The Renormalization Group
for Disordered Systems

Thesis codirected between Dipartimento di Fisica, Università La Sapienza, Rome, Italy and Laboratoire de Physique Théorique et Modèles Statistiques, Université Paris Sud, Orsay, France.

Scuola Dottorale in Scienze Astronomiche, Chimiche, Fisiche, Matematiche e della Terra "Vito Volterra".
École Doctorale ED517 "Particules, Noyaux et Cosmos".
Dottorato di Ricerca in Fisica – XXIII Ciclo

Candidate

Michele Castellana
ID number 694948

Thesis Advisors

Professor Giorgio Parisi
Professor Marc Mézard

Thesis defended on January 31, 2012
in front of a Board of Examiners composed by:

Professor Federico Ricci-Tersenghi (chairman)
Professor Alain Billoire
Professor Marc Mézard
Professor Giorgio Parisi
Professor Emmanuel Trizac
Professor Francesco Zamponi

a Laureen

Abstract

In this thesis we investigate the Renormalization Group (RG) approach in finite-dimensional glassy systems, whose critical features are still not well-established, or simply unknown. We focus on spin and structural-glass models built on hierarchical lattices, which are the simplest non-mean-field systems where the RG framework emerges in a natural way. The resulting critical properties shed light on the critical behavior of spin and structural glasses beyond mean field, and suggest future directions for understanding the criticality of more realistic glassy systems.

Acknowledgments

Thanks to all those who supported me and stirred up my enthusiasm and my willingness to work.

I am glad to thank my italian thesis advisor Giorgio Parisi, for sharing with me his experience and scientific knowledge, and especially for teaching me a scientific frame of mind which is characteristic of a well-rounded scientist. I am glad to thank my french thesis advisor Marc Mézard, for showing me how important scientific open-mindedness is, and in particular for teaching me the extremely precious skill of tackling scientific problems by considering only their fundamental features first, and of separating them from details and technicalities which would avoid an overall view.

Thanks to my family for supporting me during this thesis and for pushing me to pursue my own aspirations, even though this implied that I would be far from home.

My heartfelt thanks to Laureen for having been constantly by my side with mildness and wisdom, and for having constantly pushed me to pursue my ideas, and to keep the optimism about the future and the good things that it might bring.

Finally, I would like to thank two people who closely followed me in my personal and scientific development over these three years. Thanks to my friend Petr Šulc for the good time we spent together, and in particular for our sharing of that dreamy way of doing Physics that is the only one that can keep passion and imagination alive. Thanks to Elia Zarinelli, collaborator and friend, for sharing the experience of going abroad, leaving the past behind, and looking at it with new eyes. Thanks to him also for the completely free and pleasing environment where our scientific collaboration took place, and which should lie at the bottom of any scientific research.

Contents

x

Part I

Introduction

Chapter 1

Historical outline

Paraphrasing P. W. Anderson [4], "*the deepest and most interesting unsolved problem in solid state theory is probably the nature of glass and the glass transition*". Indeed, the complex and rich behavior of simplified models for real, physical glassy systems has interested theoreticians for its challenging complexity and difficulty, and opened new avenues in a large number of other problems such as computational optimization and neural networks.

When speaking of glassy systems, one can distinguish between two physically different classes of systems: spin glasses and structural glasses.

Spin glasses have been originally [59] introduced as models to study disordered uniaxial magnetic materials, like a dilute solution of, say, Mn in Cu, modeled by an array of spins on the Mn arranged at random in the matrix of Cu, interacting with a potential which oscillates as a function of the separation of the spins. Typical examples of spin-glass systems are $FeMnTiO_3$ [76, 71, 85, 14], $(H_3O)Fe_3(SO_4)_2(OH)_6$ [56], $CdCr_{1.7}In_{0.3}S_4$ [81, 156], $Eu_{0.5}Ba_{0.5}MnO_3$ [129] and several others.

Spin glasses exhibit a very rich phenomenology. Firstly, the very first magnetization measurements of $FeMnTiO_3$ in a magnetic field showed [76] the existence of a cusp in the susceptibility as a function of the temperature. Occurring at a finite temperature T_{sg}, this experimental observation is customary interpreted as the existence of a phase transition.
Later on, further experimental works confirmed this picture [71], and revealed some very rich and interesting features of the low-temperature phase: the chaos and memory effect. Consider a sample of $CdCr_{1.7}In_{0.3}S_4$ in a low-frequency magnetic field [81]. The system is cooled from above $T_{sg} = 16.7K$ down to $5K$, and is then heated back with slow temperature variations. The curve for the out-of-phase susceptibility χ'' as a function of the temperature obtained upon reheating will be called the reference curve, and is depicted in Fig. 1.1.
One repeats the cooling experiment but stops it at $T_1 = 12K$. Keeping the system at T_1, one waits 7 hours. In this lapse of time χ'' relaxes downwards, i. e. the system undergoes an aging process. When the cooling process is restarted, χ'' merges back with the reference curve just after a few Kelvins. This immediate merging back is the chaos phenomenon: aging at T_1 does not affect the dynamics of the system
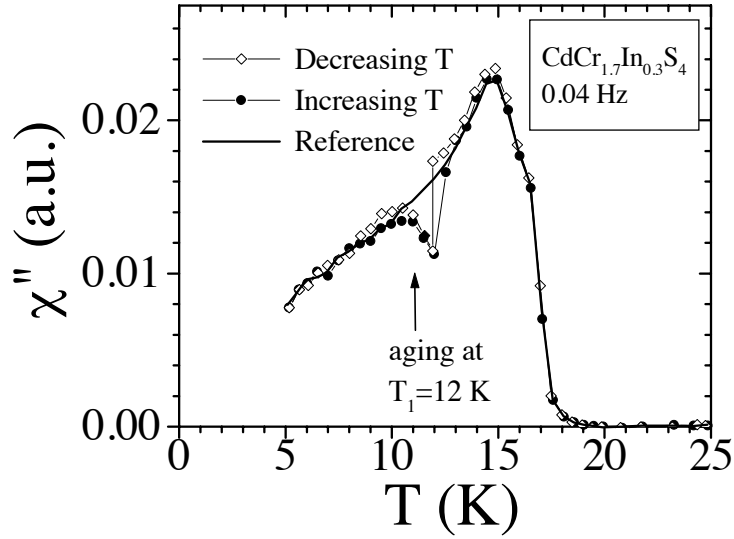
Figure 1.1. Out out phase susceptibility χ'' of $CdCr_{1.7}In_{0.3}S_4$ as a function of the temperature. The solid curve is the reference curve. The open diamonds-curve is obtained by cooling the system and stopping the cooling process at $T_1 = 7K$ for seven hours. The solid circles-curve is obtained upon re-heating the system after the above cooling process. Data is taken from [81].

at lower temperatures. From a microscopic viewpoint, the aging process brings the system at an equilibrium configuration at T_1. When cooling is restarted, such an equilibrium configuration behaves as a completely random configuration at lower temperatures, because the susceptibility curve immediately merges the reference curve. The effective randomness of the final aging configuration reveals a chaotic nature of the free-energy landscape.

The memory effect is even more striking. When the system is reheated at a constant rate, the susceptibility curve retraces the curve of the previous stop at T_1. This is quite puzzling, because even if the configuration after aging at T_1 behaves as a random configuration at lower-temperatures, the memory of the aging at T_1 is not erased.

Such a rich phenomenology challenged the theoreticians for decades. The theoretical description of such models, even in the mean-field approximation, revealed a complex structure of the low-temperature phase that could be responsible for such a rich phenomenology. Still, such a complex structure has been shown to be correct only in the mean-field approximation, and the physical features of the low-temperature phase beyond mean field are still far from being understood.

Structural glasses, also known as glass-forming liquids or glass-formers, are liquids that have been cooled fast enough to avoid crystallization [16, 150]. When cooling a sample of $o-$ Terphenyl [103], or Glycerol [112], the viscosity η or the relaxation time τ can change of fifteen order of magnitude when decreasing the temperature of

a factor two, as shown in Fig. 1.2.
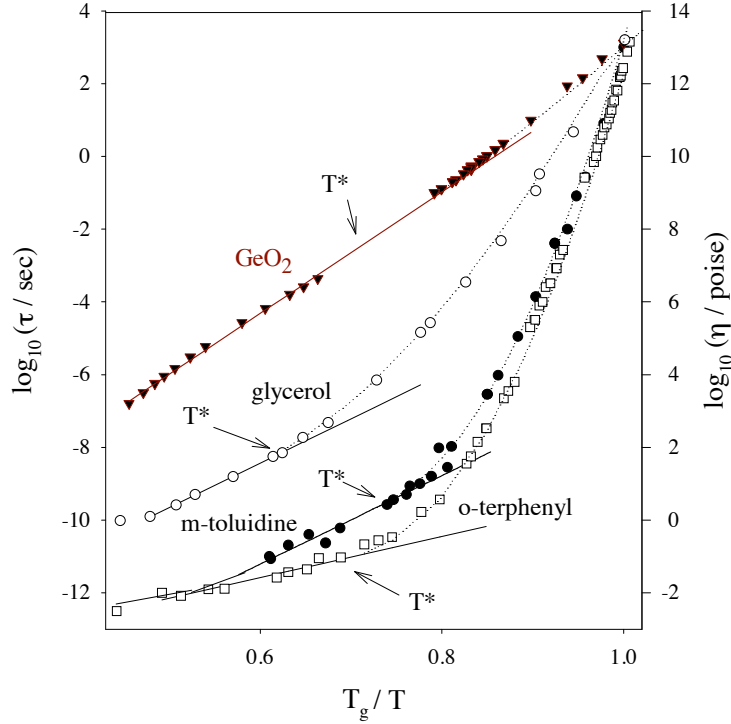
Figure 1.2. Base-10 logarithm of the relaxation time τ and of the viscosity η as a function of the logarithm of the inverse reduced temperature T_g/T, where T_g is the glass-transition temperature, for several glass formers. Data is taken from [150].

This striking increase of the viscosity can be interpreted in terms of a particle jamming process, and suggests that a phase transition occurs at a finite temperature T_g. The physical features of this transition are strikingly more complex than the ordinary first order transitions yielding a crystal as the low-temperature state.

Indeed, crystals break the translational symmetry at low temperatures, the particles being arranged on a periodic structure. Ergodicity is broken as well, because the only accessible microscopic configuration of the particles is the crystal. The sharp increase in the viscosity of a glass below the glass-transition point yields also evidence of ergodicity breaking: elementary particle moves become extremely slow, and energetically expensive, in such a way that the system is stuck in a mechanically-stable state. Differently from the crystal, this state has the same symmetry properties as the liquid: no evident symmetry breaking occurs, and there is no static order parameter to signal the transition. Moreover, at T_g the excess entropy S_e of the glass over the crystal is remarkably high, suggesting that there is a big degeneracy of mechanically-stable states a glass can get stuck in below the transition point.

Once the system is frozen in one of these exponentially many configurations, there is no way to keep it equilibrated below T_g. Accordingly, the equilibrium properties in the whole temperature phase cannot be investigated in experiments. Still, interesting properties of the low-temperature phase result from the pioneering works of Kauzmann [93], who first realized that if the excess entropy of a glass

former [143] is extrapolated from above T_g down in the low-temperature phase, there is a finite temperature T_K, the Kauzmann temperature, where this vanishes. This is rather startling because, if the geometry of the crystal is not too different from that of the liquid, one expects the entropy of the liquid to be always larger than that of the crystal. There have been countless speculations on the solution of this paradox [93, 16, 150], and the existence of a Kauzmann temperature in a real glass-former is nowadays a still hotly-debated and untamed problem from both an experimental and theoretical viewpoint.

Despite the triking difference between these two kinds of systems spin glasses and structural glasses have some deep common features. Indeed, according to a wide part of the community, spin-glass models with quenched disorder are good candidates to mimic the dynamically-induced disorder of glass-forming liquids [16], even if some people are still critical about this issue [102]. There are several points supporting the latter statement. For instance, it has been shown that hard particle lattice models [18] describing the phenomenology of structural glasses, display the phenomenology of spin systems with quenched disorder like spin glasses. Accordingly, there seems to be an underlying universality between the dynamically-induced disorder of glass-formers and the quenched disorder of spin glasses, in such a way that the theoretical description of spin glasses and that of structural glasses shared an important interplay in the last decades. More precisely, in the early 80's the solution of mean-field versions of spin [136] and structural [53] glasses were developed, and new interesting features of the low temperature phase were discovered. Since then, a huge amount of efforts has been done to develop a theoretical description of real, non-mean-field spin and structural glasses. A contribution in this direction through the implementation of the Renormalization Group (RG) method would hopefully shed light on the critical behavior of such systems.

Before discussing how the RG framework could shed light on the physics of finite-dimensional spin and structural glasses, we give a short outline of the mean-field theory of spin and structural glasses, and on the efforts that have been done to clarify their non-mean-field regime.

The Sherrington-Kirkpatrick model

The very first spin-glass model, the Edwards-Anderson (EA) model, was introduced in the middle 70's [59] as a model describing disordered uniaxial magnetic materials. Later on, Sherrington and Kirkpatrick (SK) [144] introduced a mean-field version of the EA model, which is defined as a system of N spins $S_i = \pm 1$ with Hamiltonian

$$H[\vec{S}] = - \sum_{i>j=1}^{N} J_{ij} S_i S_j, \qquad (1.1)$$

with J_{ij} independent random variables distributed according to a Gaussian distribution with zero mean and variance $1/N$.

The model can be solved with the replica method [119]: given n replicas $\vec{S}_1, \vec{S}_2, \ldots, \vec{S}_n$ of the system's spins, the order parameter is the $n \times n$ matrix $Q_{ab} \equiv 1/N \sum_{i=1}^{N} S_{a,i} S_{b,i}$ representing the overlap between replica a and replica

b. The free energy is computed as an integral over the order parameter, and thermodynamic quantities are calculated with the saddle-point approximation, which is exact in the thermodynamic limit. SK first proposed a solution for the saddle point Q_{ab}^*, which was later found to be inconsistent, since it yields a negative entropy at low temperatures. This solution is called the replica-symmetric (RS) solution, because the matrix Q_{ab}^* has a uniform structure, and there is no way to discern between two distinct replicas. Some mathematically non-rigorous aspects of the replica approach had been blamed [155] to explain the negative value of the entropy at low-temperatures. Amongst these issues, there is the continuation of the replica index n from integer to non-integer values, and the exchange of the $n \to 0$-limit with the thermodynamic limit $N \to \infty$. Still, no alternative approach was found to avoid these issues.

In the late 70's Parisi started investigating more complicated saddle points. In the very first work [134], an approximate saddle point was found, yielding a still negative but small value of the entropy at low temperatures. The solution was called replica-symmetry-broken solution, because Q_{ab}^* was no more uniform, but presented a block structure. Notwithstanding the negative values of the entropy at low temperatures, the solution was encouraging, since it showed a good agreement with Monte Carlo (MC) simulations [95], whereas the replica-symmetric solution showed a clear disagreement with MC data. Later on, better approximation schemes for the saddle point were considered [135], where the matrix Q_{ab}^* was given by a hierarchical structure of blocks, blocks into blocks, and so on. The step of this hierarchy is called the replica-symmetry-breaking (RSB) step K. The final result of such works was presented in the papers of 1979 and 1980 [133, 136], where the full-RSB ($K = \infty$) solution was presented. According to this solution, the saddle point Q_{ab}^* is uniquely determined in terms of a function $q(x)$ in the interval $0 \leq x \leq 1$, being the order parameter of the system. Parisi's solution resulted from a highly nontrivial ansatz for the saddle point Q_{ab}^*, and there was no proof of its exactness. Still, the entropy of the system resulting from Parisi's solution is always non-negative, and vanishes only at zero temperature, and the quantitative results for thermodynamic quantities such as the internal energy showed a good agreement [133] with the Thouless-Almeida-Palmer (TAP) solution [153] at low temperatures. These facts were rather encouraging, and gave a strong indication that Parisi's approach gave a significant improvement over the original solution by SK.

Still, the physical interpretation of the order parameter stayed unclear until 1983 [137], when it was shown that the function $q(x)$ resulting from the baffling mathematics of Parisi's solution is related to the probability distribution $P(q)$ of the overlap q between two real, physical copies of the system, through the relation $x(q) = \int_{-\infty}^{q} dq' P(q')$. Accordingly, in the high temperature phase the order parameter $q(x)$ has a trivial form, resulting in a $P(q) = \delta(q)$, while in the low-temperature phase the nontrivial form of $q(x)$ predicted by Parisi's solution implies a nontrivial structure of the function $P(q)$. In particular, the smooth form of $P(q)$ implies the existence of many pure states.

Further investigations in 1984 [117] and 1985 [121] gave a clear insight into the way these pure states are organized: below the critical temperature the phase space is

fragmented into several ergodic components, and each component is also fragmented into sub-components, and so on. The free-energy landscape could be qualitatively represented as an ensemble of valleys, valleys inside the valleys, and so on. Spin configurations can be imagined as the leaves of a hierarchical tree [119], and the distance between two of them is measured in terms of number of levels k one has to go up in the tree to find a common root to the two leaves. To each hierarchical level k of the tree one associates a value of the overlap q_k, where the set of possible values q_k of the overlap is encoded into the function $q(x)$ of Parisi's solution.

Parisi's solution was later rederived with an independent method in 1986 by Mézard et al [118], who reobtained the full-RSB solution starting from simple physical grounds, and presented it in a more compact form.

Finally, the proof of the exactness of Parisi's solution came in 2006 by Talagrand [149], whose results are based on previous works by Guerra [69], and who showed with a rigorous formulation that the full-RSB ansatz provides the exact solution of the problem.

This ensemble of works clarified the nature of the spin-glass phase in the mean-field case. According to its clear physical interpretation, the RSB mechanism of Parisi's solution became a general framework to deal with systems with a large number of quasi-degenerate states. In particular, in 2002 the RSB mechanism was applied in the domain of constraint satisfaction problems [120, 122, 123, 19], showing the existence of a new replica-symmetry broken phase in the satisfiable region which was unknown before then.

Despite the striking success in describing mean-field spin glasses, it is not clear whether the RSB scheme is correct also beyond mean field. Amongst the other scenarios describing the low-temperature phase of non-mean-field spin glasses, the droplet picture has been developed in the middle 80's by Bray, Moore, Fisher, Huse and McMilllan [111, 64, 61, 60, 62, 63, 27]. According to this framework, in the whole low-temperature phase there is only one ergodic component and its spin reversed counterpart, as in a ferromagnet. Differently from a ferromagnet, in a finite-dimensional spin glass spins arrange in a random way determined by the interplay between quenched disorder and temperature.

On the one hand, there have been several efforts to understand the striking phenomenological features of three-dimensional systems in terms of the RSB [78], the droplet or alternative pictures [81]. Still, none of these was convincing enough for one of these pictures to be widely accepted by the scientific community as the correct framework to describe finite-dimensional systems.

On the other hand, there is no analytical framework describing non-mean-field spin glasses. Perturbative expansions around Parisi's solution have been widely investigated by De Dominicis and Kondor [52, 55], but proved to be difficult and non-predictive. Similarly, several efforts have been done in the implementation in non-mean-field spin glasses of a perturbative field-theory approach based on the replica method [72, 99, 39], but they turned out to be non-predictive, because nonper-

turbative effects are completely untamed. Amongst the possible underlying reasons, there is the fact that such field-theory approaches are all based on a ϕ^3-theory, whose upper critical dimension is $d_c = 6$. Accordingly, a predictive description of physical three-dimensional systems would require an expansion in $\epsilon = d_c - 3 = 3$, which can be quantitatively predictive only if a huge number of terms of the ϵ-series were known [173]. Finally, high-temperature expansions for the free energy [141] turn out to be badly behaved in three dimensions [51], and non-predictive.

Since analytical approaches do not give a clear answer on such finite-dimensional systems, most of the knowledge comes from MC simulations, which started with the first pioneering works from Ogielsky [131], and were then intensively carried on during the 90's and 00's [15, 109, 110, 104, 108, 132, 100, 7, 87, 171, 89, 91, 82, 47, 83, 48, 106, 73, 10, 49, 86, 3, 8]. None of these gave a definitive answer on the structure of the low-temperature phase, and on the correct physical picture describing it. This is because a sampling of the low-temperature phase of a strongly-frustrated system like a non-mean-field spin glass has an exponential complexity in the system size [9, 160]. Accordingly, all such numerical simulations are affected by small system sizes, which prevent from discerning which is the correct framework describing the low-temperature phase. An example of how finite-size effects played an important role in such analyses is the following. According to the RSB picture, a spin-glass phase transition occurs also in the presence of an external magnetic field [119], while in the droplet picture no transition occurs in such a field [64]. MC studies [89, 92] of a one-dimensional spin glass with power-law interactions yielded evidence that there is no phase transition beyond mean field in a magnetic field. Later on, a further MC analysis [105] claimed that the physical observables considered in such a previous work were affected by strong finite-size effects, and yielded evidence of a phase transition in a magnetic field beyond mean field through a new method of data analysis. Interestingly, a recent analytical work [126] based on a replica analysis suggests that below the upper critical dimension the transition in the presence of an applied magnetic field does disappear, in such a way that there is no RSB in the low-temperature phase [124].

This exponential complexity in probing the structure of the low-temperature phase has played the role of a perpetual hassle in such numerical investigations, and strongly suggests that the final answer towards the understanding of the spin-glass phase in finite dimensions will not rely on numerical methods [75].

The Random Energy Model

The simplest mean-field model for a structural glass was introduced in 1980 by Derrida [53, 54], who named it the Random Energy Model (REM). In the original paper of 1980, the REM was introduced from a spin-glass model with quenched disorder, the p-spin model. It was shown that in the limit $p \to \infty$ where correlations between the energy levels are negligible, the p-spin model reduces to the REM: a model of N spins $S_i = \pm 1$, where the energy $\epsilon[\vec{S}]$ of each spin configuration $\vec{S}$ is a random variable distributed according to a Gaussian distribution with zero mean and variance $1/N$. Accordingly, for every sample of the disorder $\{\epsilon[\vec{S}]\}_{\vec{S}}$, the partition

function of the REM is given by

$$Z = \sum_{\vec{S}} e^{-\beta\epsilon[\vec{S}]}. \tag{1.2}$$

This model became interesting because, despite its striking simplicity, its solution reveals the existence of a phase transition reproducing all the main physical features of the glass transition observed in laboratory phenomena. Indeed, there exists a finite value T_c of the temperature, such that in the high temperature phase the system is ergodic, and has an exponentially-large number of states available, while in the low-temperature phase the system is stuck in a handful of low-lying energy states. The switchover between these two regimes is signaled by the fact that the entropy is positive for $T > T_c$, while it vanishes for $T < T_c$. Interestingly, this transition does not fall in any of the universality classes of phase transitions for ferromagnetic systems [173]. Indeed, on the one hand the transition is strictly second order, since there is no latent heat. On the other hand, the transition presents the typical freezing features of first-order phase transitions of crystals [115].

Later on, people realized that the phenomenology of the REM is more general, and typical of some spin-glass models with quenched disorder, like the p-spin model. Indeed, the one-step RSB solution scheme of the SK model was found [50] to be exact for both of the p-spin model and the REM [115], and the resulting solutions show a critical behavior very similar to each other. Accordingly, the REM, the p-spin model and other models with quenched disorder are nowadays considered to belong to the same class, the 1-RSB class [16].

The solution of the p-spin spherical model reveals that the physics of such 1-RSB mean-field models is the following [16]. There exists a finite temperature T_d such that for $T > T_d$ the system is ergodic, while for $T < T_d$ it is trapped in one amongst exponentially-many metastable states: These are the Thouless Almeida Palmer (TAP) [153] states. Since the energy barriers between metastable states are infinite in mean-field models, the system cannot escape from the metastable state it is trapped in. The nature of this transition is purely dynamical, and it shows up in the divergence of dynamical quantities like the relaxation time τ, while there is no footprint of it in thermodynamic quantities. We will denote by $f_*(T)$ the free energy of each of these TAP states and by $f_p(T)$ the free energy of the system in its paramagnetic state. Accordingly, the total free energy of the glass below T_d is given by $f_*(T) - T\Sigma(T)$. Since there is no mark of the dynamical transition in thermodynamic quantities, one has that the free energy of the glass below T_d must coincide with $f_p(T)$

$$f_p(T) = f_*(T) - T\Sigma(T). \tag{1.3}$$

Below T_d, there exists a second finite temperature $T_K < T_d$, such that the complexity vanishes at and below T_K: the number of TAP states is no more exponential, and the system is trapped in a bunch of low-lying energy minima: the system undergoes a Kauzmann transition at T_K. The nature of this transition is purely static, and shows up in the singularities of thermodynamic quantities such as the entropy.

An important physical question is whether this mean-field phenomenology persists beyond mean field. In 1989 Kirkpatrick, Thirumalai and Wolynes (KTW) [96] proposed a theoretical framework to handle finite-dimensional glass formers, which is known as the Random First Order Transition Theory (RFOT). Their basic argument was inspired by the following analogy with ferromagnetic systems. Consider a mean-field ferromagnet in an external magnetic field $h > 0$. The free energy has two minima, f_+ and f_-, with positive and negative magnetization respectively. Being $h > 0$, one has $f_- > f_+$. Even though the $+$-state has a lower free energy, it cannot nucleate because the free-energy barriers are infinite in mean field. Differently, in finite dimensions d the free-energy barriers are finite, and the free-energy cost for nucleation of a droplet of positive spins with radius R reads

$$\Delta f = C_1 R^{d-1} - (f_- - f_+) C_2 R^d, \qquad (1.4)$$

where the first addend is the surface energy cost due to the mismatch between the positive orientation of the spins inside the droplet and the negative orientation of the spins outside the droplet, while the second addend represents the free-energy gain due to nucleation of a droplet of positive spins, and is proportional to the volume of the droplet. According to the above free-energy balance, there exists a critical value R_* such that droplets with $R < R_*$ do not nucleate and shrink to zero, while droplets with $R > R_*$ grow indefinitely. Inspired by the physics emerging from mean-field models of the 1-RSB class, KTW applied a similar argument to glass-forming liquids. Before discussing KTW theory, is important to stress that the dynamical transition at T_d occurring in the mean-field case disappears in finite dimensions. This is because the free-energy barriers between metastable states are no more infinite in the thermodynamic limit. Thus, the sharp mean-field dynamical transition is smeared out in finite dimensions, and it is plausible that T_d is replaced by a crossover temperature T_*, separating a free flow regime for $T > T_*$ from an activated dynamics regime for $T < T_*$ [16].

According to KTW, for $T < T_*$ the system is trapped in a TAP state with free energy f_*. Following the analogy with the ferromagnetic case, the TAP state is associated with the $-$-state, while the paramagnetic state with the $+$-state. Accordingly, by Eq. (1.3) one has $f_- - f_+ = T\Sigma$. Nucleation of a droplet of size R of spins in the liquid state into a sea of spins in the TAP state has a free-energy cost

$$\Delta f = C_1 R^\theta - T\Sigma C_2 R^d,$$

where the exponent θ is the counterpart of $d-1$ in the ferromagnetic case, Eq. (1.4). Since the presence of disorder is expected to smear out such a surface effects with respect to the ferromagnetic case, one has $\theta < d-1$. Liquid droplets with radius smaller than $R_* \equiv \left(\frac{C_1 \theta}{T\Sigma C_2 d} \right)^{\frac{1}{d-\theta}}$ disappear, while droplets with radius larger that R_* extend to infinity. Since there are many spatially localized TAP states, droplets can't extend to infinity as in the mean-field case. The system is rather said to be in a mosaic state, given by liquid droplets that are continually created and destroyed [16].

In analogy with the 1-RSB phenomenology, RFOT theory predicts that Σ vanishes at a finite temperature $T_K < T_*$. Below this temperature liquid droplets cannot

nucleate anymore, because $R_* = \infty$, and the system is said to be in a ideal glassy state, i. e. a collectively-frozen and mechanically-stable low-lying energy state. Sill, the crucial question of the existence of a Kauzmann transition in real glass-formers is an open issue. It cannot be amended experimentally, because real glasses are frozen in an amorphous configuration below T_g, and the entropy measured in laboratory experiments in this temperature range does not give an estimate of the number of degenerate metastable states. Accordingly, analytical progress in non-mean-field models of the 1-RSB class describing the equilibrium properties below T_g would yield a significant advance on this fundamental issue.

A clear way to explore critical properties of non-mean-field systems came from the RG theory developed by Wilson in his papers of 1971 [164, 165]. The RG theory started from a very simple physical feature observed experimentally in physical systems undergoing a phase transition [161]. Consider, for instance, a mixture of water and steam put under pressure at the boiling temperature. As the pressure approaches a critical value, steam and water become indistinguishable. In particular, bubbles of steam and water of all length scales, from microscopic ones to macroscopic ones, appear. This empirical observation implies that the system has no characteristic length scale at the critical point. In particular, as the critical point is approached, any typical correlation length of the system must tend to infinity, in such a way that no finite characteristic length scale is left at the critical point. Accordingly, if we suppose to approach the critical point by a sequence of elementary steps, the physically important length scales must grow at each step. This procedure was implemented in the original work of Wilson, by integrating out all the length scales smaller than a given threshold. As a result, a new system with a larger typical length scale is obtained, and by iterating this procedure many times one obtains a system whose only characteristic length is infinite, and which is said to be critical.

The above RG scheme yields a huge simplification of the problem. Indeed, systems having a number of microscopic degrees of freedom which is typically exponential in the number of particles are reduced to a handful of effective long-wavelength degrees of freedom. These are the only physically relevant degrees of freedom in the neighborhood of the critical point, and all the relevant physical information can be extracted from them.

In the first paper of 1971 Wilson's made quantitative the above qualitative picture for the Ising model. Following Kadanoff's picture [84], short-wavelengths

degrees of freedom were integrated out by considering blocks of spins acting as a unit, in such a way that one could treat all the spins in a block as an effective spin. Given the values of the spins in the block, the value of this effective spin could be easily fixed to be +1 if the majority of spins in the block are up, and −1 otherwise. The resulting approximate RG equations were analyzed in the second paper of 1971 [165], where Wilson considered a simplified version of the Ising model and showed that this framework could make precise predictions on physical quantities like the critical exponents, which were extracted in perturbation theory. There the author realized that if the dimensionality d of the system was larger than 4 the resulting physics in the critical regime was the mean-field one, while for $d < 4$ non-mean-field effects emerge. These RG equations for the three-dimensional Ising model were treated perturbatively in the parameter $\epsilon \equiv 4 - d$, measuring the distance from the upper critical dimension $d = 4$, in a series of papers in the 70's [169, 166]. The validity of this perturbative framework was later confirmed by the reformulation of Wilson's RG equations in the language of field theory. There, the mapping of the Ising model into a ϕ^4-theory and the solution of the resulting Callan-Symanzik (CS) equations [28, 147, 173] for this theory made the RG method theoretically grounded, and the proof of the renormalizability of the ϕ^4-theory [29] to all orders in perturbation theory served as a further element on behalf of this whole theoretical framework. Finally, the picture was completed some years later by high-order implementations of the ϵ-expansion for the critical exponents [157, 41, 40, 43, 42, 94, 68, 97, 98] which were in excellent agreement with experiments [173, 1] and MC simulations [140, 5].

Because of this ensemble of works, the RG served as a fundamental tool in understanding the critical properties of finite-dimensional systems. Hence, it is natural to search for a suitable generalization of Wilson's ideas to describe the critical regime of non-mean-field spin or structural glasses. The drastic simplification resulting from the reduction of exponentially many degrees of freedom to a few long-wavelength degrees of freedom would be a breakthrough to tackle the exponential complexity limiting our understanding of the physics of such systems.

Still, a construction of a RG theory for spin or structural glasses is far more difficult than the original one developed for ferromagnetic systems. Indeed, in the ferromagnetic case it is natural to identify the order parameter, the magnetization, and then implement the RG transformation with Kadanoff's majority rule. Conversely, in non-mean-field spin or structural glasses, the order parameter describing the phase transition is fundamentally unknown.

For non-mean-field spin glasses, the RSB and droplet picture make two radically different predictions on the behavior of a tentative order parameter in the low-temperature phase. In the RSB picture the order parameter is the probability distribution of the overlap $P(q)$, being $P(q) = \delta(q)$ in the high-temperature phase and $P(q)$ a smooth function of q in the low-temperature phase [133]. Such a smooth function reflects the hierarchical organization of many pure states in the low-temperature phase. In the droplet picture [64] $P(q)$ reduces to two delta functions centered on the value of a scalar order parameter, the Edwards-Anderson order parameter q_{EA} [59]. Such an order parameter is nonzero if the local magnetizations are nonzero, i. e. if the system is frozen in the unique low-lying ergodic component of the configuration space.

For structural glasses, after important developments in the understanding of the critical regime came in 2000 [66], a significant progress in the identification of the order parameter has been proposed in 2004 [25] and numerically observed in 2008 [17] by Biroli et al., who suggested that the order parameter is the overlap between two equilibrated spin-configurations with the same boundary conditions: the influence of the boundary conditions propagates deeper and deeper into the bulk as the system is cooled, signaling the emergence of an amorphous order at low temperatures.

A justification of the difficulty in the definition of a suitable order parameter for a spin or structural glass has roots in the frustrated nature of the spin-spin interactions. To illustrate this point, let us consider a spin system like the SK where the sign of the couplings J_{ij} are both positive and negative, Eq. (1.1), and try to mimic Wilson's block-spin transformation [164] for the SK model. Given the values of the spins in a block, Kadanoff's majority rule does not give any useful information on which should the value of the effective spin. Indeed, choosing the effective spin to be $+1$ if most of the spins in the block are up and -1 otherwise does not make sense: being the J_{ij}s positive or negative with equal probability, the magnetization inside the block is simply zero on average, and does not give any useful information on which value should be assigned to the effective spin. Again, frustration is the main stumbling block in the theoretical understanding of such systems.

In order to overcome this difficulty, we recall that Wilson's approximate RG equations were found to be exact [161] on a particular non-mean-field model for ferromagnetic interactions, where the RG recursion formulas have a strikingly simple and natural form. This is Dyson's Hierarchical Model (DHM), and was introduced by Dyson in 1969 [57]. There, the process of integrating out long-wavelength degrees of freedom emerged naturally in an exact integral equation for the probability distribution of the magnetization. This equation was the forerunner of Wilson's RG equations.

The aim of this thesis is to consider a suitable generalization of DHM describing non-mean-field spin or structural glasses, and construct a RG framework for them. These models will be generally denoted by Hierarchical Models (HM), and will be introduced in Section 2.2. The definition of HM is quite general, and by making some precise choices on the form of the interactions, one can build up a HM capturing the main physical features a non-mean-field spin or structural glass. Thanks to their simplicity, HM allow for a simple and clear construction of a RG framework. Our hope is that such a RG framework could shed light on the

criticality of the glass transition beyond mean field, and on the identification of the order parameter describing the emergence of an amorphous long-range order, if present. As a long-term future direction, the RG method on HM could also be useful to understand the features of the low-temperature phase of such glassy systems.

The thesis is structured as follows. In Chapter 2 of Part I we discuss DHM, and introduce HM for spin or structural glasses. In Part II we study a HM mimicking the physics of a non-mean-field structural glass, the Hierarchical Random Energy Model (HREM), being a hierarchical version of the REM. In this Part we show how one can work out a precise solution for thermodynamic quantities of the system, signaling the existence of a Kauzmann phase transition at finite temperature. The HREM constitutes the first non-mean-field model of a structural glass explicitly exhibiting such a freezing transition as predicted by RFOT. Interestingly, the solution suggests also the existence of a characteristic length growing as the critical point is approached, in analogy with the predictions of KTW. In Part III we study a HM mimicking the physics of a non-mean-field spin glass, the Hierarchical Edwards-Anderson model (HEA), being a hierarchical version of the Edwards-Anderson model. The RG transformation is first implemented with the standard replica field-theory approach, which turns out to be non-predictive because nonperturbative effects are completely untamed. Consequently, a new RG method in real space is developed. This method avoids the cumbersome formalism of the replica approach, and shows the existence of a phase transition, making precise predictions on the critical exponents. The real-space method is also interesting from a purely methodological viewpoint, because it yields the first suitable generalization of Kadanoff's RG decimation rule for a strongly frustrated system. Finally, in Part IV we discuss the overall results of this work, by paying particular attention to its implications and future directions in the physical understanding of realistic systems with short-range interactions.

Chapter 2

Hierarchical models

In this Chapter we introduce hierarchical models. In Section 2.1 we first introduce the ferromagnetic version of hierarchical models originally introduced by Dyson, and in Section 2.2 we extend this definition to the disordered case, in the perspective to build up a non-mean-field hierarchical model of a spin or structural glass.

2.1 Hierarchical models for ferromagnetic systems

A hierarchical model for ferromagnetic systems has been introduced in the past to describe non-mean-field spin systems [57], and is known as Dyson's Hierarchical Model (DHM). DHM has been of great interest in the past, because Wilson's RG equations [164, 165, 163, 167, 168, 169] turn out to be exact in models with power-law ferromagnetic interactions built on hierarchical lattices like DHM. Indeed, in this model one can explicitly write an exact RG transformation for the probability distribution of the magnetization of the system. All the relevant physical information on the paramagnetic, ferromagnetic and critical fixed point, and the existence of a finite-temperature phase transition are encoded into these RG equations. Moreover, all the physical RG ideas emerge naturally from these recursion relations, whose solution can be explicitly built up with the ϵ-expansion technique [31, 44, 45, 46].

DHM is defined [57, 31] as a system of 2^{k+1} Ising spins $S_1, \ldots, S_{2^{k+1}}$, $S_i = \pm 1$, with an energy function which is built up recursively by coupling two systems of 2^k spins

$$
\begin{aligned}
H_{k+1}^F \left[S_1, \ldots, S_{2^{k+1}}\right] \;=\; & H_k^F \left[S_1, \ldots, S_{2^k}\right] + H_k^F \left[S_{2^k+1}, \ldots, S_{2^{k+1}}\right] + \quad (2.1) \\
& -JC_F^{k+1} \left(\frac{1}{2^{k+1}} \sum_{i=1}^{2^{k+1}} S_i\right)^2,
\end{aligned}
$$

where

$$
C_F \equiv 2^{2(1-\sigma_F)}, \tag{2.2}
$$

and F stands for ferromagnetic. The model is defined for

$$
1/2 < \sigma_F < 1. \tag{2.3}
$$

17

The limits (2.3) can be derived by observing that for $\sigma_F > 1$ the interaction energy goes to 0 for large k, and no finite-temperature phase transition occurs, while for $\sigma_F < 1/2$ the interaction energy grows with k faster than 2^k, i. e. faster than the system volume, in such a way that the model is thermodynamically unstable.

The key issue of DHM is that the recursive nature of the Hamiltonian function encoded in Eq. (2.1) results naturally into an exact RG equation. This equation can be easily derived by defining the probability distribution of the magnetization m for a 2^k-spin DHM, as

$$p_k(m) \equiv \mathcal{C} \sum_{\vec{S}} \mathrm{e}^{-\beta H_k^F[\vec{S}]} \delta \left(\frac{1}{2^k} \sum_{i=1}^{2^k} S_i - m \right), \tag{2.4}$$

where δ denotes the Dirac delta function, and $\mathcal{C}$ a constant enforcing the normalization condition $\int dm p_k(m) = 1$. Starting from Eq. (2.1), one can easily derive a recursion equation relating p_k to p_{k+1}. This equation is derived in Section A.1 of Appendix A, and reads

$$p_{k+1}(m) = \mathrm{e}^{\beta J C_F^{k+1} m^2} \int d\mu \, p_k(m + \mu) p_k(m - \mu), \tag{2.5}$$

where any m-independent multiplicative constant has been omitted to simplify the notation. Eq. (2.5) relies the probability distribution of a DHM with 2^k spins with that of a DHM with 2^{k+1} spins. Accordingly, Eq. (2.5) is nothing but the flow of the function $p_k(m)$ under reparametrization $2^k \to 2^{k+1}$ of the length scale of the system. Historically, Eq. (2.5) has been derived by Dyson [57], and then served as the starting point for the construction of the RG theory for ferromagnetic systems like the Ising model. Indeed, Wilson's RG recursion formulas for the Ising model [164, 165, 163] are approximate, while they turn out to be exact when applied to DHM, because they reduce to Eq. (2.5). DHM has thus played a crucial role in the construction of the RG theory for ferromagnetic systems, because in a sense the work of Wilson on finite-dimensional systems has been pursued in the effort to generalize the exact recursion formula (2.5) to more realistic systems with no hierarchical structure, like the three-dimensional Ising model.

Equation (2.5) has also been an important element in the probabilistic formulation of RG theory, originally foreseen by Bleher, Sinai [20] and Baker [6], and later developed by Jona-Lasinio and Cassandro [79, 31]. Indeed, Eq. (2.5) aims to establish the probability distribution of the average of 2^k spin variables $\{S_i\}_i$ for $k \to \infty$. In the case where the spins are independent and identically distributed (IID), the above analogy becomes transparent, because the answer to the above question is yield by the central limit theorem. Following this connection between RG and probability theory, one can even prove the central limit theorem starting from the RG equations (2.5) [31].

Equation (2.5) has been of interest in the last decades also because it is simple enough to be solved with high precision, and the resulting solution gives a clear insight into the critical properties of the system, showing the existence of a phase transition. The crucial observation is that Eq. (2.5) can be iterated $k \gg 1$ times in 2^k operations. Indeed, the magnetization m of a 2^k-spin DHM can take $2^k + 1$

possible values $\{-1, -1 + 2/2^k, \cdots, 0, \cdots, 1 - 2/2^k, 1\}$. According to Eq. (2.4), the function $p_k(m)$ is nonzero only if m is equal to one of these $2^k + 1$ values. It follows that in order to compute $p_{k+1}(m)$, one has to perform a sum in the right-hand side of Eq. (2.5), involving $2^k + 1$ terms. This implies that the time to calculate $p_k(m)$ for $k \gg 1$ is proportional to 2^k. Thus, the use of the hierarchical structure encoded in Eq. (2.5) yields a significant improvement in the computation of $p_k(m)$ with respect to a brute-force evaluation of the sum in the right-hand side of Eq. (2.4), which involves 2^{2^k} terms.

Let us now discuss the solution of Eq. (2.5). For Eq. (2.5) to be nontrivial for $k \to \infty$, one needs to rescale the magnetization variable. Otherwise, the C_F^{k+1}-term in the right-hand side of Eq. (2.5) would diverge for $k \to \infty$. Setting

$$\mathfrak{p}_k(m) \equiv p_k(C_F^{-k/2} m), \tag{2.6}$$

Eq. (2.5) becomes

$$\mathfrak{p}_{k+1}(m) = e^{\beta J m^2} \int d\mu \, \mathfrak{p}_k \left(\frac{m + \mu}{C_F^{1/2}} \right) \mathfrak{p}_k \left(\frac{m - \mu}{C_F^{1/2}} \right). \tag{2.7}$$

The structure of the fixed points of Eq. (2.7) is discussed in Section A.2 of Appendix A. In particular, it is shown that there exists a value β_{cF} of β, such that if $\beta < \beta_{cF}$ Eq. (2.7) converges to a high-temperature fixed point, while if $\beta > \beta_{cF}$ Eq. (2.7) converges to a low-temperature fixed point. Both of these fixed points are stable, and can be qualitatively represented as basins of attraction in the infinite-dimensional space where $\mathfrak{p}_k(m)$ flows [163]. These basins of attraction are separated by an unstable fixed point $\mathfrak{p}_*(m)$, which is reached by iterating Eq. (2.7) with $\beta = \beta_{cF}$. $\mathfrak{p}_*(m)$ is called the critical fixed point, and is characterized by the fact that the convergence of $\mathfrak{p}_k$ to $\mathfrak{p}_*$ for $\beta = \beta_{cF}$ implies the divergence of the characteristic length scale ξ_F of the system in the thermodynamic limit $k \to \infty$. Accordingly, in what follows β_{cF} will denote the inverse critical temperature of DHM. In the neighborhood of the critical temperature the divergence of ξ_F is characterized by a critical exponent ν_F, defined by

$$\xi_F \overset{T \to T_{cF}}{\approx} \frac{A}{(T - T_{cF})^{\nu_F}}, \tag{2.8}$$

where A is independent of the temperature. The critical exponent ν_F is an important physical quantity characterizing criticality, and is quantitatively predictable from the theory. In Section A.3 of Appendix A we show how ν_F can be computed starting from the RG equation (2.7). This derivation serves as an important example of the techniques that will be employed in generalizations of DHM involving quenched disorder, that will be discussed in the following Sections.

The calculation of ν_F relies on the fact that for $0 < \sigma_F \leq 3/4$ the critical fixed point $\mathfrak{p}_*(m)$ is a Gaussian function of m, while for $3/4 < \sigma_F < 1$ $\mathfrak{p}_*(m)$ is not Gaussian, as illustrated in Section A.2. We recall [44, 45, 31, 163, 173, 174] that a Gaussian $\mathfrak{p}_*(m)$ corresponds to a mean-field regime of the model. The expression mean field is due to the following. Consider for instance the thermal average at the

critical point of a physical observable $O(1/2^k \sum_{i=1}^{2^k} S_i)$, depending on the spins $\vec{S}$ through the magnetization of the system. This can be expressed as an average of $O(m)$ with weight $p_*(m)$, where $p_*(m) = \mathfrak{p}_*(C_F^{k/2} m)$

$$\mathbb{E}_{\vec{S}}^F[O] = \int dm \, p_*(m) O(m), \tag{2.9}$$

where $\mathbb{E}_{\vec{S}}^F$ stands for the thermal average

$$\mathbb{E}_{\vec{S}}^F[O] \equiv \frac{\sum_{\vec{S}} e^{-\beta H_k^F[\vec{S}]} O(1/2^k \sum_{i=1}^{2^k} S_i)}{\sum_{\vec{S}} e^{-\beta H_k^F[\vec{S}]}}.$$

In the mean-field approximation one evaluates integrals like that in the right-hand side of Eq. (2.9) with the saddle-point approximation [173, 74, 130]. If $0 < \sigma_F \leq 3/4$, $\mathfrak{p}_*(m)$ is Gaussian, and so is $p_*(m)$, in such a way that the saddle-point approximation is exact, i. e. the mean-field approximation is correct. On the contrary, for $3/4 < \sigma_F \leq 1$, $\mathfrak{p}_*(m)$ is not Gaussian, and the system has a non-mean-field behavior. In particular, fluctuations around the mean-field saddle point in the right-hand side of Eq. (2.9) are not negligible. According to this discussion, we call $\sigma_F = 3/4$ the upper critical dimension [74, 173, 174, 77] of DHM.

In the mean-field region $0 < \sigma_F \leq 3/4$, ν_F can be computed exactly, and is given by Eqs. (A.16), (A.17). In the non-mean-field region ν_F can be calculated by supposing that the physical picture emerging for $0 < \sigma_F \leq 3/4$ is slightly modified in the non-mean-field region. As discussed in Section A.2, this assumption is equivalent to saying that corrections to the mean-field estimate of integrals like (2.9) are small, i. e. they can be handled perturbatively. Whether this assumption is correct or not can be checked a posteriori, by expanding physical quantities like ν_F in powers of $\epsilon_F = \sigma_F - 3/4$, and investigating the convergence properties of the expansion. If the ϵ_F-expansion is found to be convergent or resummable [173], the original assumption is confirmed to be valid. If it is not, the non-mean-field physics is presumably radically different from that arising in the mean-field region, and cannot be handled perturbatively. As an example, the result to $O(\epsilon_F)$ for ν_F is given by Eqs. (A.16), (A.19). In [46, 44], the ϵ_F-expansion has been performed to high orders, and found to be nonconvergent. Even though, the authors showed that the application of a resummation method originally presented in [107] yields a convergent series for ν_F, which is in quantitative agreement with the values of the exponent obtained by Bleher [23]. Finally, we mention that the results from the ϵ_F-expansion of DHM have been found to be in excellent agreement with those obtained with the high-temperature expansion, which has been studied by Y. Meurice et al. [114].

Since DHM allows for a relatively simple implementation of the RG equations for a non-mean-field ferromagnet, it is natural to ask oneself whether there exists a suitable generalization of DHM that can describe a non-mean-field spin or structural glass. This generalization will be exposed in the following Section.

2.2 Hierarchical models for spin and structural glasses

In the effort to clarify the non-mean-field scenario of both spin glasses and structural glasses, it is useful to consider a suitable generalization of DHM to the disordered case. Concerning this, it is important to observe that the extension of DHM to the random case has been performed only for some particular models.

Firstly, models with local interactions on hierarchical lattices built on diamond plaques [11], have been widely studied in their spin-glass version, and lead to weakly frustrated systems even in their mean-field limit [67]. Notwithstanding this, such models yield a very useful and interesting playground to show how to implement the RG ideas in disordered hierarchical lattices, and in particular on the construction of a suitable decimation rule for a frustrated system.

Secondly, a RG analysis for random weakly frustrated models on Dyson's hierarchical lattice has been done in the past by A. Theumann [151, 152], and the structure of the physical and unphysical infrared (IR) fixed points has been obtained with the ϵ-expansion technique. Unfortunately, in these models spins belonging to the same hierarchical block interact with each other with the same [151] random coupling, in such a way that frustration turns out to be relatively weak and they are not a good representative for realistic strongly frustrated systems. This is because these models are obtained from DHM by replacing the coupling J in Eq. (2.1) with a random variable J_k. Thus, the interaction energy between spins $S_1, \ldots, S_{2^k}$ is fixed, and purely ferromagnetic or antiferromagnetic, depending on the sign of J_k. Differently, in strongly frustrated systems like the SK model, the coupling J_{ij} between any spin pair S_i, S_j is never fixed to be ferromagnetic or antiferromagnetic, because its sign is randomly drawn for any i and j.

Thirdly, disordered spin models on Dyson's hierarchical lattice have been studied by A. Naimzhanov [127, 128], who showed that the probability distribution of the magnetization converges to a Gaussian distribution in the infinite-size limit. Also in this case, the interaction between spins $S_1, \ldots, S_{2^k}$ is fixed to be ferromagnetic or antiferromagnetic, depending on the sign of a random energy ε_k which is equal to ± 1 with equal probability.

Here we present a different generalization of DHM to a disordered and strongly frustrated case, first introduced in [65], and simply call these models *hierarchical models* (HM). Indeed, the definition (2.1) holding in the ferromagnetic case can be easily generalized as follows. We define a HM as a system of 2^{k+1} spins $S_1, \ldots, S_{2^{k+1}}$, $S_i = \pm 1$, with an energy function defined recursively by coupling two systems, say system 1 and system 2, of 2^k Ising spins

$$H_{k+1}\left[S_1, \ldots, S_{2^{k+1}}\right] = H_k^1\left[S_1, \ldots, S_{2^k}\right] + H_k^2\left[S_{2^k+1}, \ldots, S_{2^{k+1}}\right] + \quad (2.10)$$
$$+\epsilon_{k+1}\left[S_1, \ldots, S_{2^{k+1}}\right].$$

The energies H_k^1, H_k^2 are to be considered as the energy of system 1 and system 2 respectively, while ϵ_k is the coupling energy between system 1 and system 2. Differently from the ferromagnetic case, here the coupling energy $\epsilon_{k+1}\left[S_1, \ldots, S_{2^{k+1}}\right]$

of any spin configuration $S_1, \cdots, S_{2^{k+1}}$ is a random variable, which is chosen to have zero mean for convenience.

Since the interaction energy ϵ_{k+1} couples 2^{k+1} spins, and since its order of magnitude is give by its variance, one must have

$$\mathbb{E}_\epsilon[\epsilon_{k+1}^2] < 2^{k+1}, \tag{2.11}$$

where $\mathbb{E}_\epsilon$ stands for the expectation value with respect to all the coupling energies ϵ_k of the model. Eq. (2.11) states that the interaction energy between 2^{k+1} spins is sub extensive with respect to the system volume 2^{k+1}, and ensures [119, 130] that HM are non-mean-field models. The mean-field limit will be constantly recovered in the following chapters as the limit where $\mathbb{E}_\epsilon[\epsilon_{k+1}^2]$ becomes of the same order of magnitude as the volume 2^{k+1}.

As we will show in the following, the form (2.10) of the Hamiltonian corresponds to dividing the system in hierarchical embedded blocks of size 2^k, so that the interaction between two spins depends on the distance of the blocks to which they belong [65, 34, 35], as shown in Fig 2.1.
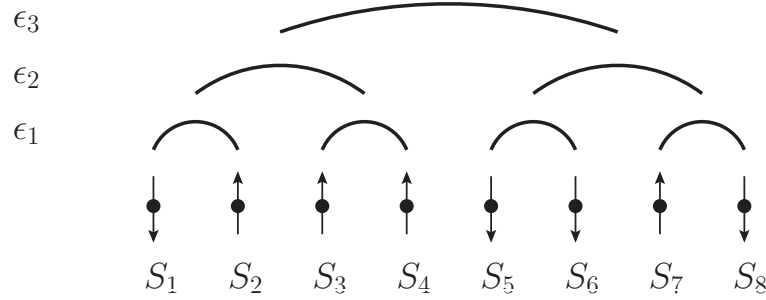
Figure 2.1. A 2^3-spin hierarchical model obtained by iterating Eq. (2.10) until $k = 3$. The arcs coupling pairs of spins represent the energies ϵ_1 at the first hierarchical level $k = 1$. Those coupling quartets of spins represent ϵ_2 at the second hierarchical level $k = 2$. Those coupling octets of spins represent the energies ϵ_3 at the third hierarchical level $k = 3$.

The random energies ϵ_k of HM can be suitably chosen to mimic the interactions of a strongly frustrated structural glass (Part II), or of a spin glass (Part III), in the perspective to give some insight into the non-mean-field behavior and criticality of both of these models. In this thesis such features will be investigated by means of RG techniques. Indeed, as for DHM, the recursive nature of the definition (2.10) suggests that HM are particularly suitable for an explicit implementation of the RG transformation. As a matter of fact, the definition (2.10) is indeed a RG flow transformation from the length scale 2^k to the length scale 2^{k+1}. As we will show explicitly in Part III, one can analyze the fixed points of such an RG flow, in order to establish if a phase transition occurs, and investigate the critical properties of the system.

It is important to observe that without the hierarchical structure this would be extremely difficult. This is mainly because of the intrinsic and deep difficulty in

identifying the correct order parameter discussed in Section 1, and thus write an RG equation for a function (or functional) of it without making use of the replica method [55, 119] which, up to the present day, could not be used to make predictions for the non-mean-field systems under consideration in this thesis.

After introducing HM in their very general form, we now make a precise choice for the random energies ϵ_k in order to build up a hierarchical model for a structural glass, the Hierarchical Random Energy Model, and discuss its solution.

Part II

The Hierarchical Random Energy Model

As discussed in Section 1, the REM is a mean-field spin model mimicking the phenomenology of a supercooled liquid. Given the general definition of HM, it is easy to make a particular choice for the random energies ϵ_k in (2.10), to build up a non-mean-field version of the REM, i. e. a HM being a candidate for describing the phenomenology of a supercooled liquid beyond mean field. Indeed, we choose the energies ϵ_k to be independent variables distributed according to a Gaussian distribution with zero mean and variance proportional to C^{2k}

$$\mathbb{E}_\epsilon[\epsilon_k^2] \sim C^{2k}, \tag{2.12}$$

where we set

$$C^2 = 2^{1-\sigma}. \tag{2.13}$$

For $\sigma < 0$ the thermodynamic limit $k \to \infty$ is ill-defined, because the interaction energy $\mathbb{E}_\epsilon[\epsilon_k^2]$ grows faster than the volume 2^k. For $\sigma > 1$, $\mathbb{E}_\epsilon[\epsilon_k^2]$ goes to 0 as $k \to \infty$, implying that there is no phase transition at finite temperature. Hence, the interesting region that we will consider in the following is

$$0 < \sigma < 1, \tag{2.14}$$

which is the equivalent of Eq. (2.3) for DHM. As we will discuss in the following, this HM reproduces the REM in the mean-field case $\sigma = 0$, and will thus be called the *Hierarchical Random Energy Model* (HREM) [33, 36]. According to the general classification of models with quenched disorder given in Section 1, the HREM has to be considered as a model mimicking a structural glass.

Before discussing the solution of the HREM, it is important to focus our attention on some important features of the model that make it interesting in the perspective of investigating the non-mean-field regime of a structural glass.

Firstly, the hierarchical structure of the HREM allows an almost explicit solution with two independent and relatively simple methods.
The first method will be described very shortly here (a complete discussion can be found in [33, 32]) and relies on the fact that the recursive nature of Eq. (2.10) implies a recursion relation for the function $\mathcal{N}_k(E)$, defined as the number of states with energy E at the k-the step of the recursion. By solving this recursion equation for large k, one can compute the entropy of the system

$$s(E) \equiv \frac{1}{2^k} \log\left[\mathcal{N}_k(E)\right], \tag{2.15}$$

and thus investigate its equilibrium properties. The computation time needed to implement this recursion at the k-th step is proportional to a power of 2^k, and represents a neat improvement on the exact computation of the partition function, involving a time proportional to 2^{2^k}. This recursive method is also significantly better than estimating thermodynamic quantities with MC simulations, because the latter are affected by a severe increase of the thermalization time when approaching the critical point, as discussed in Section 1.
The second method investigates the thermodynamic properties of the HREM by a perturbative expansion in the parameter C, physically representing the coupling
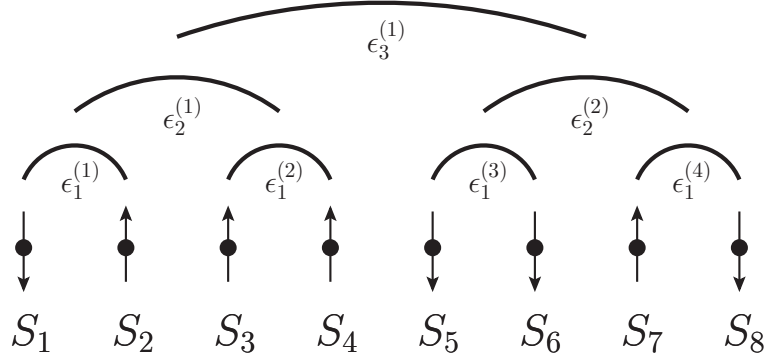
Figure 2.2. A 2^3-spin HREM and its interaction structure. Each arc represents an interaction energy $\epsilon_j^{(i)}$ amongst spins falling below the arc.

constant between spins. As a matter of fact, the relatively simple structure of the model allows for a fully automated expansion in C of the equilibrium thermodynamic quantities, which exhibits a neat and clear convergence when increasing the perturbative order as discussed in Chapter 3.

It follows that the HREM is a model that hopefully encodes the non-mean-field features of a structural glass, and that is solvable with relatively simple and reliable methods, such as the recursion equation for $\mathcal{N}(E)$ and the perturbative expansion in C. In particular, as we will show in Chapter 3, with such methods one can identify the existence of a phase transition in the HREM, and then analyze its physical features.

Secondly, it turns out that the 2^{2^k} energy levels $\{H_k[\vec{S}]\}_{\vec{S}}$ of the HREM are not independent variables as in the REM [53], because here they are correlated to each other. Indeed, by iterating k times Eq. (2.10), one obtains explicitly the Hamiltonian for a HREM with 2^k spins

$$H_k[\vec{S}] = \sum_{j=0}^{k} \sum_{i=1}^{2^{k-j}} \epsilon_j^{(i)}[\vec{S}^{(j,i)}], \tag{2.16}$$

where $\vec{S} \equiv \{S_1, \cdots, S_{2^k}\}$, while $\vec{S}^{(j,i)} \equiv \{S_{2^j(i-1)+1}, \cdots, S_{2^j i}\}$ are the spins in the i-th embedded block at the j-th hierarchical level, and $\epsilon_j^{(i)}$ is the interaction energy ϵ_j (see Eq. (2.10)) of the i-th hierarchical embedded block. The interaction energies $\epsilon_j^{(i)}$ of Eq. (2.16) are depicted in Fig 2.2 for a HREM with 2^3 spins.

According to Eq. (2.16), the energy levels are clearly correlated to each other. As we will show in Chapter 3, this fact implies that some critical features of the HREM turn out to be quite different from to those of the REM. In particular, we will show by an explicit calculation how a naive estimate of the critical temperature based on the hypothesis that the energy levels are uncorrelated fails miserably, proving the relevance of energy correlations in the critical regime.

Thirdly, the existence of the hierarchical structure depicted in Fig. 2.10 allows for the introduction of a notion of distance between spins in the HREM, whereas in the REM there is no notion of distance, because mean-field models have no

spatial geometry [119]. As we will show in Chapter 4, such a length scale can be introduced in the HREM by defining a suitable correlation function, and extracting the characteristic length scale associated with its exponential decay at large distances. It is then interesting to ask oneself whether such a length diverges at the critical point as in ferromagnetic systems [74, 101, 173, 174, 163, 162, 138]. This point will be investigated in Chapter 4, by means of the perturbative expansion method.

We will now present the perturbative computation of the equilibrium properties of the HREM, and discuss the results on the critical behavior of the model [33].

Chapter 3

Perturbative computation of the free energy

Given a sample of the random energies $\{\epsilon\} \equiv \{\epsilon_j^{(i)}\}_{j,i}$, the free energy of a HREM with 2^k spins is defined as [115, 119]

$$f[T, \{\epsilon\}] \equiv -\frac{1}{\beta 2^k} \log \left[Z\left[T, \{\epsilon\}\right] \right], \tag{3.1}$$

where

$$Z\left[T, \{\epsilon\}\right] \equiv \sum_{\vec{S}} \exp\left(-\beta H_k[\vec{S}]\right), \tag{3.2}$$

$\beta \equiv 1/T$ is the inverse temperature, and $H_k[\vec{S}]$ is given by Eq. (2.16). To simplify the notation, in the following we omit the volume label k in the free energy f and in the partition function Z unless necessary.

The free energy (3.1) of a *typical* sample $\{\epsilon\}$ can be computed by hypothesizing that the self-averaging property holds. According to this property, holding in the thermodynamic limit of a broad class of disordered systems with quenched disorder [119, 37], the free energy computed on a fixed and typical sample of the disorder is equal to the average value of the free energy over the disorder. Here we hypothesize that this property holds, so that in the thermodynamic limit $k \to \infty$ we compute $f[T, \{\epsilon\}]$ on a typical sample $\{\epsilon\}$ as the average of Eq. (3.1) over the random energies

$$\lim_{k \to \infty} f[T, \{\epsilon\}] = \lim_{k \to \infty} \mathbb{E}_\epsilon\left[f[T, \{\epsilon\}]\right]. \tag{3.3}$$

The advantage of using the self-averaging property is that the right-hand side of Eq. (3.3) is easier to compute than the left-hand side by using the replica trick [119, 115]

$$\mathbb{E}_\epsilon\left[f[T, \{\epsilon\}]\right] = -\frac{1}{\beta 2^k} \lim_{n \to 0} \frac{\mathbb{E}_\epsilon\left[Z[T, \{\epsilon\}]^n\right] - 1}{n}. \tag{3.4}$$

According to the general prescriptions of the replica trick [119, 136, 133, 37], the argument of the limit in Eq. (3.4) is here computed for integer n, and an analytic function of n is obtained. The left-hand side of (3.4) is then computed by continuing such a function to real n, and taking its $n \to 0$ limit.

As observed in Section 1, the use of the replica trick in mean-field models can be non-rigorous, because of the assumption that one can exchange the thermodynamic limit and the $n \to 0$ limit [119, 115, 136, 37]. It is important to observe that this issue does not occur in this case. Indeed, by using Eqs. (3.1), (3.3) and (3.4), one has

$$\lim_{k \to \infty} f[T, \{\epsilon\}] = \lim_{k \to \infty} \lim_{n \to 0} \frac{1 - \mathbb{E}_\epsilon \left[Z[T, \{\epsilon\}]^n \right]}{n\beta 2^k}. \tag{3.5}$$

In order to compute Eq. (3.5) in mean-field models, one hypothesizes that one can first compute the right-hand side of Eq. (3.6) in the thermodynamic limit $k \to \infty$ by using the saddle-point approximation, and then take $n \to 0$, by exchanging the limits. Being the HREM a non-mean-field model, the saddle-point approximation is wrong even in the thermodynamic limit, so that the right-hand side of Eq. (3.5) cannot be computed by taking its saddle point, and we do not need to exchange the limits. Hence, the subtleties resulting from the exchange of the limits do not occur in this case. In other words, here the replica trick is simply a convenient way to perform the computation of the quenched free energy, and a direct inspection of Eq. (3.5) in perturbation theory shows that one can do the computation without replicas, and obtain the same result as that obtained with the replica trick to any order in C. We observe that this fact is true also in the mean-field theory of spin glasses, where the full-RSB solution [133] can be rederived [118] without making use of the replica method.

Let us now focus on the explicit computation of the right-hand side of Eq. (3.5) for integer n and on the $n \to 0$-limit. One has

$$\mathbb{E}_\epsilon \left[Z[T, \{\epsilon\}]^n \right] = \sum_{\{\vec{S}_a\}_{a=1,\cdots,n}} \exp\left(\frac{\beta^2}{4} \sum_{j=0}^{k} C^{2j} \sum_{i=1}^{2^{k-j}} \sum_{a,b=1}^{n} \delta_{\vec{S}_a^{(j,i)}, \vec{S}_b^{(j,i)}} \right), \tag{3.6}$$

where $\vec{S}_1, \cdots, \vec{S}_n$ denote the spin configurations of the n replicas of the system [136, 137, 37, 130]. We then expand Eq. (3.6) in power of C^2, and take the $n \to 0, k \to \infty$-limits. It is important to observe that this C^2-expansion is equivalent to a high-temperature expansion. Indeed, in Eq. (3.6) any power C^{2j} of the coupling constant is multiplied by a factor β^2, so that the smallness of C^2 is equivalent to the smallness of the inverse temperature β.
By Eq. (3.5), the expansion of Eq. (3.6) in powers of C^2 results into an expansion for $f[T, \{\epsilon\}]$, that can be written as

$$f[T, \{\epsilon\}] = \sum_{i=0}^{\infty} C^{2i} \phi_i(T), \tag{3.7}$$

where for simplicity we omit the $k \to \infty$-limit, and the dependence of f on $\{\epsilon\}$ has disappeared because of the self-averaging property (3.3). The coefficients $\phi_i(T)$ can be explicitly calculated for large i by means of a symbolic manipulation program [170], handling the tensorial operations on the replica indices [33, 32]. This computation is carried on for integer n and an analytic function of n is obtained, so that the limit $n \to 0$ can be safely taken. In Appendix B we give an example of how these computations are performed, by doing the explicit calculation of the coefficient ϕ_0.

In the following, the expansion (3.7) will be worked out at a fixed order l, under the underlying assumption that the resulting free energy

$$f_l(T) \equiv \sum_{i=0}^{l} C^{2i} \phi_i(T) \tag{3.8}$$

approximates the exact free energy (3.7) as l is large

$$f_l(T) \overset{l \to \infty}{\to} f_\infty(T) = f[T, \{\epsilon\}].$$

Before discussing the result of this computation for $0 < \sigma < 1$, it is interesting to test perturbation theory in the region $\sigma < 0$ for the following reason. As stated in Section 2.2, for $\sigma < 0$ the thermodynamic limit of the model is ill-defined. This is because the interaction energy ϵ_k defined in Eq. (2.10) grows with k faster than the volume 2^k according to Eq. (2.12). Notwithstanding this, having the HREM 2^k spins, one can redefine the inverse temperature

$$\beta \to 2^{k\sigma/2}\beta, \tag{3.9}$$

in such a way that the variance of ϵ_k defined in Eq. (2.12) becomes

$$\mathbb{E}_\epsilon[\epsilon_k^2] \to 2^k. \tag{3.10}$$

The thermodynamic limit is now well-defined, because the coupling energy scales as the volume, and the model is a purely mean-field one. A direct numerical inspection of the expansion (3.8) after such a redefinition of β for $\sigma < 0$ shows that as l is increased the free energy of the HREM converges to that of a REM [53, 54] with critical temperature

$$T_{cU}^{\sigma<0} \equiv \frac{1}{2\sqrt{\log 2(1 - 2^\sigma)}}. \tag{3.11}$$

The label U in Eq. (3.14) stands for uncorrelated, because the value (3.14) of the critical temperature can be easily worked out by hypothesizing that the energy levels are uncorrelated as in the REM. Indeed, the fact that the free energy (3.8) converges to that of the REM for $\sigma < 0$ tells us that in this region correlations are irrelevant, and the model reduces to a purely mean-field one with the same features as the REM. This is what we expected from the fact that the energy scales as the system volume (Eq. (3.10)), and serves as an important test of the perturbative expansion (3.7).

We now focus on the region $0 < \sigma < 1$. From a direct analysis of the data for the free energy $f_l(T)$, it turns out that there exists an l-dependent critical temperature T_c^l, defined in such a way that the entropy at the l-th order in C^2 vanishes at $T = T_c^l$

$$s_l(T_c^l) \equiv -\left.\frac{df_l(T)}{dT}\right|_{T=T_c^l} = 0. \tag{3.12}$$

As discussed in Section 1, in the REM the fact that the entropy vanishes at a given temperature signals a Kauzmann phase transition. Hence, by definition T_c^l can be

considered as the l-th order critical temperature of the system. Since perturbation theory is approximate, and there is no guarantee that a perturbative expansion converges at a critical point [74, 173, 174, 138], it is important to check the behavior of T_c^l as l is increased. In Fig. 3.1, T_c^l as a function of l is depicted for $\sigma = 0.1$. Even for $l \leq 10$, a clear convergence is observed, and the resulting 'exact' critical temperature T_c^∞ is easily determined by fitting T_c^l vs. l with a function of the form $a - b \times c^l$, with $c < 1$, and setting $T_c^\infty = a$. In this way, T_c^∞ as a function of σ is determined in the region $0 \leq \sigma \leq 0.15$, where T_c^l vs. l for $l \leq 10$ exhibits a clear convergence as a function of l, and the extrapolation for $l \to \infty$ is meaningful.

The HREM has a finite temperature phase transition à la Kauzmann.

According to Eq. (3.12), the entropy of the HREM

$$s(T) \equiv -\frac{df_\infty(T)}{dT} \tag{3.13}$$

vanishes for $T = T_c^\infty$. This allows a straightforward interpretation of the phase transition occurring at $T = T_c^\infty$, resembling to that occurring in the REM [53]: for $T > T_c^\infty$ the entropy is positive, and the system explores an exponentially large number of states in the configuration space, while for $T < T_c^\infty$ the system is trapped in a handful of low-lying energy states. We have thus shown that the HREM undergoes a phase transition à la Kauzmann at a finite temperature T_c^∞, whose features are similar to that of the phase transition of the REM and, more generally, of mean-field structural glasses [16].

In the inset of Fig. 3.1, T_c^∞ as a function of σ is depicted, and T_c^∞ turns out to be a decreasing function of σ. This fact is physically meaningful, because according to Eq. (2.13), the larger σ the smaller the coupling C between spins, and so the smaller the temperature T_c^∞ such that for $T < T_c^\infty$ all the spins are frozen in a low-lying energy state.

As in the $\sigma < 0$-case, we can hypothesize that the energy levels act as uncorrelated random variables, in such a way that the HREM behaves as a REM. In this case, the critical temperature can be computed exactly, and is given by

$$T_{cU}^{\sigma>0} \equiv \frac{1}{2\sqrt{\log 2(1 - 2^{-\sigma})}}. \tag{3.14}$$

Differently from the $\sigma < 0$-case, here the decorrelation hypothesis turns out to be wrong. Indeed, by looking at the inset of Fig 3.1, T_c^∞ does not coincide with $T_{cU}^{\sigma>0}$. This fact is a clear evidence that correlations between the energy levels play a crucial role in the region $\sigma > 0$, and cannot be neglected.

In Fig 3.2 the free energy $f_l(T)$ as a function of the temperature T for $\sigma = 0.1$ and different values of $l \leq 10$ is depicted. $f_l(T)$ is found to converge to a finite value $f_\infty(T)$ for $T > T_c^\infty$, while for $T < T_c^\infty$ the lower the temperature the worse the convergence of the sequence $f_l(T)$ vs. l. Hence, when descending into the low-temperature phase from $T > T_c^\infty$, a breakdown of perturbation theory occurs, signaling the possibility of a nonanalyticity of the free energy at the critical point, resembling to the nonanalytical behavior of physical quantities occurring in second-order phase transitions for ferromagnetic systems [74, 101, 173, 174, 138].
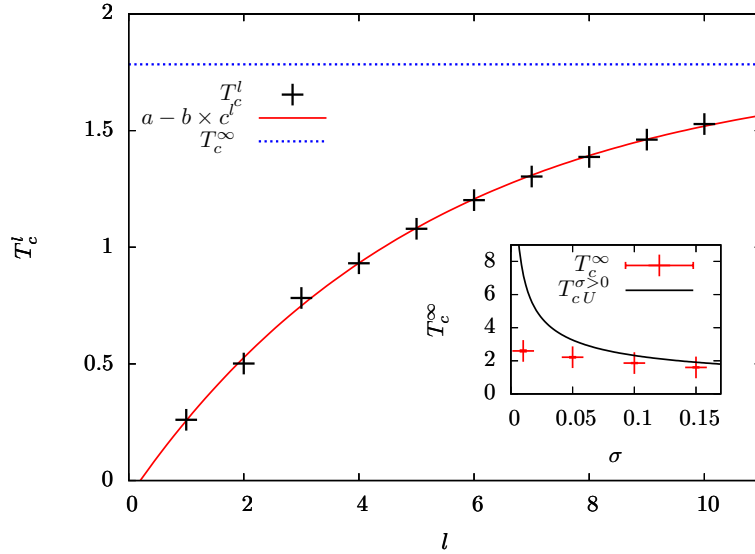
Figure 3.1. Critical temperature T_c^l (black points), its fitting function $a - b \times c^l$ (red solid curve) and asymptotic value $T_c^\infty = 1.861 \pm 0.021$ (blue dashed line) as a function of l for $\sigma = 0.1$. $T_c^\infty = a$ has been determined as a fit parameter. Inset: critical temperature T_c^∞ (red points) in the region $0 < \sigma < 0.15$ where the first 10 orders of the perturbative expansion show a clear convergence, and critical temperature $T_{cU}^{\sigma > 0}$ (black curve), as a function of σ. The error bars on T_c^∞ are an estimate of the error resulting from the fit on the parameter a. T_c^∞ is clearly non-consistent with $T_{cU}^{\sigma > 0}$, showing that correlations between energy levels are important. The $\sigma \to 0^+$-limit of T_c^∞ does not coincide with the $\sigma \to 0^-$-limit of $T_{cU}^{\sigma < 0}$ because of the abrupt change (3.9) in the normalization of the temperature when switching from $\sigma > 0$ to $\sigma < 0$.

According to the above discussion, the perturbative expansion (3.7) yields a reliable method to estimate physical quantities in the high-temperature phase $T > T_c^\infty$. Notwithstanding this, no conclusions can be drawn on the behavior of the free energy in the low-temperature phase with this perturbative framework. In particular, this method gives no insight into the structure of the states of the system in the low-temperature phase. An interesting approach yielding a tentative solution in the low-temperature phase can be worked out by hypothesizing that the n replicas $\vec{S}_1, \cdots, \vec{S}_n$ in Eq. (3.6) are grouped into n/x groups, where each group is composed by x replicas [119, 115]. For any two replicas a, b in the same group one has $\vec{S}_a = \vec{S}_b$. We can look at the small C^2-expansion (3.7) in the particular case where the replicas are grouped as described above. We call the free energy to the l-th order obtained with this ansatz $f_l^{\mathrm{RSB}}(T, x)$. RSB stands for replica-symmetry-breaking, and has the same physical interpretation as the ordinary RSB mechanism described in Section 1 for structural glasses: as in the REM, a replica-symmetry-broken structure in the low-temperature phase implies that the system is no more ergodic, because it is trapped in a handful of low-lying energy states [16, 119, 130, 53, 54, 136, 137, 115]. By performing the computation explicitly, it is easy to find out that $f_l^{\mathrm{RSB}}(T, x) = f_l(T/x)$. According to the general prescriptions of the replica approach [119, 115, 136, 133, 137], as we take the $n \to 0$-limit the parameter x, originally defined as an integer number, has to be treated as a real
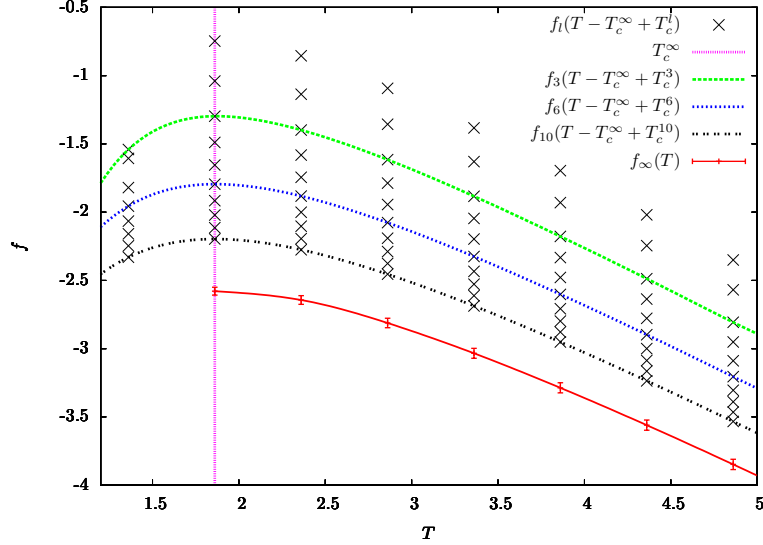
Figure 3.2. Free energy f as a function of temperature T for $\sigma = 0.1$. We depict $f_l(T - T_c^\infty + T_c^l)$ for $l = 1, 2, \cdots, 10$ (gray points), $f_3(T - T_c^\infty + T_c^3)$ (green dashed curve), $f_6(T - T_c^\infty + T_c^6)$ (blue dashed curve), $f_{10}(T - T_c^\infty + T_c^{10})$ (black dashed curve), and the extrapolated free energy $f_\infty(T)$ as a function of T (red points and solid curve). We also depict the critical temperature T_c^∞ (violet dashed line). For any fixed T, $f_\infty(T)$ has been obtained by fitting the sequence $f_l(T - T_c^\infty + T_c^l)$ vs. l with a function of the form $a - b \times c^l$, with $c < 1$, and setting $f_\infty(T) = a$. To compute $f_\infty(T)$, we used the sequence $f_l(T - T_c^\infty + T_c^l)$ vs. l instead of $f_l(T)$ vs. l because the former has the same limit as the latter for $l \to \infty$, and exhibits a better convergence for the accessible values of $l \le 10$. The error bars on $f_\infty(T)$ are given by an estimate of the fit error on the parameter a.

number lying in the interval $[0, 1]$. Hence, the maximization of $f_l^{\mathrm{RSB}}(T, x)$ with respect to x gives $x = 1$ for $T \ge T_c^l$, and $x = T/T_c^l$ for $T < T_c^l$. It follows that according to this this RSB ansatz the exact free energy reads

$$f_\infty^{\mathrm{RSB}}(T) = \begin{cases} f_\infty(T_c^\infty) & T < T_c^\infty \\ f_\infty(T) & T \ge T_c^\infty \end{cases}. \tag{3.15}$$

The form (3.15) of the RSB free energy is the same as that of the REM [119, 53, 54], and predicts that in the low-temperature phase the HREM has a one-step RSB, reflecting ergodicity breaking. On the one hand, this RSB ansatz predicts a free energy $f_\infty(T)$ which is exact for $T \ge T_c^\infty$, because it coincides with the free energy computed with perturbation theory without making use of any ansatz. On the other hand, there is no guarantee that f^{RSB} is exact in the low-temperature phase. In particular, the n replicas could be grouped in a more complicated pattern than the RSB one described above, and this configuration could yield a free energy that is larger than f^{RSB} for $T < T_c^\infty$. Since in the replica method the exact free energy is not the minimum, but the maximum of the free energy as a function of the order parameter configurations [115, 119], such a more complicated pattern would yield the exact free energy of the system. The investigation of the existence of such an optimal pattern is an extremely interesting question that could be subject of future work, and give some insight into the low-temperature phase of the HREM, and more generally into the low-temperature features of non-mean-field structural glasses.

Once the existence of a phase transition has been established, we ask ourselves what are its physical features. In particular, an interesting question is whether, as in second-order phase transitions [74, 163, 162, 173, 174], the system has no characteristic scale length at the critical point. Indeed, answering this question for the HREM is particularly interesting, because an analysis of the characteristic length scales of the system in the critical region could give some insight into the construction of a RG theory for non-mean-field structural glasses.

Chapter 4

Spatial correlations of the model

Being a non-mean-field model, the HREM allows for the definition of a distance between spins. This definition is yield naturally by the hierarchical structure of the couplings shown in Fig. 2.1. Indeed, given two spin sites i and j, one can define their ultrametric distance m as the number of levels one has to get up in the binary tree starting from the leaves, until one finds a root that is shared by i and j. This geometrical construction of the ultrametric distance is depicted in Fig. 4.1 for a HREM with $k = 3$. One can thus define the distance between i and j as

$$\| i - j \| \equiv 2^m. \tag{4.1}$$
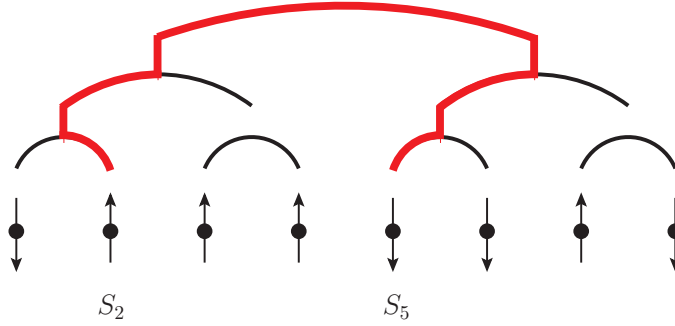
Figure 4.1. Ultrametric distance between spins S_2 and S_5 in a HREM with $k = 3$. In order to find a root shared by S_2 and S_5, one has to go 2 levels up in the binary tree. Hence, the ultrametric distance between S_2 and S_5 is $m = 2$.

Once the notion of distance has been clarified, we want to know if the system has a characteristics length defined in terms of this distance, and what is the behavior of this length in the critical region. In order to do so [32], we define a correlation function whose exponential decay at large distances yields a characteristic length scale ξ of the system. This correlation function is defined as

$$Y(2^m, T) \equiv \mathbb{E}_\epsilon \left[\mathbb{E}_{\vec{S}_1, \vec{S}_2} \left[\prod_{i=1}^{2^m} \delta_{S_{1,i}, S_{2,i}} \right] \right] \overset{m \to \infty}{\equiv} \exp\left[-\frac{2^m}{\xi(T)} \right], \tag{4.2}$$

where $\mathbb{E}_{\vec{S}}$ stands for the thermal average

$$\mathbb{E}_{\vec{S}}[\mathcal{O}[\vec{S}]] \equiv \frac{\sum_{\vec{S}} e^{-\beta H_k[\vec{S}]} \mathcal{O}[\vec{S}]}{Z[T, \{\epsilon\}]}, \tag{4.3}$$

and δ_{S_i, S_j} denotes the Kronecker delta function. The correlation function (4.2) has the following physical meaning. Given two spin configurations $\vec{S}_1$, $\vec{S}_2$, $Y(2^m, T)$ physically represents the mean overlap between $\vec{S}_1$ and $\vec{S}_2$ on the sites $1, \cdots, 2^m$ of the lattice.

Before studying the behavior of ξ in the region $0 < \sigma < 1$, we compute ξ in the region $\sigma < 0$ where the model is purely mean field. As discussed in Chapter 3, for the thermodynamic limit to be well-defined for $\sigma < 0$, one has to rescale the temperature according to Eq. (3.9). By plugging Eq. (3.9) into Eq. (4.2) and taking $\sigma < 0$, one easily obtains the correlation function in the mean-field case

$$Y(2^m, 2^{-k\sigma/2}T) \quad \stackrel{k \to \infty}{=} \quad \frac{\sum_{\vec{S}_1, \vec{S}_2} \prod_{i=1}^{2^m} \delta_{S_{1,i}, S_{2,i}}}{2^{2 \, 2^k}} \tag{4.4}$$

$$= \quad \exp(-2^m \log 2).$$

Comparing Eq. (4.4) to the definition of $\xi(T)$ in Eq. (4.2), we obtain the mean-field value of the correlation length

$$\xi_{MF}(T) = \frac{1}{\log 2}. \tag{4.5}$$

Eq. (4.5) is consistent with the fact that in the mean-field case there must be no notion of physical distance between spins [130], and so the system has no physical length scale signaling the range of spatial correlations between spins.

This picture should radically change for $0 < \sigma < 1$, where a physical spatial structure and distance does exist. In Chapter 3 we showed that the HREM has a phase transition at T_c^∞. According to the above physical meaning of the correlation function (4.2), one expects long-range spatial correlations to occur at T_c^∞, because for $T \to T_c^\infty$ both $\vec{S}_1$ and $\vec{S}_2$ should stay trapped in the same handful of low-lying energy states, and exhibit a high degree of overlap with each other. Hence, $Y(2^m, T)$ should tend to 1, in such a way that ξ diverges.

In the following we compute ξ for $0 < \sigma < 1$ in the same perturbative framework as in Chapter 3, to investigate the existence of such a long-range spatial correlations at the critical point. Firstly, Eq. (4.2) can be rewritten with the replica trick

$$
\begin{aligned}
Y(2^m, T) &= \mathbb{E}_\epsilon \left[\frac{\sum_{\vec{S}_1, \vec{S}_2} e^{-\beta(H_k[\vec{S}_1] + H_k[\vec{S}_2])} \prod_{i=1}^{2^m} \delta_{S_{1,i}, S_{2,i}}}{Z[T, \{\epsilon\}]^2} \right] \\
&= \mathbb{E}_\epsilon \left[\lim_{n \to 0} \sum_{\vec{S}_1, \cdots, \vec{S}_n} e^{-\beta \sum_{a=1}^n H_k[\vec{S}_a]} \prod_{i=1}^{2^m} \delta_{S_{1,i}, S_{2,i}} \right] \\
&= \lim_{n \to 0} \sum_{\vec{S}_1, \cdots, \vec{S}_n} \exp\left(\frac{\beta^2}{4} \sum_{j=0}^k C^{2j} \sum_{i=1}^{2^{k-j}} \sum_{a,b=1}^n \delta_{\vec{S}_a^{(j,i)}, \vec{S}_b^{(j,i)}} \right) \prod_{i=1}^{2^m} \delta_{S_{1,i}, S_{2,i}}.
\end{aligned} \tag{4.6}
$$

The last line of Eq. (4.6) is very similar to (3.6), used in Chapter 3 to compute the free energy of the HREM. Hence, the very same techniques used to compute f in perturbation theory can be employed here to calculate the correlation function Y. In particular, one can expand the correlation function (4.6) in the coupling constant C^2

$$Y(2^m, T) = \sum_{i=0}^{\infty} C^{2i} \Upsilon_{m,i}(T), \tag{4.7}$$

and explicitly evaluate the coefficients $\Upsilon_{m,i}$ by a symbolic manipulation program [170] until the order $i = 9$. In Appendix C we present the steps of the computation of $\Upsilon_{m,0}(T)$, to give some insight into the main techniques employed in the calculation to high orders.

For any fixed m and T, the exact value of $Y(2^m, T)$ has been computed by extrapolating the sequence

$$Y_l(2^m, T) \equiv \sum_{i=0}^{l} C^{2i} \Upsilon_{m,i}(T) \tag{4.8}$$

to $l \to \infty$, with the underlying assumption that for large l Eq. (4.8) converges to the exact value of the correlation function

$$Y_l(2^m, T) \overset{l \to \infty}{\to} Y_\infty(2^m, T) = Y(2^m, T).$$

The sequence $Y_l(2^m, T)$ as a function of m for fixed σ, l and T is shown in Fig. 4.2 for $m = 3, T = 3.5$. Even though Y_l is nicely convergent even to relatively low orders for the values of m and T considered in Fig. 4.2, an explicit analysis of $Y_l(2^m, T)$ for different values of m shows that the larger m, the larger the number of orders needed to see a nice convergence with respect to l. This fact can be easily understood by recalling that the C^2-expansion is equivalent to a high-temperature expansion (see Chapter 3). It is a general feature of high-temperature expansions [172, 30, 146, 51] that with a finite number of orders of the β-series, one cannot describe arbitrarily large length scales. Hence, with a finite number of orders (9 in our case) for $Y_l(2^m, T)$, one cannot describe the correlations $Y_l(2^m, T)$ for too large m.

Another important fact is that, for any fixed m the convergence of $Y_l(2^m, T)$ gets worse as the temperature T is decreased, because more terms in the β-expansion, and so in the C^2 expansion, are needed.

Practically speaking, these limitations of the perturbative expansion made us take $m \leq 3$ and $T > T_0$, where T_0 is a σ-dependent value of the temperature signaling a breakdown of perturbation theory. As we will discuss in the following, notwithstanding the very small values of m here available, it has been possible to compute the correlation length $\xi(T)$ defined in Eq. (4.2) in a wide interval of temperatures.

The correlation length $\xi(T)$ has been computed for every temperature T by fitting the data for $Y_\infty(2^m, T)$ vs. m, according to the definition of $\xi(T)$ given in Eq. (4.2).

Once $\xi(T)$ is known, we investigate its behavior at low temperatures. As stated above, one cannot take too low values of T because of the non-convergence of the
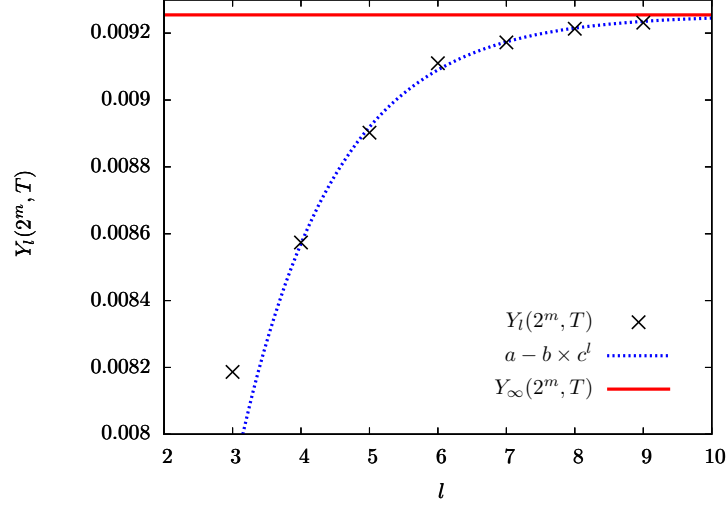
Figure 4.2. $Y_l(2^m, T)$ (black points), its fitting function $a - b \times c^l$ (blue dashed curve) as
a function of l, and $Y_\infty(2^m, T) = a$ (red solid line), determined as a fit parameter. Here
$\sigma = 0.1, m = 3$ and $T = 3.5$.

perturbative expansion. Notwithstanding this, it is still possible to approach enough
the critical point T_c^∞ and investigate the existence of long-range spatial correlations.
In particular, we test the validity of the hypothesis of a diverging $\xi(T)$ for $T \to T_c^\infty$.
In order to do so, we check whether the data for $\xi(T)$ is consistent with a power-law
divergence at some temperature T_c^ξ

$$\xi(T) \overset{T \to T_c^\xi}{\approx} \frac{C}{(T - T_c^\xi)^\nu}. \tag{4.9}$$

The validity of the hypothesis (4.9) has been tested in the following way. We suppose
that Eq. (4.9) holds, and determine the value of T_c^ξ such that the data for $\xi(T)$ best
fits with Eq. (4.9). We fit the data for $\log [\xi(T)]$ vs. $\log(T - T_c^\xi)$ for different values
of T_c^ξ. The value T_c^ξ such that $\log [\xi(T)]$ vs. $\log(T - T_c^\xi)$ best fits with a straight line,
is such that the data for $\xi(T)$ is consistent with a power-law divergence at T_c^ξ, accord-
ing to (4.9). The top panel of Fig. 4.3 shows that for $\sigma = 0.1$ the optimal value of
T_c^ξ is compatible with the critical temperature T_c^∞ for $\sigma = 0.1$ obtained in Chapter 3.

The data for the
correlation length
of the HREM is
consistent with a
power-law
divergence at the
Kauzmann
transition
temperature.

The data for $\xi(T)$ is thus consistent with a diverging correlation length at the
Kauzmann transition temperature T_c^∞. In the bottom panel of Fig. 4.3, $\xi(T)$ as
a function of T for $\sigma = 0.1$ is depicted, together with its fitting function (4.9)
with $T_c^\xi = T_c^\infty$. $\xi(T)$ increases as the temperature is decreased, and its shape is
compatible with a power-law divergence at the Kauzmann transition temperature
T_c^∞.

Since this work establishes the existence of a thermodynamic phase transition
and the possibility of a diverging correlation length in the HREM, it also shows the
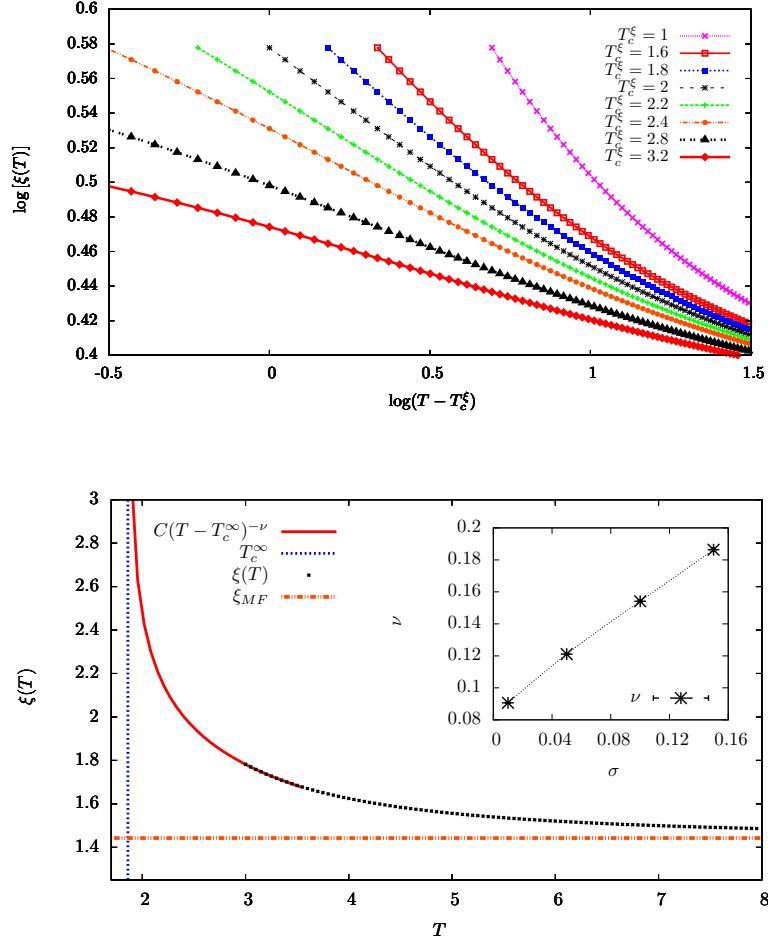
Figure 4.3. Top: $\log[\xi(T)]$ vs. $\log(T - T_c^\xi)$ for different tentative values of $1 < T_c^\xi < 3.2$ and $\sigma = 0.1$. The value of T_c^ξ such that $\xi(T)$ best fits with the hypothesis (4.9) is such that $\log[\xi(T)]$ vs. $\log(T - T_c^\xi)$ best fits with a straight line. This value lies in the interval $[1.8, 2]$, and is thus consistent with the Kauzmann transition temperature $T_c^\infty = 1.861 \pm 0.021$ of the model. Bottom: $\xi(T)$ (black points), its fitting function (4.9) with $T_c^\xi = T_c^\infty$ (solid red curve), ξ_{MF} (orange dashed line) as a function of T for $\sigma = 0.1$, and the Kauzmann transition temperature T_c^∞ (blue dashed line). In the region $0 < \sigma < 1$, the correlation length $\xi(T)$ at low temperature is significantly larger than the mean-field value ξ_{MF}, because of the existence of physical spatial correlations between spins. Inset: critical exponent ν defined by Eq. (4.9) as a function of σ. ν has been computed by setting $T_c^\xi = T_c^\infty$ and fitting $\xi(T)$ with Eq. (4.9). Error bars on ν are an estimate of the uncertainty resulting from the determination of ν as a fit parameter.

way forward to the study of finite-dimensional spin or structural-glass models.
For instance, the REM has been found [154, 26] to have a dynamical phase transition
at finite temperature if a particular dynamics is chosen: it would be interesting
to study these dynamical properties in the HREM, by introducing some suitable
dynamics of the spins, and by investigating the existence of a dynamical phase
transition, and of a diverging dynamical correlation length.
Another interesting future direction would be to generalize the techniques used in
the solution of the REM to more realistic non-mean-field spin or structural-glass
models, like p-spin models [50] built on a hierarchical lattice. Indeed, even though
the HREM serves as a model representing a non-mean-field structural glass, its
structure is still far from being realistic: strictly speaking, the spins $\vec{S}$ in the HREM
are not physical degrees of freedom, but serve as mere labels for the energy variables
$H_k[\vec{S}]$ as in the REM [53, 115, 130]. Moreover, a criticism one could address to the
solution techniques developed in Chapters 3 and 4 is that these do not give any
insight into the construction of a suitable RG protocol. In particular, a decimation
rule on spins is still lacking.

In the following Part we introduce a HM of a spin glass, in the effort to address
these two points: in such a HM spins are real physical degrees of freedom, in such a
way that a decimation rule on spins naturally emerges, and one can explicitly solve
the resulting RG equations.

Part III

The Hierarchical Edwards-Anderson Model

As discussed in Section 1, the SK model is a mean-field spin glass, whose critical properties have been clarified in Parisi's solution [133, 136, 137, 119, 115, 130]. Whether the physical features of this solution persist also in a non-mean-field version of the SK, or the non-mean-field case is described by a radically different scheme [111, 64, 61, 60, 62, 63, 27, 125], is one of the most hotly debated topics in statistical physics. Being this a very difficult question, it is interesting to consider non-mean-field versions of the SK that presumably capture all the non-mean-field physics, and that are simple enough to be solved quite easily, by means of an explicit implementation of the RG transformation.

Starting from the general definition (2.10) of Hierarchical models given in Section 2.2, here we explicitly chose the random energies ϵ_k to build up a non-mean-field version of the SK model having these features: the Hierarchical Edwards-Anderson model (HEA) [65, 34, 35, 36]. The HEA is defined by choosing the random energy ϵ_k in the following way [65]

$$\epsilon_{k+1}[S_1, \ldots, S_{2^{k+1}}] \equiv -\left(\frac{C^2}{2}\right)^{k+1} \sum_{i<j=1}^{2^{k+1}} J_{12,ij} S_i S_j, \qquad (4.10)$$

where C is still defined by Eq. (2.13), and $J_{12,ij}$ are Gaussian random variables with zero mean and unit variance.

Starting from Eq. (4.10) and from the definition of the J_{12}s, it is easy to show that ϵ_{k+1} has zero mean, and that its variance satisfies

$$\mathbb{E}_\epsilon[\epsilon_k^2] \overset{k\to\infty}{\sim} 2^{2k(1-\sigma)}. \qquad (4.11)$$

It follows that for $\sigma < 1/2$ the interaction energy (6.35) grows faster than the volume 2^k, and the thermodynamic limit $k \to \infty$ is not defined. The purely mean-field case, i. e. the case where the interaction energy scales with k as the volume 2^k, is recovered for $\sigma = 1/2$. Moreover, for $\sigma > 1$ the interaction energy (6.35) goes to 0 as $k \to \infty$, in such a way that no phase transition can occur. Hence, in the following we will take

$$1/2 < \sigma < 1, \qquad (4.12)$$

which is the equivalent of Eq. (2.3) for DHM.

Physically speaking, the interaction energy (4.10) of the HEA introduces two-spin interactions, while the interaction energy of the HREM defined in Part II has 2^{k+1}-spin interactions. Another fundamental difference between the HEA and the HREM is that, according to the general classification of models with quenched disorder given in Section 1, the HEA has to be considered as a model for a spin glass, while the HREM as a model mimicking the physics of a structural glass [16]. Compared to the HREM, the HEA is a more realistic model, because according to the definition (4.10), here the spins of the system are physical degrees of freedom, and not mere labels for the energy variables as in the REM and in the HREM. As we will see in the following, the HEA also allows for an explicit construction of a suitable decimation rule on spins, and so of a RG transformation.

An equivalent definition of the HEA can be given without using the recursion relation (2.10). Indeed, one can recover Eq. (2.10) by defining the HEA as a system of 2^k spins $S_i = \pm 1$, $0 \leq i \leq 2^k - 1$, with Hamiltonian

$$H_k[\vec{S}] = -\sum_{i,j=0}^{2^k-1} J_{ij} S_i S_j, \tag{4.13}$$

where the J_{ij}s are Gaussian random variables with zero mean and variance ς_{ij}^2. ς_{ij}^2 is given by the following expression: consider the binary representation of the points i, j

$$i = \sum_{a=0}^{k-1} c_a 2^{k-1-a}, \; j = \sum_{a=0}^{k-1} d_a 2^{k-1-a}.$$

If only the last m digits $\{c_{k-m}, \cdots, c_{k-1}\}$ of the binary representation of i are different from the last m digits $\{d_{k-m}, \cdots, d_{k-1}\}$ of the binary representation of j, one has

$$\varsigma_{ij}^2 = 2^{-2\sigma m}. \tag{4.14}$$

The definition (4.13) is equivalent to the definition given by (2.10) and (4.10).

The form (4.13) of the Hamiltonian can be obtained by dividing the system in hierarchical embedded blocks of size 2^m, as shown in Fig. 2.1. More precisely, the integer m can be considered as the ultrametric distance between spins S_i and S_j defined in Fig. 4.1 for the HREM.

The HEA is a hierarchical counterpart of the one-dimensional spin glass with power-law interactions (PLSG) [99], which has received attention recently [90, 88, 89, 104, 106]. The only difference between this PLSG and the HEA is the form of ς_{ij}^2. In the PLSG, Eq. (4.14) is replaced by $\varsigma_{ij}^2 = |i - j|^{-2\sigma}$, where $|i - j|$ denotes the ordinary absolute value of $i - j$. This form of the interaction structure, even though apparently simpler than that of the HEA, makes the implementation of a RG transformation extremely harder to pursue practically. Indeed, the form (4.14) of the interactions of the HEA keeps track of the hierarchical structure of the model, and so of a symmetry that is absent in the PLSG. Differently from the PLSG, thanks to this symmetry the RG equations of the HEA allow for a direct solution that can be in principle computed with extremely high precision [34, 35], as we will show in Chapter 5.

We now proceed by exposing the techniques developed to solve the HEA [34, 35, 36]. An important observation is that an explicit evaluation of the partition function for large k is practically impossible, because this would involve 2^k spins, and so a sum of 2^{2^k} terms. Moreover, as discussed in Section 1, there is no guarantee [75] that even the most refined MC techniques [58, 145, 73, 8, 3, 10] work properly at low temperatures for reasonably large system sizes, because of the existence of many metastable minima in the energy landscape.
An interesting method to overcome these difficulties is to use the hierarchical structure of the model. Indeed, the recursion equation (2.10) stemming from this structure results into some RG equations, whose thermodynamic limit $k \to \infty$ can be studied with some suitable approximation schemes. In Chapter 5, we derive

these RG equations with the replica approach, and analyze their fixed points with standard field-theory techniques. We show that notwithstanding their simplicity, the perturbative solution of these RG equations results into a perturbative series which is probably non-convergent. Hence, an alternative real-space approach which does not rely on the replica method is developed in Chapter 6. In this latter approach, the hierarchical structure of the model is again used to write some RG equations that can be solved numerically with high precision. The replica RG approach and the real-space approach are then compared, by considering their predictions on the critical exponents of the model.

Chapter 5

The RG in the replica approach

In this Chapter we derive and solve the RG equations for the HEA model with the replica approach [34, 35]. These RG equations can be derived with two different methods. The first, exposed in Section 5.1, derives the RG equations by using directly the hierarchical structure of the model. We will call this approach method à la Wilson, because it implements a coarse-graining RG step relating a 2^k-spin HEA to a 2^{k+1}-spin HEA, and this yields a RG equation similar to the RG equations originally obtained by Dyson [57, 44, 45, 31] for DHM, and so analogous to Wilson's RG equations [161, 164, 165, 163]. The second approach, exposed in Section 5.2, reformulates the problem in terms of a ϕ^3-field theory [173], and the resulting RG equations are nothing but the Callan-Symanzik equations [173, 174] for such a field theory. The two formulations are tested to be equivalent by an explicit computation of the critical exponents.

5.1 The RG method à la Wilson

Let us consider the partition function $Z[T, \{\epsilon\}]$ of a HEA with 2^k spins, which is defined by Eq. (3.2). According to the general features of the replica approach [119, 115, 130, 65], the physics of the model is encoded into the $n \to 0$ limit of the n-times replicated partition function

$$\mathbb{E}_\epsilon[Z[T, \{\epsilon\}]^n] = \mathbb{E}_\epsilon \left[\sum_{\{\vec{S}_a\}_{a=1,\ldots,n}} \exp \left(-\beta \sum_{a=1}^n H_k[\vec{S}_a] \right) \right], \qquad (5.1)$$

where $\mathbb{E}_\epsilon$ denotes the expectation value with respect to the random distribution of the energies ϵ_k, i. e. with respect to all the random couplings $J_{12,ij}$ of Eq. (4.10), and $\vec{S}_a$ is the spin configuration of the a-th replica of the system. One can then consider the $n \times n$ matrix Q_{ab} [119, 115, 130] physically representing the overlap between replicas a and b, which is defined as

$$\begin{aligned} Q_{ab} &\equiv & \frac{1}{2^k} \sum_{i=1}^{2^k} S_{a,i} S_{b,i} \ \forall a \neq b, \\ Q_{aa} &\equiv & 0 \ \forall a. \end{aligned}$$

An interesting quantity which is derived from (5.1) is the probability distribution of the overlap over the quenched disorder $\{\epsilon\}$

$$P_k[Q] \equiv \mathbb{E}_\epsilon \left[\sum_{\{\vec{S}_a\}_{a=1,\ldots,n}} \exp\left(-\beta \sum_{a=1}^n H_k[\vec{S}_a] \right) \prod_{a<b=1}^n \delta\left(Q_{ab} - \frac{1}{2^k} \sum_{i=1}^{2^k} S_{a,i} S_{b,i} \right) \right],$$

(5.2)

where the volume dependence has been explicitly restored with the label k in P_k, and δ denotes the Dirac delta function. The quantity $P_k[Q]$ is interesting because when one iterates the recursion equation (2.10), and a 2^{k+1}-spin HEA is built up, the resulting P_{k+1} can be related to P_k by a simple recursion equation, which is

$$P_{k+1}[Q] = \exp\left(\frac{\beta^2 C^{4(k+1)}}{4} \text{Tr}[Q^2] \right) \int [dQ_1 dQ_2] P_k[Q_1] P_k[Q_2] \times$$

(5.3)

$$\times \prod_{a<b=1}^n \delta\left(Q_{ab} - \frac{Q_{1,ab} + Q_{2,ab}}{2} \right),$$

where Tr denotes the trace over the replica indices $a, b, \ldots$, and the integral over the matrix Q is denoted by $\int[dQ] \equiv \int \prod_{a<b=1}^n dQ_{ab}$. Eq. (5.3) is equivalent to the recursion equation (2.5) for DHM [57], and it yields the flow of the function P_k obtained by coupling two systems with volume 2^k to obtain a system with volume 2^{k+1}. It follows that Eq. (5.3) can be considered as the flow of P_k under the reparametrization $2^k \to 2 \times 2^k$ of the length scale [164, 165, 163, 173, 174, 77, 138, 74]. According to these considerations, Eq. (5.3) is a RG equation.

The very same techniques developed in Section 2.1 and in Appendix A to solve Eq. (2.5) for DHM can be used to solve Eq. (5.3). Notwithstanding this, the solution of Eq. (5.3) turns out to be much more cumbersome than that of Eq. (2.5), because the former is a flow equation for a function $P_k[Q]$ of a matrix Q_{ab}, while the latter is a flow equation for a function $p_k(m)$ of a number m. In what follows we will show the main steps of the solution of Eq. (5.3).

First of all, we seek for a solution of Eq. (5.3) for $k \to \infty$, in order to investigate the critical properties of the HEA in the thermodynamic limit. To this end, let us rescale the variable Q in Eq. (5.3), by setting

$$\mathscr{P}_k[Q] \equiv P_k[C^{-2k} Q],$$

(5.4)

in such a way that Eq. (5.3) becomes

$$\mathscr{P}_k[Q] = \exp\left(\frac{\beta^2}{4} \text{Tr}[Q^2] \right) \int [dP] \, \mathscr{P}_{k-1}\left[\frac{Q+P}{C^2} \right] \mathscr{P}_{k-1}\left[\frac{Q-P}{C^2} \right].$$

(5.5)

Similarly to Eq. (2.6), Eq. (5.4) is the correct rescaling for Eq. (5.3) to converge to a nontrivial fixed point for $k \to \infty$, because according to Eqs. (2.13), (4.12) one has $C > 1$, and the $C^{4(k+1)}$-term in the right-hand side of Eq. (5.3) is an increasing function of k allowing for no nontrivial fixed point for $k \to \infty$. It follows that physically speaking, this rescaling aims to look at the RG equations (5.3) on the scales that are relevant for large k, by means of a 'zoom' on the function $P_k[Q]$,

which is encoded in the definition (5.4). An analogous rescaling will be presented in the real-space approach discussed in Chapter 6.

Eq. (5.5) can now be solved by making an ansatz for $\mathscr{P}_k[Q]$, following the same lines as in the solution of DHM illustrated in Appendix A. The simplest form one can guess for $\mathscr{P}_k[Q]$ is the Gaussian

$$\mathscr{P}_k[Q] = \exp\left(-r_k \mathrm{Tr}[Q^2]\right). \tag{5.6}$$

This form corresponds to a mean-field solution [65]. By plugging Eq. (5.6) into Eq. (5.5), one finds an evolution equation relating r_k to r_{k-1}

$$r_k = \frac{2r_{k-1}}{C^4} - \frac{\beta^2}{4}. \tag{5.7}$$

Even though the mean-field solution (5.6) is a fixed point of the RG equation (5.5), there is no guarantee that more complex and physically meaningful fixed points do not exist. By hypothesizing that $\mathscr{P}_k[Q]$ can be expanded in powers of Q, non-gaussian fixed points can be explicitly built up in a perturbative framework, by following the same lines as in the Ising model [163] and in DHM [44, 45, 31]. Indeed, we can add non-Gaussian terms in Eq. (5.6), proportional to higher powers of Q, and consistent with the symmetry properties of the model. For instance, in principle there would be several possible replica invariants proportional to Q^3, but it is possible to show that the only invariant that is consistent with the original symmetries of the Hamiltonian H_k is $\mathrm{Tr}[Q^3]$. It follows that the simplest non-mean-field ansatz for $\mathscr{P}_k[Q]$ reads

$$\mathscr{P}_k[Q] = \exp\left[-\left(r_k \mathrm{Tr}[Q^2] + \frac{w_k}{3} \mathrm{Tr}[Q^3]\right)\right]. \tag{5.8}$$

This non-Gaussian ansatz can be handled by supposing that the coefficient w_k, representing the deviations from the Gaussian solution, is small for every k. It is important to point out that this is an hypothesis which is equivalent to assuming that the non-mean-field regime of this model can be described in terms of a perturbation of the mean-field regime [55]. As discussed in Section 1, there is no general agreement on the fact that the non-mean-field behavior of a spin glass can be described in terms of a slight modification of the mean-field picture [111, 64, 61, 60, 62, 63, 27]. Hence, one should keep in mind that this assumption is far from being trivial and surely innocuous.

As shown in Appendix D, if one plugs the ansatz (5.8) into the RG equation (5.5) and expands up to $O(w_k^3)$, one finds a recursion relation for the vector (r_k, w_k), which is expressed as a function of (r_{k-1}, w_{k-1})

$$\begin{cases} r_k &= \frac{2r_{k-1}}{C^4} - \frac{\beta^2}{4} - \frac{n-2}{4}\left(\frac{w_{k-1}}{2C^2 r_{k-1}}\right)^2 + O(w_{k-1}^4), \\ w_k &= \frac{2w_{k-1}}{C^6} + \frac{n-2}{2}\left(\frac{w_{k-1}}{2C^2 r_{k-1}}\right)^3 + O(w_{k-1}^4). \end{cases} \tag{5.9}$$

Eqs. (5.9) are analogous to Wilson's RG equations for the Ising model. Indeed, the mass r_k and the coupling constant u_k of the ϕ^4-theory describing the Ising model

[173] satisfy a recursion equation very similar to Eq. (5.9) [169, 163].

In general Eqs. (5.9) do not have a finite fixed point $r_k = r_{k-1} \equiv r_*, w_k = w_{k-1} = w_*$ for every value of β. Concerning this, let us *suppose* that there exists a finite and nonzero inverse temperature β_c such that Eqs. (5.9) have a finite fixed point. By definition, β_c physically represents the inverse temperature such that the system is invariant under the RG step $k \to k+1$, i. e. under reparametrization of the length scale. Hence, at β_c the system has no characteristic length scale, i. e. it is critical [161]. We call β_c the inverse critical temperature of the HEA, because it separates the high and low-temperature phases $\beta < \beta_c, \beta > \beta_c$ where the system is not invariant under reparametrization of lengths.

We now set $\beta = \beta_c$ and sketch qualitatively the flow of the coefficient w_k towards its fixed-point value w_*. Let us consider first the case $2/C^6 < 1$, i. e. $\epsilon < 0$, with

$$\epsilon \equiv \sigma - 2/3. \tag{5.10}$$

In this case w_k is decreased as $k \to k+1$, and tends to zero, in such a way that $\mathscr{P}_k[Q]$ tends to a Gaussian solution for large k.

The situation is different when $\epsilon > 0$. In order to better understand the case $\epsilon > 0$, let us rewrite the recursion equation for w_k as

$$w_k - w_{k-1} = \left(\frac{2}{C^6} - 1\right) w_{k-1} + \frac{n-2}{2} \left(\frac{w_{k-1}}{2C^2 r_{k-1}}\right)^3 + O(w_{k-1}^4), \tag{5.11}$$

and suppose for simplicity that w_{k-1} is positive. Being $2/C^6 > 1$, the first addend in the right-hand side of Eq. (5.11) is positive, while the second addend is negative in the physical limit $n \to 0$. Hence, the first addend aims to increase w_k, while the second aims to decrease it. As we will show in the following, these two effects compensate each other, in such a way that w_k tends to a finite and nonzero fixed point for $k \to \infty$.

Following the very same lines as Wilson, we call $\mathscr{P}_*[Q], P_*[Q]$ the fixed-point probability distributions of the overlap, obtained by setting $r_k = r_*, w_k = w_*$ in $\mathscr{P}_k[Q], P_k[Q]$ respectively. The equations for $n = 0$ yield

$$w_*^2 = \begin{cases} 0 & \epsilon \leq 0 \\ 48 \log 2 \left(\frac{\beta^2/4}{2^{1/3}-1}\right)^3 \epsilon + O(\epsilon^{3/2}) & \epsilon > 0. \end{cases} \tag{5.12}$$

As anticipated above, for $\epsilon > 0$, w_k tends to a finite and nonzero value, which is found to be proportional to ϵ in Eq. (5.12).

We recall [44, 45, 31, 163, 173, 174] that a Gaussian $\mathscr{P}_*[Q]$ corresponds to a mean-field regime of the model. Indeed, in the mean-field approximation one evaluates with the saddle-point method the functional integral yielding the replicated partition function [119, 130, 115, 133, 136]

$$\mathbb{E}_\epsilon[Z[T, \{\epsilon\}]^n] = \int [dQ] P_*[Q], \tag{5.13}$$

where Eq. (5.2) and Eq. (5.1) have been used. If $\sigma \leq 2/3$, i. e. $\epsilon < 0$, $\mathscr{P}_*[Q]$ is Gaussian, and so is $P_*[Q]$, in such a way that the saddle-point approximation is

exact in the right-hand side of Eq. (5.13), i. e. the mean-field approximation is correct. On the contrary, for $2/3 < \sigma \le 1$, $\mathscr{P}_*[Q]$ is not Gaussian, and the system has a non-mean-field behavior. In particular, fluctuations around the mean-field saddle point in the right-hand side of Eq. (5.13) cannot be neglected. Hence, we call $\sigma = 2/3$ the upper critical dimension [74, 173, 174, 77] of the HEA. In the computation of a given physical quantity $\mathcal{O}(\sigma)$ for $\sigma > 2/3$, fluctuations show up in the guise of some corrections proportional to ϵ to the mean-field value of this quantity. It is important to emphasize that these ϵ-corrections are not merely a numerical improvement on the predictions for the observable, but somehow encode the strength of the corrections to the mean-field physics. For instance, if $\mathcal{O}(\sigma)$ was expanded in powers of ϵ around $\sigma = 2/3$, and if this expansion could be resummed and made convergent, this would mean that the non-mean-field physics of the system could be considered as a 'small correction' to the mean-field physics. On the contrary, if such a non-mean-field physics were substantially different, the latter statement would be incorrect, and this fact would dramatically show up in a divergent and non-resummable ϵ-series for $\mathcal{O}(\sigma)$.

These observations can be directly illustrated by considering as observable $\mathcal{O}$ the critical exponent ν, related to the divergence of the correlation length ξ

$$\xi \overset{T \to T_c}{\sim} (T - T_c)^{-\nu}. \tag{5.14}$$

ν can be computed [163] by linearizing the transformation (5.9) in the neighborhood of r_*, w_*. Such a linearization is performed by considering the 2×2-matrix

$$\mathscr{M}_{ij} \equiv \left. \frac{\partial(r_{k+1}, w_{k+1})}{\partial(r_k, w_k)} \right|_{r_k = r_*, w_k = w_*}.$$

It can be shown that ν is related to the largest eigenvalue Λ of $\mathscr{M}$ by the relation

$$\nu = \frac{\log 2}{\log \Lambda}. \tag{5.15}$$

A straightforward calculation yields ν at order ϵ, for $n = 0$

$$\nu = \begin{cases} \frac{1}{2\sigma - 1} & \sigma \le 2/3 \\ 3 + 36\epsilon + O(\epsilon^2) & \sigma > 2/3. \end{cases} \tag{5.16}$$

A detailed analysis of the computation of Appendix E reveals that in this $O(w_k^3)$-calculation resulting in the $O(\epsilon)$-estimate of ν, one considers all the one-particle irreducible (1PI) [173, 158, 159] one-loop Feynman diagrams generated by the Q^3-vertex in Eq. (5.8). These are diagrams $\mathscr{I}_1, \mathscr{I}_7$ in Fig. 5.1. Similarly, in the computation at order w_k^5, resulting in the $O(\epsilon^2)$-estimate of ν, one considers two-loop 1PI Feynman diagrams $\mathscr{I}_2, \cdots, \mathscr{I}_6$ and $\mathscr{I}_8, \cdots, \mathscr{I}_{10}$ in Fig. 5.1, and so on.

As can be seen by Eq. (5.16), the coefficient of ϵ in Eq. (5.16) is quite large, an it is plausible that the full ϵ-series of ν does not converge. According to the above discussion, the convergence or resummability of the series would give some deep insight into how strongly the mean-field physical picture should be modified in the non-mean-field region $\sigma > 2/3$. In particular, a non-resummable series would suggest
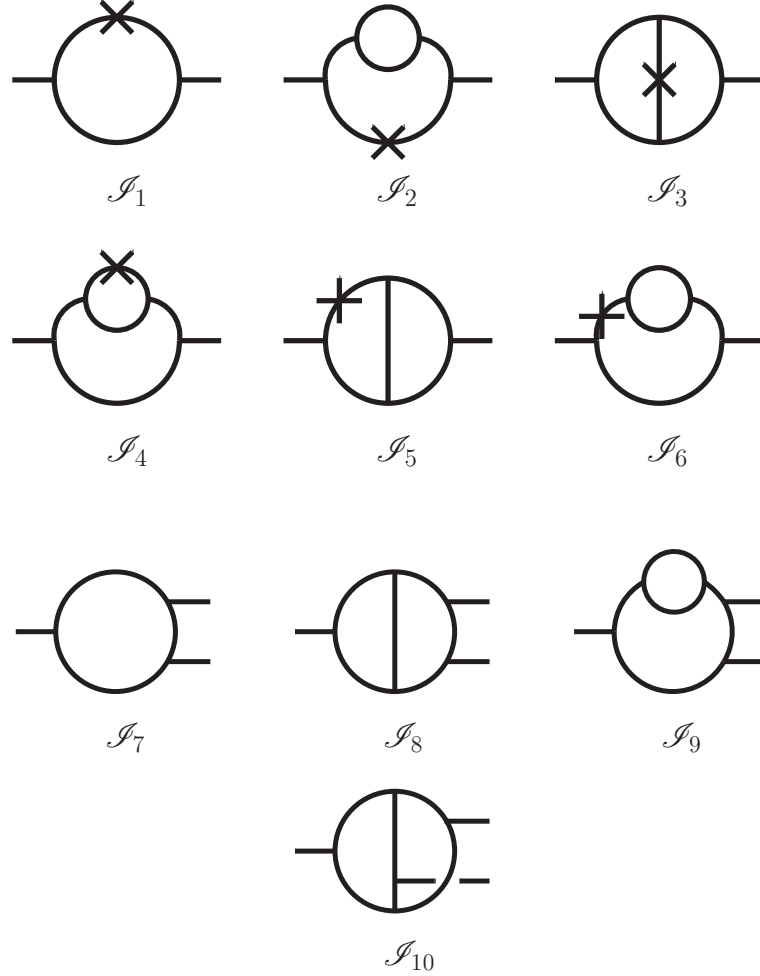
Figure 5.1. One and two-loop 1PI Feynman diagrams deriving from the $\mathrm{Tr}[Q^3]$-interaction term, which contribute to the computation of the critical exponent ν in the method à la Wilson presented in Section 5.1, and in the field-theory method presented in Section 5.2. In the method à la Wilson, diagrams $\mathscr{I}_1, \cdots, \mathscr{I}_6$ with two external lines have to be considered without crosses on the internal lines, and represent the diagrams contributing to the $\mathrm{Tr}[Q^2]$-term in $\mathscr{P}_k[Q]$. In the same method, it can be shown that diagrams $\mathscr{I}_7, \cdots, \mathscr{I}_{10}$ with three external lines contribute to the Q^3, Q^4, Q^5-terms in $\mathscr{P}_k[Q]$. In the field-theory method, diagrams $\mathscr{I}_1, \cdots, \mathscr{I}_6$ and $\mathscr{I}_7, \cdots, \mathscr{I}_{10}$ contribute to the 1PI two-point and three-point correlation functions respectively, and crosses stand for $\mathrm{Tr}[Q^2]$-insertions [173]. This graphical identification of the same diagrams in the two methods is an important test of their mutual consistency.

that the non-mean-field physics cannot be described in terms of a perturbation of the mean-field one, and would have a strong impact on the general problem of spin glasses in finite dimensions. It is thus interesting to investigate the properties of the ν-series by directly computing higher orders in ϵ, and checking the convergence or the resummability of the series.

The computation of the ϵ-expansion at high orders can be performed with a computer program. This is a particular feature of the HEA, because thanks to the hierarchical structure of the system, the RG equations (5.5) have a simple form compared to the RG equations of the PLSG [99] or of the EA model [72]. Indeed, the latter are nothing but the Callan-Symanzik equations [28, 147, 173] for a Q^3-field theory, and their solution in perturbation theory requires an explicit enumeration of all the Feynman diagrams deriving from the Q^3-vertices, and the computation of their IR-divergent part. This enumeration is extremely hard to implement in a computer program, and has never been automated even in the simplest case of the Ising model [70]. On the contrary, we believe that a symbolic manipulation program could handle Eqs. (5.5) and automate the computation to higher orders in w_k, with no need to evaluate the IR-divergent part of Feynman integrals, which is not needed in the present approach à la Wilson.
In order to perform this automation, we have evaluated by hand the first few terms of the series, which has been computed to $O(\epsilon^2)$ with the method à la Wilson, and with a quite independent field-theory method exposed in Section 5.2. Both methods give the same two-loop result for ν, which will serve as a severe test for a future automation of the ϵ-expansion to high orders. This automation is very difficult from a purely technical viewpoint, and is beyond the scope of this thesis.

Here we sketch the main steps of the two-loop computation of ν, more details are given in [35]. We showed that if we plug the ansatz (5.8) into the right-hand side of Eq. (5.5) and systematically neglect terms of order higher than w_k^3, we get a $\mathscr{P}_{k+1}[Q]$ which is still of the form (5.8), i. e. the RG equations are closed. This is not true if we keep also terms of order higher than w_k^3. Indeed, it is easy to show that in this case terms of order Q^4 arise in the right-hand side of Eq. (5.5), and these terms are not present in the original ansatz. This fact implies that to $O(w_k^4)$, $\mathscr{P}_k[Q]$ must contain also Q^4-terms, and that these terms must be proportional to w_k^4. By plugging the fourth-degree polynomial $\mathscr{P}_k[Q]$ in Eq. (5.5) and expanding the right-hand side up to $O(w_k^5)$, Q^5-terms are generated. It follows that at $O(w_k^5)$, $\mathscr{P}_k[Q]$ must contain also Q^5-terms, and that these terms must be proportional to w_k^5. If this perturbative framework is consistent, by iterating such a procedure to higher orders we reconstruct the exact function $\mathscr{P}_k[Q]$. In particular, at the j-th step of this procedure we generate n_j monomials of order Q^j, and call these monomials $\{I_l^{(j)}[Q]\}_{l=1,\dots,n_j}$. Hence, if this procedure is iterated until step number $j = p$, $\mathscr{P}_k[Q]$ can be written in the compact form

$$\mathscr{P}_k[Q] = \exp\left\{-\left[c_{1,\,k}^{(2)} I_1^{(2)}[Q] + \sum_{j=3}^{p} \frac{1}{j} \sum_{l=1}^{n_j} c_{l,\,k}^{(j)} I_l^{(j)}[Q]\right]\right\}, \qquad (5.17)$$

where

$$I^{(2)}[Q] \equiv \text{Tr}[Q^2],\ I^{(3)}[Q] \equiv \text{Tr}[Q^3],$$
$$n_3 \equiv 1,\ c_{1,\,k}^{(2)} \equiv r_k,\ c_{1,\,k}^{(3)} \equiv w_k.$$

In the present work such a procedure has been pushed up to order w_k^5, and $\mathscr{P}_k[Q]$ has been computed as a fifth-degree polynomial in Q. In particular, one generates $n_4 = 4$ invariants $I^{(4)}[Q]$ of fourth degree and $n_5 = 4$ invariants $I^{(5)}[Q]$ of fifth degree in Q. The explicit expression for all the monomials $I_l^{(j)}[Q]$ at this order is given in Table E.1 of Appendix E. The set of two RG equations (5.9) for the two-dimensional vector $(r_k, w_k) = (c_{1,\,k}^{(2)}, c_{1,\,k}^{(3)})$ obtained in the one-loop calculation here becomes a set of ten equations for the vector $c_{1,\,k}^{(2)}, c_{1,\,k}^{(3)}, c_{1,\,k}^{(4)}, \cdots, c_{4,\,k}^{(4)}, c_{1,\,k}^{(5)}, \cdots, c_{4,\,k}^{(5)}$, Eqs. (E.1)-(E.10). By linearizing these equations at the critical fixed point one can compute the 10×10-matrix $\mathscr{M}$, and extract Λ. By Eq. (5.15), one can then compute the exponent ν at two loops for $\epsilon > 0$ and $n = 0$

$$\nu = 3 + 36\epsilon + \left[432 - 27\left(50 + 55 \cdot 2^{1/3} + 53 \cdot 2^{2/3}\right)\log 2\right]\epsilon^2 + O(\epsilon^3). \tag{5.18}$$

The replica ϵ-expansion for the critical exponents of the HEA is presumably badly behaved, and non-predictive.

The coefficient of ϵ^2 in Eq. (5.18) is about -5.1×10^3: the first two orders of the ϵ-expansion show that this is probably badly-behaved and out of control. In particular, it is impossible to make any prediction on ν with the first two orders of the series. Differently, the ϵ-expansion for the critical exponents of the Ising model (consider for instance the exponent γ in [173]) is nonconvergent, but it settles to a reasonable value as the order is increased from zero up to at least three, and then it deviates from such a value when higher orders are considered (see [157, 41, 40, 43, 42, 94, 68, 97, 98] for five-loop computations of the exponents). Though, in that case the expansion can be resummed and made finite, giving a result for the exponents which is in excellent agreement with experiments [1] and MC simulations [140, 5].

As anticipated above, it is interesting to reproduce the two-loop result (5.18) with an independent method. Indeed, in the effort to build up a fully automated ϵ-expansion it is important to check that the prediction (5.18) is not only correct, but also well-defined, i. e. it does not depend on the RG scheme used in the calculation. For instance, in this approach à la Wilson the IR limit of the theory is taken by requiring invariance under the transformation $k \to k + 1$, which doubles the system volume at each step. On the contrary, in Section 5.2 we perform the IR limit by considering a real parameter λ physically representing the typical energy scale of the system, and by sending it smoothly to zero. As we will show in the next Section, these two independent ways of taking the IR limit yield the same two-loop result for ν.

5.2 The RG method in the field-theory approach

The replica formulation for the HEA allows for a quite general treatment of the IR behavior of the system, based on the path-integral formulation. This formulation

can be developed along the lines of the path-integral formulation of the Ising model [173, 174, 138, 159]. In the latter the partition and correlation functions are represented in terms of a path integral over a field ϕ, weighted with a ϕ^4-action. Setting $\varepsilon \equiv 4 - d$ (for the Ising model we use a different font for ε, to avoid confusion with the ϵ of the HEA defined in Eq. (5.10)), one finds that in the physically relevant case $\varepsilon > 0$ this ϕ^4-field theory presents IR divergences occurring when the temperature T approaches its critical value. These divergences are removed by means of the observation that one can construct an auxiliary field theory, the renormalized one, which makes the same physical predictions as the original one and has no IR divergences. Indeed, it has been shown that these divergences can be removed at any order in perturbation theory [29], and reabsorbed in the renormalization constants. Once the renormalized theory has been built up, one can extract the critical exponents in perturbation theory from the ε-expansion of the renormalization constants.

Here we show how the result (5.18) for ν can be reproduced along these lines, more details can be found in [35], while an extensive treatment of the renormalization group theory used here is given in [173].

First, this computation is better performed by taking a definition of the HEA which is slightly different from that of Eqs. (2.10), (4.10), and that has the same critical exponent ν. First, let us relabel the spins $S_1, \cdots, S_{2^k}$ as $S_0, \cdots, S_{2^k-1}$. We redefine the interaction term in Eq. (4.10) as

$$\epsilon_{k+1}[S_0, \ldots, S_{2^{k+1}-1}] \to -\left(\frac{C^2}{2}\right)^{k+1} \sum_{i=0}^{2^k-1} \sum_{j=2^k}^{2^{k+1}-1} J_{12,ij} S_i S_j. \qquad (5.19)$$

The redefinition (5.19) has the following physical meaning. In the original definition (4.10), one couples two systems, say system 1 and system 2, with 2^k spins each, and obtains a 2^{k+1}-spin system. The interaction energy between 1 and 2 is given by couplings between spins belonging to 1 (given by the terms in the sum in Eq. (4.10) with $1 \leq i, j \leq 2^k$), couplings between spins belonging to 2 (given by the terms in the sum in Eq. (4.10) with $2^k + 1 \leq i, j \leq 2^{k+1}$), and couplings between 1 and 2 (given by the terms in the sum in Eq. (4.10) with $1 \leq i \leq 2^k$, $2^k + 1 \leq j \leq 2^{k+1}$). In the redefinition (5.19), only the latter couplings are kept, and neither couplings within system 1 nor 2 appear in the definition.

The equivalence between the two definitions can be shown as follows. If one considers two spins S_i, S_j and their interaction energy, it is easy to show [65] that in the model defined by Eq. (5.19) the variance of such an interaction energy scales with the ultrametric distance between S_i and S_j in the same way as in the model defined by Eq. (4.10), and that the two variances differ only in a constant multiplicative factor. It follows that the long-wavelength features of the two models are the same. According to general universality arguments, both of the models must have the same critical exponents, because these depend only on the long-wavelength features of the system, like the way interactions between spins decay at large distances [163, 161]. Notwithstanding this fact, non-universal quantities are generally different in the two models. For instance, it is well known that if one multiplies the interaction strength between spins by a constant factor, one changes the microscopic energy scale of the

system. According to dimensional analysis [173], the critical temperature must be proportional to this energy scale, and is thus multiplied by the same factor. Hence, the critical temperature of the model defined by Eq. (4.10) is different from that of the model defined by Eq. (5.19). This can be verified by considering how the recursion relation (5.5) is modified when one applies the redefinition (5.19). Indeed, if one starts from Eq. (5.19) and goes through the steps of the derivation of Eq. (5.5), one finds a recursion equation that differs from Eq. (5.5) by a factor multiplying β. The reason why the definition (5.19) is more suitable for this field-theory approach will be clarified below.

The path-integral formulation of the HEA can now be introduced by observing that one can write the replicated partition function (5.1) in terms of a functional integral over a *local* overlap field $Q_{i,ab} \equiv S_i^a S_i^b$, $0 \le i \le 2^k - 1$

$$\mathbb{E}_\epsilon[Z[T, \{\epsilon\}]^n] = \int \mathscr{D}Q \, \mathrm{e}^{-\mathrm{S}[Q]}, \tag{5.20}$$

where $\int \mathscr{D}Q \equiv \int \prod_{i=0}^{2^k-1} \prod_{a<b=1}^{n} dQ_{i,ab}$ stands for the functional integral over the field $Q_{i,ab}$. The action $\mathrm{S}[Q]$ can be worked out by supposing that there exists a critical temperature T_c such that the characteristic length of the system diverges as T approaches T_c. We stress that this hypothesis has been made also in the RG approach à la Wilson, where we assumed the existence of a T_c such that the RG equations (5.9) have a nontrivial fixed point, i. e. a fixed point such that the system has no finite characteristic length.

By taking $T \approx T_c$, one can select the IR-dominant terms in $\mathrm{S}[Q]$, and obtain

$$\mathrm{S}[Q] = \frac{1}{2} \sum_{i,j=0}^{2^k-1} \Delta'_{i,j} \mathrm{Tr}[Q_i Q_j] + \frac{g}{3!} \sum_{i=0}^{2^k-1} \mathrm{Tr}[Q_i^3]. \tag{5.21}$$

In Eq. (5.21) the propagator $\Delta'_{i,j}$ depends on i,j through the difference $\mathcal{I}(i) - \mathcal{I}(j)$, where for any $0 \le i \le 2^k - 1$ the function $\mathcal{I}(i)$ is defined in terms of the expression in base 2 of i as

$$i = \sum_{j=0}^{k-1} a_j 2^j, \, \mathcal{I}(i) \equiv \sum_{j=0}^{k-1} a_{k-1-j} 2^j. \tag{5.22}$$

According to the above definition of $\mathcal{I}(i)$, the quadratic term of Eq. (5.21) is not invariant under spatial translations $i \to i + l$. Accordingly [158, 173], the Fourier transform of the propagator $\Delta'_{i,j}$ does not depend only on the momentum p associated with the variable $i - j$, but it generally depend on both of the momenta p, q associated with the variables i, j respectively. With this complicated form of the propagator, any explicit computation of the loop integrals, which is necessary for the computation of the critical exponents, is extremely difficult to perform. This problem can be overcome with a simple relabeling of the sites of the lattice. Indeed, if one sets

$$\mathcal{I}(i) \to i, \, \forall i = 0, \ldots, 2^k - 1,$$

it is easy to show that Eq. (5.20) still holds, with an action $\mathrm{S}[Q]$ which now reads

$$\mathrm{S}[Q] \to \frac{1}{2} \sum_{i,j=0}^{2^k-1} \Delta_{i,j} \mathrm{Tr}[Q_i Q_j] + \frac{g}{3!} \sum_{i=0}^{2^k-1} \mathrm{Tr}[Q_i^3], \tag{5.23}$$

where $\Delta_{i,j} \equiv \Delta'_{\mathcal{I}^{-1}(i),\mathcal{I}^{-1}(j)}$. Since $\Delta'_{i,j}$ depends on i, j through the difference $\mathcal{I}(i) - \mathcal{I}(j)$, $\Delta_{i,j}$ depends on i, j through the difference $i - j$. It follows that S$[Q]$ is now translationally invariant, and the ordinary Fourier transform techniques [148, 113] can be used. In particular, the Fourier transform $\Delta(p)$ of $\Delta_{i,j}$ depends only on the dyadic norm $|p|_2$ (see [139] for a precise definition of the dyadic norm) of the momentum p relative to the variable $i - j$, and can be written as

$$\Delta(p) = |p|_2^{2\sigma-1} + m, \tag{5.24}$$

where the mass m is proportional to $T - T_c$, and has dimensions $[m] = 2\sigma - 1$.

The action defined by Eq. (5.23) yields a Tr$[Q^3]$-field theory, which is known to describe the spin-glass transition in both short-range [39] and long-range [38, 99] spin glasses. Notwithstanding this, an interesting and novel feature of the propagator (5.24) is that it depends on the momentum p through its dyadic norm $|p|_2$. This fact is rather interesting, because it implies a direct analogy with the original derivation of the RG equations for the Ising model in finite dimensions, in particular with the Polyakov derivation [163, 142]. Indeed, the basic approximation scheme in the Polyakov derivation consists in introducing an ultrametric structure in momentum space, such that the momentum space is divided into shells and the sum of two momenta in a given shell cannot give a momentum of a higher momentum scale cell. This feature is analogous to a general property of the dyadic norm, such that if p_1, p_2 are two integers in $0, \ldots, 2^k - 1$, their dyadic norms satisfy [139] $|p_1 + p_2|_2 \leq \max(|p_1|_2, |p_2|_2)$. This fact implies that if p_1, p_2 are inside a shell of radius $\max(|p_1|_2, |p_2|_2)$, the momentum $p_1 + p_2$ is still in that shell. Thus, the dyadic structure of Eq. (5.24) emerges naturally in more general contexts where there is no hierarchical structure, such as finite-dimensional systems with short-range interactions.

A perturbative expansion in g of the two and three-point 1PI correlation functions deriving from the action (5.23) reveals that if $\epsilon < 0$ the field theory (5.23) is well-defined and finite, while if $\epsilon > 0$ IR divergences occur when $m \to 0$. According to a simple dimensional argument, if $\epsilon < 0$ the critical exponent ν is given by the first line of Eq. (5.16). On the contrary, if $\epsilon > 0$ a more elaborated treatment is needed to deal with IR divergences and compute ν.

For $\epsilon > 0$, IR divergences can be eliminated by defining a renormalized field theory having a renormalized mass and coupling constant m_r, g_r, which are defined in terms of the bare mass and coupling constant

$$m = m_r + \delta m, \tag{5.25}$$

$$g = m_r^{\frac{3\epsilon}{2\sigma-1}} g_r Z_g, \tag{5.26}$$

where δm is the mass shift due to renormalization, and Z_g is the renormalization constant of the coupling g. According to general results on models with long-range interactions, the field $Q_{i,ab}$ is not renormalized, i. e. its renormalization constant Z_Q is equal to one. On the contrary, one has to introduce a renormalization constant Z_{Q^2} enforcing the renormalization of the Tr$[Q_i^2]$-field. According to the minimal

subtraction scheme, the renormalization constants $\delta m, Z_g, Z_{Q^2}$ are chosen in such a way that they subtract the divergences occurring in the two and three-point 1PI correlation functions of the renormalized theory. In the IR limit $m_r \to 0$, these divergences appear in the shape of poles in ϵ. Since here $\delta m, Z_g, Z_{Q^2}$ are expanded in powers of the renormalized coupling g_r, and since these IR divergences are subtracted order by order in g_r, the constants $\delta m, Z_g, Z_{Q^2}$ are given by a series in g_r whose coefficients contain poles in ϵ. From a detailed analysis it turns out that these series contain only even powers of g_r, that only Z_g and Z_{Q^2} are needed to compute ν, and that a-loops Feynman diagrams contribute to order g_r^{2a} in Z_g, Z_{Q^2}. In Appendix F we sketch the main steps of the one-loop computation of Z_g, Z_{Q^2}, which are given in Eqs. (F.7), (F.8).

By following the very same techniques as those exposed in Appendix F, we computed Z_g, Z_{Q^2} at two loops. For $n = 0$ one has

$$
Z_g = 1 + \frac{g_r^2}{48\epsilon \log 2} + g_r^4 \left[\frac{1}{1536\epsilon^2(\log 2)^2} + \frac{5 + 2 \cdot 2^{2/3}}{512\epsilon \log 2} \right] + O(g_r^6), \qquad (5.27)
$$

$$
Z_{Q^2} = 1 + \frac{g_r^2}{24\epsilon \log 2} + g_r^4 \left[\frac{1}{576\epsilon^2(\log 2)^2} - 5\frac{(1 + 11 \cdot 2^{1/3} + 7 \cdot 2^{2/3})}{2304\epsilon \log 2} \right] +
$$
$$
+ O(g_r^6). \qquad (5.28)
$$

One can also show that $\delta m = O(g_r^4)$.

Eqs. (5.27), (5.28) explicitly construct the renormalized theory, which is free of IR divergences. In this theory, we can safely perform the IR limit, and in particular compute physical quantities in this limit. In order to do this, we introduce a function $g(\lambda)$, physically representing the effective coupling constant of the model at the energy scale λ. $g(\lambda)$ can be computed from the Callan-Symanzik equations [28, 147], as the solution of the differential equation

$$
\beta(g(\lambda)) = \lambda \frac{dg(\lambda)}{d\lambda}, \qquad (5.29)
$$

where the β-function is defined as

$$
\beta(g_r) \equiv \mu \left. \frac{\partial g_r}{\partial \mu} \right|_{g,m}, \qquad (5.30)
$$

and $\mu \equiv m_r^{\frac{1}{2\sigma - 1}}$. Eq. (5.29) states that $\beta(g_r)$ governs the flow of the effective coupling $g(\lambda)$ under changes in the energy scale λ of the system. $\beta(g_r)$ can be explicitly computed in terms of the renormalization constant Z_g, Eq. (5.27)

$$
\beta(g_r) = -3\epsilon g_r + \frac{g_r^3}{8\log 2} + 3\frac{5 + 2 \cdot 2^{2/3}}{128\log 2} g_r^5 + O(g_r^7). \qquad (5.31)
$$

The effective coupling $g(\lambda)$ in the IR limit is obtained by letting the energy scale λ go to zero, and is given by $g_r^* \equiv g(\lambda = 0)$. By definition, g_r^* is a fixed point of the flow equation (5.29), and is obtained perturbatively in the shape of a series in ϵ, as the solution of the fixed-point equation $\beta(g_r^*) = 0$. Moreover, one can show from

Eq. (5.31) that the IR fixed point $g_r^* = 0$ is stable only for $\epsilon < 0$, while for $\epsilon > 0$ a nontrivial fixed point $g_r^* \neq 0$ of order $\sqrt{\epsilon}$ arises. The same fixed-point structure arises in Wilson's method, Eq. (5.12). Notwithstanding this, in Wilson's method the IR limit is reached by doing a set of discrete steps $k \to k + 1$ each of which doubles the volume of the system, while in this approach this limit is reached by letting the energy scale λ go to zero smoothly.

Once the effective coupling in the IR limit is known, the scaling relations yield the critical exponent ν in terms of g_r^* and of the renormalization constant Z_{Q^2}

$$\nu = \frac{1}{\eta_2(g_r^*) + 2\sigma - 1}, \tag{5.32}$$

where

$$\eta_2(g_r) \equiv \mu \left. \frac{\partial \log Z_{Q^2}}{\partial \mu} \right|_{g,\,m}. \tag{5.33}$$

By plugging the two-loop result (5.28) for Z_{Q^2} into Eqs. (5.33) and evaluating $\eta(g_r)$ for $g_r = g_r^*$, we can extract ν for $n = 0$ from Eq. (5.32). The result is exactly the same as that of with Wilson's method, Eq. (5.18).

The fact that the method à la Wilson and the field-theory method yield the same two-loop prediction for ν shows that the IR limit of the HEA is well-defined, because it does not depend on the RG framework used to reach it: even though the two methods have a few underlying common features, they yield the same result for the universal quantities of the system, which are encoded into the coefficients of the ϵ-expansion. We want to stress that these universal quantities stay the same when changing the RG approach and redefining the microscopical details of the model, Eq. (5.19). Accordingly, this picture suggests that the ordinary RG ideas for the Ising model work consistently also in this disordered case: the HEA has a characteristic length diverging at the critical point, and the universal physical features in the critical region are governed by long-wavelength degrees of freedom.

Notwithstanding the positiveness of this result, the ϵ-expansion is still non-predictive, because the first few terms of the series (5.18) have a nonconvergent behavior. On the one hand, one could test empirically the reliability of the present perturbative approach, and so the convergence properties of the perturbative series, by solving Eq. (5.5) numerically for integer $n > 0$ and by comparing the result to the first three orders of the perturbative expansion. On the other hand, it would be much more difficult to test whether the series could be made resummable by some suitable techniques, by explicitly computing high orders of the expansion. To this end, our two-loop result constitutes a starting point and a severe test of this high-order computation. An eventual evidence of the resummability of the series would suggest that the non-mean-field behavior of this model can be considered as a

perturbation of the mean-field one. On the contrary, a failure of the resummation techniques would imply that the non-mean-field behavior is radically different from the mean-field one.

Another weak spot of this replica RG approach is that the method does not identify the correct spin-decimation rule in a non-mean-field strongly frustrated case, which, as discussed in Section 1, is one of the fundamental questions and difficulties in the construction of a RG theory for finite-dimensional spin glasses.

Both of these weak spots of the replica RG approach made us seek for an alternative methodology which, based on a transparent spin-decimation rule, could overcome over the difficulties of the replica method, and make quantitative predictions for the critical exponents. This methodology will be illustrated in Chapter 6, and does not rely on the replica method, but on a real-space RG criterion.

Chapter 6

# The RG approach in real space

As discussed in Section 1, a fundamental ingredient for constructing of a RG theory is the introduction of a decimation rule. Through decimation, one practically implements a coarse-graining process that changes the length scale with which one looks at the physics of the system. For ferromagnetic systems, a suitable spin decimation rule has been originally introduced by Kadanoff [84], and relies on the construction of block spins. As discussed in Section 1, Kadanoff's decimation rule does not work in a disordered system like the HEA, because the average over disorder of the magnetization inside a block of spins is trivially zero. In this Chapter we propose a real-space decimation rule for the HEA which overcomes this problem, and which is not directly based on the block-spin construction. This method will be first applied to DHM in Section 6.1, and then generalized to the HEA in Section 6.2.

6.1 The RG approach in real space for Dyson's Hierarchical Model

Let us consider a DHM, defined by Eqs. (2.1), (2.2). The real-space RG method is built up by initially iterating exactly the recursion equation (2.1) for $k = k_0$ steps, assuming for simplicity that $H_0^F[S] = 0$. In this way, a DHM with 2^{k_0} spins $S_1, \cdots, S_{2^{k_0}}$ and Hamiltonian $H_{k_0}^F[S_1, \cdots, S_{2^{k_0}}]$ is obtained exactly. Practically speaking, this means that in the following we compute exactly the physical observables of this 2^{k_0}-spin DHM. For instance, if $k_0 = 2$ we have a 4-spin DHM whose Hamiltonian is

$$
\begin{aligned}
H_2^F[S_1, \cdots, S_4] &= -\left\{ C_F J \left[\left(\frac{S_1 + S_2}{2} \right)^2 + \left(\frac{S_3 + S_4}{2} \right)^2 \right] + \right. \\
&\left. + C_F^2 J \left(\frac{S_1 + S_2 + S_3 + S_4}{4} \right)^2 \right\}.
\end{aligned}
\tag{6.1}
$$

We recall for future purpose that in the Hamiltonian (6.1), and similarly for arbitrary values of k_0, when one goes one hierarchical level up, the couplings are multiplied by a factor C_F. In particular, the first addend in braces in Eq. (6.1) physically represents the couplings at the first hierarchical level, while the second addend represents the couplings at the second hierarchical level.
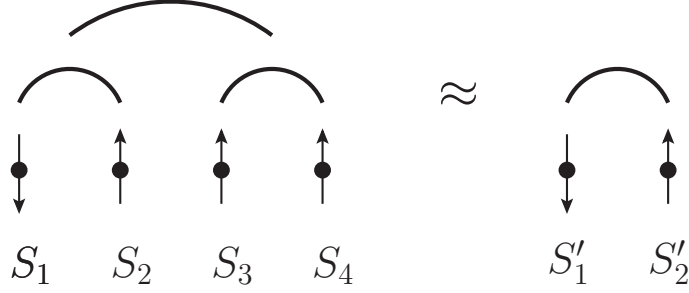
Figure 6.1. Approximation of the real-space approach for $k_0 = 2$. In the implementation of the real-space approach to DHM exposed in Section 6.1, a 2^2-spin DHM with spins $S_1, \cdots, S_4$ and Hamiltonian (6.1) is approximated by a 2-spin DHM with spins S_1', S_2' and Hamiltonian (6.2).

In the implementation of the real-space approach to the HEA exposed in Section 6.2, a 2^2-spin HEA with spins $S_1, \cdots, S_4$ and Hamiltonian (6.11) is approximated by a 2-spin HEA with spins S_1', S_2' and Hamiltonian (6.12).

We now want to build up a 2^{k_0+1}-spin DHM starting from such a 2^{k_0}-spin DHM. As shown in Section 2.1, DHM is a special case where this procedure can be iterated k times in 2^k operations, by using the hierarchical structure of the system resulting in the recurrence equation (2.5). On the contrary, if the recurrence equations (2.5) did not hold, in order to build up a 2^k-spin DHM one should compute exactly the partition function, which involves 2^{2^k} operations. To our knowledge, for the HEA model there is no known recursion equation analogous to (2.5). Indeed, the only recursion equation that one can derive for the HEA is Eq. (5.3), which relies on the replica approach. To derive a recurrence equation for a function or functional of a suitably defined order parameter without relying on the replica approach is very difficult. The origin of this difficulty is nothing but the problem of how to identify of a suitable order parameter and a function of it, which should replace the magnetization m and its probability $p_k(m)$ in the recursion equation (2.5) of DHM. Since we have not been able to derive such a recurrence equation without relying on the replica approach, the construction of a 2^k-spin HEA model still requires a computational effort of 2^{2^k}. It is hence clear that an approximation scheme is needed to reach the thermodynamic limit $k \to \infty$ for the HEA. We now illustrate this approximation scheme for DHM first, and then generalized it to the HEA in Section 6.2.

Once a 2^{k_0}-spin DHM has been built exactly, we consider 2^{k_0-1}-spin DHM, where J is replaced by another coupling J'. More precisely, such a 2^{k_0-1}-spin DHM is defined by iterating $k_0 - 1$ times Eq. (2.1) with $J \to J'$, and for the sake of clarity its spins will be denoted by $S_1', \cdots, S_{2^{k_0-1}}'$, and its Hamiltonian by $H'^F_{k_0-1}[S_1', \cdots, S_{2^{k_0-1}}']$. For $k_0 = 2$ the Hamiltonian of this DHM reads

$$H'^F_1[S_1', S_2'] = -C_F J' \left(\frac{S_1' + S_2'}{2} \right)^2. \tag{6.2}$$

Given J, the coupling J' is chosen in such a way that the 2^{k_0-1}-spin DHM represents as well as possible the 2^{k_0}-spin DHM, as qualitatively depicted in Fig. 6.1. The precise meaning of this representation will be illustrated shortly.

According to the iterative construction of Eq. (2.1), a new DHM is then constructed by taking two copies of the 2^{k_0-1}-spin DHM. Say that the first copy has spins $S'_1, \cdots, S'_{2^{k_0-1}}$ and Hamiltonian $H'^F_{k_0-1}[S'_1, \cdots, S'_{2^{k_0-1}}]$, while the second copy has spins $S'_{2^{k_0-1}+1}, \cdots, S'_{2^{k_0}}$ and Hamiltonian $H'^F_{k_0-1}[S'_{2^{k_0-1}+1}, \cdots, S'_{2^{k_0}}]$. We make these two copies interact and form a 2^{k_0}-spin DHM with Hamiltonian

$$H'^F_{k_0-1}[S'_1, \cdots, S'_{2^{k_0-1}}] + H'^F_{k_0-1}[S'_{2^{k_0-1}+1}, \cdots, S'_{2^{k_0}}] - J'C_F^{k_0}\left(\frac{1}{2^{k_0}}\sum_{i=1}^{2^{k_0}}S'_i\right)^2 . \quad (6.3)$$

Since each of the DHMs that we make interact represents a 2^{k_0}-spin DHM, the model defined by Eq. (6.3) represents a 2^{k_0+1}-spin DHM. Once again, this DHM is then approximated by a 2^{k_0-1}-spin DHM with coupling, say, J'', and two copies of such a 2^{k_0-1}-spin DHM are then taken and coupled again, to obtain a system representing a 2^{k_0+2}-spin DHM. Such a recursive construction is iterated k times, and a system representing a 2^{k_0+k}-spin DHM is obtained. Setting $J_0 \equiv J, J_1 \equiv J', J_2 \equiv J'', \cdots$, this procedure establishes a relation between J_k and J_{k+1}. Since at each step k of this procedure we double the system size, this flow physically represents the RG flow of the coupling J_k under reparametrization of the unit length $2^k \to 2^{k+1}$.

Let us now describe how a 2^{k_0}-spin system has been approximated by a 2^{k_0-1}-spin system. Consider a physical observable $O^F_{k_0}(\beta J)$ of the 2^{k_0}-spin DHM, whose spins are $S_1, \cdots, S_{2^{k_0}}$, and whose Hamiltonian is $H^F_{k_0}[S_1, \cdots, S_{2^{k_0}}]$. Consider also an observable $O^F_{k_0-1}(\beta J')$ of the 2^{k_0-1}-spin DHM, whose spins are $S'_1, \cdots, S'_{2^{k_0-1}}$, and whose Hamiltonian is $H'^F_{k_0-1}[S'_1, \cdots, S'_{2^{k_0-1}}]$. The normalized magnetizations on the left and right half of the 2^{k_0}-spin system are

$$\begin{aligned}
m_L &\equiv \frac{\frac{1}{2^{k_0-1}}\sum_{i=1}^{2^{k_0-1}}S_i}{\sqrt{\mathbb{E}_{\vec{S}}\left[\left(\frac{1}{2^{k_0-1}}\sum_{i=1}^{2^{k_0-1}}S_i\right)^2\right]}}, \\
m_R &\equiv \frac{\frac{1}{2^{k_0-1}}\sum_{i=2^{k_0-1}+1}^{2^{k_0}}S_i}{\sqrt{\mathbb{E}_{\vec{S}}\left[\left(\frac{1}{2^{k_0-1}}\sum_{i=2^{k_0-1}+1}^{2^{k_0}}S_i\right)^2\right]}}
\end{aligned} \quad (6.4)$$

respectively, where $\mathbb{E}_{\vec{S}}$ stands for the thermal average at fixed temperature T, performed with the Boltzmann weight $\exp(-\beta H^F_{k_0})$. Similarly, the normalized magnetizations on the left and right half of the 2^{k_0-1}-spin system are

$$\begin{aligned}
m'_L &\equiv \frac{\frac{1}{2^{k_0-2}}\sum_{i=1}^{2^{k_0-2}}S'_i}{\sqrt{\mathbb{E}_{\vec{S'}}\left[\left(\frac{1}{2^{k_0-2}}\sum_{i=1}^{2^{k_0-2}}S'_i\right)^2\right]}}, \\
m'_R &\equiv \frac{\frac{1}{2^{k_0-2}}\sum_{i=2^{k_0-2}+1}^{2^{k_0-1}}S'_i}{\sqrt{\mathbb{E}_{\vec{S'}}\left[\left(\frac{1}{2^{k_0-2}}\sum_{i=2^{k_0-2}+1}^{2^{k_0-1}}S'_i\right)^2\right]}}
\end{aligned} \quad (6.5)$$

respectively, where $\mathbb{E}_{\vec{S}'}$ stands for the thermal average with the Boltzmann weight $\exp(-\beta H'^F_{k_0-1})$.

According to Kadanoff's block-spin rule, in order that the 2^{k_0-1}-spin DHM might be a good approximation of the 2^{k_0}-spin DHM, one should map the block of spins in the left half of the 2^{k_0}-spin DHM into the block of spins in the left half of the 2^{k_0-1}-spin DHM, and so for the right half. Accordingly, one should find a method which quantitatively implements the qualitative equalities

$$m_L = m'_L, \; m_R = m'_R. \tag{6.6}$$

To this end, we choose the following observables

$$\begin{aligned}
O^F_{k_0}(\beta J) &\equiv \mathbb{E}_{\vec{S}}\left[m_L m_R\right], \\
O^F_{k_0-1}(\beta J') &\equiv \mathbb{E}_{\vec{S}'}\left[m'_L m'_R\right].
\end{aligned} \tag{6.7}$$

According to Eqs. (6.6), Kadanoff's block-spin rule described in Eq. (6.6) can be practically implemented by imposing the constraint

$$O^F_{k_0}(\beta J) = O^F_{k_0-1}(\beta J'). \tag{6.8}$$

For any fixed J, Eq. (6.8) is the equation determining J' as a function of J, as the value of the coupling of the 2^{k_0-1}-spin DHM such that this is the best-possible approximation of the 2^{k_0}-spin DHM. According to the above discussion, Eq. (6.8) is the RG equation relating the coupling J at the scale 2^k to the coupling J' at the scale 2^{k+1}.

The RG Eq. (6.8) is not exact, because it relies on the fact that a 2^{k_0}-spin DHM is approximated by a 2^{k_0-1}-spin DHM. Even though, such an approximation becomes asymptotically exact for large k_0, as we will explicitly show in the following. Another important issue of this RG scheme is that there is a considerable amount of freedom in the choice of the observables $O^F_{k_0}, O^F_{k_0-1}$, and that the RG equations (6.8) depend on this choice. This is the reason why in what follows the whole method will be systematically tested a posteriori, by comparing its predictions to the predictions obtained heretofore with other methods, if these exist. As we will show shortly, the encouraging outcome of this comparison makes us guess that if k_0 is large enough, the results of this RG approach do not depend on the choice of the observables, if this is reasonable.

Quite large values of k_0 can be achieved by using the hierarchical structure of the system. Indeed, thanks to this structure the thermal averages appearing in Eqs. (6.7), which would involve $2^{2^{k_0}}$ terms in a brute-force computation, can be computed in 2^{k_0} operations, as shown in Appendix G.

Back to the predictions of Eq. (6.8), one can show that for any k_0 they reproduce the interval (2.3). Indeed, for $\sigma_F > 1$ Eq. (6.8) gives $J' < J \, \forall J, \beta$, in such a way that the coupling J goes to 0 when the RG transformation is iterated many times, and no phase transition occurs. On the contrary, for $\sigma_F < 1/2$ one has $J' > J \, \forall J, \beta$, in such a way that the model is thermodynamically unstable. The fact that the interval
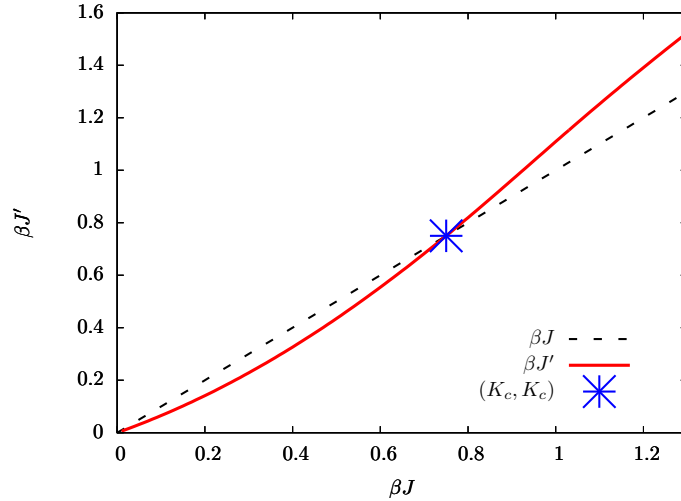
Figure 6.2. $\beta J'$ as a function of βJ for $C_F = 1.2$, $k_0 = 8$, and point (K_c, K_c) where the two curves intersect. According to the discussion in the text, $\beta \lesseqgtr \beta_{cF}^{RS}$ implies that $J' \lesseqgtr J$.

(2.3) is reproduced is a first test of the correctness of the real-space approach. For $1/2 < \sigma_F < 1$ there is a finite inverse temperature β_{cF}^{RS} such that for $\beta < \beta_{cF}^{RS}$ one has $J' < J$, while for $\beta > \beta_{cF}^{RS}$ one has $J' > J$, where the label RS stands for real space. For $\beta = \beta_{cF}^{RS}$, $J' = J$, i. e. the system is invariant under reparametrization of the length scale $2^k \to 2^{k+1}$. Hence β_{cF}^{RS} is the critical temperature of the model [161, 163].

The RG transformation (6.8) is illustrated in Fig 6.2, where $\beta J'$ is depicted as a function of βJ for a given C_F and k_0-value. Interesting properties about universality emerge from this plot. Indeed, the curve $\beta J'$ as a function of βJ intersects the straight line βJ for a unique value of the coupling $\beta J \equiv K_c$. Now let us iterate the RG transformation several times, starting with a given $J = J_0$, then determining $J' = J_1, J'' = J_2$, and so on. At the first step of the iteration, $J_1 = J_0$ if and only if $\beta J_0 = K_c$. It follows that $\beta_{cF}^{RS} = K_c/J_0$. Similarly, at the next steps K_c/J_0 is the only value of the inverse temperature such that $J_k = J_0 \forall k$. Since K_c is defined as the solution of the equations $O_{k_0}^F(K_c) = O_{k_0-1}^F(K_c)$, it does not depend on the initial condition J_0, and thus it is universal. As an analogy, K_c corresponds to the dimensionless nearest-neighbor critical coupling of the Ising model, which has been extensively measured in three dimensions by means of Monte Carlo Renormalization Group (MCRG) calculations [5, 140]. On the other hand, dimensional quantities like $\beta_{cF}^{RS} = K_c/J_0$ are not universal. Indeed, $\beta_{cF}^{RS} = K_c/J_0$ depends on the coupling J_0 at the initial step of the iteration, i. e. at microscopic length scales. This is in agreement with the very general RG picture of ferromagnetic systems like the Ising model [163], where the critical temperature is not universal because it depends on the microscopic properties of the lattice.

An important universal quantity is the critical exponent ν_F, defined in terms of the correlation length by Eq. (2.8). According to the general RG theory in the

neighborhood of the critical fixed point K_c, ν_F is given by

$$\nu_F = \frac{\log 2}{\log \Lambda_{F\,RS}}, \tag{6.9}$$

where $\Lambda_{F\,RS}$ is here defined as

$$\Lambda_{F\,RS} \equiv \left.\frac{d\beta J'}{d\beta J}\right|_{\beta J = K_c}. \tag{6.10}$$

Since in this case the RG transformation involves only one variable J, $\Lambda_{F\,RS}$ is simply the largest eigenvalue of the 1×1 matrix linearizing the transformation in the neighborhood of the critical fixed point. A more complex case where the RG transformation involves an infinite number of variables will be discussed in Section 6.2. In Fig. 6.3 we depict $\Lambda_{F\,RS}$ from Eq. (6.10) together with the values of Λ_F (Eq. (A.16)) presented in [46] resulting from the field-theory approach of Section 2.1 and Appendix A, as a function of $1/2 < \sigma_F < 1$. The field-theory method makes the exact prediction (A.17) for Λ_F in the region $1/2 < \sigma_F < 3/4$ where the mean-field approximation is exact, while it estimates Λ_F in the non-mean-field region $3/4 < \sigma_F < 1$ by means of a resummed $\epsilon_F = \sigma_F - 3/4$-expansion. The first order of this expansion is given by Eq. (A.19).

The real-space RG approach makes a prediction for the critical exponents of Dyson's Hierarchical Model which is in good agreement with that obtained with other methods.

As k_0 is increased, $\Lambda_{F\,RS}$ computed with the real-space method approaches the field-theory value Λ_F, confirming the validity of the real-space RG approach. Notice that according to Eqs. (A.17) and (A.19), the derivative with respect to σ_F of Λ_F is discontinuous at $\sigma_F = 3/4$. On the contrary, $\Lambda_{F\,RS}$ is a smooth function of σ_F. This discrepancy is presumably due to the fact that k_0 is not large enough, and should disappear for larger k_0, because the real-space approach is exact for $k_0 \to \infty$.

Since the real-space approach for DHM reproduces the interval (2.3) and, for large k_0, also the critical exponents obtained with other methods, it is natural to generalize it to the HEA model. Accordingly, its predictions will be compared to those obtained with the replica approach in the mean-field region $1/2 < \sigma \leq 2/3$ where the latter is predictive, yielding a precise consistency test of the two approaches. On the contrary, in the non-mean-field region $2/3 < \sigma < 1$ the replica approach is not predictive, and thus a quantitative comparison of the values of the critical exponents would be meaningless. Even though, an interesting question is whether the real-space approach is predictive in this non-mean-field region. These points will be addressed in the following Section.

6.2 The RG approach in real space for the Hierarchical Edwards-Anderson model

It turns out that the definition of the HEA which is suitable to implement the real-space approach is the one where the interaction energies are redefined by Eq. (5.19). Accordingly, in what follows the HEA will be defined by Eqs. (2.10), (5.19), and we set for simplicity $H_0[S] = 0$.
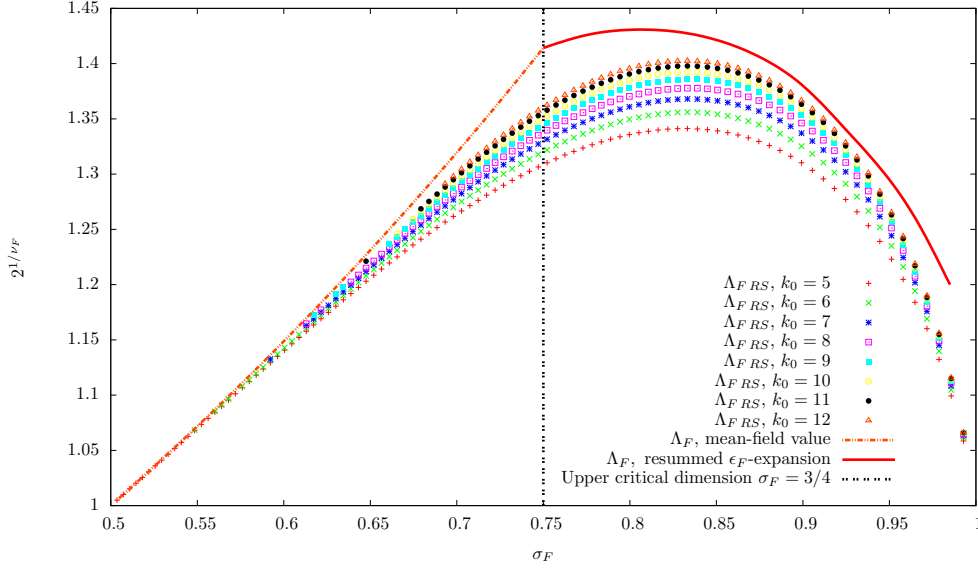
Figure 6.3. Λ_{FRS} and Λ_F as a function of σ_F for $1/2 < \sigma_F < 1$. The black dashed line represents the upper critical dimension $\sigma_F = 3/4$ discussed in Section 2.1 and Appendix A. The points represent Λ_{FRS} for $5 \leq k_0 \leq 12$. The orange dashed curve and the red solid curve represent Λ_F obtained with the field-theory method in the mean-field region $1/2 < \sigma_F \leq 3/4$ and in the non-mean-field region $3/4 < \sigma_F < 1$ respectively. The orange dashed curve represent the exact mean-field value of Λ_F given by Eq. (A.17), and the red continuous curve represents Λ_F computed with the resummed $\epsilon_F = \sigma_F - 3/4$-expansion [46] (see Eq. (A.19) for the first order of the ϵ_F-expansion).

6.2.1 Simplest approximation of the real-space method

Let us now illustrate how to implement in the spin-glass case the real-space approach presented in Section 6.1 for $k_0 = 2$. The reader should follow our derivation in close analogy with the one exposed in Section 6.1 for DHM. A HEA model with 2^2 spins $S_1, \cdots, S_4$ is built up exactly by means of the recursion equation (2.10). Setting $\mathcal{J}_{ij} \equiv C^2/2 J_{ij}$, the Hamiltonian of this model is

$$H_2[S_1, \cdots, S_4] = -\Bigg\{ [\mathcal{J}_{12}S_1S_2 + \mathcal{J}_{34}S_3S_4] + \frac{C^2}{2}[\mathcal{J}_{13}S_1S_3 + \mathcal{J}_{14}S_1S_4 +$$
$$+ \mathcal{J}_{23}S_2S_3 + \mathcal{J}_{24}S_2S_4] \Bigg\}. \tag{6.11}$$

By definition, the couplings $\{\mathcal{J}_{ij}\}_{ij}$ are IID random variables, and the probability distribution of each of them will be denoted by $p(\mathcal{J})$.

Thus, we consider a 2-spin HEA model, defined by iterating once Eq. (2.10). For the sake of clarity its spins will be denoted by S'_1, S'_2, and its Hamiltonian reads

$$H'_1[S'_1, S'_2] = -\mathcal{J}'_{12}S'_1S'_2. \tag{6.12}$$

For each realization of the couplings $\{\mathcal{J}_{ij}\}_{ij}$, we choose $\mathcal{J}'_{12}$ as a function of $\{\mathcal{J}_{ij}\}_{ij}$ in such a way that the 2-spin HEA model yields the best-possible approximation of the 2^2-spin HEA. This procedure is analogous to that exposed in Section

6.1 for DHM, and is qualitatively depicted in Fig. 6.1. By choosing $\mathcal{J}'_{12}$ in this way, the distribution $p(\mathcal{J})$ induces a distribution of $\mathcal{J}'_{12}$, that we will denote by $p'(\mathcal{J}'_{12})$. The technical details on how $p'(\mathcal{J})$ is computed from $p(\mathcal{J})$ will be given shortly.

According to the iterative construction of Eq. (2.10), a new HEA is then constructed by taking two realizations of the 2-spin HEA. Each realization is given by drawing the coupling $\mathcal{J}'$ according to its probability distribution $p'(\mathcal{J}')$. Say that the first realization has spins S'_1, S'_2 and Hamiltonian $H'_1[S'_1, S'_2] = -\mathcal{J}'_{12}S'_1S'_2$, while the second realization has spins S'_3, S'_4 and Hamiltonian $H'_1[S'_3, S'_4] = -\mathcal{J}'_{34}S'_3S'_4$. We make these two copies interact and form a 2^2-spin HEA with Hamiltonian

$$H'_1[S'_1, S'_2] + H'_1[S'_3, S'_4] - \frac{C^2}{2}[\mathcal{J}'_{13}S'_1S'_3 + \mathcal{J}'_{14}S'_1S'_4 + \mathcal{J}'_{23}S'_2S'_3 + \mathcal{J}'_{24}S'_2S'_4], \quad (6.13)$$

where $\mathcal{J}'_{13}, \mathcal{J}'_{14}, \mathcal{J}'_{23}, \mathcal{J}'_{24}$ have been drawn independently from the distribution $p'(\mathcal{J}')$. Since each of the HEA models that we made interact represents a 2^2-spin HEA, the model defined by Eq. (6.13) represents a 2^3-spin HEA. At the next step of the iteration, this HEA model is again approximated by a 2-spin HEA with coupling, say, $\mathcal{J}''_{12}$, and the probability distribution $p''(\mathcal{J}''_{12})$ of $\mathcal{J}''_{12}$ is computed from $p'(\mathcal{J}')$. Two realizations of such a 2-spin HEA are then taken and coupled again, to obtain a system representing a 2^4-spin HEA. This step is repeated k-times, and a system representing a 2^{2+k}-spin HEA is obtained.

Setting $p_0(\mathcal{J}) \equiv p(\mathcal{J}), p_1(\mathcal{J}) \equiv p'(\mathcal{J}), p_2(\mathcal{J}) \equiv p''(\mathcal{J}), \cdots$, this procedure establishes a relation between $p_k(\mathcal{J})$ and $p_{k+1}(\mathcal{J})$. Since at each step k of this procedure we double the system size, this physically represents the RG flow of the probability distribution of the coupling $p_k(\mathcal{J})$ under reparametrization of the unit length $2^k \to 2^{k+1}$.

A 2^2-spin HEA has been approximated by a 2-spin HEA as follows. Consider a physical observable $O_2(\{\beta\mathcal{J}_{ij}\}_{ij})$ of the 2^2-spin HEA, depending on the 6 couplings $\{\mathcal{J}_{ij}\}_{ij}$ and β through the dimensionless quantities $\{\beta\mathcal{J}_{ij}\}_{ij}$. Consider also an observable $O_1(\beta\mathcal{J}'_{12})$ of the 2-spin HEA, depending on the coupling $\mathcal{J}'_{12}$ and β through the dimensionless quantity $\beta\mathcal{J}'_{12}$. We recall that in the real-space approach for DHM with $k_0 = 2$ we built up the observables (6.7) as products of the magnetizations inside the left and right-half of the 2^2-spin DHM and of the 2-spin DHM. In a sense that choice was natural, because we know that the magnetization is the correct order parameter of DHM. When one tries to generalize that choice to the HEA, one has to face the fact that the order parameter for non-mean-field spin glasses is not known, and so the choice of the observables is more difficult and ambiguous. Inspired by the fact that the order parameter in the mean-field case is the overlap [133, 136, 137, 119, 130], here we will build up O_2, O_1 as thermal averages of products of spin overlaps. We want to stress that to a certain extent this choice relies on the underlying assumption that the overlap is still the good quantity describing the physics of the system, and should be thus be verified a posteriori. In particular, there is no guarantee that this choice is correct for values of σ lying in the non-mean-field region $2/3 < \sigma < 1$. A detailed analysis of the predictions of this real-space approach for the critical exponents in this region will be exposed in the following.

To build up O_2 and O_1, consider two *real* replicas $\vec{S}^1, \vec{S}^2$ of the spins of the 2^2-spin model, and two real replicas $\vec{S'}^1, \vec{S'}^2$ of the spins of the 2-spin model. The normalized overlap between $\vec{S}^1$ and $\vec{S}^2$ on the left and on the right leaf of the 2^2-spin HEA are

$$
\begin{aligned}
Q_L &= \frac{\frac{S_1^1 S_1^2 + S_2^1 S_2^2}{2}}{\sqrt{\mathbb{E}_{\vec{S}^1, \vec{S}^2}\left[\left(\frac{S_1^1 S_1^2 + S_2^1 S_2^2}{2}\right)^2\right]}}, \\
Q_R &= \frac{\frac{S_3^1 S_3^2 + S_4^1 S_4^2}{2}}{\sqrt{\mathbb{E}_{\vec{S}^1, \vec{S}^2}\left[\left(\frac{S_3^1 S_3^2 + S_4^1 S_4^2}{2}\right)^2\right]}}
\end{aligned}
\tag{6.14}
$$

respectively, where $\mathbb{E}_{\vec{S}}$ denotes the thermal average at fixed disorder $\{\mathcal{J}\}_{ij}$ and temperature, performed with the Hamiltonian (6.11). The normalized overlap between $\vec{S'}^1$ and $\vec{S'}^2$ on the left and on the right leaf of the 2-spin HEA are

$$
\begin{aligned}
Q_L' &= S_1'^1 S_1'^2, \\
Q_R' &= S_2'^1 S_2'^2
\end{aligned}
\tag{6.15}
$$

respectively. Following Kadanoff's decimation rule, we want to map the 2^2-spin HEA into the 2-spin HEA by imposing that the spins S_1, S_2 correspond to the spin S_1', and that the spins S_3, S_4 correspond to the spin S_2'. This mapping results in a correspondence between the overlaps in Eq. (6.14) and those in Eq. (6.15), which can be qualitatively written as

$$
Q_L = Q_L', \; Q_R = Q_R'.
\tag{6.16}
$$

Making the following choice for the observables

$$
\begin{aligned}
O_2(\{\beta\mathcal{J}_{ij}\}) &\equiv \mathbb{E}_{\vec{S}^1, \vec{S}^2}[Q_L Q_R], \\
O_1(\beta\mathcal{J}_{12}') &\equiv \mathbb{E}_{\vec{S'}^1, \vec{S'}^2}[Q_L' Q_R'],
\end{aligned}
\tag{6.17}
$$

Kadanoff's decimation rule encoded in Eq. (6.16) can be practically implemented by enforcing the constraint

$$
O_2(\{\beta\mathcal{J}_{ij}\}) = O_1(\beta\mathcal{J}_{12}'),
\tag{6.18}
$$

where $\mathbb{E}_{\vec{S'}}$ denotes the thermal average at fixed disorder $\mathcal{J}_{12}'$ and temperature, performed with the Hamiltonian (6.12). For any realization of the couplings $\{\mathcal{J}_{ij}\}_{ij}$, Eq. (6.18) determines $\mathcal{J}_{12}'$ as a function of $\{\mathcal{J}_{ij}\}_{ij}$ in such a way that the 2-spin HEA yields the best-possible approximation of the 2^2-spin HEA. The mapping (6.18) results into a mapping between the probability distribution $p(\mathcal{J})$ of each of the couplings $\{\mathcal{J}_{ij}\}_{ij}$ and $p'(\mathcal{J}_{12}')$. Indeed, Eq. (6.18) can be easily rewritten as

$$
O_2(\{\beta\mathcal{J}_{ij}\}) = \tanh^2(\beta\mathcal{J}_{12}').
$$

and thus the mapping between $p(\mathcal{J})$ and $p'(\mathcal{J}')$ is

$$
\begin{aligned}
p'(\mathcal{J}') &= \int \left[\prod_{i<j} p(\mathcal{J}_{ij}) d\mathcal{J}_{ij}\right] \frac{1}{2}\left[\delta\left(\mathcal{J}' - \frac{1}{\beta}\operatorname{arctanh}\left(\sqrt{O_2(\{\beta\mathcal{J}_{ij}\})}\right)\right) + \right. \\
&\quad \left. + \delta\left(\mathcal{J}' + \frac{1}{\beta}\operatorname{arctanh}\left(\sqrt{O_2(\{\beta\mathcal{J}_{ij}\})}\right)\right)\right].
\end{aligned}
\tag{6.19}
$$

Eq. (6.19) is the RG flow relating the distribution of the disorder $p(\mathcal{J})$ at length scale 2^k with the distribution of the disorder $p'(\mathcal{J}')$ at length scale 2^{k+1}, and is the generalization of Eq. (6.8) holding for DHM. We recall that the RG equation (6.8) for DHM yields a flow for a number J, while Eq. (6.19) yields a flow for a function $p(\mathcal{J})$, which can be seen as a set $\{p(\mathcal{J})\}_{\mathcal{J}}$ of an infinite number of degrees of freedom, each of which is the value of $p(\mathcal{J})$ at a point $\mathcal{J}$. Accordingly, the solution of Eq. (6.19) is slightly more complicated than that of Eq. (6.8), and it has been worked out with two independent techniques. The first one transforms Eq. (6.19) into a recursion equation relating the moments of $p(\mathcal{J})$ to the moments of $p'(\mathcal{J}')$, which is built up perturbatively by means of a high-temperature expansion, and is presented in Section 6.2.1.1. The second one is purely numerical, and solves Eq. (6.19) by means of the population dynamics algorithm, as illustrated in Section 6.2.1.2. In the following two Sections we thus illustrate these solution techniques for Eq. (6.19), and analyze the resulting fixed-points structure and show how the critical exponents can be calculated in the $k_0 = 2$-approximation. Then, we illustrate how the very same techniques can be implemented in better approximations of the real-space approach, i. e. $k_0 > 2$, and analyze the predictions of the real-space approach for the critical exponents as a function of k_0.

6.2.1.1 Solution of the real-space RG equations with the high-temperature expansion

Since it is not easy to handle analytically the continuous set of degrees of freedom $\{p(\mathcal{J})\}_{\mathcal{J}}$ in Eq. (6.19), it is better to transform the latter into an equation for the moments of $p(\mathcal{J}), p'(\mathcal{J}')$. Since there is $\pm\mathcal{J}$-symmetry, $p(\mathcal{J}), p'(\mathcal{J}')$ are even functions of $\mathcal{J}, \mathcal{J}'$ respectively. Hence, setting

$$\begin{aligned} m_a &\equiv \int d\mathcal{J}\, p(\mathcal{J})\mathcal{J}^a, \\ m'_a &\equiv \int d\mathcal{J}'\, p'(\mathcal{J}')(\mathcal{J}')^a, \end{aligned}$$

one has $m_{2a+1} = m'_{2a+1} = 0$, and Eq. (6.19) can be transformed into an equation relating $\{m_{2a}\}_a$ to $\{m'_{2a}\}_a$. Indeed, let us call the 6 couplings $\mathcal{J}_{12}, \mathcal{J}_{13}, \ldots, \mathcal{J}_{34}$ $\mathcal{J}_1, \cdots, \mathcal{J}_6$ respectively, and integrate both sides of Eq. (6.19) with respect to $\mathcal{J}'$

$$\begin{aligned} m'_{2a} &= \int \left[\prod_{\alpha=1}^{6} d\mathcal{J}_\alpha p(\mathcal{J}_\alpha) \right] \frac{1}{\beta^{2a}} \left[\operatorname{arctanh}^{2a}\left(\sqrt{O_2(\{\beta\mathcal{J}_\gamma\}_\gamma)} \right) \right] \\ &\equiv F_{2a}[\{m_{2b}\}_b]. \end{aligned} \tag{6.20}$$

The function F_{2a} depends in a complicated way on the even moments $\{m_{2b}\}_b$, and we have not been able to compute it explicitly. Still, this dependence can be systematically worked out by expanding in powers of β the square brackets in the right-hand side of Eq. (6.20). If we truncate the expansion at a given order β^{2m}, the right-hand side of Eq. (6.20) becomes a linear combination of $\{m_{2b}\}_{b=1,\ldots,m}$ which can be computed explicitly. Hence, if we take Eq. (6.20) for $a = 1, \ldots, m$, we obtain a set of equations relating $\{m'_{2a}\}_{a=1,\ldots,m}$ to $\{m_{2b}\}_{b=1,\ldots,m}$. This set of equations is nothing but the flow $p(\mathcal{J}) \to p'(\mathcal{J}')$ represented with the discrete set of degrees of freedom $\{m_{2a}\}_{a=1,\ldots,m} \to \{m'_{2b}\}_{b=1,\ldots,m}$.

In Appendix H we show explicitly these equations for $m = 2$, Eq. (H.1), and discuss their solution. In particular, we show that if we consider only the leading terms in the β-expansion, the RG equations relating $\{m'_{2a}\}_{a=1,...,m}$ to $\{m_{2b}\}_{b=1,...,m}$ reproduce the condition $\sigma > 1/2$ that has been previously derived in Eq. (4.12). On the contrary, they do not reproduce the condition $\sigma < 1$. This is presumably due to the fact that the present approach implements the lowest-order approximation $k_0 = 2$ of the real-space method. Indeed, in Section 6.2.2 we will show that the numerical implementation of the real-space method for $k_0 > 2$ yields a better description of the region where σ significantly deviates from $1/2$, and the condition $\sigma < 1$ should be recovered for k_0 large enough.

It is easy to see that Eq. (H.1) has an attractive high-temperature fixed point $m_{2a} = 0 \,\forall a$, and an attractive low-temperature fixed point $m_{2a} = \infty \,\forall a$. These fixed points are separated by a repulsive critical fixed point $\{m^*_{2a}\}_{a=1,...,m}$. In order to investigate the latter, one can introduce a critical temperature β_c^{RS} such that Eq. (H.1) converges to $\{m^*_{2a}\}_{a=1,...,m}$ for $\beta = \beta_c^{RS}$. This fixed point is determined by means of an expansion in powers of $\sigma - 1/2$, physically representing the distance from the purely mean-field regime $\sigma = 1/2$ of the model. The critical exponent ν defined by Eq. (5.14) is expressed in terms of the largest eigenvalue Λ_{RS} of the matrix linearizing Eq. (H.1) in the neighborhood of $\{m^*_{2a}\}_{a=1,...,m}$ through the relation

$$\nu = \frac{\log 2}{\log \Lambda_{RS}},$$

and is given by Eq. (H.7).

This computation can be performed to higher orders. If the expansion is done up to $O(\beta^{2m})$, Λ_{RS} can be computed to order $(\sigma - 1/2)^{m-1}$. The calculation has been done for $m = 5$ by means of a symbolic manipulation program [170], and the result is

$$
\begin{aligned}
\Lambda_{RS} &= 1 + 2\log 2 \,(\sigma - 1/2) - \frac{219(\log 2)^2}{20}(\sigma - 1/2)^2 + \\
&\quad -\frac{113453(\log 2)^3}{1200}(\sigma - 1/2)^3 + \frac{56579203(\log 2)^4}{403200}(\sigma - 1/2)^4 + \\
&\quad +O((\sigma - 1/2)^5).
\end{aligned}
\tag{6.21}
$$

Even though only the first four terms of the expansion are available, Eq. (6.21) yields an accurate estimate of Λ_{RS} in a relatively wide range of values of σ. This is shown in Table 6.1, where the values of $\Lambda_{RS}^{(i)}$ obtained by truncating the expansion (6.21) to order $(\sigma - 1/2)^i$ are listed for different values of $0.54 \leq \sigma \leq 0.62$ and i. Since $\Lambda_{RS}^{(i)}$ increases by less than 1% when increasing i from 3 to 4, in this region we can extract the exact value of Λ_{RS} with good accuracy.

It turns out that the high-temperature expansion cannot be implemented for $k_0 > 2$, because the symbolic manipulations become too difficult. Still, the values of the critical exponent ν computed with the high-temperature expansion for $k_0 = 2$

Table 6.1. $\Lambda_{RS}^{(i)}$ as a function of i for different values of $0.54 \leq \sigma \leq 0.62$. The relative change in $\Lambda_{RS}^{(i)}$ obtained as one increases the order i from 3 to 4 is less than 1%, and yields an estimate of the error on the critical exponent ν.

σ	$\Lambda_{RS}^{(1)}$	$\Lambda_{RS}^{(2)}$	$\Lambda_{RS}^{(3)}$	$\Lambda_{RS}^{(4)}$
0.54	1.05545	1.04703	1.04502	1.0451
0.58	1.1109	1.07723	1.06111	1.06244
0.62	1.16636	1.0906	1.03619	1.04291

will serve as an important test of a different, purely numerical implementation of the RG equations (6.19) for $k_0 = 2$, that will be illustrated in the following Section. Once the agreement between the numerical and analytical approach will be established for $k_0 = 2$, the numerical method will be easily implemented for $k_0 > 2$, yielding an estimate of the exact value of the exponents obtained as k_0 is increased.

6.2.1.2 Solution of the real-space RG equations with the population-dynamics method

The RG equations (6.19) are nonlinear integral equations, and it is difficult to solve them analytically and determine $p'(\mathcal{J}')$ as a functional of $p(\mathcal{J})$. Accordingly, one can use some numerical methods. Here we describe a stochastic approach known as population dynamics, yielding an extremely simple and powerful solution of Eq. (6.19). Historically, population dynamics appeared first in the theory of localization of electrons in disordered systems [2], and was later developed for spin glasses [116] and constraint-satisfaction problems [115].

In population dynamics one represents the function $p(\mathcal{J})$ as a population of P numbers $\{\mathcal{J}_i\}_{i=1,\ldots,P}$, where each $\mathcal{J}_i$ has been drawn with probability $p(\mathcal{J}_i)$. Accordingly if P is large enough, once we know $p(\mathcal{J})$ we can compute the population $\{\mathcal{J}_i\}_i$, while once we know the population $\{\mathcal{J}_i\}_i$ we can compute $p(\mathcal{J})$ from the relation

$$p(\mathcal{J})dJ \sim \frac{1}{P} \sum_{i=1}^{P} \mathbb{I}[\mathcal{J}_i \in (J, J + dJ)], \tag{6.22}$$

where the function $\mathbb{I}[\mathcal{J}_i \in (J, J + dJ)]$ equals one if $\mathcal{J}_i \in (J, J + dJ)$ and zero otherwise, and dJ is a suitably chosen small binning interval. Thus, there is a one-to-one correspondence between $p(\mathcal{J})$ and $\{\mathcal{J}_i\}_{i=1,\ldots,P}$, and these are different representations of the same object

$$p(\mathcal{J}) \leftrightarrow \{\mathcal{J}_i\}_{i=1,\ldots,P}. \tag{6.23}$$

In practice, once one knows the population $\{\mathcal{J}_i\}_i$ the corresponding $p(\mathcal{J})$ is computed by setting

$$\mathcal{J}_{\text{MAX}} \equiv \max_i(|\mathcal{J}_i|), \tag{6.24}$$

choosing $dJ = 2\mathcal{J}_{\text{MAX}}/B$, and using Eq. (6.22), where B is a suitably chosen large integer number.

Routine 1 Population-dynamics routine

---

for $i = 1, \ldots, P$

    for $\alpha = 1, \ldots, 6$

        draw uniformly a random number j in $\{1, \ldots, P\}$.

        set $\mathcal{J}_\alpha^{temp} = \mathcal{J}_r$.

    end

    draw uniformly a random sign $s = \pm 1$.

    set $\mathcal{J}_i' = s \frac{1}{\beta} \operatorname{arctanh} \left(\sqrt{O_2(\{\beta \mathcal{J}_\alpha^{temp}\}_\alpha)} \right)$.

end

return $\{\mathcal{J}_i'\}_i$.

The mapping $p(\mathcal{J}) \to p'(\mathcal{J}')$ given by Eq. (6.19) yields a mapping between $\{\mathcal{J}_i\}_{i=1,\ldots,P}$ and the population $\{\mathcal{J}_i'\}_i$ representing $p'(\mathcal{J}')$

$$p'(\mathcal{J}') \leftrightarrow \{\mathcal{J}_i'\}_{i=1,\ldots,P}. \tag{6.25}$$

Indeed, once $\{\mathcal{J}_i\}_i$ is known, it is easy to show that one can compute $\{\mathcal{J}_i'\}_i$ by means of the pseudocode illustrated in Routine 1.

The reader should notice that the population dynamics Routine is extremely simple and versatile to implement, and that it requires no evaluation of the integrals in the right-hand side of Eq. (6.19). Once $\{\mathcal{J}_i'\}_i$ is known, this routine is iterated to compute $\{\mathcal{J}_i''\}_i$ from $\{\mathcal{J}_i'\}_i$, and so on. In particular, by iterating k times Routine 1 one can compute the population $\{\mathcal{J}_{k\,i}\}_i$ representing the probability distribution $p_k(\mathcal{J}_k)$. Accordingly, the algorithm is named population dynamics after the fact that k is analogous to the dynamical-evolution time of the population $\{\mathcal{J}_{k\,i}\}_i$.

The structure of the fixed points of Eq. (6.19) can be now investigated numerically. Indeed, by iterating the population-dynamics Routine at fixed β and by computing $p_k(\mathcal{J})$ as a function of k, it is easy to show that there is a finite value of $\beta = \beta_c^{RS}$ such that for $\beta < \beta_c^{RS}$ $p_k(\mathcal{J})$ converges to $\delta(\mathcal{J})$ as k is increased, while for $\beta > \beta_c^{RS}$ $p_k(\mathcal{J})$ broadens, i. e. its variance is an increasing function of k. The reader should observe that this flow to weak and strong coupling for $p(\mathcal{J})$ in the high and in the low-temperature phase respectively is the analog of the flow to weak and strong coupling for the number J in the real-space approach for DHM, depicted in Fig. (6.2). The physical interpretation of these two temperature regimes is that for $\beta < \beta_c^{RS}$ $p_k(\mathcal{J})$ flows to an attractive high-temperature fixed point with $\mathcal{J} = 0$ where spins are decorrelated, while for $\beta > \beta_c^{RS}$ it flows to an attractive low-temperature fixed point with $\mathcal{J} = \infty$ where spins are strongly correlated. This fact implies that as the temperature is lowered below T_c a phase transition occurs, and this transition yields a collective and strongly interacting behavior of spins in

the low-temperature phase. Even though this result has been derived in the $k_0 = 2$-approximation, the implementations of the real-space method for $k_0 > 2$ will confirm this picture. The existence of a finite-temperature phase transition for a diluted version of the HEA model has been established heretofore with MC simulations by means of finite-size scaling techniques [65]. Since the critical properties of such a diluted version of the HEA should be the same [65] as those of the HEA defined here, the real-space approach confirms the picture on the criticality of the system given by MC simulations.

An important feature of the population-dynamics approach is that for $\sigma < 1/2$ the thermodynamic limit is ill-defined, which has been discussed in Part III, Eq. (4.12). Indeed, the numerics show that for $\sigma \to 1/2$ $\beta_c^{RS} \to 0$, in such a way that the system is always in the low-temperature phase, i. e. the variance of $p_k(\mathcal{J})$ is an increasing function of k, and the thermodynamic limit $k \to \infty$ is ill-defined. On the other hand, according to Eq. (4.12) one should have that $\beta_c^{RS} \to \infty$ as $\sigma \to 1$, because for $\sigma > 1$ no finite-temperature phase transition occurs. Unfortunately, this condition is not reproduced by the real-space approach. As discussed in Section 6.2.1.1, this is presumably due to the fact that k_0 is small, i. e. that Eq. (6.19) implements only the lowest-order approximation of the real-space method ($k_0 = 2$). This hypothesis is supported by the fact that the estimate of the critical exponents that we will give in what follows significantly improve as k_0 is increased in the region where σ differs significantly from $1/2$, while they hardly change in the region $\sigma \approx 1/2$, implying that the closer σ to 1, the larger the values of k_0 needed. Accordingly, for $\sigma \to 1$ a significantly better description would be obtained if larger values of k_0 were accessible, and the $\sigma < 1$-limit would be recovered.

The numerical implementation of Routine 1 also shows that there is a repulsive critical fixed point, that we will call $p_*(\mathcal{J})$, which is reached by iterating Routine 1 with $\beta = \beta_c^{RS}$

$$
\begin{aligned}
p_*(\mathcal{J}) &= \int \left[\prod_{\alpha=1}^{6} p_*(\mathcal{J}_\alpha) d\mathcal{J}_\alpha \right] \frac{1}{2} \left[\delta \left(\mathcal{J} - \frac{1}{\beta_c^{RS}} \operatorname{arctanh} \left(\sqrt{O_2(\{\beta_c^{RS} \mathcal{J}_\alpha\}_\alpha)} \right) \right) + \right. \\
&\quad \left. + \delta \left(\mathcal{J} + \frac{1}{\beta_c^{RS}} \operatorname{arctanh} \left(\sqrt{O_2(\{\beta_c^{RS} \mathcal{J}_\alpha\}_\alpha)} \right) \right) \right].
\end{aligned}
\tag{6.26}
$$

This critical fixed point is analogous to the critical value of the coupling K_c in the real-space method for DHM, depicted in Fig. (6.2). In the numerical implementation both β_c^{RS} and $p_*(\mathcal{J})$ are computed by iterating Routine 1 and by dynamically adjusting β at each step to its critical value, which is approximately determined as the value of β such that $\int d\mathcal{J}' p'(\mathcal{J}')(\mathcal{J}')^2 = \int d\mathcal{J} p(\mathcal{J})\mathcal{J}^2$. In order to do so, one starts with two values of the temperature $T_{\min}, T_{\text{MAX}}$ such that

$$
T_{\min} < T_c^{RS} < T_{\text{MAX}},
\tag{6.27}
$$

and then iterates the bisection Routine 2.

Each iteration k of Routine 2 is one step of the RG transformation performed at temperature $T = (T_{\min} + T_{\text{MAX}})/2$, and if the second moment of $p'(\mathcal{J}')$ is smaller than that of $p(\mathcal{J})$, T is in the high-temperature phase, and the interval $[T_{\min}, T_{\text{MAX}}]$

Routine 2 Bisection routine

---

for $k = 1, \ldots, k_{\mathrm{MAX}}$

> **set** $T = (T_{\min} + T_{\mathrm{MAX}})/2$.
>
> **set** $\varsigma^2 = \frac{1}{P} \sum_{i=1}^{P} \mathcal{J}_i^2$.
>
> **compute** $\{\mathcal{J}_i'\}_i$ from Routine 1 and set $\mathcal{J}_i = \mathcal{J}_i' \; \forall i = 1, \ldots, P$.
>
> **set** $\varsigma'^2 = \frac{1}{P} \sum_{i=1}^{P} \mathcal{J}'^2_i$.
>
> **if** $\varsigma'^2 > \varsigma^2$ **set** $T_{\min} = T_{\min} + x(T_{\mathrm{MAX}} - T_{\min})$.
>
> **else**   **set** $T_{\mathrm{MAX}} = T_{\mathrm{MAX}} - x(T_{\mathrm{MAX}} - T_{\min})$.

end

return $T_c^{RS} = T$ and $\{\mathcal{J}_i\}_i \leftrightarrow p_*(\mathcal{J})$

---

is reduced by $0 < x < 1$ by lowering the upper limit T_{MAX}, and vice versa if T is in the low-temperature phase. By iterating this procedure $k_{\mathrm{MAX}} \gg 1$ times, the Routine returns an estimate of the critical temperature $T_c^{RS} = T$ and of the critical fixed point $\{\mathcal{J}_i\}_i \leftrightarrow p_*(\mathcal{J})$.

Since population dynamics is a stochastic approach, this bisection Routine is not deterministic, and might give slightly different results when one runs it several times if the population size P is not large enough. In particular, such a stochastic character can introduce some instabilities when approaching the repulsive fixed point, and these might let the bisection Routine flow towards the low or high-temperature fixed point, far away from $p_*(\mathcal{J})$. Accordingly, the parameter x has been chosen by hand in order to minimize this instability, and the numerical implementation of the bisection Routine has shown that $x \sim 0.1$ yields a good estimate of the critical fixed point.

The critical fixed point $p_*(\mathcal{J})$ obtained with this bisection method is depicted in Fig. 6.4 for a given σ-value, where we also represent $p_*(\mathcal{J})$ obtained with the $k_0 = 3, 4$-approximations that will be described in what followins.

Once the fixed point $p_*(\mathcal{J})$ has been computed numerically, the critical exponents can be determined by linearizing the transformation (6.19) in the neighborhood of $p_*(\mathcal{J})$. Being the RG equations (6.19) a flow for a continuous set of degrees of freedom $\{p(\mathcal{J})\}_{\mathcal{J}}$, the matrix linearizing the RG transformation in the neighborhood
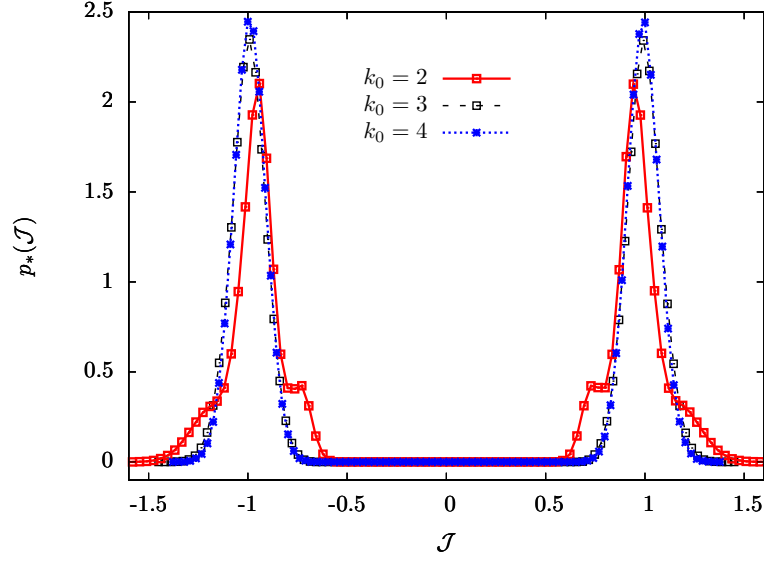
Figure 6.4. Fixed point $p_*(\mathcal{J})$ as a function of $\mathcal{J}$ for $\sigma = 0.5146$ and $k_0 = 2, 3, 4$, obtained by iterating Routine 2 starting with $p_0(\mathcal{J}) = 1/\sqrt{2\pi}\mathrm{e}^{-\mathcal{J}^2/2}$. For $k_0 = 2$, $k_{\mathrm{MAX}} = 50, P = 2 \times 10^6, x = 0.1$ and $B = 96$. For $k_0 = 3$, $k_{\mathrm{MAX}} = 50, P = 10^6, x = 0.1$ and $B = 96$. For $k_0 = 4$, $k_{\mathrm{MAX}} = 20, P = 2 \times 10^4, x = 0.1$ and $B = 96$. $p_*(\mathcal{J})$ has compact support and a convergent behavior as k_0 is increased. This convergence indicates that k_0 is large enough in such a way that the real-space approach is asymptotically exact for this value of σ.

of $p_*(\mathcal{J})$ has continuous indices $\mathcal{J}, \mathcal{J}'$, and is defined as

$$
\begin{aligned}
\mathscr{M}^{RS}_{\mathcal{J},\mathcal{J}'} &\equiv \left. \frac{\delta p'(\mathcal{J})}{\delta p(\mathcal{J}')} \right|_{p=p_*, \beta=\beta_c^{RS}} \\
&= \sum_{\gamma=1}^{6} \int \left[\prod_{\lambda\neq\gamma=1}^{6} p_*(\mathcal{J}_\lambda) d\mathcal{J}_\lambda \right] \times \\
&\quad \times \frac{1}{2} \left[\delta\left(\mathcal{J} - \frac{1}{\beta_c^{RS}} \operatorname{arctanh}\left(\sqrt{O_2(\{\beta_c^{RS}\mathcal{J}_\lambda\}_\lambda^{\gamma,\mathcal{J}'})} \right) \right) + \right. \\
&\quad \left. + \delta\left(\mathcal{J} + \frac{1}{\beta_c^{RS}} \operatorname{arctanh}\left(\sqrt{O_2(\{\beta_c^{RS}\mathcal{J}_\lambda\}_\lambda^{\gamma,\mathcal{J}'})} \right) \right) \right],
\end{aligned}
\tag{6.28}
$$

where $\{\beta_c^{RS}\mathcal{J}_\lambda\}_\lambda^{\gamma,\mathcal{J}'} \equiv \{\beta_c^{RS}\mathcal{J}_1, \ldots, \beta_c^{RS}\mathcal{J}_{\gamma-1}, \beta_c^{RS}\mathcal{J}', \beta_c^{RS}\mathcal{J}_{\gamma+1}, \ldots, \beta_c^{RS}\mathcal{J}_6\}$ and in the second line of Eq. (6.28) Eq. (6.19) has been used.

In the rigorous treatment [45] of the ϵ_F-expansion for DHM, the linearization of the transformation $\mathfrak{p}_k(m) \to \mathfrak{p}_{k+1}(m)$ in the neighborhood of $\mathfrak{p}_*(m)$ is formulated in terms of a linear functional acting on a suitably defined space of functions $\phi(m)$, and the critical exponents are extracted from the eigenvalues of this functional. These eigenvalues are determined by the theory of linear functionals, in particular by the theory of Hermite polynomials. Similarly, here the matrix $\mathscr{M}^{RS}$ defines a linear functional $\mathcal{L}$ acting on a suitably defined space of functions $\phi(\mathcal{J})$, and yielding a

function $\mathcal{L}[\phi](\mathcal{J})$

$$\mathcal{L}[\phi](\mathcal{J}) \equiv \int d\mathcal{J}' \mathscr{M}^{RS}_{\mathcal{J},\mathcal{J}'} \phi(\mathcal{J}').$$

Unfortunately, the complicated form (6.28) of $\mathscr{M}^{RS}$ did not allow for an analytic treatment, and in particular the spectrum of $\mathscr{M}^{RS}$, and so the critical exponents, could not be determined in terms of the spectrum of well-known linear functionals. Hence, a completely numerical analysis of the spectrum of $\mathscr{M}^{RS}$ has been done. This analysis is illustrated in Appendix I. As a result, the critical exponent ν defined by Eq. (5.14) is determined from the spectrum of $\mathscr{M}^{RS}$. In Fig. 6.5 we depict $\lambda^{(n_*)}$ obtained with this $k_0 = 2$-approximation, $\lambda^{(n_*)}$ obtained with the $k_0 = 3, 4$-approximations that will be discussed in what follows, and Λ_{RS} obtained with the high-temperature expansion as a function of σ. We also depict the prediction for $2^{1/\nu}$ of the replica approach discussed in Chapter 5, in both the mean-field region $\sigma \leq 2/3$ and the non-mean-field region $\sigma > 2/3$. Fig. 6.5 shows that the prediction Λ_{RS} for $2^{1/\nu}$ obtained with the high-temperature expansion and the prediction $\lambda^{(n_*)}$ for $2^{1/\nu}$ obtained with population dynamics are in excellent agreement, confirming the validity of both methods. Even though, the agreement between $\Lambda_{RS}, \lambda^{(n_*)}$ and $2^{1/\nu}$ obtained with the replica approach is good only if σ is sufficiently close to $1/2$. As we will see shortly, this discrepancy progressively disappears when implementing approximations with $k_0 > 2$. Since these have been developed along the lines of the $k_0 = 2$-approximation, in the following Section we will sketch only the main steps of the derivation of the real-space RG equations for $k_0 > 2$, and of the resulting computation of the critical exponents.

6.2.2   Improved approximations of the real-space method

In the real-space approach developed in Section 6.2.1 a 2^{k_0}-spin HEA is approximated by a 2^{k_0-1}-spin HEA, with $k_0 = 2$. This approximation can be implemented for larger k_0 and, as discussed above, it becomes asymptotically exact for $k_0 \to \infty$. In order to generalize the real-space approach to $k_0 > 2$, let us consider a 2^{k_0}-spin HEA with spins $S_1, \ldots, S_{2^{k_0}}$ and Hamiltonian $H_{k_0}[\vec{S}]$, where H_{k_0} is obtained by iterating the recursion equations (2.10), (5.19). Let us set $C^2/2J_{ij} \equiv \mathcal{J}_{ij}$, where J_{ij} are the couplings defined in Eq. (2.10), (5.19).

Let us then consider a 2^{k_0-1}-spin HEA with spins $S'_1, \ldots, S'_{2^{k_0-1}}$ and Hamiltonian $H_{k_0-1}[\vec{S}']$, where H_{k_0-1} is obtained by iterating the recursion equations (2.10), (5.19). Let us set $C^2/2J'_{ij} \equiv \mathcal{J}'_{ij}$, where J'_{ij} are the couplings defined in Eq. (2.10), (5.19). Let us also call the $M \equiv 2^{k_0}(2^{k_0} - 1)/2$ couplings $\mathcal{J}_{12}, \mathcal{J}_{13}, \ldots, \mathcal{J}_{2^{k_0}-1\, 2^{k_0}}$ $\mathcal{J}_1, \cdots, \mathcal{J}_M$ respectively, and let us call the $M' \equiv 2^{k_0-1}(2^{k_0-1} - 1)/2$ couplings $\mathcal{J}'_{12}, \mathcal{J}'_{13}, \ldots, \mathcal{J}'_{2^{k_0-1}-1\, 2^{k_0-1}}$ $\mathcal{J}'_1, \cdots, \mathcal{J}'_{M'}$ respectively.

According to the analysis of Section 6.2.1, for each sample of the couplings $\{\mathcal{J}_\alpha\}_\alpha$ we choose $\{\mathcal{J}'_\alpha\}_\alpha$ as a function of $\{\mathcal{J}_\alpha\}_\alpha$ in such a way that the 2^{k_0-1}-spin HEA yields the best-possible approximation of the 2^{k_0}-spin HEA. This procedure is qualitatively depicted in Fig. 6.6 for $k_0 = 3$.

Since in this case the number of couplings of the 2^{k_0-1}-spin HEA is M', we need a set of M' equations to determine the optimal couplings $\{\mathcal{J}'_\alpha\}_\alpha$. This set of equations ensuring that the 2^{k_0-1}-spin HEA approximates the 2^{k_0}-spin HEA can
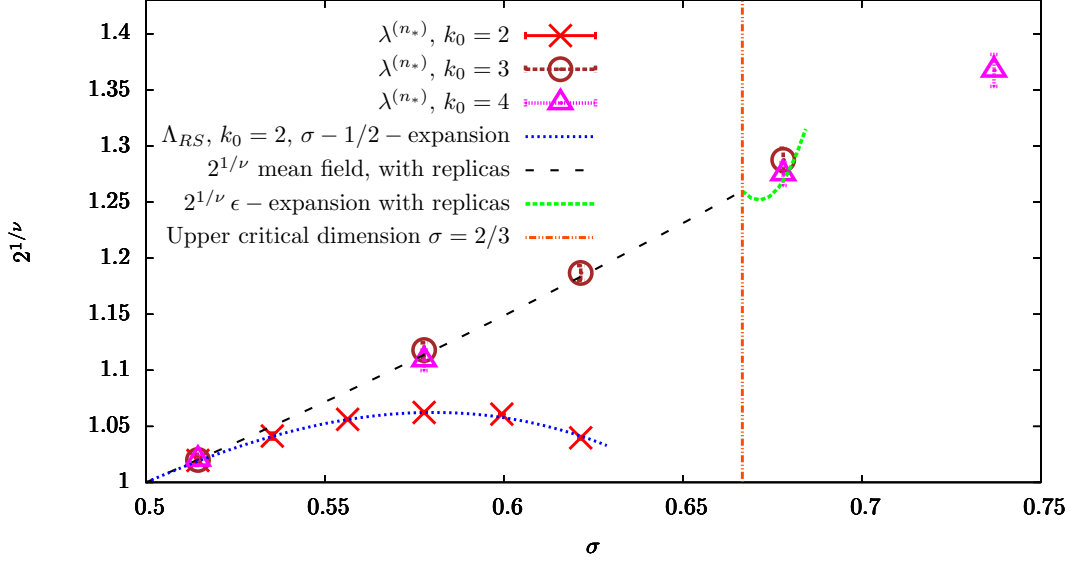
Figure 6.5. $2^{1/\nu}$ as a function of σ. The red points represent $\lambda^{(n_*)}$ computed with the population-dynamics implementation of the real-space RG equations with $k_0 = 2$ and $48 \leq B \leq 96, k_{\text{MAX}} = 50, 10^6 \leq P \leq 2 \times 10^7, x = 0.1$ and initial distribution $p_0(\mathcal{J}) = 1/\sqrt{2\pi}e^{-\mathcal{J}^2/2}$. The brown points represent $\lambda^{(n_*)}$ computed with the population-dynamics implementation of the real-space RG equations with $k_0 = 3$ and $48 \leq B \leq 100, k_{\text{MAX}} = 50, 4 \times 10^4 \leq P \leq 10^6, x = 0.1$ and initial distribution $p_0(\mathcal{J}) = 1/\sqrt{2\pi}e^{-\mathcal{J}^2/2}$. The violet points represent $\lambda^{(n_*)}$ computed with the population-dynamics implementation of the real-space RG equations with $k_0 = 4$ and $48 \leq B \leq 96, k_{\text{MAX}} = 20, 5 \times 10^3 \leq P \leq 2 \times 10^4, x = 0.1$ and initial distribution $p_0(\mathcal{J}) = 1/\sqrt{2\pi}e^{-\mathcal{J}^2/2}$. For any fixed k_0 one cannot compute ν for too large σ, because the bisection routine used to determine the critical fixed point is unstable for large σ. The blue dashed curve represents Λ_{RS} computed with the high-temperature expansion of the real-space RG equations to fourth order in $\sigma - 1/2$, see Eq. (6.21). The black dashed curve and the green dashed curve represent $2^{1/\nu}$ obtained with the replica approach presented in Chapter 5: the black dashed curve represents the mean-field value of $2^{1/\nu}$ for $\sigma \leq 2/3$ given by the first line in Eq. (5.16), while the green dashed curve represents the two-loop result (5.18) for $\sigma > 2/3$. The orange dashed curve represents the upper critical dimension $\sigma = 2/3$ resulting from the replica approach and discussed in Chapter 5.

be obtained by considering M' physical observables $\{O_{k_0}^\alpha(\{\beta\mathcal{J}_\gamma\}_\gamma)\}_{\alpha=1,\dots,M'}$ of the 2^{k_0}-spin HEA, depending on the M couplings $\{\mathcal{J}_\alpha\}_\alpha$ and on β through the dimensionless quantities $\{\beta\mathcal{J}_\alpha\}_\alpha$. Consider also M' observables $\{O_{k_0-1}^\alpha(\{\beta\mathcal{J}'_\gamma\}_\gamma)\}_{\alpha=1,\dots,M'}$ of the 2^{k_0-1}-spin HEA, depending on the couplings $\{\mathcal{J}'_\alpha\}_\alpha$ and on β through the dimensionless quantity $\{\beta\mathcal{J}'_\alpha\}_\alpha$.

In order to build up $O_{k_0}^\alpha$ and $O_{k_0-1}^\alpha$, consider two real replicas $\vec{S}^1, \vec{S}^2$ of the spins of the 2^{k_0}-spin HEA, and two real replicas $\vec{S'}^1, \vec{S'}^2$ of the spins of the 2^{k_0-1}-spin HEA. Now consider the 2^{k_0-1} pairs of contiguous spins $(S_1, S_2), (S_3, S_4), \dots, (S_{2^{k_0}-1}, S_{2^{k_0}})$ of the 2^{k_0}-spin HEA, and the normalized overlaps between $\vec{S}^1$ and $\vec{S}^2$ on each of the
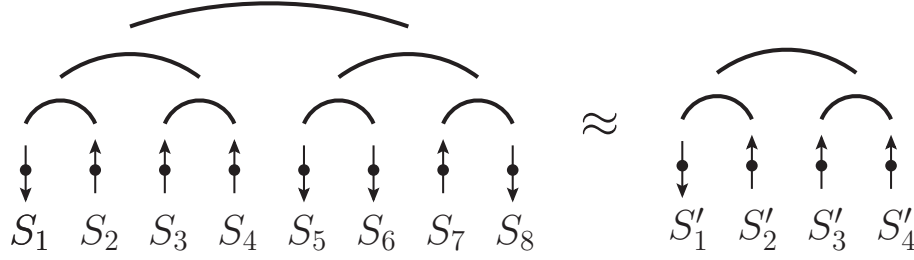
Figure 6.6. Approximation of the real-space approach for $k_0 = 3$. A 2^3-spin HEA with spins $S_1, \cdots, S_8$ and Hamiltonian $H_8[\vec{S}]$ is approximated by a 2^2-spin HEA with spins $S'_1, \ldots, S'_4$ and Hamiltonian $H_2[\vec{S}']$.

leaves defined by these pairs

$$Q_\alpha = \frac{\frac{S^1_{2\alpha-1}S^2_{2\alpha-1}+S^1_{2\alpha}S^2_{2\alpha}}{2}}{\sqrt{\mathbb{E}_{\vec{S}^1,\vec{S}^2}\left[\left(\frac{S^1_{2\alpha-1}S^2_{2\alpha-1}+S^1_{2\alpha}S^2_{2\alpha}}{2}\right)^2\right]}},$$

where $\alpha = 1, \ldots, 2^{k_0-1}$, and $\mathbb{E}_{\vec{S}^1,\vec{S}^2}$ denotes the expectation value with respect to $\vec{S}^1, \vec{S}^2$ with Boltzmann weight $e^{-\beta H_{k_0}}$. Now consider the normalized overlaps between $\vec{S}'^1$ and $\vec{S}'^2$ on each of the spins of the 2^{k_0-1}-spin HEA

$$Q'_\alpha = S'^1_\alpha S'^2_\alpha,$$

where $\alpha = 1, \ldots, 2^{k_0-1}$.

Kadanoff's decimation rule is implemented by imposing the correspondence between Q_α and Q'_α $\forall \alpha = 1, \ldots, 2^{k_0-1}$. This can be done by choosing the following observables

$$\begin{aligned}
O^1_{k_0}(\{\beta\mathcal{J}_\gamma\}_\gamma) &= \mathbb{E}_{\vec{S}^1,\vec{S}^2}[Q_1 Q_2], \\
O^2_{k_0}(\{\beta\mathcal{J}_\gamma\}_\gamma) &= \mathbb{E}_{\vec{S}^1,\vec{S}^2}[Q_1 Q_3], \\
&\cdots \\
O^{M'}_{k_0}(\{\beta\mathcal{J}_\gamma\}_\gamma) &= \mathbb{E}_{\vec{S}^1,\vec{S}^2}[Q_{2^{k_0-1}-1} Q_{2^{k_0-1}}],
\end{aligned} \tag{6.29}$$

$$\begin{aligned}
O^1_{k_0-1}(\{\beta\mathcal{J}'_\gamma\}_\gamma) &= \mathbb{E}_{\vec{S}'^1,\vec{S}'^2}[Q'_1 Q'_2], \\
O^2_{k_0-1}(\{\beta\mathcal{J}'_\gamma\}_\gamma) &= \mathbb{E}_{\vec{S}'^1,\vec{S}'^2}[Q'_1 Q'_3], \\
&\cdots \\
O^{M'}_{k_0-1}(\{\beta\mathcal{J}'_\gamma\}_\gamma) &= \mathbb{E}_{\vec{S}'^1,\vec{S}'^2}[Q'_{2^{k_0-1}-1} Q'_{2^{k_0-1}}],
\end{aligned} \tag{6.30}$$

where $\mathbb{E}_{\vec{S}'^1,\vec{S}'^2}$ denotes the expectation value with respect to $\vec{S}'^1, \vec{S}'^2$ with Boltzmann weight $e^{-\beta H_{k_0-1}}$. The 2^{k_0}-spin HEA can now be approximated by the 2^{k_0-1}-spin HEA by enforcing the constraints

$$O^\alpha_{k_0}(\{\beta\mathcal{J}_\gamma\}_\gamma) = O^\alpha_{k_0-1}(\{\beta\mathcal{J}'_\gamma\}_\gamma) \; \forall \alpha = 1, \ldots, M'. \tag{6.31}$$

In what follows we assume that Eq. (6.31) can be written as

$$\mathcal{J}'_\alpha = 1/\beta f_\alpha(\{\beta\mathcal{J}_\gamma\}_\gamma), \tag{6.32}$$

where in Eq. (6.32) we have used the fact that the right-hand side of Eq. (6.31) depends on $\{\mathcal{J}'_\alpha\}_\alpha$ through the dimensionless products $\{\beta\mathcal{J}'_\alpha\}_\alpha$.

Now suppose that the couplings $\{\mathcal{J}_\alpha\}$ are independent and that each of them is distributed according to a given $p(\mathcal{J})$. According to Eq. (6.32), the couplings $\{\mathcal{J}'_\alpha\}_\alpha$ are not independent, because the entangled structure of Eq. (6.32) introduces some correlation between them. Accordingly, the joint probability distribution of $\{\mathcal{J}'_\alpha\}_\alpha$ is

$$p'_C(\{\mathcal{J}'_\alpha\}_\alpha) = \int \left[\prod_{\alpha=1}^{M'} p(\mathcal{J}_\alpha)d\mathcal{J}_\alpha\right] \prod_{\alpha=1}^{M'} \delta\left(\mathcal{J}'_\alpha - \frac{1}{\beta}f_\alpha(\{\beta\mathcal{J}_\gamma\}_\gamma)\right), \tag{6.33}$$

where the label C stands for correlated. Hence, starting with a set of uncorrelated couplings $\{\mathcal{J}_\alpha\}_\alpha$, after one step of the RG transformation we generate some correlation between the couplings. This situation occurs in many cases where one performs an effective reduction of the degrees of freedom of a system under reparametrization of the length scale. Indeed, it is a quite general fact that if one starts with a set of degrees of freedom at a given length scale L, additional degrees of freedom are generated at the length scale $2L$. A typical example is the RG flow for the Ising model in dimensions $d \approx 4$, where in the effective ϕ^4-theory one generates additional $\phi^6, \phi^8, \cdots$-terms after one RG step (see [164, 165, 163, 162, 168] for a general discussion in the approach à la Wilson and [173] for a discussion in the field-theory approach for the Ising model). Notwithstanding this, it turns out that in the field-theory RG approach [173] these terms are finite, i. e. non singular in $1/(4-d)$, so they do not need to be absorbed into the renormalization constants, and do not contribute to the critical exponents. This fact is intrinsically related to the perturbative renormalizability of the ϕ^4-theory [173], and implies that the RG equations can be written in closed form.

It is not easy to tell if the above correlation can be consistently neglected in this real-space approach, and the answer to this question could be intrinsically related to the renormalizability of the theory. In our approach we will not address this delicate point, and we will simply get rid of the above correlation between the $\mathcal{J}'_\alpha$s by assuming that they are independent, and that each of them is distributed according to a distribution $p'(\mathcal{J}')$ given by the average of M' marginalized distributions, each of which is obtained by integrating $p'_C(\{\mathcal{J}'_\alpha\}_\alpha)$ over $M'-1$ couplings

$$p'(\mathcal{J}') = \frac{1}{M'} \sum_{\alpha=1}^{M'} \int \left[\prod_{\gamma=1,\gamma\neq\alpha}^{M'} d\mathcal{J}'_\gamma\right] p'_C(\mathcal{J}'_1, \ldots, \mathcal{J}'_{\alpha-1}, \mathcal{J}', \mathcal{J}'_{\alpha+1}, \ldots, \mathcal{J}'_{M'}). \tag{6.34}$$

By plugging Eq. (6.33) into Eq. (6.34) we obtain the RG equation relating $p(\mathcal{J})$ to $p(\mathcal{J}')$

$$p'(\mathcal{J}') = \frac{1}{M'} \sum_{\alpha=1}^{M'} \int \left[\prod_{\gamma=1}^{M'} p(\mathcal{J}_\gamma)d\mathcal{J}_\gamma\right] \delta\left(\mathcal{J}' - \frac{1}{\beta}f_\alpha(\{\beta\mathcal{J}_\gamma\}_\gamma)\right). \tag{6.35}$$

A procedure along the lines of that presented in Section 6.2.1 can be applied to Eq. (6.35): once a 2^{k_0}-spin HEA has been approximated by a 2^{k_0-1}-spin HEA, one takes two realizations of the latter and couples them to obtain a system representing a 2^{k_0+1}-spin HEA, and iterates this procedure. In this way one obtains a sequence $p(\mathcal{J}) \equiv p_0(\mathcal{J}), p'(\mathcal{J}') \equiv p_1(\mathcal{J}'), p''(\mathcal{J}'') \equiv p_2(\mathcal{J}''), \dots$ physically representing the RG flow of the disorder distribution.

In the numerical implementation $p(\mathcal{J})$ and $p'(\mathcal{J}')$ are represented by two populations, and the RG equations (6.35) are implemented in population dynamics by generalizing Routine 1. The numerical implementation of Eq. (6.35) shows that the main qualitative features of the $k_0 = 2$-case stay the same here. In particular, there is a finite value of β, that we will call β_c^{RS}, such that for $\beta < \beta_c^{RS}$ $p_k(\mathcal{J})$ converges to the high-temperature fixed point $\delta(\mathcal{J})$ as k is increased, while for $\beta > \beta_c^{RS}$ the width of $p_k(\mathcal{J})$ is an increasing function of k, and $p_k(\mathcal{J})$ converges to the low-temperature fixed point. If one iterates Eq. (6.35) with $\beta = \beta_c^{RS}$, the iteration converges to a finite critical-fixed-point $p_*(\mathcal{J})$.

The critical fixed point $p_*(\mathcal{J})$ is obtained by implementing Routine 2, and is depicted in Fig. 6.4 as a function of $\mathcal{J}$ for a given σ-value and $k_0 = 3, 4$.

The matrix $\mathcal{M}_{\mathcal{J},\mathcal{J}'}^{RS}$ linearizing the RG transformation in the neighborhood of $p_*(\mathcal{J})$ is defined in the same way as in Eq. (6.28), and its eigenvalue $\lambda^{(n_*)}$ defined by Eq. (I.14) yields the critical exponent ν defined by Eq. (5.14) according to Eq. (I.15).

$\lambda^{(n_*)}$ for $k_0 = 3, 4$ is depicted in Fig 6.5 as a function of σ. Fig. 6.5 shows that even though for $k_0 = 2$ $\lambda^{(n_*)}$ is significantly different from the mean-field value obtained with the replica approach, as k_0 is increased both $\lambda^{(n_*)}$ for $k_0 = 3$ and $\lambda^{(n_*)}$ for $k_0 = 4$ agree very well with the mean-field value obtained with the replica approach in the whole mean-field region $1/2 < \sigma \leq 2/3$. This is an important a posteriori test of the whole real-space RG framework presented here. The situation subtler in the non-mean-field region $\sigma > 2/3$. In this region the ϵ-expansion based on the replica approach is non-predictive, because the first few orders (5.18) of the series have a nonconvergent behavior. Still, the data of the real-space approach can be compared to that of MC simulations [65] performed on a diluted version of the HEA, where ν is an increasing function of σ in the non-mean-field region $\sigma > 2/3$, which disagrees with the results of the real-space approach, Fig. 6.5.

The real-space RG method makes precise predictions for the critical exponents of the Hierarchical Edwards-Anderson model, which are in agreement with those of the replica method in the classical region. In the non-classical region these predictions cannot be compared to those of the replica method.

There might be several reasons for this disagreement [36]. A first issue might be the smallness of k_0 in the real-space approach: it is plausible that for larger k_0 the derivative of $\lambda^{(n_*)}$ at $\sigma = 2/3_+$ turns out to be negative, in agreement with the MC results. Another issue might be that the exponent ν is not universal: the exponent ν of the HEA model studied here might be different from that of the diluted version of the HEA studied in MC simulations. Indeed, universality in non-mean-field spin glasses has never been established rigorously [75]. On the one hand, universality violation in finite-dimensional systems [12, 13] resulted from numerical studies done heretofore, even though more recent analyses based on MC simulations [91] and high-temperature expansion [51] suggest that universality holds. A third important issue might be that the couplings correlation has been neglected in the real-space

approach for $k_0 > 2$, see Eq. (6.34). Indeed, this couplings correlation might play a vital role in the non-mean-field region $2/3 < \sigma < 1$, and it might yield a radically different critical behavior of the system if one took it into account.

These issues could be investigated in some future directions of this real-space method. For instance, it would be interesting to find a way to handle couplings correlation in the real-space approach. One could then investigate the relevance of this correlation in both the mean and the non-mean-field region, and compare the resulting values of the critical exponents to those obtained with MC simulations. Another interesting future direction would be to implement this approach in the presence of an external magnetic field. Indeed, by analyzing the existence of a critical fixed point one could establish whether there is a phase transition in the non-mean-field region, which has been a hotly debated issue in the last years [89, 105], and could give some insight into the correct picture describing the low-temperature phase of the system [64]. Finally, it would be interesting to implement the present approach for more realistic spin-glass systems, like the three-dimensional EA model. Indeed, a simple analysis shows that this method can be easily generalized to models with short-range interactions built on a finite-dimensional hypercube.

Part IV

Conclusions

This thesis has investigated the implementation of renormalization-group (RG) techniques in finite-dimensional glassy systems, in order to shed light on the critical behavior of spin and structural glasses beyond mean field. In finite dimensions the existence of a phase transition in structural glasses is not well-established, and the structure of the low-temperature phase for both spin and structural glasses is fundamentally unknown and controversial. Since Wilson's RG equations emerge in a natural and simple way in ferromagnetic spin models with a hierarchical interaction structure, in this work we considered two finite-dimensional models of spin and structural glasses built on Dyson's hierarchical lattice [57].

After giving a brief introduction on spin and structural glasses in Part I, in Part II we focused on a structural-glass model built on a hierarchical lattice, the Hierarchical Random Energy Model (HREM) [33, 32]. In this study, we showed the first evidence of a non-mean-field model of a supercooled liquid undergoing a Kauzmann phase transition. On the one hand, the features of the phase transition are different from the mean-field case [53]. The free energy is found to be nonanalytical at the critical point, and our study of the correlation length of the system in the critical region shows that the data is consistent with the existence of a diverging correlation length. On the other hand, by investigating the properties of the low-temperature phase we showed that the free energy has a one-step replica-symmetry-breaking (RSB) saddle point in the low-temperature phase, describing a fragmentation of the free-energy landscape into disconnected components.

A first future direction of this work would be to generalize it to more realistic models, like 1-RSB models with p-spin interactions and $p \geq 3$, which have an entropy-crisis transition in the mean-field case: it would be interesting to build up a non-mean-field version of these models on a hierarchical lattice, and to implement a suitable generalization of the RG techniques used for the HREM to study their critical behavior. A second future direction would be to study the dynamics of the HREM and of these hierarchical 1-RSB models. In particular, 1-RSB models have a dynamical phase transition in the mean-field case mimicking the dynamical arrest in glass-formers at the glass-transition temperature predicted by the Mode Coupling Theory. If one could check whether this transition persists or is smeared out in such hierarchical counterparts of mean-field 1-RSB models, one could test directly some of the building blocks of the Random First Order Transition Theory.

In Part III we presented the study of a spin-glass model built on a hierarchical lattice, the Hierarchical Edwards-Anderson Model (HEA). Differently from the HREM, in the HEA the spins are not mere labels for the energy variables, but they are physical degrees of freedom. This fact allowed for an implementation of a RG decimation protocol, which has been implemented with two different approaches. The first approach is based on the replica method [34, 35], while the second one does not rely on the replica formalism, but on a real-space picture [36].

In the replica RG approach the infrared (IR) limit of the theory has been taken with two different methods, and both of them yield the same two-loop prediction for the ϵ-expansion of the critical exponents. This shows that the IR limit of the theory is well defined, and suggests the existence of a diverging correlation length in the system. Unfortunately, this approach makes predictions for the critical exponents only in the classical region, i. e. in the parameter region where the mean-field approximation is exact. In the non-classical region the two-loop ϵ-expansion has a nonconvergent behavior, in such a way that no conclusion can be drawn on the actual values of the critical exponents.

In the real-space RG approach a generalization of Kadanoff's block-spin decimation is implemented in spin glasses, and the resulting RG equations are worked out by means of a series of approximation steps. These equations have been solved by means of the high-temperature expansion and of the population-dynamics method, yielding consistent results. Similarly to the replica RG method, the real-space approach shows that a phase transition occurs in the HEA and that the correlation length diverges at the critical point. At variance with the replica RG method, this method makes precise predictions for the critical exponents in both the classical region, where the critical exponents are in excellent agreement with those of the replica method, and in the non-classical region. The real-space predictions in this region are in disagreement with Monte Carlo (MC) simulations done for a diluted version of the HEA. There might be several possible reasons for this disagreement: the discrepancy should disappear if better approximation steps were considered in the real-space approach, or the critical exponents of the HEA model defined here might be different from those of the diluted HEA, i. e. universality might be violated.

There are several future directions for the replica and for the real-space approach. As far as the replica approach is concerned, the two-loop calculation that we have done here is a base of departure for an automated computation of the ϵ-expansion for the critical exponents. Despite its highly technical nature, the calculation of high orders of the ϵ-series would clarify whether the ϵ-expansion can be resummed and made convergent, and so whether the non-mean-field physics of the system can be considered as a small perturbation of the mean-field one. As far as the real-space approach is concerned, it would be interesting to improve the approximation scheme to check whether the disagreement with MC simulations disappears. If the disagreement does not disappear, one could test the universality of the exponents by checking directly whether the critical indices stay the same when changing the details of the quenched-disorder probability distribution. Moreover, in order to shed light on the structure of the low-temperature phase, it would be interesting to implement the real-space method in the presence of an external magnetic field and to verify the existence of a phase transition in the non-classical region, by searching for a critical fixed point of the RG equations. Indeed, the existence of a phase transition in a field is one of the fundamental elements discriminating between the RSB and the droplet picture for finite-dimensional spin glasses, and it would shed light on the features of the low-temperature phase of these systems.

Appendix A

Properties of Dyson's Hierarchical Model

A.1   Derivation of Eq. (2.5)

Let us derive Eq. (2.5) first. We start from the definition (2.4), omit any m-independent multiplicative constant to simplify the notation, and we have

$$
\begin{aligned}
p_{k+1}(m) &= \sum_{\vec{S}} \mathrm{e}^{-\beta(H_k^F[\vec{S}_1]+H_{k-1}^F[\vec{S}_2])+\beta JC_F^{k+1}\left(\frac{1}{2^{k+1}}\sum_{i=1}^{2^k} S_i\right)^2} \times \\
&\quad \times \delta\left(\frac{1}{2^{k+1}}\sum_{i=1}^{2^{k+1}} S_i - m\right)\int dm_1 dm_2 \delta\left(\frac{1}{2^k}\sum_{i=1}^{2^k} S_i - m_1\right) \times \\
&\quad \times \delta\left(\frac{1}{2^k}\sum_{i=2^k+1}^{2^{k+1}} S_i - m_2\right) \\
&= \mathrm{e}^{\beta JC_F^{k+1}m^2}\int dm_1 dm_2 \delta\left(\frac{m_1+m_2}{2}-m\right) \times \\
&\quad \times \left[\sum_{\vec{S}_1}\mathrm{e}^{-\beta H_k^F[\vec{S}_1]}\delta\left(\frac{1}{2^k}\sum_{i=1}^{2^k} S_i - m_1\right)\right] \times \\
&\quad \times \left[\sum_{\vec{S}_2}\mathrm{e}^{-\beta H_k^F[\vec{S}_2]}\delta\left(\frac{1}{2^k}\sum_{i=2^k+1}^{2^{k+1}} S_i - m_2\right)\right] \\
&= \mathrm{e}^{\beta JC_F^{k+1}m^2}\int dm_1 dm_2 \delta\left(\frac{m_1+m_2}{2}-m\right)p_k(m_1)p_k(m_2), \quad \text{(A.1)}
\end{aligned}
$$

where we set $\vec{S}_1 \equiv \{S_1,\ldots,2^k\}$, $\vec{S}_2 \equiv \{S_{2^k+1},\ldots,2^{k+1}\}$, in the first line we used Eq. (2.1) and multiplied by a factor equal to one, and in the third line we used the fact that the quantities in square brackets in the second line are equal to $p_k(m_1), p_k(m_2)$ because of the definition (2.4). By changing the variables of integration, Eq. (A.1) leads to Eq. (2.5).

A.2   Structure of the fixed points of Eq. (2.7)

Taking $H_0^F[S] = 0$, the Hamiltonian $H_k^F[\vec{S}]$ has $\pm\vec{S}$ symmetry, and thus according to Eqs. (2.4), (2.6), $\mathfrak{p}_k(m)$ is an even function of m. Hence, the simplest approximation is to assume that it is a Gaussian

$$\mathfrak{p}_k(m) = \mathrm{e}^{-r_k^F m^2}, \tag{A.2}$$

by neglecting higher powers of m in the exponential. Non-Gaussian terms will be later added in the argument of the exponential of Eq. (A.2). For the integral of $\mathfrak{p}_k(m)$ with respect to m to be finite, we have $r_k^F > 0$.

By plugging Eq. (A.2) into Eq. (2.7), we obtain a recursion equation for r_k^F

$$r_{k+1}^F = \frac{2r_k^F}{C_F} - \beta J. \tag{A.3}$$

Eq. (A.3) can be solved explicitly, and yields

$$r_k^F = \left(\frac{2}{C_F}\right)^k \left(r_0^F - \frac{\beta J}{\frac{2}{C_F} - 1}\right) + \frac{\beta J}{\frac{2}{C_F} - 1}. \tag{A.4}$$

It follows that if $\beta = \beta_{cF}$, with

$$\beta_{cF} \equiv r_0^F / J(2/C_F - 1), \tag{A.5}$$

r_k^F has a finite limit $r_* = r_0$ for $k \to \infty$. This fixed point will be called the critical fixed point. The critical fixed point is unstable, because any small deviation of β from β_{cF} would let r_k^F flow away from r_*^F towards another fixed point, as one can see from Eq. (A.4). If $\beta < \beta_{cF}$ or $\beta > \beta_{cF}$, this attractive fixed point is called the high or low-temperature fixed point respectively. According to Eq. (A.5), the critical temperature depends on the value r_0^F at the initial step of the iteration, i. e. at microscopic length scales $2^k \sim 1$. This fact is in agreement with the very general picture occurring in ferromagnetic systems like the Ising model [163], where the critical temperature is not universal, because it depends on the microscopic properties of the lattice, like the nearest-neighbor couplings between spins.

Another important feature of the solution of Eq. (A.3) is the following. Take $\beta < \beta_{cF}$ and $k \gg 1$. According to Eqs. (2.6), (A.2) and (A.4), one has

$$p_k(m) = \exp\left[-2^k \left(r_0^F - \frac{\beta J}{\frac{2}{C_F} - 1}\right) m^2\right]. \tag{A.6}$$

Eq. (A.6) shows that for large k the variable $m = 1/2^k \sum_{i=1}^{2^k} S_i$ is distributed according to a Gaussian distribution with variance proportional to $1/2^k$. This is the result that one could have guessed with the central limit theorem, supposing the spins S_i to be independent. Now take $\beta = \beta_{cF}$. According to Eqs. (2.6), (A.2) and to the fact that $r_k = r_* \forall k$, for large k one has

$$p_k(m) = \mathrm{e}^{-r_* C_F^k m^2}. \tag{A.7}$$

Eq. (A.7) shows that the distribution of m is still Gaussian, but its variance is proportional to $1/C_F^k$, while supposing the spins to be independent by means of the central limit theorem, one would predict the variance to be proportional to $1/2^k$. The physical interpretation of these facts resulting from Eqs. (A.6), (A.7) is the following. For $\beta < \beta_{cF}$ spins can be considered as independent, and so m has the k-dependence predicted by the central limit theorem. On the contrary, at the critical point strong correlations are developed, resulting in a collective behavior of spins which cannot be considered as independent anymore, and yielding a magnetization m with a k-dependence different from that predicted with the independence hypothesis.

Let us now seek for a more accurate approximation of $\mathfrak{p}_k$, by adding a quartic term in the exponential in the right-hand side of Eq. (A.2)

$$\mathfrak{p}_k(m) = e^{-(r_k^F m^2 + w_k^F m^4)}, \tag{A.8}$$

where for the integral of $\mathfrak{p}_k(m)$ with respect to m to be finite, one has $w_k^F > 0$.

In the following we will suppose that the non-Gaussian term w_k^F is small for every k, i. e. that an expansion in powers of w_k^F is meaningful. Practically speaking, this is equivalent to supposing that the above qualitative picture resulting from the Gaussian ansatz (A.2) is slightly modified from the introduction of non-Gaussian terms in Eq. (A.8). The correctness of this assumption will be tested a posteriori by checking if the resulting perturbative series for physical quantities is convergent, or if it can be made convergent with some suitable resummation technique [173]. Plugging Eq. (A.8) into Eq. (2.7) and developing in powers of w_k^F, one has

$$
\begin{aligned}
\mathfrak{p}_{k+1}(m) &= e^{-\frac{2r_k^F}{C_F}m^2 + \beta J m^2} \left\{ 1 - \frac{1}{8(r_k^F)^2} \left[3 + \frac{8m^2 r_k^F (3C_F + 2m^2 r_k^F)}{C_F^2} \right] w_k^F + \right. \\
&\quad + \frac{1}{128 C_F^4 (r_k^F)^4} [105 C_F^4 + 720 C_F^3 r_k^F m^2 + 1824 C_F^2 (r_k^F)^2 m^4 + \\
&\quad \left. + 768 C_F (r_k^F)^3 m^6 + 256 (r_k^F)^4 m^8](w_k^F)^2 + O((w_k^F)^3) \right\}.
\end{aligned} \tag{A.9}
$$

The right-hand side of Eq. (A.9) does not have the same form as the ansatz (A.8). Notwithstanding this, one can rewrite the term in braces in the right-hand side of Eq. (A.9) as an exponential up to order $(w_k^F)^2$, and obtain

$$
\begin{aligned}
\mathfrak{p}_{k+1}(m) &= \exp \left\{ - \left[\frac{2r_k^F}{C_F} - \beta J + \frac{3}{C_F r_k^F} w_k^F - \frac{9}{2C_F (r_k^F)^3} (w_k^F)^2 \right] m^2 + \right. \\
&\quad \left. - \left[\frac{2}{C_F^2} w_k^F - \frac{9}{C_F^2 (r_k^F)^2} (w_k^F)^2 \right] m^4 + O((w_k^F)^3) \right\}.
\end{aligned} \tag{A.10}
$$

Comparing Eq. (A.10) to Eq. (A.8), one has

$$
\begin{cases}
r_{k+1}^F = \frac{2r_k^F}{C_F} - \beta J + \frac{3}{C_F r_k^F} w_k^F - \frac{9}{2C_F (r_k^F)^3}(w_k^F)^2 + O((w_k^F)^3), \\
w_{k+1}^F = \frac{2}{C_F^2} w_k^F - \frac{9}{C_F^2 (r_k^F)^2}(w_k^F)^2 + O((w_k^F)^3).
\end{cases} \tag{A.11}
$$

The second line of Eq. (A.11) can be rewritten as

$$w_{k+1}^F - w_k^F = \left(\frac{2}{C_F^2} - 1 \right) w_k^F - \frac{9}{C_F^2 (r_k^F)^2} (w_k^F)^2 + O((w_k^F)^3).$$

If follows that $\sigma_F \lessgtr 3/4$ implies $2/C_F^2 \lessgtr 1$, and so $w_{k+1}^F \lessgtr w_k^F$. Hence, for $\sigma \leq 3/4$ $w_k^F \to 0$ for $k \to \infty$, and any fixed point is Gaussian, while for $\sigma_F > 3/4$ a non-Gaussian fixed point arises for $k \to \infty$. Historically, the analysis of Gaussian fixed points of Eq. (2.6) was first done in [20, 22, 21], while non-Gaussian fixed points have been studied first in [24], and their analysis was later developed in [46, 45, 44, 80]. According to the above assumption that an expansion in powers of w_k^F is meaningful, the structure of the fixed points of Eq. (2.7) discussed in the Gaussian case must still hold. Let us set

$$\epsilon_F \equiv \sigma_F - \frac{3}{4} \tag{A.12}$$

and show this explicitly in Fig. A.1, where a parametric plot of (r_k^F, w_k^F) as a function of k is depicted for three different temperatures $T < T_{cF}, T > T_{cF}$ and $T \approx T_{cF}$ for a given ϵ_F and J-value, with $\epsilon_F > 0$. The Figure shows the existence of two attractive fixed points, the high-temperature fixed point and the low-temperature fixed point, and of an unstable critical fixed point separating them, as illustrated in the Gaussian case. Given an initial condition, the parameters r_k^F, w_k^F converge to the critical fixed point only if β is equal to its critical value β_{cF}.

Let us now focus on the critical fixed point. This is obtained by setting $\beta = \beta_{cF}$ and by requiring that $r_{k+1}^F = r_k^F = r_*^F$, $w_{k+1}^F = w_k^F = w_*^F$ in Eq. (A.11)

$$\begin{cases} r_*^F &= \frac{2r_*^F}{C_F} - \beta_{cF} J + \frac{3}{C_F r_*^F} w_*^F - \frac{9}{2C_F (r_*^F)^3} (w_*^F)^2 + O((w_*^F)^3), \\ w_*^F &= \frac{2}{C_F^2} w_*^F - \frac{9}{C_F^2 (r_*^F)^2} (w_*^F)^2 + O((w_*^F)^3). \end{cases} \tag{A.13}$$

If w_*^F is nonzero, one can divide the second equality of Eq. (A.13) by w_*^F, and get

$$1 - \frac{2}{C_F^2} = -\frac{9}{C_F^2 (r_*^F)^2} w_*^F + O((w_*^F)^2). \tag{A.14}$$

Since w_*^F must be positive, we have $1 - 2/C_F^2 < 0$, i. e. $\epsilon_F > 0$. As anticipated above, a non-Gaussian critical fixed point $w_*^F \neq 0$ exists only if $\epsilon_F > 0$, and according to Eq. (A.14) it is proportional to ϵ_F. Accordingly, if $\epsilon_F \leq 0$ one has $w_*^F = 0$.
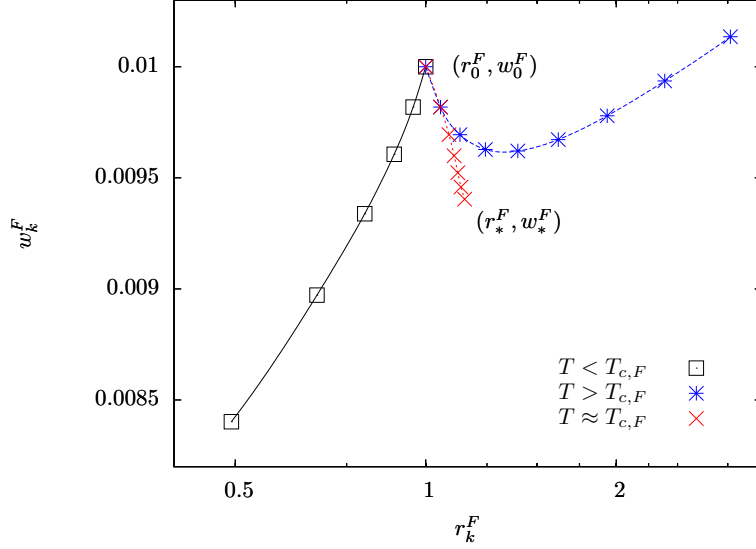
A.3   Calculation of ν_F

The critical exponent ν_F can be calculated [163] by linearizing Eq. (A.13) in the neighborhood of the critical fixed point r_*^F, w_*^F. Let us introduce the 2×2 matrix

$$\mathscr{M}_{ij}^F \equiv \left. \frac{\partial (r_{k+1}^F, w_{k+1}^F)}{\partial (r_k^F, w_k^F)} \right|_{r_k^F = r_*^F, w_k^F = w_*^F}. \tag{A.15}$$

One can show [163], that the critical exponent ν_F is related to the largest eigenvalue Λ_F of $\mathscr{M}^F$

$$\nu_F = \frac{\log 2}{\log \Lambda_F}. \tag{A.16}$$

Figure A.1. Parametric plot of (r_k^F, w_k^F) as a function of k with $\epsilon_F = 0.01, J = 1$. The black points represent (r_k^F, w_k^F) for increasing k from top to bottom, with $T < T_{cF}$. The blue points represent (r_k^F, w_k^F) for increasing k from left to right, with $T > T_{cF}$. The red points represent (r_k^F, w_k^F) for increasing k from top to bottom: here T has been dynamically adjusted as follows at each step k. At the step $k = 0$ of the iteration we consider two initial values of the temperature T_{mF}, T_{MF} such that $T_{mF} < T_{cF} < T_{MF}$. Then, we iterate the following procedure. We choose $T = (T_{mF} + T_{MF})/2$ and compute r_{k+1}^F, w_{k+1}^F as a function of r_k^F, w_k^F with Eqs. (A.11). If $r_{k+1}^F > r_k^F$, we are in the high-temperature phase, and thus we lower the upper bound on T by setting $T_{MF} \to (T_{mF} + T_{MF})/2$, otherwise we are in the low-temperature phase, and we raise the lower bound by setting $T_{mF} \to (T_{mF} + T_{MF})/2$. Then we set $k \to k + 1$ and repeat. By iterating this procedure many times, we obtain an estimate of the critical temperature T_{cF} by successive bisections of the interval $[T_{mF}, T_{MF}]$, and we also obtain an estimate of the critical fixed point r_*^F, w_*^F, which is depicted in the Figure. This bisection procedure is analog to the bisection Routine 2, illustrated in Section 6.2.1.2 for the RG approach in real space.

If $\epsilon_F \leq 0$, one has $r_*^F = \beta_{cF} J/(2/C_F - 1), w_*^F = 0$. $\mathscr{M}^F$ can be directly computed from Eq. (A.11), and one has

$$\Lambda_F = 2^{2\sigma_F - 1}. \tag{A.17}$$

Even though Eq. (A.17) has been derived by using the approximate ansatz (A.8), one can show that any ansatz including $m^6, m^8, \cdots$-terms in $\mathfrak{p}_k(m)$ would lead to Eq. (A.17). Hence, Eq. (A.17) is exact.

If $\epsilon_F > 0$, the critical fixed point r_*^F, w_*^F can be computed perturbatively as a power series in ϵ_F by observing from Eq. (A.14) that $w_*^F = O(\epsilon_F)$, and by expanding the left and the right-hand side of Eq. (A.13) in powers of ϵ_F. The result is

$$\begin{aligned}
r_*^F &= (1 + \sqrt{2})\beta_{cF} J - \frac{10}{3}(4 + 3\sqrt{2})\beta_{cF} J \log 2 \cdot \epsilon_F + O(\epsilon_F^2), \\
w_*^F &= \frac{8}{9}(3 + 2\sqrt{2})(\beta_{cF} J)^2 \log 2 \cdot \epsilon_F + O(\epsilon_F^2).
\end{aligned} \tag{A.18}$$

Using Eqs. (A.15), (A.11), (A.18), one has

$$\Lambda_F = \sqrt{2} \left(1 + \frac{2}{3} \log 2 \cdot \epsilon_F + O(\epsilon_F^2) \right). \tag{A.19}$$

Differently from Eq. (A.17), Eq. (A.19) is not exact, because it is the first order of a series in ϵ_F.

Appendix B

Calculation of ϕ_0

In order to calculate ϕ_0, let us consider Eq. (3.6) for $C = 0$. One has

$$
\begin{aligned}
\mathbb{E}_\epsilon[Z[T, \{\epsilon\}]^n] &= \sum_{\{\vec{S}_a\}_{a=1,\ldots,n}} \exp\left(\frac{\beta^2}{4} \sum_{i=1}^{2^k} \sum_{a,b=1}^{n} \delta_{S_{a,i}, S_{b,i}}\right) \tag{B.1}\\
&= \sum_{\{\vec{S}_a\}_{a=1,\ldots,n}} \exp\left(\frac{\beta^2}{4} \sum_{i=1}^{2^k} \sum_{a,b=1}^{n} \frac{1 + S_{a,i} S_{b,i}}{2}\right)\\
&= \sum_{\{\vec{S}_a\}_{a=1,\ldots,n}} \exp\left(\frac{\beta^2}{8} \sum_{i=1}^{2^k} \sum_{a,b=1}^{n} S_{a,i} S_{b,i}\right) [1 + O(n^2)]\\
&= \sum_{\{\vec{S}_a\}_{a=1,\ldots,n}} \exp\left[\frac{\beta^2}{8} \sum_{i=1}^{2^k} \left(\sum_{a=1}^{n} S_{a,i}\right)^2\right]\\
&= \sum_{\{\vec{S}_a\}_{a=1,\ldots,n}} \prod_{i=1}^{2^k} \sqrt{\frac{2}{\pi}} \int_{-\infty}^{\infty} dx_i \exp\left(-2x_i^2 + \beta x_i \sum_{a=1}^{n} S_{a,i}\right)\\
&= \prod_{i=1}^{2^k} \sqrt{\frac{2}{\pi}} \int_{-\infty}^{\infty} dx_i e^{-2x_i^2} [2\cosh(\beta x_i)]^n\\
&= \left\{\sqrt{\frac{2}{\pi}} \int_{-\infty}^{\infty} dx e^{-2x^2} \left[1 + n\log[2\cosh(\beta x)] + O(n^2)\right]\right\}^{2^k}\\
&= 1 + n 2^k \sqrt{\frac{2}{\pi}} \int_{-\infty}^{\infty} dx e^{-2x^2} \log[2\cosh(\beta x)] + O(n^2).
\end{aligned}
$$

In the second line of Eq. (B.1) we write explicitly $\delta_{S_{a,i}, S_{b,i}}$ in terms of the spins. In the third line we observe that the first addend in the exponential is $O(n^2)$, and so we don't have to calculate it because, according to Eq. (3.5), in order to compute f we need only the terms in $\mathbb{E}_\epsilon[Z[T, \{\epsilon\}]^n]$ that are linear in n. In the fifth line we write the exponential in terms of a Gaussian integral, according to the Hubbard-Stratonovich transformation [173]. In the sixth line we sum over the spins. The expression obtained in the sixth line is an explicit function of n, in such a way that in the seventh and eighth line we develop such an expression in powers of n up

to linear terms.

Plugging Eq. (B.1) in Eq. (3.5) and using Eq. (3.7), one has

$$\phi_0(T) = -\frac{1}{\beta}\sqrt{\frac{2}{\pi}}\int_{-\infty}^{\infty} dx\, e^{-2x^2}\log\left[2\cosh(\beta x)\right].$$

This calculation has been automated with a symbolic manipulation program [170], and the coefficients $\phi_i(T)$ have been computed for $0 \leq i \leq 10$.

Appendix C

Calculation of $\Upsilon_{m,0}$

From the last line of Eq. (4.6) with $C = 0$, one has

$$
\begin{aligned}
\Upsilon_{m,0}(T) &= \lim_{n \to 0} \sum_{\{\vec{S}_a\}_{a=1,\ldots,n}} \exp\left(\frac{\beta^2}{4} \sum_{i=1}^{2^k} \sum_{a,b=1}^{n} \delta_{S_{a,i},S_{b,i}}\right) \prod_{i=1}^{2^m} \delta_{S_{1,i},S_{2,i}} \qquad \text{(C.1)} \\
&= \lim_{n \to 0} \sum_{\{\vec{S}_a\}_{a=1,\ldots,n}} \exp\left(\frac{\beta^2}{4} \sum_{i=1}^{2^k} \sum_{a,b=1}^{n} \frac{1 + S_{a,i}S_{b,i}}{2}\right) \prod_{i=1}^{2^m} \delta_{S_{1,i},S_{2,i}} \\
&= \lim_{n \to 0} \sum_{\{\vec{S}_a\}_{a=1,\ldots,n}} \exp\left(\frac{\beta^2}{8} \sum_{i=1}^{2^k} \sum_{a,b=1}^{n} S_{a,i}S_{b,i}\right) \prod_{i=1}^{2^m} \delta_{S_{1,i},S_{2,i}}[1 + O(n^2)] \\
&= \lim_{n \to 0} \sum_{\{\vec{S}_a\}_{a=1,\ldots,n}} \exp\left[\frac{\beta^2}{8} \sum_{i=1}^{2^k} \left(\sum_{a=1}^{n} S_{a,i}\right)^2\right] \prod_{i=1}^{2^m} \delta_{S_{1,i},S_{2,i}} \\
&= \lim_{n \to 0} \sum_{\{\vec{S}_a\}_{a=1,\ldots,n}} \left[\prod_{i=1}^{2^k} \sqrt{\frac{2}{\pi}} \int_{-\infty}^{\infty} dx_i \exp\left(-2x_i^2 + \beta x_i \sum_{a=1}^{n} S_{a,i}\right)\right] \times \\
&\quad \times \prod_{i=1}^{2^m} \delta_{S_{1,i},S_{2,i}} \\
&= \lim_{n \to 0} \left\{ \sum_{\{\vec{S}_I^a\}_{a=1}^{n}} \left[\prod_{i=1}^{2^m} \sqrt{\frac{2}{\pi}} \int_{-\infty}^{\infty} dx_i \exp\left(-2x_i^2 + \beta x_i \sum_{a=1}^{n} S_{a,i}\right)\right] \times \right. \\
&\quad \left. \prod_{i=1}^{2^m} \delta_{S_{1,i},S_{2,i}} \right\} \times \\
&\quad \times \left\{ \sum_{\{\vec{S}_O^a\}_{a=1}^{n}} \left[\prod_{i=2^m+1}^{2^k} \sqrt{\frac{2}{\pi}} \int_{-\infty}^{\infty} dx_i \exp\left(-2x_i^2 + \beta x_i \sum_{a=1}^{n} S_{a,i}\right)\right]\right\}
\end{aligned}
$$

$$
= \lim_{n \to 0} \left\{ \sum_{\{\vec{S}_I^a\}_{a=1}^n} \left[\prod_{i=1}^{2^m} \sqrt{\frac{2}{\pi}} \int_{-\infty}^{\infty} dx_i \exp\left(-2x_i^2 + \beta x_i \sum_{a=1}^n S_{a,i} \right) \right] \times \right.
$$

$$
\left. \times \prod_{i=1}^{2^m} \delta_{S_{1,i},S_{2,i}} \right\} \times
$$

$$
\times \left\{ \prod_{i=2^m+1}^{2^k} \sqrt{\frac{2}{\pi}} \int_{-\infty}^{\infty} dx_i e^{-2x_i^2} [2\cosh(\beta x_i)]^n \right\}
$$

$$
= \lim_{n \to 0} \sum_{\{\vec{S}_I^a\}_{a=1}^n} \left[\prod_{i=1}^{2^m} \sqrt{\frac{2}{\pi}} \int_{-\infty}^{\infty} dx_i \exp\left(-2x_i^2 + \beta x_i \sum_{a=1}^n S_{a,i} \right) \right] \times
$$

$$
\times \prod_{i=1}^{2^m} \delta_{S_{1,i},S_{2,i}} [1 + O(n)]
$$

$$
= \lim_{n \to 0} \sum_{\{\vec{S}_I^a\}_{a=2}^n} \prod_{i=1}^{2^m} \sqrt{\frac{2}{\pi}} \int_{-\infty}^{\infty} dx_i \exp\left[-2x_i^2 + \beta x_i (2S_{2,i} + S_{3,i} + \cdots + S_{n,i}) \right]
$$

$$
= \lim_{n \to 0} \left\{ \prod_{i=1}^{2^m} \sqrt{\frac{2}{\pi}} \int_{-\infty}^{\infty} dx_i e^{-2x_i^2} \frac{2\cosh(2\beta x_i)}{[2\cosh(\beta x_i)]^{2-n}} \right\}
$$

$$
= \left[\sqrt{\frac{2}{\pi}} \int_{-\infty}^{\infty} dx\, e^{-2x^2} \frac{2\cosh(2\beta x)}{[2\cosh(\beta x)]^2} \right]^{2^m}
$$

In the second line of Eq. (C.1) we write explicitly $\delta_{S_{a,i},S_{b,i}}$ in terms of the spins. In the third line we observe that the first addend in the exponential is $O(n^2)$, and so we don't have to compute it in the limit $n \to 0$. In the fifth line we write the exponential in terms of a Gaussian integral, according to the Hubbard-Stratonovich transformation [173]. In the sixth line we split the sum over the spins into a sum involving spins $\vec{S}_I^a \equiv S_{a,1}, \cdots, S_{a,2^m}$, and a sum involving spins $\vec{S}_O^a \equiv S_{a,2^m+1}, \cdots, S_{a,2^k}$. In the seventh line we explicitly calculate the latter sum, and in the eighth line we observe that this is given by $1 + O(n)$. In the ninth line we drop the $O(n)$ terms, and sum over $\vec{S}_I^1$, while in the tenth line we sum over the remaining spins. The expression obtained in the tenth line is an explicit function of n, in such a way that in the last line the limit $n \to 0$ can be taken.

This calculation has been automated with a symbolic manipulation program [170], and the coefficients $\Upsilon_{m,i}(T)$ have been computed for $0 \le i \le 9$.

Appendix D

Derivation of the recurrence equations (5.9)

Plugging Eq. (5.8) into Eq. (5.5), one finds

$$
\mathscr{P}_k[Q] = \exp\left\{-\left[\left(\frac{2r_{k-1}}{C^4} - \frac{\beta^2}{4}\right)\text{Tr}[Q^2] + \frac{2w_{k-1}}{3C^6}\text{Tr}[Q^3]\right]\right\} \times \quad \text{(D.1)}
$$
$$
\times \int [dP]\exp\left[-S_{k-1}[P,Q]\right],
$$
$$
S_{k-1}[P,Q] \equiv \frac{2r_{k-1}}{C^4}\text{Tr}[P^2] + \frac{2w_{k-1}}{C^6}\text{Tr}[QP^2].
$$

The integral in Eq. (D.1) is Gaussian, and thus it can be calculated exactly by using standard formulas [173]. Indeed, defining $\forall a > b$ the index $A \equiv (a,b)$, the $n(n-1)/2$ integration variables $\{P_{ab}\}_{a<b=1,\dots,n}$ can be labeled with the index A: $\{P_{ab}\}_{a<b=1,\dots,n} \to \{P_A\}_{A=1,\dots,n(n-1)/2}$. In order to compute the Gaussian integral in Eq. (D.1), we observe that

$$
\frac{\partial^2 S_{k-1}[P,Q]}{\partial P_A \partial P_B} = \frac{8r_{k-1}}{C^4}\delta_{AB} + \frac{4w_{k-1}}{C^6}M_{AB}[Q],
$$

where

$$
M_{ab,cd}[Q] \equiv N_{ab,cd}[Q] + N_{ab,dc}[Q], \quad \text{(D.2)}
$$
$$
N_{ab,cd}[Q] \equiv \delta_{bc}Q_{da} + \delta_{ac}Q_{db}. \quad \text{(D.3)}
$$

Calculating the Gaussian integral, Eq. (D.1) becomes

$$
\mathscr{P}_k[Q] = \exp\left\{-\left[\left(\frac{2r_{k-1}}{C^4} - \frac{\beta^2}{4}\right)\text{Tr}[Q^2] + \frac{2w_{k-1}}{3C^6}\text{Tr}[Q^3]\right]\right\} \times
$$
$$
\times \left[\det\left(\frac{8r_{k-1}}{C^4}\delta_{AB} + \frac{4w_{k-1}}{C^6}M_{AB}[Q]\right)\right]^{-\frac{1}{2}}, \quad \text{(D.4)}
$$

where in Eq. (D.4) and in the following, Q-independent multiplicative constants are omitted.

Supposing that w_k is small for every k, the determinant in the right-hand side of Eq. (D.4) can now be expanded in powers of w_{k-1}. Calling **Tr** the trace over

A-type indices, we use the relation $\log \det = \mathbf{Tr} \log$ for the matrix in round brackets in Eq. (D.4)

$$\left[\det \left(\frac{8r_{k-1}}{C^4} \delta_{AB} + \frac{4w_{k-1}}{C^6} M_{AB}[Q] \right) \right]^{-\frac{1}{2}} = \tag{D.5}$$

$$\exp \left\{ -\frac{1}{2} \left[\frac{w_{k-1}}{2C^2 r_{k-1}} \mathbf{Tr}[M[Q]] - \frac{1}{2} \left(\frac{w_{k-1}}{2C^2 r_{k-1}} \right)^2 \mathbf{Tr}[M[Q]^2] + \right. \right.$$

$$\left. \left. +\frac{1}{3} \left(\frac{w_{k-1}}{2C^2 r_{k-1}} \right)^3 \mathbf{Tr}[M[Q]^3] + O(w_{k-1}^4) \right] \right\}.$$

By using the definitions (D.2) and (D.3), one has $\mathbf{Tr}[M[Q]] = 0$. Then, by using Eqs. (D.2), (D.3), one has

$$
\begin{aligned}
\mathbf{Tr}[M[Q]^2] &= \sum_{AB} M[Q]_{AB} M[Q]_{BA} \\
&= \sum_{a>b,c>d} (N_{ab,cd}[Q] + N_{ab,dc}[Q]) (N_{cd,ab}[Q] + N_{cd,ba}[Q]) \\
&= \sum_{a\neq b,c\neq d} N_{ab,cd}[Q] N_{cd,ab}[Q] \\
&= \sum_{a\neq b,c\neq d} (\delta_{bc} Q_{da} + \delta_{ac} Q_{db})(\delta_{da} Q_{bc} + \delta_{ca} Q_{bd}) \\
&= \sum_{a\neq b,c\neq d} \delta_{ca} Q_{bd}^2 \\
&= \sum_{abcd} (1 - \delta_{ab})(1 - \delta_{cd}) \delta_{ca} Q_{bd}^2 \\
&= (n-2) \sum_{ab} Q_{ab}^2 \\
&= (n-2) \mathrm{Tr}[Q^2].
\end{aligned}
\tag{D.6}
$$

In the second line of Eq. (D.6) we write the sum over the indices $A, B, \ldots$ in terms of a sum over the replica indices $a, b, \ldots$. In the third line we use the symmetry of $N_{ab,cd}[Q]$ with respect to $a \leftrightarrow b$ and rewrite the sum over $a > b$, $c > d$ in terms of a sum with $a \neq b$, $c \neq d$. In the fifth line we find out that only one of the terms stemming from the product $(\delta_{bc} Q_{da} + \delta_{ac} Q_{db})(\delta_{da} Q_{bc} + \delta_{ca} Q_{bd})$ does not vanish, because of the constraints $a \neq b$, $c \neq d$, $Q_{aa} = 0$ (see Eq. (5.2)), and because of the Kronecker δs in the sum. Once we are left with the nonvanishing term, in the sixth line we write explicitly the sum over $a \neq b$, $c \neq d$ in terms of an unconstrained sum over a, b, c, d by adding the constraints $(1 - \delta_{ab})(1 - \delta_{cd})$. In the seventh line we calculate explicitly the sum over the replica indices, and write everything in terms of the replica invariant $I_1^{(2)}[Q] \equiv \mathrm{Tr}[Q^2]$ (see Table E.1).

By following the steps shown Eq. (D.6), all the other tensorial operations can be done. In particular, one finds

$$\mathbf{Tr}[M[Q]^3] = (n-2) \mathrm{Tr}[Q^3]. \tag{D.7}$$

By plugging Eqs. (D.6), (D.7) into Eq. (D.5), and then substituting Eq. (D.5) into the recursion relation (D.4), one finds

$$
\begin{aligned}
\mathscr{P}_k[Q] \;=\; \exp\Bigg\{ &-\Bigg[\left(\frac{2r_{k-1}}{C^4} - \frac{\beta^2}{4} - \frac{n-2}{4}\left(\frac{w_{k-1}}{2C^2 r_{k-1}}\right)^2 \right) \mathrm{Tr}[Q^2] + \quad \text{(D.8)} \\
&+ \frac{1}{3}\left(\frac{2w_{k-1}}{C^6} + \frac{n-2}{2}\left(\frac{w_{k-1}}{2C^2 r_{k-1}}\right)^3 \right) \mathrm{Tr}[Q^3] + O(w_{k-1}^4) \Bigg] \Bigg\}.
\end{aligned}
$$

Comparing Eq. (D.8) to the ansatz (5.8) for $\mathscr{P}_k$, one finds the recursion relations (5.9) for the coefficients r_k, w_k.

Appendix E

Results of the two-loop RG calculation à la Wilson

Here we sketch the results of the perturbative calculation to the order w_k^5 mentioned in Section 5.1. The invariants $I_l^{(j)}[Q]$ yielding $\mathscr{P}_k[Q]$ as a fifth-degree polynomial in Q are given in Table E.1.

The recurrence RG equation (5.5) relating $\mathscr{P}_{k-1}[Q]$ to $\mathscr{P}_k[Q]$ yields a set of equations relating the coefficients $\{c_{l,k-1}^{(j)}\}_{j,l}$ to $\{c_{l,k}^{(j)}\}_{j,l}$. After a quite involved calculation, one finds that these are

$$
\begin{aligned}
c_{1,k}^{(2)} &= \frac{2c_{1,k-1}^{(2)}}{C^4} - \frac{\beta^2}{4} - \frac{n-2}{4}\left(\frac{c_{1,k-1}^{(3)}}{2C^2 c_{1,k-1}^{(2)}}\right)^2 + (2n-1)\frac{c_{1,k-1}^{(4)}}{8C^4 c_{1,k-1}^{(2)}} + \\
&\quad + \frac{c_{2,k-1}^{(4)}}{2C^4 c_{1,k-1}^{(2)}}\left[1 + \frac{n(n-1)}{4}\right] + (n-2)\frac{c_{3,k-1}^{(4)}}{8C^4 c_{1,k-1}^{(2)}} + \frac{3c_{4,k-1}^{(4)}}{8C^4 c_{1,k-1}^{(2)}} + \\
&\quad + O\left((c_{1,k-1}^{(3)})^6\right),
\end{aligned}
\tag{E.1}
$$

Table E.1. Invariants generated to the order $p = 5$. In each line of the table we show the invariants $I_1^{(j)}[Q], \ldots, I_{n_j}^{(j)}[Q]$ from left to right.

j		$I_l^{(j)}[Q]$		
2		$\mathrm{Tr}[Q^2]$		
3		$\mathrm{Tr}[Q^3]$		
4	$\mathrm{Tr}[Q^4]$	$\mathrm{Tr}[Q^2]^2$	$\sum_{a\neq c} Q_{ab}^2 Q_{bc}^2$	$\sum_{ab} Q_{ab}^4$
5	$\mathrm{Tr}[Q^5]$	$\mathrm{Tr}[Q^2]\mathrm{Tr}[Q^3]$	$\sum_{abcd} Q_{ab}^2 Q_{bc}Q_{bd}Q_{cd}$	$\sum_{abc} Q_{ab}^3 Q_{ac}Q_{bc}$

$$c_{1,k}^{(3)} = \frac{2c_{1,k-1}^{(3)}}{C^6} + \frac{n-2}{2}\left(\frac{c_{1,k-1}^{(3)}}{2C^2 c_{1,k-1}^{(2)}}\right)^3 + \frac{3n c_{1,k-1}^{(5)}}{4C^6 c_{1,k-1}^{(2)}} +$$

$$+ (n+3)\frac{3c_{2,k-1}^{(5)}}{20C^6 c_{1,k-1}^{(2)}} + \frac{9c_{3,k-1}^{(5)}}{20C^6 c_{1,k-1}^{(2)}} +$$

$$+ \frac{3c_{4,k-1}^{(5)}}{20C^6 c_{1,k-1}^{(2)}}[12 + n(n-1)] +$$

$$- \frac{3c_{1,k-1}^{(3)}}{4C^6 c_{1,k-1}^{(2)}}\left[\frac{(n-1)c_{1,k-1}^{(4)}}{2C^4 c_{1,k-1}^{(2)}} + \frac{2c_{2,k-1}^{(4)}}{C^4 c_{1,k-1}^{(2)}} + \frac{c_{3,k-1}^{(4)}}{2C^4 c_{1,k-1}^{(2)}}\right] +$$

$$+ O\left((c_{1,k-1}^{(3)})^7\right), \tag{E.2}$$

$$c_{1,k}^{(4)} = \frac{2c_{1,k-1}^{(4)}}{C^8} - \frac{n}{2}\left(\frac{c_{1,k-1}^{(3)}}{2C^2 c_{1,k-1}^{(2)}}\right)^4 + O\left((c_{1,k-1}^{(3)})^6\right), \tag{E.3}$$

$$c_{2,k}^{(4)} = \frac{2c_{2,k-1}^{(4)}}{C^8} - \frac{3}{2}\left(\frac{c_{1,k-1}^{(3)}}{2C^2 c_{1,k-1}^{(2)}}\right)^4 + O\left((c_{1,k-1}^{(3)})^6\right), \tag{E.4}$$

$$c_{3,k}^{(4)} = \frac{2c_{3,k-1}^{(4)}}{C^8} + 8\left(\frac{c_{1,k-1}^{(3)}}{2C^2 c_{1,k-1}^{(2)}}\right)^4 + O\left((c_{1,k-1}^{(3)})^6\right), \tag{E.5}$$

$$c_{4,k}^{(4)} = \frac{2c_{4,k-1}^{(4)}}{C^8} + 4\left(\frac{c_{1,k-1}^{(3)}}{2C^2 c_{1,k-1}^{(2)}}\right)^4 + O\left((c_{1,k-1}^{(3)})^6\right), \tag{E.6}$$

$$c_{1,k}^{(5)} = \frac{2c_{1,k-1}^{(5)}}{C^{10}} + \frac{n+6}{2}\left(\frac{c_{1,k-1}^{(3)}}{2C^2 c_{1,k-1}^{(2)}}\right)^5 + O\left((c_{1,k-1}^{(3)})^7\right), \tag{E.7}$$

$$c_{2,k}^{(5)} = \frac{2c_{2,k-1}^{(5)}}{C^{10}} - 40\left(\frac{c_{1,k-1}^{(3)}}{2C^2 c_{1,k-1}^{(2)}}\right)^5 + O\left((c_{1,k-1}^{(3)})^7\right), \tag{E.8}$$

$$c_{3,k}^{(5)} = \frac{2c_{3,k-1}^{(5)}}{C^{10}} + 30\left(\frac{c_{1,k-1}^{(3)}}{2C^2 c_{1,k-1}^{(2)}}\right)^5 + O\left((c_{1,k-1}^{(3)})^7\right), \tag{E.9}$$

$$c_{4,k}^{(5)} = \frac{2c_{4,k-1}^{(5)}}{C^{10}} + 5\left(\frac{c_{1,k-1}^{(3)}}{2C^2 c_{1,k-1}^{(2)}}\right)^5 + O\left((c_{1,k-1}^{(3)})^7\right). \tag{E.10}$$

Appendix F

One-loop RG calculation in the field-theory approach

In this Appendix we present the computation of the RG functions Z_g, Z_{Q^2} to order g_r^2.

In the bare theory, 1PI correlation functions are defined by the action (5.23), and they can be obtained as the derivative of the bare 1PI generating functional $\Gamma[\mathcal{Q}]$ with respect to $\mathcal{Q}_{i,ab}$. Similarly, the renormalized 1PI correlation functions are the derivatives with respect to $\mathcal{Q}$ of the generating functional $\Gamma_r[\mathcal{Q}]$ of the renormalized theory, which depends on the renormalized parameters m_r, g_r. Accordingly, $\Gamma_r[\mathcal{Q}]$ can be expanded in powers of g_r by means of the loop expansion

$$\Gamma_r[\mathcal{Q}] = \frac{1}{2}\sum_{i,j=0}^{2^k-1}\Delta_{ij}\mathrm{Tr}[\mathcal{Q}_i\mathcal{Q}_j] + \frac{m_r^{3\epsilon}g_r}{3!}\sum_i \mathrm{Tr}[\mathcal{Q}_i^3]\bigg(Z_g + \tag{F.1}$$
$$+\frac{n-2}{8}m_r^{\frac{6\epsilon}{2\sigma-1}}\mathscr{I}_7 g_r^2\bigg) + O(g_r^5).$$

The Feynman diagram $\mathscr{I}_7$ is depicted in Fig. 5.1, and is equal to

$$\mathscr{I}_7 = \frac{1}{2^k}\sum_{p=0}^{2^k-1}\frac{1}{\left(m_r + \delta m + |p|_2^{2\sigma-1}\right)^3}. \tag{F.2}$$

It is easy to show that $\mathscr{I}_7$ has a finite limit for $k \to \infty$. Indeed, the propagator (5.24) in the sum in the right-hand side of Eq. (F.2) depends on p through its dyadic norm. Hence, the sum over p in the right-hand side of Eq. (F.2) can be easily transformed into a sum over all the possible values of $|p|_2$. In order to do so, we recall [139] that the number of integers $0 \leq p \leq 2^k - 1$ which satisfy $|p|_2 = 2^{-j}$ is given by 2^{-j+k-1}. This number is the volume of a shell in a space of integer numbers p, where the distance between two integers p_1, p_2 is given by the dyadic norm $|p_1 - p_2|_2$. Hence, Eq. (C.1) becomes

$$\mathscr{I}_7 = \sum_{j=0}^{k-1}2^{-j-1}\frac{1}{\left[m_r + \delta m + 2^{-j(2\sigma-1)}\right]^3} \tag{F.3}$$
$$\stackrel{k\to\infty}{=} \sum_{j=0}^{\infty}2^{-j-1}\frac{1}{\left[m_r + \delta m + 2^{-j(2\sigma-1)}\right]^3},$$

where in the second line of Eq. (F.3) the $k \to \infty$ limit has been taken, because the sum in the first line is convergent in this limit. One can also show that $\delta m = O(g_r^2)$, and thus rewrite (F.3) as

$$\mathscr{I}_7 = \sum_{j=0}^{\infty} 2^{-j-1} \frac{1}{\left[m_r + 2^{-j(2\sigma-1)}\right]^3} + O(g_r^2). \tag{F.4}$$

Looking at Eq. (F.4), we observe that $\mathscr{I}_7$ is divergent for $m_r \to 0$. In particular, the smaller m_r, the larger the values of j dominating the sum. It follows that in the IR limit $m_r \to 0$ the sum in the right-hand side of Eq. (F.4) can be approximated by an integral, because in the region $j \gg 1$ dominating the sum the integrand function is almost constant in the interval $[j, j+1]$. Setting $q \equiv 2^{-j}$, for $m_r \to 0$ we have $-q \log 2 \, dj = dq$, and

$$
\begin{aligned}
\mathscr{I}_7 &= \frac{1}{2 \log 2} \int_0^1 \frac{dq}{[m_r + q^{2\sigma-1}]^3} + O(g_r^2) \\
&= \frac{m_r^{-\frac{6\epsilon}{2\sigma-1}}}{2 \log 2} \int_0^{m_r^{-\frac{1}{2\sigma-1}}} \frac{dx}{(1 + x^{2\sigma-1})^3} + O(g_r^2) \\
&= \frac{m_r^{-\frac{6\epsilon}{2\sigma-1}}}{2 \log 2} \int_0^{\infty} \frac{dx}{(1 + x^{2\sigma-1})^3} + O(g_r^2),
\end{aligned}
\tag{F.5}
$$

where in the last line of Eq. (F.5) the $m_r \to 0$-limit has been taken. By considering the asymptotic behavior for $x \to \infty$ of the integrand function in the last line of Eq. (F.5), one finds that its integral is convergent for $\epsilon > 0$ and divergent for $\epsilon < 0$, in such a way that it has a singularity for $\epsilon \to 0^+$. Its ϵ-divergent part can be easily evaluated

$$
\begin{aligned}
\mathscr{I}_7 &= \frac{m_r^{-\frac{6\epsilon}{2\sigma-1}}}{4 \log 2} \Gamma\left(3 + \frac{1}{1-2\sigma}\right) \Gamma\left(1 + \frac{1}{1-2\sigma}\right) + O(g_r^2) \\
&= m_r^{-\frac{6\epsilon}{2\sigma-1}} \left[\frac{1}{12\epsilon \log 2} + O_\epsilon(1)\right] + O(g_r^2),
\end{aligned}
\tag{F.6}
$$

where Γ is the Euler's Gamma function, and in the second line of Eq. (F.6) we developed the right-hand side in the first line in powers of ϵ around $\epsilon = 0$, where $O_\epsilon(1)$ denotes terms which stay finite as $\epsilon \to 0$.

We now plug Eq. (F.6) into Eq. (F.1), and require that $\Gamma_r[\mathcal{Q}]$, the generating functional of the renormalized theory, is finite, i. e. that it has no terms singular in ϵ. Accordingly, we require that the ϵ-singular part of $\mathscr{I}_7$ is canceled by Z_g: this is the minimal subtraction scheme. Taking $n = 0$, this subtraction implies that

$$Z_g = 1 + \frac{1}{48\epsilon \log 2} g_r^2 + O(g_r^4). \tag{F.7}$$

A very similar calculation can be done by considering the generating functional $\Gamma[\mathcal{Q}, K]$, whose derivatives with respect to $\mathcal{Q}_{i,ab}$ and K_j yield 1PI correlation functions with $Q_{i,ab}$ and $\mathrm{Tr}[Q_j^2]$-insertions, and by introducing the corresponding

functional of the renormalized theory $\Gamma_r[\mathcal{Q}, K]$. By requiring that $\Gamma_r[\mathcal{Q}, K]$ is finite, we obtain

$$Z_{Q^2} = 1 + \frac{1}{24\epsilon \log 2} g_r^2 + O(g_r^4). \tag{F.8}$$

Eqs. (F.7), (F.8) are the one-loop renormalization constants Z_g, Z_{Q^2}.

Appendix G

Computation of the observables 6.7 in Dyson's Hierarchical Model

In order to compute the observables (6.7), it is convenient to introduce for any k a discrete magnetization variable μ taking $2^k + 1$ possible values $\{-1, -1 + 2/2^k, \cdots, 0, \cdots, 1 - 2/2^k, 1\}$, and its probability distribution

$$\pi_k(\mu) \equiv \frac{\sum_{\vec{S}} \mathrm{e}^{-\beta H_k^F[\vec{S}]} \delta\left(\frac{1}{2^k} \sum_{i=1}^{2^k} S_i = \mu\right)}{Z_k}, \tag{G.1}$$

where

$$Z_k \equiv \sum_{\vec{S}} \mathrm{e}^{-\beta H_k^F[\vec{S}]},$$

and δ denotes the Kronecker delta. Eq. (2.1) implies [57] that $\pi_k(\mu)$ satisfies a recursion equation analogous to Eq. (2.5)

$$\pi_{k+1}(\mu) = \mathrm{e}^{J\beta C_F^{k+1} \mu^2} \sum_{\mu_1, \mu_2} \pi_k(\mu_1) \pi_k(\mu_2) \delta\left(\frac{\mu_1 + \mu_2}{2} = \mu\right), \tag{G.2}$$

where a μ-independent multiplicative constant has been omitted in the right-hand side of Eq. (G.2).

Given βJ, the recursion equation (G.2) can be iterated numerically $k_0 - 1$ times in 2^{k_0} operations. Once $\pi_{k_0}(\mu)$ is known, the observable $O_{k_0}^F(\beta J)$ can be easily computed. Indeed, according to Eqs. (6.7), (6.4), we have

$$O_{k_0}^F(\beta J) = \frac{\mathbb{E}_{\vec{S}}\left[\left(\frac{1}{2^{k_0-1}} \sum_{i=1}^{2^{k_0-1}} S_i\right)\left(\frac{1}{2^{k_0-1}} \sum_{i=2^{k_0-1}+1}^{2^{k_0}} S_i\right)\right]}{\mathbb{E}_{\vec{S}}\left[\left(\frac{1}{2^{k_0-1}} \sum_{i=1}^{2^{k_0-1}} S_i\right)^2\right]}. \tag{G.3}$$

The numerator of Eq. (G.3) is

$$\mathbb{E}_{\vec{S}}\left[\left(\frac{1}{2^{k_0-1}}\sum_{i=1}^{2^{k_0-1}}S_i\right)\left(\frac{1}{2^{k_0-1}}\sum_{i=2^{k_0-1}+1}^{2^{k_0}}S_i\right)\right] =$$

$$= \frac{1}{Z_{k_0}}\sum_{\vec{S}}\exp\left[-\beta\left(H_{k_0-1}^F[\vec{S}_1]+H_{k_0-1}^F[\vec{S}_2]\right)+\beta JC_F^{k_0}\left(\frac{1}{2^{k_0}}\sum_{i=1}^{2^{k_0}}S_i\right)^2\right]\times$$

$$\times\left(\frac{1}{2^{k_0-1}}\sum_{i=1}^{2^{k_0-1}}S_i\right)\left(\frac{1}{2^{k_0-1}}\sum_{i=2^{k_0-1}+1}^{2^{k_0}}S_i\right)\times$$

$$\times\sum_{\mu_1,\mu_2}\delta\left(\frac{1}{2^{k_0-1}}\sum_{i=1}^{2^{k_0-1}}S_i=\mu_1\right)\delta\left(\frac{1}{2^{k_0-1}}\sum_{i=2^{k_0-1}+1}^{2^{k_0}}S_i=\mu_2\right)$$

$$= \frac{Z_{k_0-1}^2}{Z_{k_0}}\sum_{\mu_1,\mu_2}e^{\beta JC_F^{k_0}\left(\frac{\mu_1+\mu_2}{2}\right)^2}\mu_1\mu_2\pi_{k_0-1}(\mu_1)\pi_{k_0-1}(\mu_2), \tag{G.4}$$

where $S_1\equiv\{S_1,\cdots,S_{2^{k_0-1}}\}, S_2\equiv\{S_{2^{k_0-1}+1},\cdots,S_{2^{k_0}}\}$, and in the first line of Eq. (G.4) we used the recurrence relation (2.1), and we multiplied by a factor equal to one, while in the second line we used the definition (G.1). By following the same steps as in Eq. (G.4), the denominator in Eq. (G.3) is

$$\mathbb{E}_{\vec{S}}\left[\left(\frac{1}{2^{k_0-1}}\sum_{i=1}^{2^{k_0-1}}S_i\right)^2\right]=\frac{Z_{k_0-1}^2}{Z_{k_0}}\sum_{\mu_1,\mu_2}e^{\beta JC_F^{k_0}\left(\frac{\mu_1+\mu_2}{2}\right)^2}\mu_1^2\pi_{k_0-1}(\mu_1)\pi_{k_0-1}(\mu_2).$$
$$\tag{G.5}$$

By dividing Eq. (G.4) by Eq. (G.5), the multiplicative constants cancel out, and we are left with

$$O_{k_0}^F(\beta J)=\frac{\sum_{\mu_1,\mu_2}e^{\beta JC_F^{k_0}\left(\frac{\mu_1+\mu_2}{2}\right)^2}\mu_1\mu_2\pi_{k_0-1}(\mu_1)\pi_{k_0-1}(\mu_2)}{\sum_{\mu_1,\mu_2}e^{\beta JC_F^{k_0}\left(\frac{\mu_1+\mu_2}{2}\right)^2}\mu_1^2\pi_{k_0-1}(\mu_1)\pi_{k_0-1}(\mu_2)}. \tag{G.6}$$

The right-hand side of Eq. (G.6) can be computed in 2^{k_0} operations.

Appendix H

Solution of the real-space RG equations with the high-temperature expansion

In this Appendix we show how the RG equations (6.20) can be solved with a systematic expansion in powers of β, by illustrating an explicit example where this expansion is performed up to order β^4.

Expanding in powers of β the arctanh term in the right-hand side of Eq. (6.20) we have

$$\begin{cases} m'_2 &= \frac{C^4}{2}m_2 + \frac{C^4}{2}\beta^2(m_2)^2 + \frac{C^8}{8}\beta^2(m_2)^2 - \frac{C^8}{24}\beta^2 m_4, \\ m'_4 &= \frac{3C^8}{16}(m_2)^2 + \frac{C^8}{16}m_4. \end{cases} \tag{H.1}$$

An important feature of Eq. (H.1) is that it reproduces the fact that for $\sigma < 1/2$ the thermodynamic limit is ill-defined, as we discussed in Part III, Eq. (4.12). In order to see this, let us look at the first line of Eq. (H.1). The first addend in the right-hand side is the $O(\beta^2)$-term resulting from the β-expansion of the term in square brackets in the right-hand side of Eq. (6.20), while the other addends are $O(\beta^4)$-terms. Keeping only the first term and using Eq. (2.13), we have $m'_2 = 2^{1-2\sigma}m_2$. Accordingly, if $\sigma < 1/2$ we have $m'_2 > m_2$, i. e. the variance of the coupling $\mathcal{J}$ increases at each RG step, in such a way that in the thermodynamic limit $k \to \infty$ the interaction energy diverges, and the model is ill-defined. On the other hand, Eq. (H.1) does not reproduce the condition $\sigma < 1$. This fact will emerge also in the numerical solution of the RG equations (6.19), and it will be discussed in Section 6.2.1.1.

Eq. (H.1) is formally analogous to Eq. (A.11) for DHM, and to Eq. (5.9), (E.1), (E.2) for the HEA. Accordingly, it is easy to see that Eq. (H.1) has a stable high-temperature fixed point $m_2 = m_4 = 0$, and a stable low-temperature fixed point $m_2 = m_4 = \infty$. These fixed points are separated by an unstable critical fixed point $m_2 = m_2^*, m_4 = m_4^*$. By iterating k times Eq. (H.1) we generate the sequence m_{2k}, m_{4k}, and we depict the flow $\{m_{2k}, m_{4k}\}_k$ in Fig. H.1 for different values of the temperature. Fig. H.1 shows that there is a value of the temperature T_c^{RS} such that

for $T = T_c^{RS}$ $\{m_{2\,k}, m_{4\,k}\}_k$ converges to m_2^*, m_4^*, while for $T \gtrless T_c^{RS}$ $\{m_{2\,k}, m_{4\,k}\}_k$ converges to the high or low-temperature fixed point respectively.
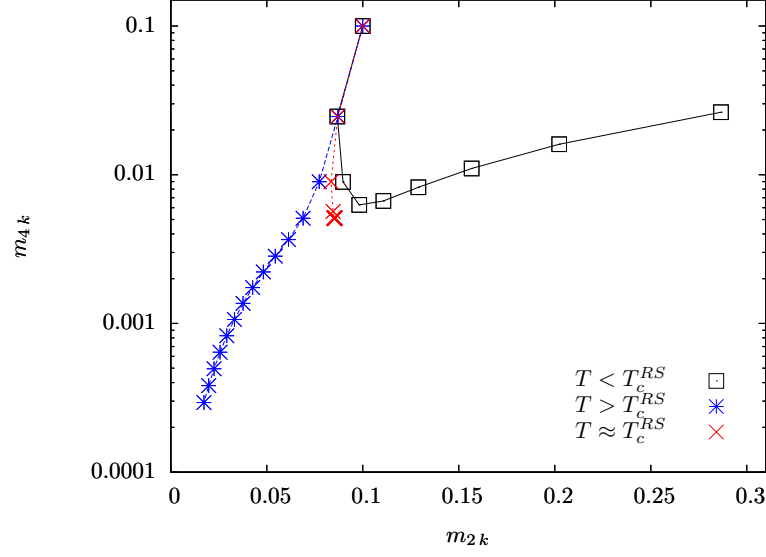
Figure H.1. Parametric plot of $(m_{2\,k}, m_{4\,k})$ as a function of k with $\sigma = 0.6$. The black points represent $(m_{2\,k}, m_{4\,k})$ for increasing k from left to right, with $T < T_c^{RS}$. The blue points represent $(m_{2\,k}, m_{4\,k})$ for increasing k from top to bottom, with $T > T_c^{RS}$. The red points represent $(m_{2\,k}, m_{4\,k})$ for increasing k from top to bottom: here T has been dynamically adjusted to T_c^{RS} at each step k with the same procedure as that described in the Caption of Fig A.1 for DHM.

We now use the same procedure as that illustrated in Section A.2 to calculate m_2^*, m_4^*, by taking $\beta = \beta_c^{RS}$ in such a way that Eq. (H.1) has a nontrivial fixed point $m_a = m_a' = m_a^*$

$$\begin{cases} m_2^* = \frac{C^4}{2}m_2^* + \frac{C^4}{2}(\beta_c^{RS})^2(m_2^*)^2 + \frac{C^8}{8}(\beta_c^{RS})^2(m_2^*)^2 - \frac{C^8}{24}(\beta_c^{RS})^2 m_4^*, \\ m_4^* = \frac{3C^8}{16}(m_2^*)^2 + \frac{C^8}{16}m_4^*. \end{cases} \quad \text{(H.2)}$$

The second line in Eq. (H.2) yields

$$m_4^* = 3C^8(m_2^*)^2/[16(1 - C^8/16)], \quad \text{(H.3)}$$

and by plugging Eq. (H.3) into the first line of Eq. (H.2) we obtain

$$m_2^* = \frac{C^4}{2}m_2^* \left\{ 1 + \left[1 + \frac{C^4}{4} + \frac{C^{12}}{2^6(-1 + C^8/16)} \right] (\beta_c^{RS})^2 m_2^* \right\}. \quad \text{(H.4)}$$

Eq. (H.4) has a solution $m_2^* = 0$ which is ruled out, and a nonzero solution $m_2^* \propto 1 - C^4/2$. In the following we will compute this solution with an expansion in the neighborhood of $\sigma = 1/2$. According to Eq. (2.13) one has $1 - C^4/2 = O(\sigma - 1/2)$, thus we have $m_2^* = O(\sigma - 1/2)$, and $m_4^* = O((\sigma - 1/2)^2)$. More precisely, from Eqs. (H.4), (H.3) we have

$$\begin{aligned} m_2^* &= \frac{3\log 2}{2(\beta_c^{RS})^2}(\sigma - 1/2) + O((\sigma - 1/2)^2), \\ m_4^* &= \frac{9(\log 2)^2}{4(\beta_c^{RS})^4}(\sigma - 1/2)^2 + O((\sigma - 1/2)^3). \end{aligned} \quad \text{(H.5)}$$

Once the critical fixed point has been found, we can linearize the RG transformation (H.1) in the neighborhood of m_2^*, m_4^* to extract the critical exponents. To this end, we introduce the 2×2 matrix

$$\mathrm{M}_{ij} \equiv \left. \frac{\partial m'_{2i}}{\partial m_{2j}} \right|_{\vec{m}=\vec{m}^*} \tag{H.6}$$

and its largest eigenvalue Λ_{RS}. From Eqs. (H.6), (H.1), (H.5) one finds

$$\Lambda_{RS} = 1 + 2 \log 2 \, (\sigma - 1/2) + O((\sigma - 1/2)^2). \tag{H.7}$$

This high-temperature expansion can be implemented to higher orders in β. More precisely, it turns out that if the expansion of the term in square brackets in Eq. (6.20) is done up to order β^{2m}, one obtains a set of m RG equations analogous to Eq. (H.1), relating $\{m_{2a}\}_{a=1,\dots,m}$ to $\{m'_{2a}\}_{a=1,\dots,m}$. The critical fixed point and the matrix M linearizing the RG transformation in its neighborhood are then extracted. The largest eigenvalue Λ_{RS} of M can be computed as a power series in $\sigma - 1/2$ up to order $(\sigma - 1/2)^{m-1}$. This computation has been done for $m \leq 5$ by means of a symbolic manipulation program [170], and the result is given in Eq. (6.21).

Appendix I

Numerical discretization of the matrix $\mathscr{M}^{RS}$ in the $k_0 = 2$-approximation

In this Section we describe the numerical computation of the matrix $\mathscr{M}^{RS}$ and of its spectrum through a discretization of the continuous variable $\mathcal{J}$.

Suppose that by iterating Routine 2 we computed the critical fixed point $p_*(\mathcal{J}) \leftrightarrow \{\mathcal{J}_i\}_i$. As shown in Fig. 6.4, $p_*(\mathcal{J})$ has a compact support $[-\mathcal{J}_{\mathrm{MAX}}, \mathcal{J}_{\mathrm{MAX}}]$, where $\mathcal{J}_{\mathrm{MAX}}$ is defined by Eq. (6.24). This feature of the critical fixed point suggests a rather natural way to compute $\mathscr{M}^{RS}_{\mathcal{J}, \mathcal{J}'}$, based on a discretization of the continuous variable $\mathcal{J}$ in the compact interval $[-\mathcal{J}_{\mathrm{MAX}}, \mathcal{J}_{\mathrm{MAX}}]$. Let us consider

$$\mathcal{J}(i) \equiv \left[\frac{1}{2} + (i-1) \right] \frac{2\mathcal{J}_{\mathrm{MAX}}}{B} - \mathcal{J}_{\mathrm{MAX}}, \ \forall i = 1, \ldots, B, \tag{I.1}$$

and the $B \times B$ matrix

$$\mathfrak{M}_{ij} \equiv \mathscr{M}^{RS}_{\mathcal{J}(i), \mathcal{J}(j)}. \tag{I.2}$$

The matrix $\mathfrak{M}$, and so $\mathscr{M}^{RS}$, can be easily computed numerically with a population-dynamics routine which is quite similar to Routine 1.

In Fig. I.1 we depict $\mathscr{M}^{RS}_{\mathcal{J}, \mathcal{J}'}$ as a function of $\mathcal{J}, \mathcal{J}'$, computed by means of Eq. (I.2) for a given σ-value, and we show that by taking B large enough the discretization method reconstructs a smooth function of $\mathcal{J}, \mathcal{J}'$.

The eigenvalues of $\mathfrak{M}$ can be easily extracted numerically, and the eigenvalues of $\mathscr{M}^{RS}$, which are related to the critical exponents, can be easily obtained from those of $\mathfrak{M}$ as follows. The n-th eigenvalue $\lambda^{(n)}$ and the left and right eigenfunctions $\phi_n^L(\mathcal{J}), \phi_n^R(\mathcal{J})$ of $\mathscr{M}^{RS}$ are defined by

$$\int d\mathcal{J}' \mathscr{M}^{RS}_{\mathcal{J}, \mathcal{J}'} \phi_n^R(\mathcal{J}') = \lambda^{(n)} \phi_n^R(\mathcal{J}), \tag{I.3}$$

$$\int d\mathcal{J} \phi_n^L(\mathcal{J}) \mathscr{M}^{RS}_{\mathcal{J}, \mathcal{J}'} = \lambda^{(n)} \phi_n^L(\mathcal{J}'). \tag{I.4}$$
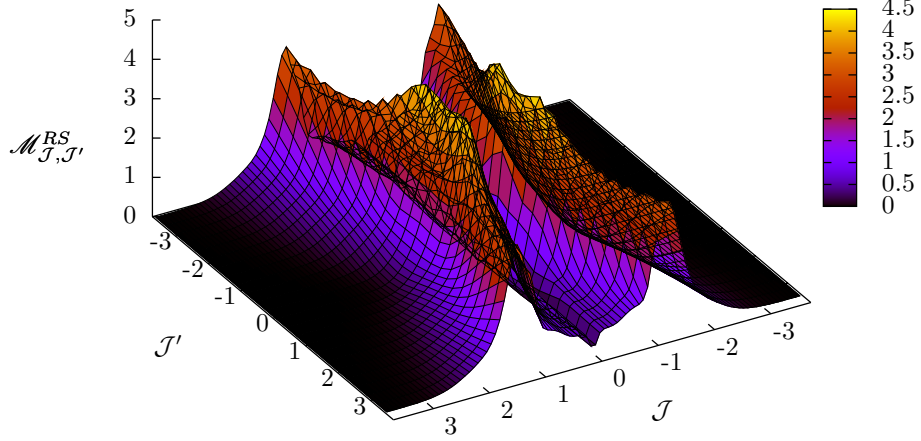
Figure I.1. Matrix $\mathscr{M}^{RS}_{\mathcal{J},\mathcal{J}'}$ as a function of $\mathcal{J}, \mathcal{J}'$ in the $k_0 = 2$-approximation obtained with the discretization method (I.2) with $\sigma = 0.6215$, $P = 10^7$, $B = 96$, $k_{\mathrm{MAX}} = 50$, $x = 0.1$. The matrix is not symmetric, and thus some eigenvalues are complex. Notwithstanding this, the explicit numerical computation of the spectrum of $\mathscr{M}^{RS}$ shows that the eigenvalue yielding the critical exponent ν is real.

The n-th eigenvalue $\lambda_D^{(n)}$ and the left and right eigenvectors $\phi_{D\,n}^L(i), \phi_{D\,n}^R(i)$ of $\mathfrak{M}$ are defined by

$$\sum_{j=1}^{B} \mathfrak{M}_{ij} \phi_{D\,n}^R(j) \;=\; \lambda_D^{(n)} \phi_{D\,n}^R(i), \tag{I.5}$$

$$\sum_{i=1}^{B} \phi_{L\,n}^R(i) \mathfrak{M}_{ij} \;=\; \lambda_D^{(n)} \phi_{D\,n}^L(j). \tag{I.6}$$

If we multiply Eqs. (I.5), (I.6) by $dJ \equiv 2\mathcal{J}_{\mathrm{MAX}}/B$, take the large-$B$ limit, transform the sums in Eqs. (I.5), (I.6) into integrals and use the definition (I.2), by comparing Eqs. (I.5), (I.6) to Eqs. (I.3), (I.4) we obtain the following identifications holding in the $B \to \infty$-limit

$$\lambda_D^{(n)} \times dJ \;=\; \lambda^{(n)}, \tag{I.7}$$

$$\phi_{D\,n}^R(i) \;=\; \phi_n^R(\mathcal{J}(i)), \tag{I.8}$$

$$\phi_{D\,n}^L(i) \;=\; \phi_n^L(\mathcal{J}(i)). \tag{I.9}$$

In particular, from Eq. (I.7) we can extract the eigenvalues of $\mathscr{M}^{RS}$ from those of $\mathfrak{M}$.

In order to extract the critical exponents, one should observe that there is an eigenvalue, that we will call $\lambda^{(1)}$, which can be calculated analytically and which does not contribute to ν even though it is part of the spectrum of $\mathscr{M}^{RS}$. Indeed, by multiplying Eq. (6.28) by $p_*(\mathcal{J}')$, integrating with respect to $\mathcal{J}'$ and using Eq. (6.26), we obtain

$$\int d\mathcal{J}' \mathscr{M}^{RS}_{\mathcal{J},\mathcal{J}'} p_*(\mathcal{J}') = 6 p_*(\mathcal{J}), \tag{I.10}$$

while by multiplying Eq. (6.28) by a constant A and integrating with respect to $\mathcal{J}$

we have

$$\int d\mathcal{J} A \, \mathscr{M}^{RS}_{\mathcal{J},\mathcal{J}'} = 6A. \tag{I.11}$$

Comparing Eqs. (I.10), (I.11) to Eqs. (I.3), (I.4) we have

$$
\begin{aligned}
\lambda^{(1)} &= 6, \\
\phi_1^R(\mathcal{J}) &= p_*(\mathcal{J}), \\
\phi_1^L(\mathcal{J}) &= A.
\end{aligned}
\tag{I.12}
$$

Following the very same procedure as Wilson's [163], if we iterate the RG equations (6.19) k times for $T \approx T_c^{RS}$ and then iterate l times, the difference between p_{k+l} and p_* is given by

$$
\begin{aligned}
p_{k+l}(\mathcal{J}) - p_*(\mathcal{J}) &= \int d\mathcal{J}' [(\mathscr{M}^{RS})^l]_{\mathcal{J},\mathcal{J}'} [p_k(\mathcal{J}') - p_*(\mathcal{J}')] \\
&= \int d\mathcal{J}' \sum_n (\lambda^{(n)})^l \phi_n^R(\mathcal{J}) \phi_n^L(\mathcal{J}') [p_k(\mathcal{J}') - p_*(\mathcal{J}')],
\end{aligned}
\tag{I.13}
$$

where $[(\mathscr{M}^{RS})^l]_{\mathcal{J},\mathcal{J}'}$ is the $\mathcal{J},\mathcal{J}'$-th component of the matrix $(\mathscr{M}^{RS})^l$, and in the second line of Eq. (I.13) the spectral representation of $\mathscr{M}^{RS}$ has been used. According to the third line of Eq. (I.12), the integral in the second line of Eq. (I.13) vanishes for $n = 1$ because of the normalization condition $\int d\mathcal{J}' p_k(\mathcal{J}') = \int d\mathcal{J}' p_*(\mathcal{J}') = 1$. Hence, the eigenvalue $\lambda^{(1)}$ does not contribute either to the exponential divergence of p_{k+l} from p_* nor to ν [163]. This fact is rather natural, because the eigenvalue $\lambda^{(1)} = 6$ is an artefact of the $k_0 = 2$-approximation, where a 2^2-spin HEA model with exactly six couplings $\{\mathcal{J}_\alpha\}_\alpha$ is reduced to a 2-spin HEA. This fact will be elucidated further in Section 6.2.2 when illustrating the $k_0 > 2$-approximations. Indeed also for $k_0 > 2$ there is an eigenvalue $\lambda^{(1)} = 2^{k_0}(2^{k_0} - 1)/2$ which depends explicitly on the approximation degree k_0, but which does not contribute to ν.

The eigenvalue of $\mathscr{M}^{RS}$ determining ν is easily found by defining n_* in such a way that

$$|\lambda^{(n_*)}| = \max_n(|\lambda^{(n)}|) \text{ and } \int d\mathcal{J} \phi_{n_*}^L(\mathcal{J}) [p_k(\mathcal{J}) - p_*(\mathcal{J})] \neq 0, \tag{I.14}$$

and by observing that [163] the critical exponent ν defined by Eq. (5.14) is given by

$$\nu = \frac{\log 2}{\log \lambda^{(n_*)}}. \tag{I.15}$$

Part V

Reprints of the papers

PHYSICAL REVIEW LETTERS

Hierarchical Random Energy Model of a Spin Glass

Michele Castellana,[1,2] Aurélien Decelle,[1] Silvio Franz,[1] Marc Mézard,[1] and Giorgio Parisi[2]

[1]*Laboratoire de Physique Théorique et Modèles Statistiques, CNRS - Université Paris Sud, Bâtiment 100, 91405 Orsay Cedex, France*
[2]*Dipartimento di Fisica, Università di Roma "La Sapienza," 00185 Rome, Italy*

We introduce a random energy model on a hierarchical lattice where the interaction strength between variables is a decreasing function of their mutual hierarchical distance, making it a non-mean-field model. Through small coupling series expansion and a direct numerical solution of the model, we provide evidence for a spin-glass condensation transition similar to the one occurring in the usual mean-field random energy model. At variance with the mean field, the high temperature branch of the free-energy is nonanalytic at the transition point.

Clarifying the nature of glassy states is a fundamental goal of modern statistical physics. Both for spin glasses [1] and for structural glasses [2], the mean-field theory of disordered systems provides a suggestive picture of laboratory glassy phenomena as the reflection of an ideal thermodynamic phase transition. Unfortunately, the development of a first principles theory of glassy systems going beyond mean field has resisted decades of intense research [3–5]. One of the main obstacles towards this goal lies in the lack of reliable real space renormalization group (RG) schemes allowing us to reduce the effective number of degrees of freedom and identify the relevant fixed points describing glassy phases. In ferromagnetic systems, an important role in the understanding of the real space RG transformation has been played by spin systems with power law interactions on hierarchical lattices [6,7]. In these models, the RG equations take the simple form of nonlinear integral equations for an unknown function (as opposed to the functional of statistical field theory), that can be solved with high precision. In this perspective, it is natural to generalize these models to spin glasses [8,9].

In this Letter, we introduce the simplest such spin-glass model, a random energy model (REM) [13,14]. As we shall see, the hierarchical REM is such that the interaction energy between subsystems scales subextensively in the system size. It thus qualifies as a non-mean-field model. We report in what follows the results of a small coupling expansion and of an algorithmic solution of the RG equations for the entropy that, exploring complementary regions of parameter space, provide the first analytic evidence in favor of an ideal glass transition in a non-mean-field model. Interestingly, this transition turns out to have—as in the case of the standard REM—the character of an entropy catastrophe analogous to the one hypothesized long ago for the structural glasses [15,16].

The hierarchical REM can be defined as a system of $N = 2^k$ Ising spins with an energy function defined recursively. The recursion is started at the level of a single spin $k = 0$, with the definition of $H_0[S] = \epsilon_0(S)$, where the single spin energies are independent identically distributed (i.i.d.) random variables extracted from a distribution $\mu_0(\epsilon)$. At the level $k + 1$, we consider then two independent systems of 2^k spins $S_1 = \{S_{1i}\}$, $i = 1, \ldots, 2^k$ and $S_2 = \{S_{2i}\}$, $i = 1, \ldots, 2^k$ with Hamiltonians $H_{1k}[S_1]$ and $H_{2k}[S_2]$, respectively, and put them in interaction to form a composite system of 2^{k+1} spins and Hamiltonian

$$H_{k+1}[S_1, S_2] = H_{1k}[S_1] + H_{2k}[S_2] + \epsilon_k[S_1, S_2],$$

where the ϵ_k are i.i.d. random variables extracted from a distribution $\mu_{k+1}(\epsilon)$, chosen to have zero mean and variance $\langle \epsilon_k[S_1, S_2]^2 \rangle \sim 2^{(k+1)(1-\sigma)}$. The interaction term $\epsilon_k[S_1, S_2]$ is physically analogous to a surface interaction energy between the two subsystems. For $\sigma \in (0, 1)$, this model qualifies as a non-mean-field system, where the interaction energy between different parts of the system scales with volume to a power smaller than unity. On the contrary, when $\sigma \leq 0$, the interaction energy grows faster than the volume. A rescaling of the energy is then necessary to get a well-defined thermodynamic limit. The system behaves in this case as a mean-field model. Finally, for $\sigma > 1$, the interaction energy decreases with distance and asymptotically the model behaves as a free system. In the following, we focus on the most interesting region $0 < \sigma < 1$.

We have studied this model with two different methods. The first one is a replica study of the quenched free energy, performed through a small coupling perturbative expansion. The second one is a numerical estimate of the microcanonical entropy as a function of the energy. Both methods suggest that a REM-like finite-temperature phase transition occurs for all $\sigma \in (0, 1)$.

Perturbative computation of the free energy.—In order to make the calculations as simple as possible, we have chosen a Gaussian distribution for the energies ϵ_k. We then considered the perturbative expansion in $g \equiv 2^{1-\sigma}$ of the free energy $f(T) = f^{(m)}(T) + O(g^{m+1})$. Notice that the expansion of f to the mth order takes into account just
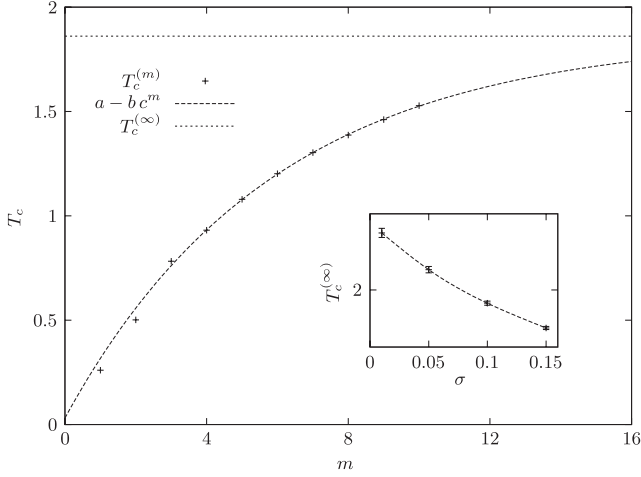
FIG. 1.   The temperatures $T_c^{(m)}$ vs m for $\sigma = .1$. Here, $T_c = 1.861 \pm .021$. Inset: T_c vs σ.
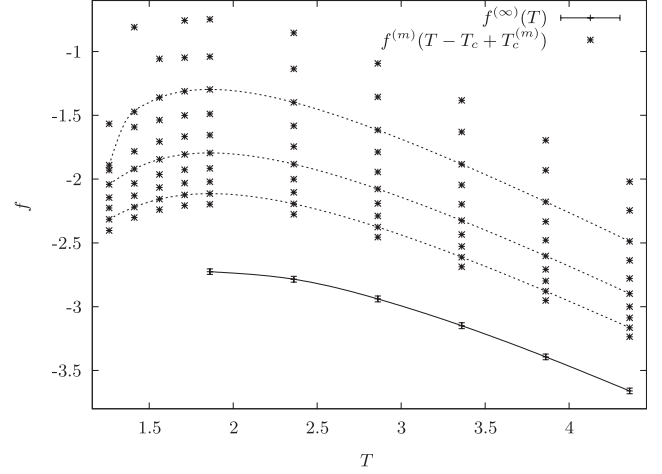

FIG. 2.   To get a better convergence for the free energy, we considered the sequence $f^{(m)}(T - T_c + T_c^{(m)})$ instead of $f^{(m)}(T)$. As $T_c^{(m)} \to T_c$ for $m \to \infty$, the two sequences have the same limit $f^{(\infty)}(T)$. Here, we see that for $\sigma = 0.1$, $f^{(m)}(T)$ has negative entropy $s^{(m)}(T)$ for $T < T_c^{(m)}$.

the interactions with range less or equal to 2^m, i.e., the first m hierarchical levels.

The computation of the free energy has been done with the replica method. In this context, it is just a mathematical tool to organize the terms of the series. We considered then the expansion of the average partition function of the system replicated n times

$$\overline{Z^n} = \sum_{S_1 \cdots S_n} \exp\left[\frac{\beta^2}{4} \sum_{j=0}^{k} g^j \sum_{i=1}^{2^{k-j}} \sum_{a,b=1}^{n} \delta_{S_a^{(j,i)} S_b^{(j,i)}} \right] \quad (1)$$

where $\beta \equiv 1/T$, and $S^{(j,i)}$ is the configuration of the ith group of spins at the jth level of the hierarchy. This representation allowed an automated computation of $f^{(m)}$ up to the value of $m = 10$.

A useful check of the method is obtained considering $\sigma < 0$. Since in this case high values of j dominate the energy in (1), correlations between the energy levels can be neglected. After rescaling the energies by $\epsilon_j \to 2^{k\sigma/2} \epsilon_j$, the free energy of the model becomes equal to the one of the standard REM [13,14] with critical temperature $T_c = \sqrt{\sum_j 2^{-\sigma j} / \log 2}$. We found that, when increasing m, $f^{(m)}$ converges to the REM free energy with exponential speed in the whole high temperature regime $\beta < \beta_c$.

We now consider $f(T)$ for $0 < \sigma < 1$. The direct inspection of the curves shows that, for $m \geq 1$, the mth order entropy $s^{(m)}(T) \equiv -df^{(m)}(T)/dT$ while positive at high temperature, becomes negative at some temperature $T_c^{(m)}$. As can be seen in Fig. 1, the sequence $T_c^{(m)}$ exhibits a good exponential convergence to a finite limit T_c for $\sigma \leq 0.15$. The stability of these data for large m clearly suggests that an entropy crisis transition is present in the model at T_c. The inset in Fig. 1 shows that T_c is a decreasing function of σ, consistently with the fact that the larger σ, the weaker the interaction strength. At high temperature also, the free-

energy series has a good exponential convergence in g (see Fig. 2).

This small g expansion gives some evidence for an entropy crisis taking place at temperature T_c. It is important to realize that this T_c cannot be simply computed from the sum of the variances of the ϵ_k: the energy correlations cannot be neglected. An entropy crisis implies the existence of a phase transition at a temperature $\geq T_c$. In a REM scenario, the phase transition would take place exactly at T_c, when the entropy vanishes. An argument in favor of such a result can be found with a one-step replica symmetry breaking ansatz. Consider the partition function (1) and suppose that the n replicas are grouped into n/x groups, so that, for any two replicas a, b in the same group, $S_a^{(j,i)} = S_b^{(j,i)}$ for all i, j. Then perform again the small g expansion, within this ansatz. To each order m, this procedure gives a free energy $f_x^{(m)}(T) = f^{(m)}(T/x)$. The maximization over x then gives $x = 1$ for $T > T_c^{(m)}$, and $x = T/T_c^{(m)}$ for $T < T_c^{(m)}$. This result is in complete analogy with the one found in the REM, so the above replica symmetry breaking Ansatz predicts a REM-like transition at $T = T_c$. In order to get distinct evidence for this scenario, we have done some numerical study.

Numerical computation of the entropy.—We exploit the hierarchical structure of the model to compute the microcanonical entropy $S_k(E)$. In order to make the computations as simple as possible, we have chosen for $\mu_k(\epsilon)$ the binomial distribution [17,18],

$$\mu_k(\epsilon) = \frac{1}{2^{M_k}} \binom{M_k}{\epsilon + \frac{M_k}{2}}.$$

At the level k, M_k is the integer part of $\gamma 2^{k(1-\sigma)}$, to have the

same scaling of the variance as in the Gaussian model. The constant γ is chosen so that for all the values of σ studied, $\lfloor(\gamma 2^{k(1-\sigma)})\rfloor/(\gamma 2^{k(1-\sigma)}) \approx 1$ for every k. Consider the disorder-dependent density of states for a sample a: $\mathcal{N}_k^a(E) = \sum_S \delta_{H_k(S),E}$. The recursion relation that defines the model's Hamiltonian implies that when two samples a and b at the level k are merged to define a sample at the level $k + 1$, the resulting density of states $\mathcal{N}_{k+1}^c(E)$ satisfies

$$\mathcal{N}_{k+1}^c(E) = \sum_{\substack{E_a, E_b, \epsilon \\ E = E_a + E_b + \epsilon}} n_k(E_a, E_b, \epsilon) \qquad (2)$$

where $n_k(E_a, E_b, \epsilon) = \sum_{S_1,S_2} \delta_{H_k^a(S_1),E_a} \times \delta_{H_k^b(S_1),E_b} \delta_{\epsilon_k(S_1,S_e),\epsilon}$ is the number of states in the composite system that have $H_a = E_a$, $H_b = E_b$ and interaction energy equal to ϵ. For given E_a and E_b, the joint distribution of the $n_k(E_a, E_b, \epsilon)$ for the different values of ϵ is multinomial with parameters $q_\epsilon = \langle n_k(E_a, E_b, \epsilon) \rangle = \mathcal{N}_k^a(E_a)\mathcal{N}_k^b(E_b)\mu_k(\epsilon)$, while n_k's with different first or second argument are independent.

Our algorithmic approach starts from the exact iteration of Eq. (2). Thanks to the use of a discrete interaction energy, the iteration time grows with k proportionally to $2^{k(3-\sigma)}$. This allowed us to reach the level $k = 12$. The results of the iteration shows that the values of the energy can be divided in bulk region of energy density around the origin where the number of states $\mathcal{N}_k(E) = e^{2^k S_k(E/2^k)}$ is exponential in the system size, and an edge region where the number of states is of order one (see Fig. 3).

In order to proceed further, we assume the existence and self-averaging property of the entropy density $S(e)$ in the thermodynamic limit. We then coarse grain our description. We discretize the energy density in the bulk region
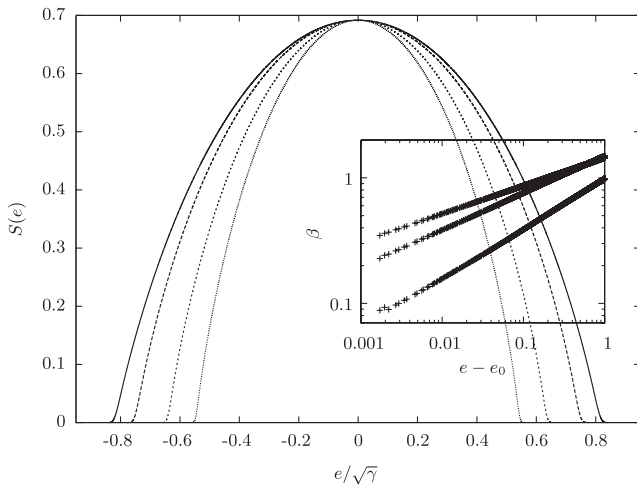
and use an approximated iteration for the entropy, where the sum (2) is approximated by its maximum term. We account for the edge region using the exact recursion for the $N_0 = 10\,000$ lowest energy levels. We can in this way iterate many times and obtain a good estimate of the thermodynamic limit behavior.

In Fig. 3, we present the average entropy density as a function of the energy density e for various values of σ. In order to identify the transition, it is more convenient to average the data obtained with a fixed energy difference from the fluctuating ground states. We can get in this way good estimates of the value of the inverse critical temperature of the model $\beta_c = s'(e_0)$. An interesting feature emerging from our analysis is that close to the ground state energy density e_0, the entropy is not analytic and behaves as $S(e) \approx \beta_c(e - e_0) + C(e - e_0)^a$ with a well fitted by the value $a = 2 - \sigma$. This behavior, when translated in the canonical formalism, implies a singularity of the free energy close to T_c, $F(T) = E_0 + \text{const} \times (T - T_c)^{(2-\sigma)/(1-\sigma)}$, corresponding to a specific heat exponent $\alpha = -\frac{\sigma}{1-\sigma}$.

Having found evidence for a thermodynamic phase transition, we turn our attention to the distribution of low-lying energy states. The REM picture suggests that, close to the ground state, the number of energy levels with given energy E are independent Poissonian variables with density $\langle \mathcal{N}_\infty(E) \rangle = e^{\beta_c(E-E_0)}$. A computation using extreme value statistics shows that the probability $Q_\ell(k)$ that the ground state and first $\ell - 1$ excited states are occupied by n levels is given by

$$Q_\ell(n) = [1 - \exp(-\ell\beta_c)]^n/(\ell\beta_c n). \qquad (3)$$

In Fig. 4, we show the $Q_\ell(n)$ obtained numerically together with a fit with the form (3). This procedure confirms the

FIG. 3. The entropy $s(e)$ vs $e/\sqrt{\gamma}$ for $\sigma = 0.9, 0.8, 0.7, 0.6$ (with $\gamma = 30, 10, 5, 5$, respectively), from the outside to the inside. Inset: power law behavior of $\beta - \beta_c$. The slopes are close to $1 - \sigma$, with $\sigma = 0.6, 0.7, 0.8$ from bottom to top.
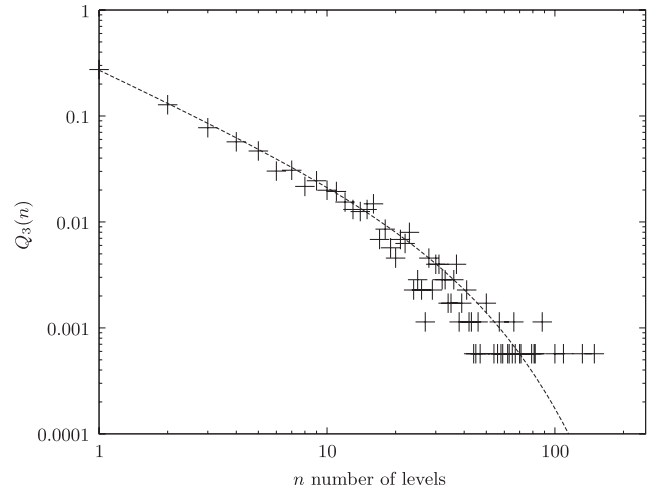

FIG. 4. Numerical data (cross) and the fitting function $Q_3(n)$ for the statistics of occupation of the ground state and the first two occupied levels. Here, $k = 10$, $\sigma = 0.6$ and $\gamma = 5$. The dashed line is a fit with the form (3) with $\beta_c = 1.20$.
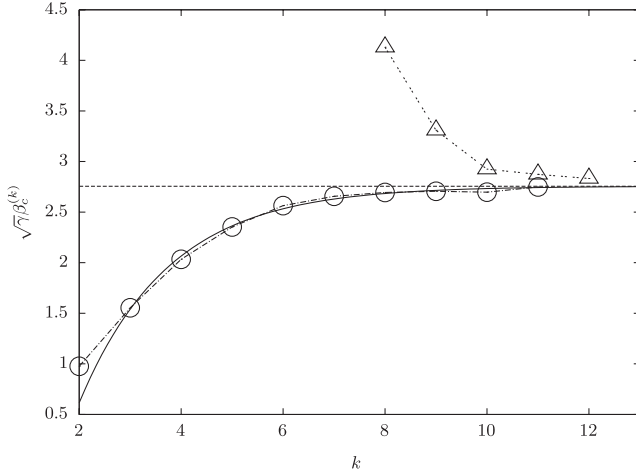
FIG. 5.   Finite volume estimation of the inverse critical temperature, $\sqrt{\gamma}\beta_c^{(k)}$ vs k, for $\sigma = 0.6$ and $\gamma = 5$ determined by (3) (circle) and by $\beta_c = s'(e_0)$ (triangles). The latter have been fitted with a function of the type $\beta_c^{(k)} = \beta_c - BC^k$ (solid line). The asymptotic value β_c is given by the dashed line.

validity of a REM-like transition, and provides an alternative way of estimating the critical temperature. As Fig. 5 shows, the two estimates for different values of k tend to the same limit from opposite directions.

Conclusions.—In this Letter, we have introduced a hierarchical, non-mean-field REM. We have analyzed it through small coupling series, through a 1RSB replica ansatz, and through an algorithmic approach. The two approaches point to the existence of a REM-like phase transition at the temperature where the entropy vanishes. At variance with the mean-field result (which predicts a discontinuity in the specific heat), one finds a nontrivial specific heat exponent at T_c. It will be interesting to study the replica structure of this hierarchical REM in order to explore other possible replica solutions at low temperatures. Another important theme of future research is the study of spin-glass models with p-body interaction [13,19,20]: at the mean-field level, these models display an entropy crisis transition similar to the one of the REM

whenever $p \geq 3$. It will be interesting to study them on hierarchical lattices.

[1] M. Mézard, G. Parisi, and M. A. Virasoro, *Spin Glass Theory and Beyond* (World Scientific, Singapore, 1987).
[2] T. Castellani and A. Cavagna, J. Stat. Mech. (2005) P05012.
[3] C. De Dominicis and I. Giardina, *Random Fields and Spin Glasses: A Field Theory Approach* (Springer, New York, 2006).
[4] J. H. Chen and T. C. Lubensky, Phys. Rev. B **16**, 2106 (1977).
[5] G. Kotliar, P. W. Anderson, and D. L. Stein, Phys. Rev. B **27**, 602 (1983).
[6] F. J. Dyson, Commun. Math. Phys. **12**, 91 (1969).
[7] P. Collet and J. Eckmann, *A Renormalization Group Analysis of the Hierarchical Model in Statistical Mechanics* (Springer-Verlag, Berlin, 1978).
[8] S. Franz, T. Jörg, and G. Parisi, J. Stat. Mech. (2009) P02002.
[9] These models should not be confused with models with local interactions on hierarchical lattices built on diamond plaquettes [10], which, starting from Ref. [11], have been widely studied in their spin-glass version and lead to weakly frustrated systems even in their mean-field limit [12].
[10] A. N. Berker and S. Ostlund, J. Phys. C **12**, 4961 (1979).
[11] S. R. McKay, A. N. Berker, and S. Kirkpatrick, Phys. Rev. Lett. **48**, 767 (1982).
[12] E. Gardner, J. Phys. (Les Ulis, Fr.) **45**, 1755 (1984).
[13] B. Derrida, Phys. Rev. Lett. **45**, 79 (1980).
[14] D. J. Gross and M. Mézard, Nucl. Phys. **B240**, 431 (1984).
[15] W. Kauzmann, Chem. Rev. **43**, 219 (1948).
[16] J. H. Gibbs and E. A. DiMarzio, J. Chem. Phys. **28**, 373 (1958).
[17] C. Moukarzel and N. Parga, Physica A (Amsterdam) **177**, 24 (1991).
[18] K. Ogure and Y. Kabashima, Prog. Theor. Phys. **111**, 661 (2004).
[19] E. Gardner, Nucl. Phys. **B257**, 747 (1985).
[20] T. R. Kirkpatrick, D. Thirumalai, and P. G. Wolynes, Phys. Rev. A **40**, 1045 (1989).

Adversarial satisfiability problem

Michele Castellana[1,2,3] and Lenka Zdeborová[3,4]

[1] Dipartimento di Fisica, Università di Roma 'La Sapienza', 00185 Rome, Italy
[2] LPTMS, CNRS and Université Paris-Sud, UMR8626, Bâtiment 100, 91405 Orsay, France
[3] Theoretical Division and Center for Nonlinear Studies, Los Alamos National Laboratory, NM 87545, USA
[4] Instiue de Physique Théorique, IPhT, CEA Saclay, and URA 2306, CNRS, 91191 Gif-sur-Yvette cedex, France
E-mail: michele.castellana@lptms.u-psud.fr and lenka.zdeborova@cea.fr

Abstract. We study the adversarial satisfiability problem, where the adversary can choose whether the variables are negated in clauses or not, in order to make the resulting formula unsatisfiable. This problem belongs to a general class of adversarial optimization problems that often arise in practice and are algorithmically much harder than the standard optimization problems. We use the cavity method to compute large deviations of the entropy in the random satisfiability problem with respect to the configurations of negations. We conclude that in the thermodynamic limit the best strategy the adversary can adopt is to simply balance the number of times every variable is negated and the number of times it is not negated. We also conduct a numerical study of the problem, and find that there are very strong pre-asymptotic effects that may be due to the fact that for small sizes exponential and factorial growth is hardly distinguishable. As a side result we compute the satisfiability threshold for balanced configurations of negations, and also the random regular satisfiability, i.e. when all variables belong to the same number of clauses.

Keywords: message-passing algorithms, random graphs, networks

J. Stat. Mech. (2011) P03023

Contents

1. Introduction

The following setting often arises in practical optimization problems. Consider two players, each of them has a given set of moves (configurations) and a cost function depending on the moves of both the players. The first player is trying to optimize a certain cost function over his set of moves (configurations), and the interest of the second player is to make this optimum as bad as possible. In the game, at first the second player (adversary) chooses his moves (a configuration), and then the first player chooses his moves. What is the best strategy (algorithm) for the adversary in the case where his set of moves is too large to be able to evaluate all the possibilities? A specific example of this adversarial optimization setting could be a police department trying to set border controls in such a way that the amount of goods smugglers can transfer is the smallest possible [1, 2], or minimax games treated in [3].

Let us call the set of moves of the adversary $\vec{u}$, and the set of moves of the first player $\vec{v}$, the cost function being $f(\vec{u}, \vec{v})$. The goal of the adversary is to find u_m that maximizes $\min_{\vec{v}} f(\vec{u}, \vec{v})$. Since in common situations both $\vec{u}$ and $\vec{v}$ have exponentially many components in the size of the system the adversarial optimization is much harder than the usual (one-player) optimization, because even evaluating the $\min_{\vec{v}} f(\vec{u}, \vec{v})$ for a given $\vec{u}$ is typically a hard optimization problem.

In the theory of algorithmic complexity the so-called NP problems are those for which it is easy (polynomial) to evaluate if a proposed solution is indeed a solution. In other words verifying a solution to an NP problem is a polynomial problem. Assume now that for a given $\vec{u}$ the problem $\exists \vec{v} \Phi(\vec{u}, \vec{v}) = \text{TRUE}$ is an NP problem (as an example consider $\Phi(\vec{u}, \vec{v}) = \text{TRUE}$ if and only if $f(\vec{u}, \vec{v}) < a$ where f is the cost function

from above, and a is a constant). Then the associated adversarial decision problem is defined as $\exists \vec{u} \ \forall \vec{v} \Phi(\vec{u}, \vec{v}) = \text{TRUE}$. Hence if the class of polynomial problems is considered easy, and the NP problems correspond to the first level of difficulty, then the adversarial problems correspond to the second level of difficulty. We could continue this construction by adding even more levels of logical quantifiers; this would lead to the so-called polynomial hierarchy of complexity classes. For more details on these notions see for instance [4, 5]. Without doubt, the theoretical understanding of hard optimization and decision problems is crucial for many areas of science, and the same holds for adversarial problems.

The most famous benchmark of an algorithmically hard problem is the K-satisfiability (K-SAT) of Boolean formulas. Call a clause a logical disjunction (operation 'or') of K variables or their negations. Given a set of N Boolean variables x_i, and a set of M clauses, the satisfiability problem consists in deciding whether all clauses can be simultaneously satisfied or not. The K-SAT problem was the first problem shown to be NP-complete, that is as hard as any other NP problems [6]. It has a large number of applications in automated verification and design. The random K-SAT problem, where variables in clauses are chosen randomly and negated with probability $1/2$, provides easy to generate hard formulas [7].

Random K-SAT thus became a common playground for new algorithms, and theoretical ideas for understanding the origin of algorithmic hardness. The statistical physics approach related to the physics of diluted spin glasses contributed tremendously to the understanding of the properties of random K-SAT formulas, see e.g. [8, 9]. Following this path in this paper we introduce a random adversarial satisfiability problem and develop a statistical mechanics framework to understand its properties. This framework can be readily applied to other random adversarial optimization and decision problems. We study the large deviation functions for the original optimization problem with respect to the moves of the adversary. The main ideas of our approach to the study of large deviations come from studies of spin glasses and the cavity method [10]–[13]. Our approach is also closely linked to the well established fact that the replicated free energy in Parisi's replica symmetry breaking (RSB) [14, 15] can be interpreted as Legendre transformation of the large deviation function. We will, however, derive our method independently of these notions, by using only the factor graph representation of the problem and the belief propagation (BP) algorithm.

One natural setting for the random adversarial satisfiability problem is to introduce the negation-variables J_{ia}, where $J_{ia} = 1$ if variable i is negated in clause a, and $J_{ia} = 0$ if not. The set of moves of the adversary is then all the possible configurations of negations $\{J_{ia}\}$, while the moves of the first player are all the possible configurations of the variables $\{x_i\}$. The graph of interactions is chosen at random as before. The goal of the adversary is to set the negations in such a way that the resulting formula is as frustrated as possible. In particular, we will be interested in the question: can the adversary make the formula unsatisfiable or not? We will call this problem random AdSAT.

An independent interest in the random AdSAT comes from the study of the random quantum satisfiability (quantum SAT) problem [16]–[18]. It was shown that if the adversary can make the random formula unsatisfiable, then also the random quantum SAT is unsatisfiable. A natural question is whether the quantum SAT is much more restrictive than the AdSAT or not.

Note also that the quantified satisfiability (QSAT) problem is another SAT-based problem that belongs to the general adversarial setting as introduced above. In the QSAT problem one introduces two types of variables: the existential variables x_i and the universal variables y_i. The QSAT then consists in deciding whether $\forall \vec{y} \exists \vec{x} G(\vec{x}, \vec{y}) = \text{TRUE}$, where $G(\vec{x}, \vec{y})$ is a satisfiability formula (with negation-variables fixed). Random ensembles of QSAT were introduced and studied in [19]. QSAT is arguably more important for industrial applications than the AdSAT that we study here. We chose the AdSAT defined as above because it is slightly simpler, and it provides information relevant to the original random SAT problem. We plan to apply our approach to the random QSAT problem in the near future.

In terms of methodology our study is also closely related to the work on optimization under uncertainty [20], where the goal is to find $\text{argmin}_{\vec{u}} \mathbb{E}_{\vec{t}} \min_{\vec{v}} f(\vec{u}, \vec{v}, t)$. In other words one needs to minimize an expectation of a result of an independent minimization, which itself can be hard to compute. In [20] the authors studied the stochastic bipartite matching problem with a message passing technique very closely related to the one we use for the adversarial SAT problem here.

The present paper is structured as follows. In section 2 we set the adversarial satisfiability problem, and describe our statistical physics approach to solve it. In section 3 we recall the standard belief and survey propagation (SP) equations for the random K-satisfiability problem. In section 4 we derive the equations to compute the large deviations with respect to the configurations of negations. In section 5 we first present and discuss the cavity result for random regular adversarial satisfiability, then we do the same for the canonical (Poissonian) random adversarial satisfiability. As a side result we obtain the satisfiability threshold for the (non-adversarial) random regular and random balanced SAT. In section 6 we compare our theoretical result to numerical simulations, performing an exhaustive search of all the solutions. Finally, in section 7 we conclude and discuss the perspectives of this work.

2. AdSAT as a large deviation calculation

The random K-SAT problem is defined as follows. Consider N Boolean variables $\{x_i\}_{i=1,\ldots,N}$, $x_i = \{0, 1\}$, and $M = \alpha N$ clauses ψ_a. Each clause depends on K random variables from the N available ones. If a variable i belongs to clause ψ_a, then we set $J_{ai} = 1$ if the variable is negated, and $J_{ia} = 0$ if it is not. The K-SAT problem can be represented via a so-called factor graph, a bipartite graph between variables (variable nodes) and clauses (function nodes), with edges between variable i and clause a if i belongs to clause a. The negation-variables can be seen as attributes of the edges. The random K-SAT instance corresponds to the case where the J_{ia}s are drawn uniformly at random. Probably, the most well known property of the random K-SAT is the existence of a phase transition at a value α_c such that if $\alpha < \alpha_c$ then with high probability (probability going to one as $N \to \infty$) there exists a configuration $\{x_i\}$ that satisfies all the clauses, and for $\alpha > \alpha_c$ no such configuration exists with high probability. We define ∂_i as the ensemble of function nodes connected to the variable node i, ∂_a as the ensemble of variable nodes connected to the function node a.

The adversarial satisfiability problem (AdSAT) is defined by drawing a random K-SAT instance as before without deciding the negation-variables $\{J_{ia}\} \equiv \mathcal{J}$. A solution to

the AdSAT problem is given by a set $\mathcal{J}$ such that the resulting instance is unsatisfiable. Just as in random K-SAT there is a threshold α_a in the random AdSAT such that for $\alpha < \alpha_a$ no solution to the AdSAT formula exists with high probability. And for $\alpha > \alpha_a$ a solution exists with high probability. We observe that $\alpha_a \leq \alpha_c$ since above α_c a random configuration of negations makes the formula unsatisfiable, recall $\alpha_c(K = 3) = 4.2667$ [21]. Also $\alpha_a \geq \alpha_p$, where $\alpha_p = 1/K$ is the percolation threshold below which the graph is basically a collection of small trees and a few single loop components, which are both satisfiable for any configuration of negations. One of the goals of the present paper is to estimate the value of the AdSAT threshold α_a.

In random K-SAT the satisfiability threshold can be found by counting the number of configurations that have a certain energy $E(\{x_i\})$ (i.e. number of unsatisfied clauses). To compute the entropy one introduces a Legendre parameter β and computes the free energy f defined as

$$\mathrm{e}^{-\beta N f(\beta)} = \sum_{\{x_i\}} \mathrm{e}^{-\beta E(\{x_i\})} = \mathrm{e}^{N[s(e) - \beta e]}, \qquad \frac{\partial s(e)}{\partial e} = \beta, \tag{1}$$

where the number of configurations having energy E is $\mathrm{e}^{S(E)}$, and the saddle-point approximation for $N \to \infty$ has been used. If $E = 0$ belongs to the support of the function $S(E)$ then the problem is in the satisfiable phase, if not than the problem is in the unsatisfiable phase. In the satisfiable phase we call $s = S(0)/N$ the entropy of satisfying configurations. The cavity method and the replica symmetry breaking serve to compute $f(\beta)$ in the thermodynamic limit $N \to \infty$ [22, 8]. There are two crucial properties that make this calculation possible. First, the energy can be written as a sum of local terms:

$$E(\{x_i\}) = \sum_a \prod_{i \in \partial a} \delta_{x_i, J_{ia}}. \tag{2}$$

Second, the underlying factor graph is locally tree-like. These computations moreover provide much more information about the problem than the value of the satisfiability threshold.

In the study of random AdSAT we will proceed analogously. We consider the number of configurations of the negations that yield a given value of the entropy of solutions s

$$s(\mathcal{J}) = \frac{1}{N} \log \left[\sum_{\{x_i\}} \prod_{a=1}^{M} \left(1 - \prod_{i \in \partial a} \delta_{x_i, J_{ia}} \right) \right]. \tag{3}$$

We define a large deviation function $\mathcal{L}(s)$ as the logarithm of this number divided by the size of the system N. Again to compute $\mathcal{L}(s)$ it is advantageous to introduce its Legendre transform

$$Z(x) = \mathrm{e}^{N\Phi(x)} = \sum_{\mathcal{J}} \mathrm{e}^{xNs(\mathcal{J})} = \mathrm{e}^{N[\mathcal{L}(s) + xs]}, \qquad \frac{\partial \mathcal{L}(s)}{\partial s} = -x, \tag{4}$$

where the saddle-point approximation for $N \to \infty$ has been used.

We stress here that $\mathcal{L}(s)$ is the large deviation function with respect to the negation-configurations; it is hence defined for a given geometry of the satisfiability formula. In what follows we assume, as is usual, that $\mathcal{L}(s)$ is self-averaging with respect to the

formula geometry, i.e. $\mathcal{L}(s)$ is almost surely the same function for two randomly chosen formulas. This assumption is a generalization of the self-averaging property of the free energy in the canonical K-SAT problem. Note also that when writing this expression we implicitly assume that the number of negation-configurations that give a certain entropy is exponential in N. If it is smaller that exponential in N computation of $\Phi(x)$ will lead to $\mathcal{L}(s) = -\infty$. We will come back to this point in section 6.

Note two special cases: for $x = 0$ the partition function (4) is simply equal to the total number of negation-configurations $\Phi(0) = K\alpha \log 2$; for $x = 1$, the partition function above is related to the annealed partition function, $\Phi(1) = \log 2 + \alpha \log(2^K - 1)$.

The major difficulty in calculating $\Phi(x)$, for a general value of x, is that the entropy $s(\mathcal{J})$ is not defined as a sum of local terms. On the other hand the geometry of the underlying factor graph is still tree-like in the random AdSAT, hence for any configuration of negations $\mathcal{J}$ we can apply the cavity method (with replica symmetry breaking if needed) to compute the entropy $s(\mathcal{J})$. In the cavity method, as is reminiscent of the Bethe approximation, the entropy (or more generally Bethe free energy) can be written as a sum of local terms. This fact enables us to calculate $\Phi(x)$.

The statistical physics treatment of the random K-SAT problem among others led to a discovery that the replica symmetry breaking approach is needed [22, 8, 9] in order to correctly compute the entropy close to the satisfiability threshold α_c. In other words, in that region the space of solutions splits into well ergodically separated clusters. We define the complexity function Σ as the logarithm of the total number of clusters per variable. The value of the complexity can then be computed with the survey propagation equations [8]. At the satisfiability threshold the complexity goes to zero, whereas the entropy density of solutions is a positive number even at the threshold. With this in mind it will be useful to define also

$$\mathrm{e}^{N\Phi_{\mathrm{SP}}(x)} = \sum_{\mathcal{J}} \mathrm{e}^{xN\Sigma(\mathcal{J})} = \mathrm{e}^{N[\mathcal{L}_{\mathrm{SP}}(\Sigma) + x\Sigma]}, \qquad \frac{\partial \mathcal{L}_{\mathrm{SP}}(\Sigma)}{\partial \Sigma} = -x, \tag{5}$$

where $\mathcal{L}_{\mathrm{SP}}(\Sigma)$ is the entropy density of negation-configurations that give a certain complexity function Σ, and the saddle-point approximation for $N \to \infty$ has been used.

3. Reminder of equations for belief and survey propagation

With the notation introduced in section 2 we write the belief propagation equations and the Bethe entropy as derived, e.g., in [23, 24]. These equations are asymptotically exact on locally tree-like graphs as long as all the correlation length scales are finite. If they are not then splitting the phase space into clusters such that within each cluster the correlations decay again might be possible. SP then estimates the total number of such clusters [8], and it does so asymptotically exactly at least close enough to the satisfiability threshold [25, 9].

Denoting by $\{m_{ia}, \hat{m}_{ai}\}$ the BP (SP) messages, we write the BP (SP) fixed-point equations as

$$m_{ia} = g_{ia}(\{\hat{m}_{bi}\}_{b \in \partial i \backslash a}, \{J_{bi}\}_{b \in \partial i}), \tag{6}$$

$$\hat{m}_{ai} = \hat{g}_{ai}(\{m_{ja}\}_{j \in \partial a \backslash i}, \{J_{ja}\}_{j \in \partial a}). \tag{7}$$

In the BP case, the messages read [24] $m_{ia} = \{\nu_{ia}^0, \nu_{ia}^1\}$, $\hat{m}_{ai} = \{\hat{\nu}_{ai}^0, \hat{\nu}_{ai}^1\}$, and

$$
\begin{aligned}
g_{ia}^r(\{\hat{\nu}_{bi}\}_{b\in\partial i\backslash a}) &= \frac{\prod_{b\in\partial i\backslash a} \hat{\nu}_{bi}^r}{\prod_{b\in\partial i\backslash a} \hat{\nu}_{bi}^0 + \prod_{b\in\partial i\backslash a} \hat{\nu}_{bi}^1}, \\
\hat{g}_{ai}^r(\{\nu_{ja}\}_{j\in\partial a\backslash i}, \{J_{ja}\}_{j\in\partial a}) &= \frac{1 - \delta_{r,J_{ai}} \prod_{j\in\partial a\backslash i} \nu_{ja}^{J_{ja}}}{2 - \prod_{j\in\partial a\backslash i} \nu_{ja}^{J_{ja}}},
\end{aligned}
\tag{8}
$$

where $r = 0, 1$. In the SP case, $m_{ia} = \{Q_{ia}^S, Q_{ia}^U, Q_{ia}^*\}$, $\hat{m}_{ai} = \hat{Q}_{ai}$, and

$$
\begin{aligned}
g_{ia}^*(\{J_{bi}\}_{b\in\partial i}, \{\hat{Q}_{bi}\}_{b\in\partial i\backslash a}) &= C \prod_{b\in\partial i\backslash a} (1 - \hat{Q}_{bi}), \\
g_{ia}^S(\{J_{bi}\}_{b\in\partial i}, \{\hat{Q}_{bi}\}_{b\in\partial i\backslash a}) &= C \prod_{b\in\mathcal{U}_{ia}} (1 - \hat{Q}_{bi}) \left[1 - \prod_{b\in\mathcal{S}_{ia}} (1 - \hat{Q}_{bi})\right], \\
g_{ia}^U(\{J_{bi}\}_{b\in\partial i}, \{\hat{Q}_{bi}\}_{b\in\partial i\backslash a}) &= C \prod_{b\in\mathcal{S}_{ia}} (1 - \hat{Q}_{bi}) \left[1 - \prod_{b\in\mathcal{U}_{ia}} (1 - \hat{Q}_{bi})\right], \\
\hat{g}_{ai}(\{Q_{ja}\}_{j\in\partial a\backslash i}) &= \prod_{j\in\partial a\backslash i} Q_{ja}^U,
\end{aligned}
\tag{9}
$$

where C is a normalization constant enforcing the relation $g_{ia}^* + g_{ia}^S + g_{ia}^U = 1$, and $\mathcal{S}_{ia}, \mathcal{U}_{ia}$ are defined as

$$
\begin{aligned}
\text{if } J_{ia} = 0 &\quad \mathcal{S}_{ia} = \partial_0 i\backslash a, &\quad \mathcal{U}_{ia} = \partial_1 i, \\
\text{if } J_{ia} = 1 &\quad \mathcal{S}_{ia} = \partial_1 i\backslash a, &\quad \mathcal{U}_{ia} = \partial_0 i,
\end{aligned}
\tag{10}
$$

where $\partial_{0/1} i = \{a \in \partial i \text{ such that } J_{ia} = 0/1\}$.

If $\{m_{ia}, \hat{m}_{ai}\}$ is a fixed point of equations (6)–(7), the Bethe entropy for BP and the complexity for SP are both written in a general form

$$
s(\{J_{ia}, m_{ia}, \hat{m}_{ai}\}) = \sum_{a=1}^M \mathbb{S}_a(\{m_{ia}, J_{ia}\}_{i\in\partial a}) + \sum_{i=1}^N \mathbb{S}_i(\{\hat{m}_{ai}, J_{ia}\}_{a\in\partial i}) - \sum_{(ia)} \mathbb{S}_{ai}(m_{ia}, \hat{m}_{ai}),
\tag{11}
$$

where for BP

$$
\begin{aligned}
\mathbb{S}_a(\{\nu_{ia}, J_{ia}\}_{i\in\partial a}) &= \log\left(1 - \prod_{i\in\partial a} \nu_{ia}^{J_{ia}}\right), \\
\mathbb{S}_i(\{\hat{\nu}_{ai}, J_{ia}\}_{a\in\partial i}) &= \log\left(\prod_{b\in\partial i} \hat{\nu}_{bi}^0 + \prod_{b\in\partial i} \hat{\nu}_{bi}^1\right), \\
\mathbb{S}_{ai}(\nu_{ia}, \hat{\nu}_{ai}) &= \log\left(\nu_{ia}^0 \hat{\nu}_{ai}^0 + \nu_{ia}^1 \hat{\nu}_{ai}^1\right),
\end{aligned}
\tag{12}
$$

while for SP

$$\mathbb{S}_a(\{Q_{ia}, J_{ia}\}_{i \in \partial a}) = \log \left(1 - \prod_{j \in \partial a} Q_{ja}^U \right),$$

$$\mathbb{S}_i(\{\hat{Q}_{ai}, J_{ia}\}_{a \in \partial i}) = \log \left[\prod_{b \in \partial_0 i} (1 - \hat{Q}_{bi}) + \prod_{b \in \partial_1 i} (1 - \hat{Q}_{bi}) - \prod_{b \in \partial i} (1 - \hat{Q}_{bi}) \right], \quad (13)$$

$$\mathbb{S}_{ai}(Q_{ia}, \hat{Q}_{ai}) = \log \left(1 - Q_{ia}^U \hat{Q}_{ai} \right).$$

Readers unfamiliar with the interpretation and derivation of the belief and the survey propagation (8)–(10) are referred to [23, 26, 24]. However, for understanding of our method in what follows the general form (6)–(7) and (11) is sufficient.

4. Computation of the large deviations function

The most important formula of section 3 is (11): in certain regimes it gives the asymptotically exact entropy or complexity in a form factorized in local terms. The remaining complication is that now everything depends on the fixed point of the BP (SP) equations. We can, however, write

$$Z(x) = \sum_{\mathcal{J}} \int \prod_{ia} dm_{ia} d\hat{m}_{ai} e^{Nxs(\{J_{ia}, m_{ia}, \hat{m}_{ai}\})} \prod_{(ia)} \delta(m_{ia} - g_{ia}(\{\hat{m}_{bi}\}_{b \in \partial i \setminus a}, \{J_{bi}\}_{b \in \partial i}))$$

$$\times \prod_{(ia)} \delta(\hat{m}_{ai} - \hat{g}_{ai}(\{m_{ja}\}_{j \in \partial a \setminus i}, \{J_{ja}\}_{j \in \partial a})). \quad (14)$$

If we now introduce auxiliary variables $\omega_{ia} \equiv \{J_{ia}, m_{ia}, \hat{m}_{ai}\}$ the partition function defined by (4) can be re-written in the common local form

$$Z(x) = \sum_{\{\omega_{ia}\}} \left\{ \left[\prod_{a=1}^{M} \Psi_a(\{\omega_{ia}\}_{i \in \partial a}) \right] \left[\prod_{i=1}^{N} \Psi_i(\{\omega_{ia}\}_{a \in \partial i}) \right] \left[\prod_{(ia)} \Psi_{ai}(\omega_{ia}) \right] \right\}, \quad (15)$$

where

$$\Psi_a(\{\omega_{ia}\}_{i \in \partial a}) \equiv e^{x\mathbb{S}_a(\{m_{ia}, J_{ia}\}_{i \in \partial a})} \prod_{i \in \partial a} \delta(\hat{m}_{ai} - \hat{g}_{ai}(\{m_{ja}\}_{j \in \partial a \setminus i}, \{J_{ja}\}_{j \in \partial a})),$$

$$\Psi_i(\{\omega_{ia}\}_{a \in \partial i}) \equiv e^{x\mathbb{S}_i(\{\hat{m}_{ai}, J_{ai}\}_{a \in \partial i})} \prod_{a \in \partial i} \delta(m_{ia} - g_{ia}(\{\hat{m}_{bi}\}_{b \in \partial i \setminus a}, \{J_{bi}\}_{b \in \partial i})), \quad (16)$$

$$\Psi_{ai}(\omega_{ia}) \equiv e^{-x\mathbb{S}_{ai}(m_{ia}, \hat{m}_{ai})}.$$

In equation (15) and in the following the sum over ω_{ia} stands for the sum over J_{ia} and the integral over m_{ia}, $\hat{m}_{ai}$.

The probability measure in equation (15) is local and can hence be represented with an auxiliary factor graph that can be viewed as decorating the original K-SAT factor graph. Figure 1 depicts this construction.

The partition function $Z(x)$ can now be computed by implementing the general BP formalism to the auxiliary graph, just as is done in the derivation of the 1RSB equations in [24] (note indeed the close formal resemblance of our approach and the 1RSB equations).
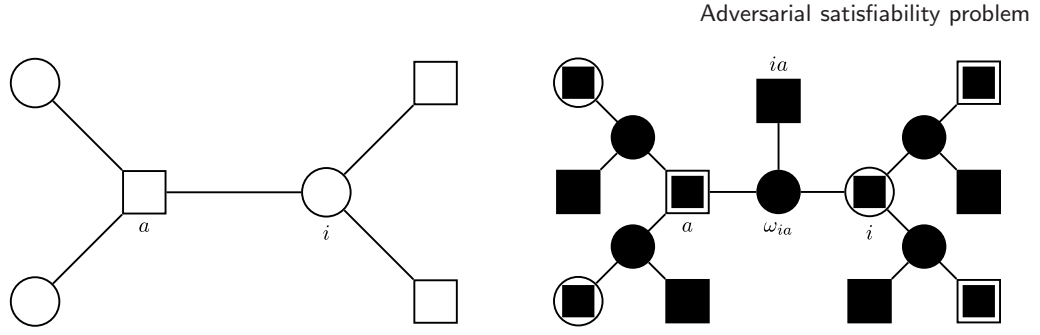
Figure 1. Left: the graph of the original K-SAT instance. Empty circles and empty squares represent variable and function nodes respectively. An edge connecting a variable node i to a function node a means that the function node ψ_a depends on x_i. Right: the auxiliary factor graph describing equation (15), built upon the graph of the K-SAT instance in the left panel. Empty squares with black-filled squares inside represent the Ψ_a function nodes, empty circles with black-filled squares inside represent Ψ_i function nodes of the auxiliary graphs. Finally, black-filled squares represent Ψ_{ia} function nodes, while black-filled circles represent ω_{ia} variable nodes of the auxiliary graph. An edge connecting ω_{ia} to a function node of the auxiliary graph means that such a function node depends on ω_{ia}.

We call $S_{ia}(\omega_{ia})$ the message going from the variable node ia to the function node a, and $\hat{S}_{ai}(\omega_{ia})$ the message going from the variable node ia to the function node i. BP equations on the auxiliary factor graph on the variables ω_{ia} then lead to fixed-point equations for these messages:

$$
\hat{S}_{ai}(\omega_{ia}) \simeq \sum_{\{\omega_{ja}\}_{j\in\partial a\setminus i}} [\hat{z}_{ai}(\{m_{ja}, J_{ja}\}_{j\in\partial a}, \hat{m}_{ai})]^x \prod_{j\in\partial a} \delta(\hat{m}_{aj} - \hat{g}_{aj}(\{m_{ka}\}_{k\in\partial a\setminus j}, \{J_{ka}\}_{k\in\partial a}))
$$
$$
\times \prod_{j\in\partial a\setminus i} S_{ja}(\omega_{ja}), \tag{17}
$$

$$
S_{ia}(\omega_{ia}) \simeq \sum_{\{\omega_{ib}\}_{b\in\partial i\setminus a}} [z_{ia}(\{\hat{m}_{bi}, J_{ib}\}_{b\in\partial i}, m_{ia})]^x \prod_{b\in\partial i} \delta(m_{ib} - g_{ib}(\{\hat{m}_{ci}\}_{c\in\partial i\setminus b}, \{J_{ci}\}_{c\in\partial i}))
$$
$$
\times \prod_{b\in\partial i\setminus a} \hat{S}_{bi}(\omega_{ib}), \tag{18}
$$

where

$$
z_{ia}(\{\hat{m}_{bi}, J_{ib}\}_{b\in\partial i}, m_{ia}) \equiv e^{\mathbb{S}_i(\{\hat{m}_{bi}, J_{ib}\}_{b\in\partial i}) - \mathbb{S}_{ai}(m_{ia}, \hat{m}_{ai})},
$$
$$
\hat{z}_{ai}(\{m_{ja}, J_{ja}\}_{j\in\partial a}, \hat{m}_{ai}) \equiv e^{\mathbb{S}_a(\{m_{ia}, J_{ia}\}_{i\in\partial a}) - \mathbb{S}_{ai}(m_{ia}, \hat{m}_{ai})}.
$$

Equations (17)–(18) can be further simplified. It is easy to check that when the fixed-point equations (6)–(7) hold, the term z_{ia} (respectively $\hat{z}_{ai}$) does not depend on the 'backward' messages m_{ia} (respectively $\hat{m}_{ai}$). Using this result, we can see that (17)–(18) are compatible with a choice of the messages S_{ia}, $\hat{S}_{ai}$ depending only on m_{ia}, J_{ia} and only on $\hat{m}_{ai}, J_{ia}$ respectively. Indeed, if we assume that $S_{ia}(\omega_{ia}) = S_{ia}(m_{ia}, J_{ai})$, and

$\hat{S}_{ai}(\omega_{ia}) = \hat{S}_{ai}(\hat{m}_{ai}, J_{ai})$, then (17)–(18) become

$$S_{ia}(m_{ia}, J_{ai}) \simeq \sum_{\{J_{bi}\}_{b\in\partial i\setminus a}} \int \prod_{b\in\partial i\setminus a} d\hat{m}_{bi} \hat{S}_{bi}(\hat{m}_{bi}, J_{bi}) \left[z_{ia}(\{\hat{m}_{bi}, J_{ib}\}_{b\in\partial i\setminus a})\right]^x$$
$$\times \, \delta(m_{ia} - g_{ia}(\{\hat{m}_{bi}\}_{b\in\partial i\setminus a}, \{J_{bi}\}_{b\in\partial i})), \tag{19}$$

$$\hat{S}_{ai}(\hat{m}_{ai}, J_{ai}) \simeq \sum_{\{J_{aj}\}_{j\in\partial a\setminus i}} \int \prod_{j\in\partial a\setminus i} dm_{ja} S_{ja}(m_{ja}, J_{ja}) \left[\hat{z}_{ai}(\{m_{ja}, J_{ja}\}_{j\in\partial a\setminus i})\right]^x$$
$$\times \, \delta(\hat{m}_{ai} - \hat{g}_{ai}(\{m_{ja}\}_{j\in\partial a\setminus i}, \{J_{ja}\}_{j\in\partial a})). \tag{20}$$

The free energy $\Phi(x)$ can then be computed using the general expression for the Bethe free entropy [24]

$$N\Phi(x) = \sum_{a=1}^{M} \mathbb{F}_a + \sum_{i=1}^{N} \mathbb{F}_i - \sum_{(ia)} \mathbb{F}_{ia}, \tag{21}$$

where

$$\mathbb{F}_a = \log\left[\sum_{\{J_{ia}\}_{i\in\partial a}} \int \prod_{i\in\partial a} dm_{ia} S_{ia}(m_{ia}, J_{ia}) e^{x\mathbb{S}_a(\{m_{ia}, J_{ia}\}_{i\in\partial a})}\right], \tag{22}$$

$$\mathbb{F}_i = \log\left[\sum_{\{J_{ia}\}_{a\in\partial i}} \int \prod_{a\in\partial i} d\hat{m}_{ai} \hat{S}_{ai}(\hat{m}_{ai}, J_{ia}) e^{x\mathbb{S}_i(\{\hat{m}_{ai}\}_{a\in\partial i})}\right], \tag{23}$$

$$\mathbb{F}_{ia} = \log\left[\sum_{J_{ia}} \int dm_{ia}\, d\hat{m}_{ai} S_{ia}(m_{ia}, J_{ia}) \hat{S}_{ai}(\hat{m}_{ai}, J_{ia}) e^{x\mathbb{S}_{ia}(m_{ia}, \hat{m}_{ia})}\right]. \tag{24}$$

Equations (19)–(20) clearly show the formal analogy with the 1RSB cavity equations [24]. The difference between equations (19)–(20) and the latter is that in the AdSAT case the negations are considered as physical degrees of freedom of the partition function $Z(x)$, and the resulting cavity equations (19)–(20) consist in a weighted average of the quantities $[z_{ia}(\{\hat{m}_{bi}, J_{ib}\}_{b\in\partial i\setminus a})]^x$, $[\hat{z}_{ai}(\{m_{ja}, J_{ja}\}_{j\in\partial a\setminus i})]^x$ over $\{J_{ia}, m_{ia}, \hat{m}_{ai}\}$. On the contrary, in the 1RSB case the only degrees of freedom are the BP messages $\{m_{ia}, \hat{m}_{ia}\}$ in such a way that the resulting 1RSB cavity equations consist in an average over $(m_{ia}, \hat{m}_{ai})$ at fixed J_{ia}s.

The biggest advantage of the formal resemblance of equations (19)–(20) to the 1RSB cavity equations is that in order to solve (19)–(20) numerically we can use the very same technique and all the related knowledge as in the case of 1RSB. We indeed use the population dynamics [22], where the distributions $S_{ia}(m_{ia}, J_{ia})$, $\hat{S}_{ai}(\hat{m}_{ai}, J_{ia})$ are represented as populations of P messages. When the size of the population P is large, we expect the populations to reproduce well the distributions $S_{ia}(m_{ia}, J_{ia})$, and $\hat{S}_{ai}(\hat{m}_{ai}, J_{ia})$. The cavity equations (19)–(20) can be written in terms of these populations. Starting from a given initial configuration, the iteration of the cavity equations yields the fixed-point populations satisfying (19)–(20). Once this fixed point is achieved the free energy $\Phi(x)$ can be computed numerically by means of (21)–(24). This is repeated for different values

of x and finally the Legendre transform $\mathcal{L}(s)$ is evaluated. Everything is done in the very same way as the 1RSB equations are usually solved, for more details see, e.g., [22, 27, 28]. The only difference is in the treatment of the negation-variables. In our case one writes the distributions $S_{ia}(m_{ia}, J_{ia})$, $\hat{S}_{ai}(\hat{m}_{ai}, J_{ia})$ as

$$S_{ia}(m_{ia}, J_{ia}) = \tfrac{1}{2} S_{ia}(m_{ia}|J_{ia}), \qquad \hat{S}_{ai}(\hat{m}_{ai}, J_{ia}) = \tfrac{1}{2}\hat{S}_{ai}(\hat{m}_{ai}|J_{ia}),$$

because $S_{ia}(J_{ia}) = \int \mathrm{d}m_{ia} S_{ia}(m_{ia}, J_{ia}) = 1/2 = \hat{S}_{ai}(J_{ia})$, as can be seen by explicitly integrating equations (19)–(20). We then introduce a pair of populations $\{S_{ia}^1[s], \hat{S}_{ai}^1[s]\}_{s=1,...,P}$ and $\{S_{ia}^0[s], \hat{S}_{ai}^0[s]\}_{s=1,...,P}$ representing the probability distributions $S_{ia}(m_{ia}|1)$, $\hat{S}_{ai}(\hat{m}_{ai}|1)$ and $S_{ia}(m_{ia}|0)$, $\hat{S}_{ai}(\hat{m}_{ai}|0)$ respectively. The population dynamics is then implemented in terms of such populations, and the resulting fixed point investigated numerically.

5. Cavity method results for random AdSAT

In this section we present the solution of the cavity equations (19)–(20), and its implications for the random AdSAT problem.

5.1. Large deviations of the entropy and complexity on regular instances

Before addressing the random AdSAT as defined in section 1 we will study it on random regular instances. On L-regular instances every variable belongs to exactly L clauses. A random L-regular instance is chosen uniformly at random from all possible ones with a given number of variables N and number of clauses M, provided that $KM = LN$. Note that, as far as we know, this ensemble of random SAT instances was not treated in the literature previously.

In the 3-SAT problem discussed in this paper the Bethe entropy is asymptotically exact only as long as the BP equations converge to a fixed point [9]; the non-convergence is equivalent to the spin glass instability, or a continuous transition to a replica symmetry breaking phase. On random regular graphs with random values of negations, BP stops converging at $L = 12$ (this is the reason why these and larger values are omitted from table 1), meaning that for $L \geq 12$ there is a need for SP (or another form of replica symmetry breaking solution). For $L \geq 15$ BP iterations for random regular 3-SAT lead to contradictions (zero normalizations) meaning that in this region the large random instances are almost surely unsatisfiable. Survey propagation on random regular 3-SAT has a trivial fixed point for $L \leq 12$, and a non-trivial fixed point for $L = 13$ with the value of complexity $\Sigma(L = 13) = 0.008$. SP does not converge for $L \geq 14$; if we ignore the non-convergence, and compute the complexity from the current values of messages, we get on average $\Sigma(L = 14) = -0.03$. This means that $L = 13$ is the largest satisfiable case.

The great advantage of random regular instances is that topologically the local neighborhood looks the same for every variable i. Moreover, we recall that in regimes where the BP equations are asymptotically exact the properties of variable i depend only on the structure of the local neighborhood of i. Hence on regular graphs all the quantities in equations (19)–(20) are independent of the indices i, j, and a, b. This so-called factorization property simplifies crucially the numerical solution of

Table 1. The Bethe free entropy on regular instances with random negation-configurations (s_{ran}), with balanced negation-configurations (s_{B}), and non-frustrated with $J_{ia} = 0 \ \forall(ia)$ (s_{U}). The entropy for the non-frustrated case and for the balanced case for even degree $L \leq 10$ can be computed analytically since the BP fixed point is factorized in these cases. In the other cases we iterate the BP equations on large random graphs and compute the entropy from the corresponding BP fixed point. The star signals that BP did not converge and the value of entropy was obtained by averaging over an interval of time. The $\times$ means that BP converged to contradictions for these densities of constraints.

L	s_{ran}	s_{B}	s_{U}
2	0.6039	0.5710	0.6196
3	0.5592	0.5324	0.5975
4	0.5134	0.4488	0.5796
5	0.4686	0.4120	0.5644
6	0.4220	0.3266	0.5513
7	0.3750	0.2902	0.5397
8	0.3302	0.2044	0.5293
9	0.2816	0.1677	0.5199
10	0.2319	0.082 *	0.5114
11	0.1813	0.042 *	0.5035
12	0.128 *	$\times$	0.4962
13	0.07 *	$\times$	0.4894
14	$\times$	$\times$	0.4831

equations (19)–(20); the $2KM$ distributions $\{S_{ia}(\nu_{ia}, J_{ia}), \hat{S}_{ai}(\hat{\nu}_{ai}, J_{ai})\}$ reduce to only two ($J = 0$ and 1) distributions $S(\nu, J), \hat{S}(\hat{\nu}, J)$. Moreover, the thermodynamic limit is taken directly without increasing the computational effort. (To avoid confusion, we recall here that for the canonical random K-SAT problem where negation-variables are chosen uniformly at random and fixed, the BP solution is not factorized. In the adversarial version one sums over the negation-variables, hence the factorization.)

In figure 2 we show the large deviation function $\mathcal{L}(s)$ of the Bethe entropy s obtained by the population dynamics over BP messages on regular graphs with $K = 3$ and variable degree $L = 4$, i.e. by solving equations (19), (20) and (21)–(24). First of all, in the 'infinite temperature' case, i.e. when the Legendre parameter $x = 0$, that is at the maximum of $\mathcal{L}(s)$, we recover the logarithm of the total number of negation-configurations $\mathcal{L}(x = 0) = L \log 2$. The corresponding value of entropy $s(x = 0) = s_{\mathrm{ran}}$ is the Bethe entropy for a random choice of negations (values summarized in table 1).

The inset of the figure shows that as the Legendre parameter $x \to \pm\infty$ both $\mathcal{L}$ and s converge to well defined ending points (the same data in a logarithmic plot show that the convergence is exponential). Let us denote the lowest entropy ending point (left, $x \to -\infty$) ($s_{\mathrm{L}}, \mathcal{L}_{\mathrm{L}}$), and the highest entropy ending point (right, $x \to \infty$) ($s_{\mathrm{R}}, \mathcal{L}_{\mathrm{R}}$). We observe systematically that the value of s_{R} is equal to s_{U}, where s_{U} is the entropy of the uniform negation-configuration which is obtained by computing a fixed point of equations (6)–(7) such that $\hat{\nu}_{ai} = \hat{\nu} \ \forall(ai)$, $\nu_{ia} = \nu \ \forall(ia)$ and $J_{ia} = 0 \ \forall(ia)$, and plugging it into equation (11). The values of s_{U} as a function of L are summarized in table 1. An edge-independent fixed point of the BP equations is called factorized. We realize that s_{U}
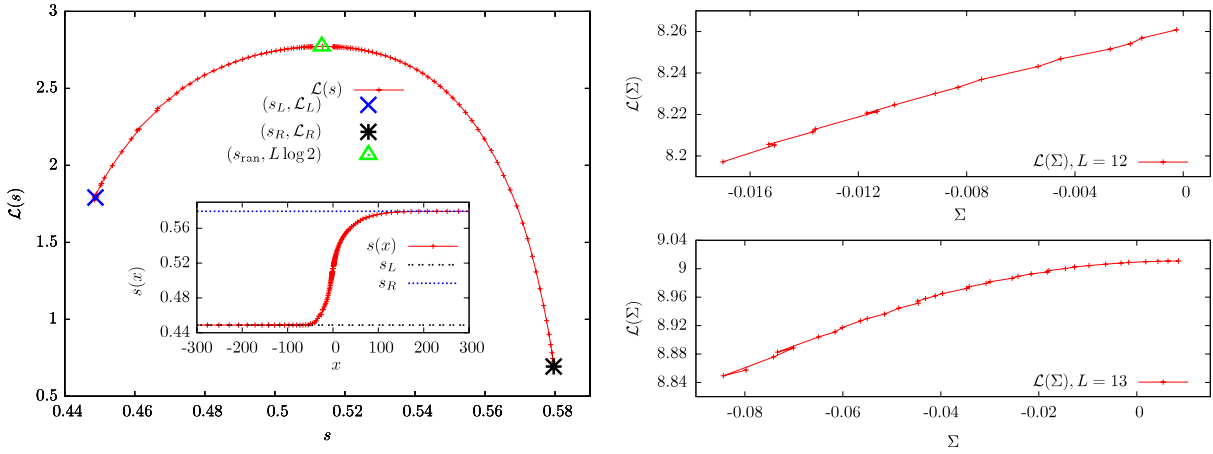
Figure 2. Left: the BP large deviation function $\mathcal{L}(s)$ versus the Bethe entropy s computed by population dynamics on regular graphs with $K = 3$, $L = 4$, population size $P = 10^4$. The left ending point $(f_{\mathrm{L}}, \mathcal{L}_{\mathrm{L}})$ corresponds to balanced configurations of negations, whereas the right ending point $(f_{\mathrm{R}}, \mathcal{L}_{\mathrm{R}})$ to the polarized configurations of negations (more details in the text). Right: the SP large deviation function $\mathcal{L}_{\mathrm{SP}}(\Sigma)$ versus the complexity Σ computed by population dynamics on regular graphs with $K = 3, L = 13, P = 10^4$ (bottom), and $K = 3, L = 12, P = 75 \times 10^3$ (top).

also corresponds to the value of the Bethe entropy when every variable is either always negated or never negated; we call such negation-configurations polarized. There are 2^{LN} polarized negation-configurations, and indeed the logarithm of the number of such choices corresponds to the value of $\mathcal{L}_{\mathrm{R}} = \log 2$. Intuitively such configurations of negation are frustrating the formula in the least possible way, and figure 2 shows that such intuition is asymptotically exact in this case.

Similarly, for the lowest entropy ending point, for even values of the degree L, we realize that $\mathcal{L}_{\mathrm{L}} = \log \binom{L}{L/2}$ and s_{L} corresponds to a value s_{B} that is obtained from a factorized BP fixed point when each variable is $L/2$ times negated and $L/2$ times non-negated; values are summarized in table 1. Such balanced configurations of negations locally frustrate the variables in a maximal way (half of the clauses want the variable to be 1, the other half 0). And the computation presented in figure 2 suggests that asymptotically there are no correlated negation-configurations that would frustrate the formula even more and decrease the value of the entropy further.

We investigate in more detail the result following from figure 2, i.e. that the most frustrated configurations of negations on the regular graphs with even degree are the balanced negations; we denote the balanced negation-configurations $\{J_{ia}\}_{\mathrm{B}} = \mathcal{J}_{\mathrm{B}}$. There are $\binom{L}{L/2}^N$ such negation-configurations. Does our result mean that all of them lead to the same number of solutions $\mathcal{N}(\mathcal{J}_{\mathrm{B}})$? We will see in section 6 that this is not true for finite N. The correct conclusion from the result presented in figure 2 is that $\lim_{N \to \infty} [\log \mathcal{N}(\mathcal{J}_{\mathrm{B}})]/N = s_{\mathrm{B}} = s_{\mathrm{L}}$ independently of the realization of $\mathcal{J}_{\mathrm{B}}$. This can also be seen directly from the solution of the BP equations on the formulas with balanced negations. Indeed, for even L the fixed point of the BP equations is factorized and

independent of the realization of negations and also of the size of the graph. We tried numerically formulas of various sizes and many possible realizations of balanced negations, and for even degree $L < 10$ BP always converges to the factorized fixed point (at $L = 10$ BP stops converging, as we will discuss later in the paper), giving always the same Bethe entropy density s_B. Further discussion about the true entropy fluctuations compared to the constant Bethe entropy in this case will be presented in section 6.

For regular graphs with odd degree L we cannot achieve ideal balancing of every variable. Instead, we call a configuration of negations balanced if for every variable there is either $(L-1)/2$ or $(L+1)/2$ negations. The total number of such configurations is then $2^N \binom{L}{(L-1)/2}^N$. The BP fixed point on the balanced instances for odd L is not factorized anymore. We can, however, solve the cavity equations (19)–(20) restricted to only balanced values of negations and we obtain that within the error-bars of the numerical resolution of the equations (that are less than 1%) all the balanced configurations give the same value of Bethe entropy also in the odd L case.

Our results for large deviations of the Bethe entropy lead to a conclusion that for the regular instances and in the limit $N \to \infty$ the most frustrated formulas are all those with balanced configurations of negations. Let us hence conclude this section by summarizing the properties of regular SAT instances with balanced negations. BP on balanced instances converges for $L \leq 9$, and leads to contradictions for $L \geq 13$. Survey propagation on balanced regular instances has a trivial fixed point for $L \leq 9$, for $L = 10$ a fixed point with complexity $\Sigma_B(L = 10) = 0.018$, and for $L \geq 11$ the complexity is negative (e.g. $\Sigma_B(L = 11) = -0.001$, $\Sigma_B(L = 12) = -0.075$).

For completeness, we also computed the large deviations of the complexity function. That is, we solved equations (19)–(20) using SP as the basic message passing scheme. Figure 2 (right) shows some of the results for $L = 12$ and 13; we indeed see that there are configurations of negations that lead to negative complexity. Unfortunately, it is hard to extract any information from these curves for very negative values of x, because of the noise introduced by the finite population size effects. This also poses a problem for $L = 10$ and 11, where we know that a non-trivial fixed point of SP exists for the balanced configurations of negations. In the population dynamics we should hence see a non-trivial solution for very negative values of x. Instead we were only able to obtain very noisy and inconclusive data from the population dynamics with population sizes up to 7.5×10^4. For $L = 10$ the SP equations have only one factorized fixed point for all the balanced configurations of negations; this again strongly suggests that instances with balanced negations are the most frustrated ones, and hence that for $L = 10$ the adversary cannot make large formulas unsatisfiable. For lower values of $L \leq 9$ the population dynamics has always only a trivial fixed point given by $S_{ia}(Q_{ia}, J_{ia}) = \delta(Q_{ia}^S)\delta(Q_{ia}^U)\delta(Q_{ia}^* - 1)/2$, $\hat{S}_{ai}(\hat{Q}_{ai}, J_{ia}) = \delta(\hat{Q}_{ai})/2$ yielding $\Phi(x) = K\alpha \log 2$. SP is hence not very useful in this case to obtain new information about the random AdSAT problem.

In summary, for $L \geq 11$ the adversary will succeed in making a large formula unsatisfiable by simply balancing the negations (for $L \geq 14$ a random choice of negations would do). On the other hand, following our previous conclusion that the balanced formulas are the most frustrated ones, for $L \leq 10$ the adversary will not be able to make large random regular SAT instances unsatisfiable by adjusting the values of negation-variables.

## 5.2. Results for random AdSAT, i.e. instances with Poisson degree distribution

In the most commonly considered ensemble of the random K-satisfiability problem, K variables appearing in each clause are chosen independently at random (avoiding repetitions). For large system sizes this procedure generates Poissonian degree distribution with mean $K\alpha$. In this case every node has a different local neighborhood and hence the fixed point of equations (19)–(20) is not factorized, and the distribution $S_{ia}(m_{ia}, J_{ai})$, $\hat{S}_{ai}(\hat{m}_{ai}, J_{ai})$ are different on every edge. We hence solve equations (19)–(20) by generating an instance of the problem (graph) of size N, associating one population of size P with every directed edge, and iterate following equations (19)–(20). This is more computationally involved, and we are able to treat only modestly large N and P, typically several hundreds. The resulting large deviation function $\mathcal{L}(s)$ is depicted in figure 3 for several values of constraint density α.

For low values of the constraint density, e.g. $\alpha = 1$ in figure 3, the location of the right (large entropy, least frustrated) ending point $(s_R, \mathcal{L}_R)$ corresponds, as in the case of random regular instances, to the value of Bethe entropy that is obtained if no negations are present in the instance ($J_{ia} = 0$ for all ia), and $\mathcal{L}_R = (1 - e^{-K\alpha})\log 2$ (corresponding to the number of negation-configurations where no variable is locally frustrated). For larger values of the constraint density, e.g. $\alpha = 2$ in figure 3, the results from population sizes as large as we were able to achieve are very noisy for large values of $x \approx 100$. We observed that the data are getting smoother as the population size is growing, however not enough to be able to confirm from these data that $(s_R, \mathcal{L}_R)$ is the right ending point.

The part of the curve corresponding to a very large negative parameter x does not converge to an ending point. Instead at some x_0 the large deviation function $\mathcal{L}(s)$ ceases to be concave, and an unphysical branch appears for $x < x_0$. This unphysical branch is not present on random regular instances with even degree; when the degree is odd the data for large negative x are inconclusive in the sense that we might see a unphysical branch or only a numerical noise. We define the left ending point as the extreme of the physical branch $s_L = s(x_0)$, and $\mathcal{L}_L = \mathcal{L}(x_0)$. We observe systematically that in the region of interest (say for $\alpha \geq 1$) the values s_L and $\mathcal{L}_L$ are very close to the values corresponding to balanced instances $(s_B, \mathcal{L}_B)$. In balanced instances each variable is negated as many times as non-negated (for variables of odd degree the absolute value of the difference between the number of negations and non-negations is one). In the thermodynamic limit the number of such balanced negation-configurations is

$$\mathcal{L}_B = \sum_{i=0}^{\infty} \log \binom{2i}{i} e^{-k\alpha} \frac{(k\alpha)^{2i}}{(2i)!} + \sum_{i=0}^{\infty} \log \left[2 \binom{2i+1}{i} \right] e^{-k\alpha} \frac{(k\alpha)^{2i+1}}{(2i+1)!}. \quad (25)$$

We made a number of attempts to obtain a value of entropy considerably smaller than the balanced entropy, $s < s_B$. First, we removed the leaves from the formula and balanced only the residual formula. This indeed leads to a lower value of the entropy, but for $\alpha > 1$ the difference was less than 1%. We tested the population dynamics limited to the balanced negation-configurations, i.e. we solved equations (19)–(24) where the sum over the negation-variables in equations (20) and (23) was limited only to the balanced negation-configurations. The large deviation function $\mathcal{L}(s)$ obtained in this way did not differ more than by 1% from the value $(s_B, \mathcal{L}_B)$, see figure 3 (left). We also investigated the results of population dynamics over the SP equations and we were not able to find cases
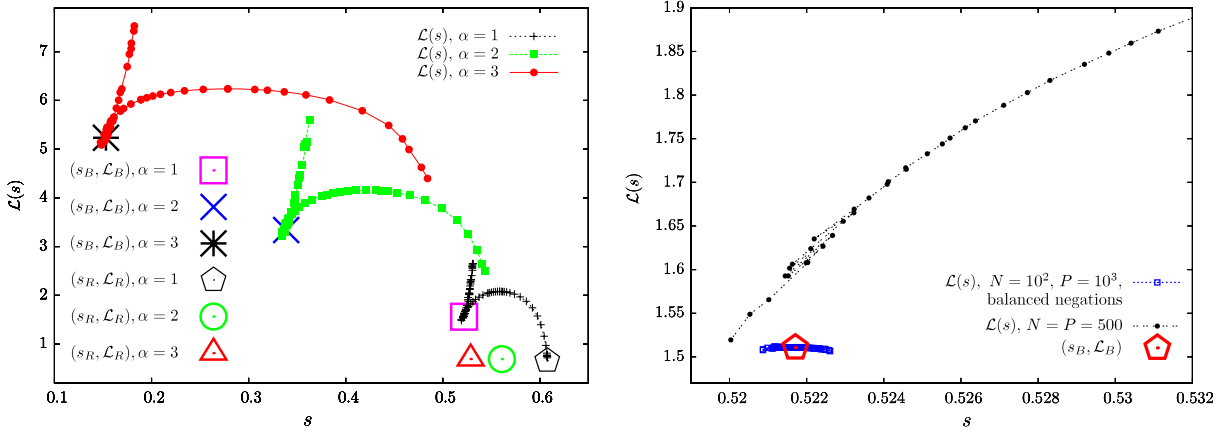
Figure 3. Left: the BP large deviation function $\mathcal{L}(s)$ versus the Bethe entropy s computed by population dynamics on Poissonian graphs with random negation-configurations, for $K = 3$, various values of the constraint density α, and both positive and negative x. For $\alpha = 1$–3 the part of the curve with $x < 0$ has been computed with $N = P = 300$. For $\alpha = 1$ the part of the curve with $x > 0$ reaches the right ending point, and has been computed with $N = P = 500$. For $\alpha = 2, 3$ the part of the curve with positive x has been computed with $N = P = 300$, and it does not reach the right ending point; even larger N and P are needed to remove the noise from the data for very large positive x. For $x < 0$, an unphysical branch (concave part of the curve) starts at $x_0 \approx -42$, $x_0 \approx -44$, $x_0 \approx -40$ for $\alpha = 1, 2, 3$ respectively. The points indicate the values for balanced configurations of negations $(s_{\mathrm{B}}, \mathcal{L}_{\mathrm{B}})$, and for configurations of negations where all the variables are non-negated $(s_{\mathrm{R}}, \mathcal{L}_{\mathrm{R}})$. Right: zoom of the large deviation function $\mathcal{L}(s)$ versus s for $\alpha = 1$ close to the low entropy ending point for $N = P = 500$. The data become noisy close to the low entropy ending point; larger graph and population sizes lead to an improvement. We plotted the data down to the lowest value of entropy s; hence the unphysical branch is not plotted. The point indicates the value $(s_{\mathrm{B}}, \mathcal{L}_{\mathrm{B}})$ for balanced configurations of negations. The blue data points show the large deviation function restricted to balanced configurations of negations for $N = 10^2, P = 10^3$. Notice the narrow range of entropies s plotted in the latter, and how little the lowest entropy we achieved differs from the balanced value.

where the complexity would decrease by more than 1% below the complexity value on the balanced instances. We also tried simulated annealing on the negation-variables using the Bethe entropy as the cost function, with the same result. All this makes us conclude that with at least 1% of precision the satisfiability threshold for random adversarial SAT equals the satisfiability threshold of the balanced random ensemble.

Let us hence summarize the results about BP and SP for the random satisfiability problem with balanced configurations of negations. For $K = 3$ the BP ceases to converge for $\alpha \geq 2.96$. SP starts to converge to a non-trivial fixed point for $\alpha > 3.20$, and the complexity decreases to zero at

$$\alpha_{\mathrm{B}} = 3.399 \pm 0.001; \tag{26}$$

this is hence the satisfiability threshold on the balanced random formulas. All our
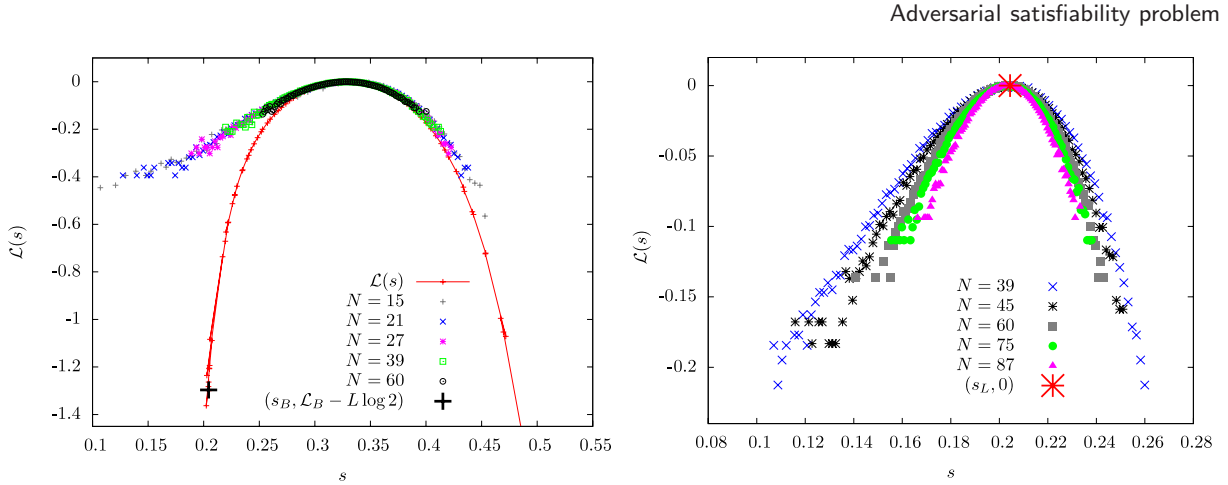
Figure 4. Left: $\mathcal{L}_N(s)$ versus s for regular random graphs with random negations, computed exactly for $15 \leq N \leq 60$ with $N_s = 10^5$ samples $\mathcal{J}$, and binning interval $\Delta s = (s_{\max} - s_{\min})/100$ with $K = 3, L = 8$, where $s_{\max}$ and $s_{\min}$ are the maximum and minimum entropies of the N_s samples respectively. We also plot $\mathcal{L}(s)$ versus s computed with the population dynamics for both negative x ($P = 5 \times 10^4$) and positive x ($P = 2 \times 10^4$). Right: $\mathcal{L}_N(s)$ versus s for regular random graphs with balanced negations, computed exactly for $39 \leq N \leq 87$, $N_s = 10^5$, binning interval $\Delta s = (s_{\max} - s_{\min})/100$, and $K = 3, L = 8$. The curves do not superpose, so the large deviations decay faster than exponentially.

observations about the large deviation function suggest that the threshold for the random adversarial satisfiability problem satisfies $\alpha_a > 3.39$.

6. Numerical results for AdSAT and large deviations

In this final section we compare theoretical predictions from the cavity method with numerical results.

6.1. Numerical results for large deviations

First, we investigate numerically the number of configurations of negations yielding a formula with a certain entropy of solutions. For one given random graph geometry of size N, we generate independently at random $I \gg 1$ different configurations of negations, and for each of them we count the number of solutions using a publicly available implementation of the exact counting algorithm relsat [29]. We define the probability $P_N(s)$ over the negation-configurations that the value of the entropy density is between s and $s + \Delta s$, where Δs is a binning interval that we will specify later.

Following the assumption of exponentially-small large deviations made in equation (4), we define

$$\mathcal{L}_N(s) = \frac{1}{N} \left[\log P_N(s) - \log \max_s P_N(s) \right]. \tag{27}$$

The numerical result for $\mathcal{L}_N(s)$ is depicted in figure 4 (left) for $L = 8$, and compared to the predictions of the large deviations of the Bethe entropy from section 5. The agreement between the numerical data point and the theoretical prediction is not good in the low

entropy region. One possibility is that this is due to pre-asymptotic effects; on the other hand this does not seem likely as the numerical curves seem to superpose nicely for different system sizes. Another possibility is that we neglected some replica symmetry breaking effects; note, however, that the large deviation calculation over survey propagation did not provide any non-trivial result. We hence leave this disagreement as an open problem.

At this point we want to recall the result from BP that we obtained on balanced regular instances with even degree (i.e. for instance $L = 8$); in that case the BP fixed point was factorized and independent of the negation-configuration even for small graphs. Let us hence investigate the numerical results for the large deviations of the entropy in this case. The data for $\mathcal{L}_N(s)$ are depicted in figure 4 (right); recall from table 1 that the maximum of the curve corresponds to s_B obtained with BP. The curves in figure 4 (right) clearly do not superpose for different system sizes. Indeed, $\mathcal{L}_N(s)$ seems to be 'closing'. From these data it is indeed plausible that in the limit $N \to \infty$, $\mathcal{L}_N(s)$ converges to a delta function on the value of entropy $s = s_B$.

Hence, the data in figure 4 (right) suggest that the probability that the entropy of a formula is different from the value predicted by BP is smaller than exponentially small. This makes us conclude that in a general case, the probability of having an entropy outside the interval (s_L, s_R) is smaller than exponentially small (we recall that for the balanced negations and even degree L regular graphs $s_L = s_R = s_B$). Hence in the thermodynamic limit there are almost surely no negation-configurations that would lead to a value of entropy outside the range (s_L, s_R).

Moreover, the large deviation function $\mathcal{L}_N(s)$ if asymptotically negative can be interpreted as a probability of generating a rare graph and configuration of negations having entropy s [30]. Since there are of order N^N regular graphs, and there is no or at least one graph with entropy $s \notin (s_L, s_R)$, we can have either $P_N(s) = 0$ or

$$P_N(s) \geq \mathrm{e}^{-c_1 N \log N},\tag{28}$$

where c_1 is some positive constant. Consider now that there are $\mathrm{e}^{N\mathcal{L}'}$ of configurations of negations (e.g. $\mathcal{L}' = K\alpha \log 2$ if we consider all the negation-configurations, or $\mathcal{L}' = \mathcal{L}_B$ if we consider just the balanced negation-configurations). The fraction of graphs with configurations of negations leading to entropy $s \notin (s_L, s_R)$ has to be small only if

$$P_N(s)\mathrm{e}^{N\mathcal{L}'} \ll 1.\tag{29}$$

If an equality holds in equation (28) then equation (29) holds in the thermodynamic limit, $N \to \infty$. However, (29) does not have to hold for finite N unless

$$N \geq N_c \equiv \exp\left(\frac{\mathcal{L}'}{c_1}\right).\tag{30}$$

Since c_1 can be considerably smaller than $\mathcal{L}'$, the crossover value of N_c might be very large and out of reach for exact numerical methods. This justifies the presence of strong pre-asymptotic effects for the system sizes treated in figure 4.

6.2. Strong finite size corrections for the AdSAT threshold

We investigate numerically the AdSAT threshold α_a by computing the probability (over random graph instances) p_s that an adversary is not able to find a configuration of
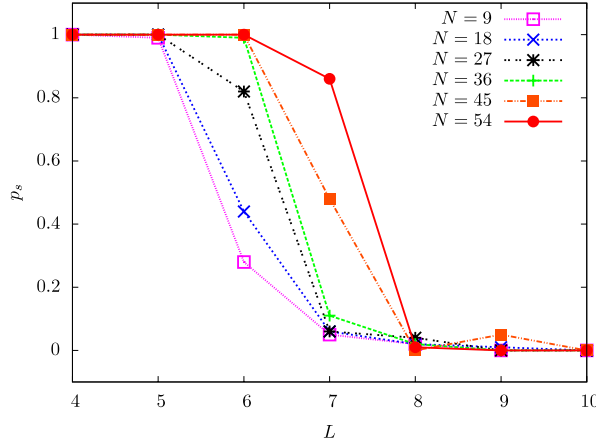
Figure 5. Probability p_s that using the simulated annealing algorithm described in the text we did not find any unsatisfiable configuration of negations for L-regular instances, as a function of L, for different system sizes $9 \leq N \leq 54$. We used the annealing rate $r = 1.1$, and number of instances $I = 100$.

negations that makes the formula unsatisfiable. We do this on regular instances because of the reduced fluctuations that arise due to the randomness of the graph.

We generate $I \gg 1$ regular instances for each value of the degree L and for each size N. Then for each instance we use simulated annealing on the negation-variables in order to minimize the number of solutions; we monitor whether an unsatisfiable formula is generated or not. This general strategy for AdSAT was suggested by [31]. In particular, we introduce an inverse temperature β. Initially we set $\beta = 1$. We choose randomly one of the negation-variables, J_{ia}, and attempt to flip it, i.e. to set $J_{ia} \rightarrow 1 - J_{ia}$. Denoting by $\mathcal{J}'$ the configuration of negations after this flip, we accept the flip with probability $\min\{1, \mathrm{e}^{-\beta(S_{\mathcal{J}'} - S_{\mathcal{J}})}\}$. The entropy $S_{\mathcal{J}}$ is computed exactly with a publicly available implementation of the exact exhaustive search algorithm relsat [29]. This algorithm has an exponential running time in the size of the system, limiting us to very small system sizes. Attempting for N negation flips is one Monte Carlo (MC) step. Every 10 MC steps we multiply the inverse temperature by a rate factor $r > 1$. We keep track of the so far minimal value of entropy $s_{\min}$ and the index n_0 of the MC step in which it was first found. The algorithm stops if either an unsatisfiable instance is encountered or no further decrease in the value of entropy $s_{\min}$ has occurred in the last $9 \times n_0 + 50$ MC steps. The probability p_s plotted in figure 5 is then given by the fraction of cases in which an unsatisfiable instance was not found.

There is of course no guarantee that our algorithm found the actual minimal possible entropy. So, strictly speaking, any result for the satisfiability threshold derived from the data for p_s is only an upper bound to the true threshold. However, given the strictness of our stopping condition we have a reasonable confidence that our results are very close to the exact results. Figure 5 depicts the fraction of regular instances of size N where we were unable to find a configuration of negations that would make the formula unsatisfiable.

On first sight the numerical data in figure 5 do not agree with our theoretical predictions. Indeed, we predicted that unsatisfiable configurations of negations exist only for $L \geq 11$, whereas, for the system sizes our simulated annealing algorithm was able

to treat, we find unsatisfiable negation-configurations for a large fraction of graphs with $L \geq 8$.

On a second sight, however, we see in figure 5 that for $L = 6$ and 7 there are very strong finite size corrections to p_s. Indeed, for $L = 6$ and size $N = 9$ we find that roughly 3/4 of the instances can be made unsatisfiable, whereas for $N = 36$ none of the $I = 100$ instances that we tried can be made unsatisfiable. Similarly for $L = 7$ and size $N = 36$ we find that most of the $I = 100$ instances can be made unsatisfiable, whereas for $N = 54$ almost none of them. If this trend continues it is perfectly plausible that in the $N \to \infty$ limit even for $L = 10$ the adversary is never successful. These results, in agreement with the conclusions of section 6.1, suggest very strong pre-asymptotic effects in the AdSAT problem. The strength of the finite size corrections hence poses a challenge to numerical verifications of our cavity method asymptotic predictions.

On the other hand, the scaling argument presented in equation (30) suggests that the system sizes at which the asymptotic behavior starts to be dominant might be quite large (perhaps thousands or more); this is in particular true in the vicinity of the satisfiability threshold. Hence, in the AdSAT problem, and likely also in other adversarial optimization problems, it is particularly important to develop techniques that predict the pre-asymptotic behavior and the finite size corrections. We saw from the results on random regular instances with even degree that BP predicts the same Bethe entropy for all balanced negation-configurations independently of the system size; hence the methods for analysis of finite size corrections and pre-asymptotic effects will have to go beyond the assumptions of the cavity method. On the other hand, analysis of the cases where the BP fixed point is factorized might be a good playground for the development of such techniques.

7. Discussion and conclusions

In this paper we studied the adversarial satisfiability problem and concluded that the most frustrated instances of random K-SAT are very close to the ones with balanced configurations of negations. For random regular 3-SAT instances this leads to a threshold $L = 11$, starting from which the adversary is able to find unsatisfiable configurations of negations (compare to $L = 14$ for the ordinary random regular 3-SAT). For the canonical (Poissonian) adversarial 3-SAT this leads to $\alpha_a = 3.399(1)$ (compare to $\alpha_c = 4.2667$ for the ordinary random 3-SAT). The satisfiability threshold values for the regular and for the balanced 3-SAT instances were obtained as a side result.

This result is rather uninteresting from the algorithmic point of view, as balancing negations is an easy problem. However, the same method we used here can be applied to more interesting situations, for instance the quantified SAT problem. Recall also that the adversarial satisfiability problem was suggested as a problem interpolation between random SAT and random quantum SAT. Note, however, that our study leads to the conclusion that the adversary SAT is much closer to the classical random SAT than to the quantum SAT. Note that in the large K limit the random satisfiability threshold scales as $\alpha \approx 2^K \log 2$; the same scaling holds for the threshold in the random K-SAT with balanced negations, since at large K the degree of the variables is so large that the difference between the Poissonian distribution of the number of non-negated variables and balanced negation-configurations does not play any role in the leading order in K. On

the other hand, the satisfiability threshold of the quantum SAT was upper-bounded by $2^K \log 2/2$ [17, 18]; hence the quantum effect must be responsible for this drastic decrease of the threshold value.

We obtained our results by studying the large deviations of the entropy in the ordinary random K-SAT. In particular, an approach leading to equations very similar to the 1RSB equations leads to the calculation of the large deviations in the case where rare instances are exponentially rare. Exponential large deviations are common in statistical physics. In some cases, see, e.g., [32], [11]–[13], the large deviations are rarer than exponentially rare. In our study this arises for regular random K-SAT instances with balanced negations and even degree. In cases where the large deviation function decays faster than exponentially with the system size extremely strong finite size corrections and pre-asymptotic effects can be induced, as we argued in section 6, where we presented numerical studies of the large deviations and of the satisfiability threshold. Interestingly, methods based on the standard cavity method are not straightforwardly applicable to study of the related finite size corrections and pre-asymptotic behavior. It remains a theoretical challenge to find out how to describe analytically and algorithmically these pre-asymptotic effects that might be crucial for solving some industrial instances of adversarial optimization problems.

Finally we did not address the possibility of replica symmetry breaking in the space of negations (due to its technical difficulty) and this should also be a subject of future works.

Acknowledgments

References

[1] McMasters A W and Mustin T M, *Optimal interdiction of a supply network*, 1970 *Nav. Res. Logist. Q.* **17** 261

[2] Wood R K, *Deterministic network interdiction*, 1993 *Math. Comput. Modelling* **17** 1

[3] Varga P, *Minimax games, spin glasses, and the polynomial-time hierarchy of complexity classes*, 1998 *Phys. Rev. E* **57** 6487

[4] Papadimitriou C H, 1994 *Computational Complexity* (Reading, MA: Addison-Wesley)

[5] Moore C and Mertens S, 2011 *The Nature of Computation* (Oxford: Oxford University Press)

[6] Cook S A, *The complexity of theorem-proving procedures*, 1971 *Proc. 3rd STOC (New York, NY)* ACM pp 151–8

[7] Mitchell D G, Selman B and Levesque H J, *Hard and easy distributions for SAT problems*, 1992 *Proc. 10th AAAI* (Menlo Park, CA: AAAI Press) pp 459–65

[8] Mézard M, Parisi G and Zecchina R, *Analytic and algorithmic solution of random satisfiability problems*, 2002 *Science* **297** 812

[9] Krzakala F, Montanari A, Ricci-Tersenghi F, Semerjian G and Zdeborová L, *Gibbs states and the set of solutions of random constraint satisfaction problems*, 2007 *Proc. Nat. Acad. Sci.* **104** 10318

[10] Rivoire O, *The cavity method for large deviations*, 2005 *J. Stat. Mech.* P07004

[11] Parisi G and Rizzo T, *Large deviations in the free energy of mean-field spin glasses*, 2008 *Phys. Rev. Lett.* **101** 117205

[12] Parisi G and Rizzo T, *Phase diagram and large deviations in the free energy of mean-field spin glasses*, 2009 *Phys. Rev. B* **79** 134205

[13] Parisi G and Rizzo T, *Large deviations of the free energy in diluted mean-field spin-glass*, 2010 *J. Phys. A: Math. Theor.* **43** 045001

[14] Parisi G, *A sequence of approximated solutions to the SK model for spin-glasses*, 1980 *J. Phys. A: Math. Gen.* **13** L115

[15] Dotsenko V, Franz S and Mezard M, *Partial annealing and overfrustration in disordered systems*, 1994 *J. Phys. A: Math. Gen.* **27** 2351

[16] Laumann C R, Moessner R, Scardicchio A and Sondhi S L, *Phase transitions and random quantum satisfiability*, 2010 *Quantum Inf. Comput.* **10** 1

[17] Bravyi S, Moore C and Russell A, *Bounds on the quantum satisfiability threshold*, 2009 arXiv:0907.1297v2

[18] Laumann C R, Lauchli A M, Moessner R, Scardicchio A and Sondhi S L, *Product, generic, and random generic quantum satisfiability*, 2010 *Phys. Rev.* A **81** 062345

[19] Chen H and Interian Y, *A model for generating random quantified boolean formulas*, 2005 *IJCAI 2005: Proc. 19th Int. Joint Conf. on Artificial Intelligence* pp 66–71

[20] Altarelli F, Braunstein A, Ramezanpour A and Zecchina R, *Statistical physics of optimization under uncertainty*, 2010 arXiv:1003.6124v1, 2010

[21] Mertens S, Mézard M and Zecchina R, *Threshold values of random k-SAT from the cavity method*, 2006 *Random Struct. Algorithms* **28** 340

[22] Mézard M and Parisi G, *The Bethe lattice spin glass revisited*, 2001 *Eur. Phys. J.* B **20** 217

[23] Yedidia J S, Freeman W T and Weiss Y, *Understanding belief propagation and its generalizations*, 2003 *Exploring Artificial Intelligence in the New Millennium* (San Francisco, CA: Morgan Kaufmann) pp 239–6

[24] Mézard M and Montanari A, 2009 *Physics, Information, Computation* (Oxford: Oxford Press)

[25] Montanari A, Parisi G and Ricci-Tersenghi F, *Instability of one-step replica-symmetry-broken phase in satisfiability problems*, 2004 *J. Phys. A: Math. Gen.* **37** 2073

[26] Mézard M and Zecchina R, *Random k-satisfiability problem: from an analytic solution to an efficient algorithm*, 2002 *Phys. Rev.* E **66** 056126

[27] Zdeborová L and Krzakala F, *Phase transitions in the coloring of random graphs*, 2007 *Phys. Rev.* E **76** 031131

[28] Montanari A, Ricci-Tersenghi F and Semerjian G, *Clusters of solutions and replica symmetry breaking in random k-satisfiability*, 2008 *J. Stat. Mech.* P04004

[29] Bayardo R J Jr and Pehousek J D, *Counting models using connected components*, 2000 *Proc. 17th AAAI* (Menlo Park, CA: AAAI Press) pp 157–62

[30] Rivoire O, *Properties of atypical graphs from negative complexities*, 2004 *J. Stat. Phys.* **117** 453

[31] Nagaj D and Scardicchio A, 2010 in preparation

[32] Monthus C and Garel T, *Matching between typical fluctuations and large deviations in disordered systems: application to the statistics of the ground state energy in the sk spin-glass model*, 2010 *J. Stat. Mech.* P02023

Renormalization group computation of the critical exponents of hierarchical spin glasses

Michele Castellana[1,2] and Giorgio Parisi[1]

[1]*Dipartimento di Fisica, Università di Roma 'La Sapienza', 00185 Rome, Italy*
[2]*LPTMS–CNRS–Universite Paris-Sud, UMR 8626, Bât. 100, 91405 Orsay, France*

The large scale behavior of the simplest non-mean-field spin-glass system is analyzed, and the critical exponent related to the divergence of the correlation length is computed at two loops within the ϵ-expansion technique with two independent methods. The techniques presented show how the underlying ideas of the renormalization group apply also in this disordered model, in such a way that an ϵ-expansion can be consistently set up. By pushing such calculation to high orders in ϵ, a consistent non-mean-field theory for such disordered system could be established, giving a substantial contribution the development of a predictive theory for real spin glasses.

The understanding of glassy systems and their critical properties is a subject of main interest in statistical physics. The mean-field theory of spin-glasses [1] and structural glasses [2] provides a physically and mathematically rich theory. Nevertheless, real spin-glass systems have short-range interactions, and thus cannot be successfully described by mean-field models [1]. This is the reason why the development of a predictive and consistent theory of glassy phenomena going beyond mean field is still one of the most hotly debated, difficult and challenging problems in this domain [3–5], so that a theory describing real glassy systems is still missing. This is because nonperturbative effects are poorly understood and not under control, and the basic properties of large scale behavior of these systems still far from being clarified.

In ferromagnetic systems, the physical properties of the paramagnetic-ferromagnetic transition emerge in a clear way already in the original approach of Wilson [7], where one can write a simple renormalization group (RG) transformation. It was later realized that Wilson's equations are exact in models with ferromagnetic power-law interactions on hierarchical lattices as the Dyson model [8,9]. This model contains all the physical RG properties, and is simple enough to yield a solution of the RG equations within the ϵ-expansion [10].

The extension of this approach to random systems is available only in a few cases. An RG analysis for random models on the Dyson hierarchical lattice has been pursued in the past [11,12], and a systematic analysis of the physical and unphysical infrared (IR) fixed points has been developed within the ϵ-expansion technique. Unfortunately, in such models spins belonging to the same hierarchical block interact each other with the same [11] random coupling J, in such a way that frustration turns out to be relatively weak and they are not a good representative of realistic strongly frustrated system. Moreover, there has recently been a new wave of interest for strongly frustrated random models on hierarchical lattices [13–15]: for example, it has been shown [14] that a generalization of the Dyson model to its disordered version [the hierarchical random energy model (HREM)] has a random energy model-like phase transition.

In this letter we present a field theory analysis of the critical behavior of a generalization of Dyson's model

to the disordered case, known as the hierarchical Edwards-Anderson Model (HEA) [13]. The HEA is of particular interest, since it is a non-mean-field strongly frustrated model with long-range interaction. It follows that its RG analysis pursued in this work makes a contribution to the development of a theory describing real glassy systems with short-range interaction. Indeed, the symmetry properties of the HEA make an RG analysis simple enough to be done with two independent methods, showing that its IR-limit is physically well-defined, independently on the computation technique that one uses. The same symmetry properties make the RG equations simple enough to make a high-order ϵ-expansion tractable by means of a symbolic manipulation program, resulting in a first predictive theory for the critical exponents for a strongly frustrated non-mean-field system mimicking a real spin-glass. It is possible that such a perturbative expansion turns out to be nonconvergent: if this happens, it may help us to pin down the nonperturbative effects. Motivated by this purpose, we show with a two-loop calculation that such ϵ-expansion can be set up consistently, and that the ordinary RG underlying ideas actually apply also in this case, so that the IR limit of the theory is well-defined independently on the regularization technique.

The Hamiltonian of the HEA is defined [13] as $H_J[S] = -\Sigma_{i,k} J_{i,k} S_i S_k$ where the spin S_is take values ± 1 and $J_{i,k}$ are Gaussian random variables with zero mean and variance $\sigma_{i,k}^2$. Everything depends on the form of $\sigma_{i,k}^2$ that will be chosen in such way to make the model simple enough, and a good candidate mimicking a real glassy system. At large distance we have that $\sigma_{i,k}^2 = O(|i-k|^{-2\sigma})$, where σ is a parameter tuning the decay of the interaction strength with distance: we recover the mean-field regime for $\sigma = 1/2$, while no transition is present for $\sigma > 1$ [13]. We will thus be interested in the case $1/2 < \sigma < 1$, where the interaction strength mimics the non-mean field forces of a real spin glass. The form of $\sigma_{i,k}^2$ is given by the following expression: if only the last m digits in the binary representation of the points i and k are different, $\sigma_{i,k}^2 = 2^{-2\sigma m}$. This form of the Hamiltonian corresponds in dividing the system in hierarchical embedded blocks of size 2^m, such that the interaction between two spins depends on the distance of the blocks to which they belong. The quantity $\sigma_{i,k}^2$ is not translational invariant, but it is invariant under a

huge symmetry group and this will be crucial in the study of the model.

We reproduce the IR behavior of the HEA by two different methods. The first method is analogous to the coarse-graining Wilson's method for the Ising model: the IR limit is obtained by imposing invariance with respect to the composition operation taking two systems of 2^k spins and yielding a system of 2^{k+1} spins, for which one can obtain closed formulas because of hierarchical structure of the Hamiltonian. The second method is more conventional: we perform the IR-limit of the theory by constructing an IR-safe renormalized theory and performing its IR limit by the Callan-Symanzik equation.

Wilson's method. As mentioned before, the hierarchical symmetry structure of the model makes the implementation of a recursionlike RG equation simple enough to be solved within an approximation scheme, yielding [13] a recurrence relation for the probability distribution of the overlap [1,2] $Q_{ab}, a = 1, \cdots, n$

$$Z_k[Q] = e^{\beta^2/4 \, \text{Tr}[Q^2]} \int [dP] Z_{k-1}\left[\frac{Q+P}{C^{1/2}}\right] \times Z_{k-1}\left[\frac{Q-P}{C^{1/2}}\right], \quad (1)$$

where $C \equiv 2^{2(1-\sigma)}$, $\beta \equiv 1/T$ is the inverse-temperature and $\int [dP]$ stands for the functional integral over P_{ab}. The recursion relation (1) can be solved by supposing $Z_k[Q]$ to be a mean-field solution, i.e., a Gaussian function of Q. As it will be explicitly shown in the following, the resulting fixed point $Z_*[Q]$ of Eq. (1) turns out [13] to be stable just for $\epsilon \equiv \sigma - \frac{2}{3} < 0$. For $\epsilon > 0$ the stable fixed point is no more Gaussian, and we search for a solution to Eq. (1) as a small perturbation to the mean-field solution

$$Z_k[Q] = \exp\{-[r_k \, \text{Tr}[Q^2] + w_k/3 \, \text{Tr}[Q^3]]\}. \quad (2)$$

General RG arguments [7] suggest that the corrections to the mean-field solution must be proportional to ϵ.

A complete reconstruction of the function $Z_k[Q]$ for $\epsilon > 0$ stems from the following systematic expansion procedure. In first approximation, we write $Z_k[Q]$ as in Eq. (2), and take into account only the cubic term. By inserting Eq. (2) into Eq. (1), and expanding in terms of w_{k-1} to up to $O(w_{k-1}^3)$, we find that $Z_k[Q]$ has the same functional form as in Eq. (2), where the coefficients r_k, w_k are given by some functions of r_{k-1}, w_{k-1} that can be directly computed. It follows that the recursion Eq. (1) yields a relation between r_k, w_k and r_{k-1}, w_{k-1}. In particular, the recursion relation giving w_k as a function of r_{k-1}, w_{k-1}

$$w_k = \frac{2w_{k-1}}{C^{3/2}} + \frac{n-2}{16C^{3/2}}\left(\frac{w_{k-1}}{r_{k-1}}\right)^3 + O(w_{k-1}^5),$$

shows that for $\epsilon < 0$ the fixed point is Gaussian, while for $\epsilon > 0$ a non-Gaussian fixed point arises. It is important point out that the value of $\epsilon = \sigma - 2/3$ is different by the $\epsilon' = \sigma - 1/2$, arising in the generalization Dyson model to its disordered version that has been already pursued in the literature [11,12]. This is because in the latter the frustration is much weaker than in the HEA, in such a way that the IR-behavior of the theory turns out to be generally different.

Higher order corrections to the Gaussian solution can be handled systematically: inserting Eq. (2) into Eq. (1), and expanding to $O(w_{k-1}^4)$, we generate in $Z_k[Q]$ four monomials $\{I_4^l[Q]\}_{l=1,\dots,4}$ of fourth degree in Q. In order to close the recursion relation (2), it is then natural to set

$$Z_k[Q] = \exp\left\{-r_k\left[\text{Tr}[Q^2] + w_k/3 \, \text{Tr}[Q^3] + \frac{1}{4}\sum_{l=1}^4 \lambda_k^l I_4^l[Q]\right]\right\}, \quad (3)$$

where $\lambda_k^l = O(w_k^4)$. By plugging Eq. (3) into Eq. (1), we obtain a recursion equation relating $r_k, w_k, \{\lambda_k^l\}_{l=1,\cdots,4}$ to $r_{k-1}, w_{k-1}, \{\lambda_{k-1}^l\}_{l=1,\cdots,4}$. This procedure can be pushed to arbitrary high order p in w_k, yielding an p-degree polynomial for

$$Z_k[Q] = \exp\left(-\sum_{j=2}^p \sum_{l=1}^{n_j} c_{j,k}^l I_j^l[Q]\right), \quad (4)$$

where the number n_j of monomials proliferates for increasing j. Following the method explained above, a recursion equation relating $\{c_{j,k}^l\}_{j,l}$ to $\{c_{j,k-1}^l\}_{j,l}$ can be obtained, and the critical fixed point $\{c_{j,*}^l\}_{j,l}$ computed by solving perturbatively in ϵ the fixed-point equations. Following the standard RG, we suppose that the system has a characteristic correlation length ξ, diverging at the critical point, where the system is invariant under change in the scale length. By linearizing the recursion relation close to such fixed point, the critical exponent ν governing the power-law divergence of ξ for $T \to T_c$ can be obtained in terms of the largest eigenvalue λ of the matrix M linearizing such transformation next to the fixed point [7]: $\nu^{-1} = \log_2 \lambda$.

We performed this systematic expansion to the order $p = 5$, generating $n_4 = 4$ invariants of fourth degree, and $n_5 = 4$ invariants of fifth degree in Q. Such computation yields ν to the order ϵ^2. For $n \to 0$, we find

$$\nu = 3 + 36\epsilon + [432 - 27(50 + 55 \cdot 2^{1/3} + 53 \cdot 2^{2/3})\log 2]\epsilon^2 + O(\epsilon^3). \quad (5)$$

The one-loop result for ν is the same as that of the power-law interaction spin-glass studied in [5] (where $\epsilon \equiv 3(\sigma - 2/3)$). Notwithstanding this, the coefficients of the expansion in these two models will be in general different at two or more loops. As a matter of fact, the binary tree structure of the interaction of the HEA emerges in the nontrivial $\log 2, 2^{1/3}$ factors in the coefficient of ϵ^2 in Eq. (5), that can't be there in the power-law case.

Before discussing the result in Eq. (5), we point out that Wilson's method explicitly implements the binary-tree structure of the model when approaching the IR limit. Nevertheless, if the IR limit is well-defined, physical observables like ν must not depend on the technique we use to compute them in such a limit. It is then important to reproduce Eq. (5) with a different approach.

Field-theoretical method. Here the ϵ-expansion is performed by constructing a functional integral field theory and by removing its IR divergences within the minimal subtraction scheme. The field theory is constructed by expressing

the average of the replicated partition function as a functional integral over the local overlap field

$$Q_{iab} \equiv S_i^a S_i^b, \quad \mathbb{E}_J[Z^n] = \int [dQ] e^{-S[Q]}. \quad (6)$$

A short computation yields the IR-dominant terms in the effective Hamiltonian for a system of 2^k spins,

$$S[Q] = \frac{1}{2} \sum_{i,j}^{0,2^k-1} (\sigma_{i,j}^2 + \tau^{2\sigma-1} \delta_{ij}) \text{Tr}[Q_i Q_j] + \frac{g}{3!} \sum_{i=0}^{2^k-1} \text{Tr}[Q_i^3], \quad (7)$$

where Tr denotes the trace over the replica indexes and $\tau^{2\sigma-1} \propto T - T_c$. The field theory defined by Eq. (7) reproduces the Q^3 interaction term of the well-know effective actions describing the spin-glass transition in short-range [16] and long-range [5,17] spin glasses. Notwithstanding this similarity, the novelty of the HEA is that a high-order ϵ-expansion can be quiet easily automated by means of a symbolic manipulation program solving the simple RG Eq. (1) to high orders in ϵ. This is not true for such short and long-range [5,16,17] models, where the only approach to compute the exponents is the field-theoretical one. Indeed, nobody ever managed to automatize at high orders a computation of the critical exponents within the field-theoretical minimal subtraction scheme, either for the simplest case of the Ising model.

To start our field-theoretical analysis, we observe that Eq. (7) presents an unusual quadratic term that is not invariant under spatial translations and it is difficult to perform explicit calculations. This difficulty can be overcome by a relabeling of the sites of the lattice $i = 0, \cdots, 2^k - 1$, following the same procedure of [18,19]. After relabeling one obtains that $\sigma_{i,j}^2 \propto |i-j|_2^{-2\sigma}$, where $|i|_2$ is the diadic norm of i, i.e., if 2^m divides i and $i/2^m$ is odd, $|i|_2 = 2^{-m}$. Even if this representation is quite unusual (if you are not an expert in p-adic numbers), in this way the variance of the couplings $J_{i,j}$ is translational invariant, since it depends only on $i-j$ (each realization of the system is not translational invariant). In the replica formalism we need to know only the variance of the couplings, not the actual couplings and therefore the effective Hamiltonian in replica space is translational invariant and we can use the standard Fourier transform [19,20] in order to compute loop integrals. The field theory defined by Eq. (7) can be now analyzed within the loop expansion framework. We expand the 1PI correlation functions

$$\Gamma_{a_1 b_1 i_1 \cdots a_m b_m i_m; j_1 \cdots j_l}^{(m,l)}$$

$$\equiv 2^{-l} \langle Q_{i_1 a_1 b_1} \cdots Q_{i_m a_m b_m} \text{Tr}[Q_{j_1}^2] \cdots \text{Tr}[Q_{j_l}^2] \rangle_{1PI},$$

in terms of the renormalized coupling constant g_r and take the small renormalized mass limit $\tau_r \to 0$. According

to general results [6] concerning long-range models, the field Q is not renormalized, and all we need are the $\text{Tr}[Q^2]$-renormalization constant Z_2, and the g-renormalization constant Z_g. An explicit evaluation of the loop integrals related to the action [Eq. (7)] shows that the IR divergences arising for $\epsilon > 0$, $\tau_r \to 0$ can be reabsorbed into Z_g, Z_2 by means of the minimal subtraction scheme [6]. An IR-safe renormalized theory can be constructed, and its IR fixed point g_r^* is computed as the zero of the β-function $\beta(g(\lambda)) = \lambda g'(\lambda)$, yielding the effective coupling constant $g(\lambda)$ of the theory at the energy scale λ. ν is given in terms of g_r^*, Z_2

$$\eta_2[g_r] \equiv \tau_r \frac{\partial \log Z_2}{\partial \tau_r} \bigg|_{g,\tau}, \quad \frac{1}{\nu} = \eta_2[g_r^*] + 2\sigma - 1. \quad (8)$$

As predicted by dimensional considerations, the fixed point $g_r^* = 0$ is stable only for $\epsilon < 0$, while for $\epsilon > 0$ a non-Gaussian fixed point g_r^* of order ϵ arises. By plugging the two-loop result for g_r^* and Z_2 into Eq. (8) and taking $n \to 0$, we reproduce exactly the result [Eq. (5)] derived within Wilson's method.

Conclusions. In this paper we consider a strongly frustrated non-mean-field spin-glass system, the HEA model, and performed an RG analysis yielding results and future developments for a predictive theory of the critical exponents for real spin-glass systems. We set up two perturbative approaches to compute the IR behavior of the HEA. The first explicitly exploits the hierarchical structure of the model, and implements a Wilson-like coarse-graining technique to reach the IR limit. The second relies on the construction of an effective field theory reproducing the IR limit by means of the Callan-Symanzik equation. In both methods, we implemented the basic RG underlying ideas. Among these, the existence of a characteristic length ξ diverging at the critical point, where the theory is invariant with respect to changes in its energy scale. The two approaches yield the same prediction for the critical exponent ν related to the divergence of ξ, showing that the IR limit of the theory is well-defined and independent on the actual method one uses to reproduce it.

Thanks to the hierarchical symmetry of the model, a high-order ϵ-expansion for the HEA could be automatized by means of a symbolic manipulation program. If such series could be made convergent [6] by means of some resummation technique, such high-order calculation would yield an analytical control on the critical exponents, resulting in a precise prediction for a non-mean-field spin-glass.

[1] M. Mézard, G. Parisi, and M. A. Virasoro, *Spin Glass Theory and Beyond* (World Scientific, Singapore, 1987).

[2] T. Castellani and A. Cavagna, J. Stat. Mech.: Theory Exp. (2005) P05012.

[3] C. De Dominicis and I. Giardina, *Random Fields and Spin Glasses: A Field Theory Approach* (Springer, New York, 2006).

[4] J. H. Chen and T. C. Lubensky, Phys. Rev. B **16**, 2106 (1977).

[5] G. Kotliar, P. W. Anderson, and D. L. Stein, Phys. Rev. B **27**, 602 (1983).

[6] J. Zinn-Justin, *Quantum Field Theory and Critical Phenomena*, Vol. 113 of The International Series of Monographs on Physics (Clarendon, Oxford, 2002).

[7] K. G. Wilson and J. B. Kogut, Phys. Rep. **12**, 75 (1974).

[8] F. J. Dyson, Commun. Math. Phys. **12**, 91 (1969).

[9] P. Collet and J. Eckmann, *A Renormalization Group Analysis of the Hierarchical Model in Statistical Mechanics* (Springer-Verlag, Berlin, 1978).

[10] M. Cassandro and G. Jona-Lasinio, Adv. Phys. **27**, 913 (1978).

[11] A. Theumann, Phys. Rev. B **21**, 2984 (1980).

[12] A. Theumann, Phys. Rev. B **22**, 5441 (1980).

[13] S. Franz, T. Jörg, and G. Parisi, J. Stat. Mech.: Theory Exp. (2009) P02002.

[14] M. Castellana, A. Decelle, S. Franz, M. Mézard, and G. Parisi, Phys. Rev. Lett. **104**, 127206 (2010).

[15] Y. V. Fyodorov, A. Ossipov, and A. Rodriguez, J. Stat. Mech.: Theory Exp. (2009) L12001.

[16] A. B. Harris, T. C. Lubensky, and J. H. Chen, Phys. Rev. Lett. **36**, 415 (1976).

[17] M. C. Chang and J. Sak, Phys. Rev. B **29**, 2652 (1984).

[18] G. Parisi and N. Sourlas, Eur. Phys. J. B **14**, 535 (2000).

[19] Y. Meurice, J. Math. Phys. **36**, 1812 (1995).

[20] M. Taibleson, *Fourier Analysis on Local Fields* (Princeton University Press, Princeton, NJ, 1976).

Renormalization-group computation of the critical exponents of hierarchical spin glasses: Large-scale behavior and divergence of the correlation length

Michele Castellana[1,2] and Giorgio Parisi[1]

[1]*Dipartimento di Fisica, Università di Roma "La Sapienza," I-00185 Rome, Italy*
[2]*Laboratoire de Physique Théorique et Modèles Statistiques (LPTMS), CNRS and Université Paris-Sud,*
UMR8626, Bâtiment 100, F-91405 Orsay, France

In a recent work [M. Castellana and G. Parisi, Phys. Rev. E **82**, 040105(R) (2010)], the large-scale behavior of the simplest non-mean-field spin-glass system has been analyzed, and the critical exponent related to the divergence of the correlation length has been computed at two loops within the ϵ-expansion technique by two independent methods. By performing the explicit calculation of the critical exponents at two loops, one obtains that the two methods yield the same result. This shows that the underlying renormalization group ideas apply consistently in this disordered model, in such a way that an ϵ-expansion can be set up. The question of the extension to high orders of this ϵ-expansion is particularly interesting from the physical point of view. Indeed, once high orders of the series in ϵ for the critical exponents are known, one could check the convergence properties of the series, and find out if the ordinary series resummation techniques, yielding very accurate predictions for the Ising model, work also for this model. If this is the case, a consistent and predictive non-mean-field theory for such a disordered system could be established. In that regard, in this work we expose the underlying techniques of such a two-loop computation. We show with an explicit example that such a computation could be quite easily automatized, i.e., performed by a computer program, in order to compute high orders of the ϵ-expansion, and so eventually make this theory physically predictive. Moreover, all the underlying renormalization group ideas implemented in such a computation are widely discussed and exposed.

I. INTRODUCTION

Spin glasses, structural glasses, and the physical description of their critical properties have interested statistical physicists for several decades. The mean-field theory of these models [1–4] provides a physically and mathematically rich picture of their physics and of their critical behavior. Notwithstanding the great success of such mean-field theories, real spin-glass systems are non-mean-field systems, because they have short-range interactions. It follows that these systems cannot be described by mean-field models. As a matter of fact, the generalization of the above mean-field theories to the non-mean-field case is an extremely difficult task that has still not been achieved, so that the development of a predictive and consistent theory of glassy phenomena for real systems is still one of the most hotly debated and challenging problems in this domain [5–11].

There are several reasons why this task is so difficult to achieve. For example, the standard field-theoretical techniques [12,13], yielding the Ising model critical exponents with striking agreement with experimental data, usually do not apply to locally interacting glassy systems. Indeed, a considerable difficulty in the setup of a loop expansion for a spin glass with local interactions is that the mean-field saddle point has a very complicated structure [3], and could even be nonuniquely defined. It follows that the predictions of a loop expansion performed around one selected saddle point could actually depend on the choice of the saddle point itself [14], resulting into an intrinsic ambiguity in the physical predictions of such an expansion. Moreover, nonperturbative effects are poorly understood and not under control, and the basic properties of the large-scale behavior of these systems

are still far from being clarified. From the physical point of view, the fact that one cannot handle perturbatively corrections to the mean-field solution could imply that the physics of real systems is radically different from the mean-field one, so that a completely new description is needed.

The physical properties of the paramagnetic-ferromagnetic transition emerge in a clear way in ferromagnetic systems, as was already discussed in the original work of Wilson [13], where one can write a simple renormalization group (RG) transformation, describing a flow under length-scale reparametrizations. These RG equations turn out to be exact in models with power-law ferromagnetic interactions built on hierarchical lattices such as the Dyson model [15,16]. As a matter of fact, in these models one can explicitly write an exact RG transformation for the probability distribution of the magnetization of the system. All the relevant physical information on the paramagnetic, ferromagnetic, and critical fixed point, and the existence of a finite-temperature phase transition are encoded into these RG equations. Moreover, all the physical RG ideas emerge naturally from these recursion relations, whose solution can be explicitly built up with the ϵ-expansion technique [16–18]. The convergence properties of such an ϵ-expansion in the Dyson model have been investigated in Ref. [17]. It turns out that the ϵ series is divergent, but can be made convergent with a suitable resummation technique.

The extension of this approach to random systems has been performed only for some particular models. On the one hand, a RG analysis for random models on the Dyson hierarchical lattice has been done in the past [19,20], and a systematic analysis of the physical and unphysical infrared (IR) fixed points has been performed within the ϵ-expansion technique.

Unfortunately, in such models spins belonging to the same hierarchical block interact with each other with the same [19] random coupling J, in such a way that frustration turns out to be relatively weak, and they are not a good representative of a realistic strongly frustrated system.

On the other hand, models with local interactions on hierarchical lattices built on diamond plaquettes [21] have been widely studied in their spin-glass version, and also lead to weakly frustrated systems even in their mean-field limit [22]. Notwithstanding this, such models yield a very useful and interesting playground to show how to implement the RG ideas in disordered hierarchical lattices, and in particular on the construction of a suitable decimation rule for a frustrated system, which is one of the basic topics in the construction of a RG for spin glasses, and so in the identification of the existence of a spin-glass phase in finite dimension.

In addition, recently there has been a new wave of interest for strongly frustrated random models on hierarchical lattices [23–25]: For example, it has been shown [24] that a generalization of the Dyson model to its disordered version [the hierarchical random energy model (HREM)] has a random energy model-like phase transition, yielding interesting new critical properties that do not appear in the mean-field case.

In a recent work [26], we performed a field theory analysis of the critical behavior of a generalization of Dyson's model to the disordered case, known as the hierarchical Edwards-Anderson model (HEA) [23], that is physically more realistic than the HREM and presents a strongly frustrated non-mean-field interaction structure, being thus a good candidate to mimic the critical properties of a real spin glass. This analysis is based on the replica method, and in particular on the assumption that the physics of the system is encoded in the $n \to 0$-limit [1,2]. Moreover, the symmetry properties of the HEA make a RG analysis simple enough to be performed with two independent methods, to check if the IR limit of the model is physically well defined independently on the computation technique that one uses. Another element of novelty of the HEA is that its hierarchical structure makes the RG equations simple enough to make a high-order ϵ-expansion eventually tractable by means of a symbolic manipulation program, resulting in a quantitative theory for the critical exponents beyond mean field for a strongly frustrated spin-glass system. It is possible that such a perturbative expansion turns out to be nonconvergent: If this happens, it may help us to pin down the nonperturbative effects. Motivated by this purpose, we have shown [26] with a two-loop calculation that such an ϵ-expansion can be set up consistently, and that the ordinary RG underlying ideas actually apply also in this case, so that the IR limit of the theory is well defined independently on the regularization technique.

In the present work, we show how the underlying RG ideas emerge in the computation of Ref. [26], and in particular how such a calculation has been performed, so that the reader can fully understand and reproduce it. Moreover, we show by an explicit example of such a computation how the ϵ-expansion could be automatized, i.e., implemented by a computer program, in such a way that high orders of the expansion could be computed to establish its summability properties.

The HEA is defined [23,26] as a system of 2^{k+1} spins, $S_0, \ldots, S_{2^{k+1}-1}, S_i = \pm 1$, with an energy function defined

recursively by coupling two systems of 2^k Ising spins

$$
\begin{aligned}
H_{k+1}^J & [S_0, \ldots, S_{2^{k+1}-1}] \\
& = H_k^{J_1}[S_0, \ldots, S_{2^k-1}] + H_k^{J_2}[S_{2^k}, \ldots, S_{2^{k+1}-1}] \\
& \quad - \frac{1}{2^{(k+1)\sigma}} \sum_{i<j}^{0,2^{k+1}-1} J_{12,ij} S_i S_j,
\end{aligned} \tag{1}
$$

where

$$
H_1^J[S_1, S_2] = -J 2^{-\sigma} S_1 S_2,
$$

and all the couplings J_{ij} are Gaussian random variables with zero mean and unit variance. Here σ is a parameter tuning the decay of the interaction strength with distance.

As we will show in the following, the form (1) of the Hamiltonian corresponds to dividing the system in hierarchical embedded blocks of size 2^k, so that the interaction between two spins depends on the distance of the blocks to which they belong [23,24].

The HEA is a hierarchical counterpart of the one-dimensional spin glass with power-law interactions [11], which has received attention recently [27–31].

It is crucial to observe [23] that the sum of the squares of the interaction terms that couple the two subsystems in Eq. (1) scales with k as $2^{2k(1-\sigma)}$. Hence, for $\sigma > 1/2$ the interaction energy scales sub-extensively in the system volume, yielding a non-mean field behavior of the model, while for $\sigma < 1/2$ it grows faster than the volume, and the thermodynamic limit is not defined. On the contrary, for $\sigma > 1$ the interaction energy goes to 0 as $k \to \infty$, so that no finite-temperature phase transition can occur. Hence, the interesting region we will study is $\sigma \in (1/2, 1)$.

An equivalent definition of the HEA can be given without using the recursion relation (1). Indeed, one can recover Eq. (1) by defining the HEA as a system of 2^k Ising spins with the Hamiltonian,

$$
H_k[S] = -\sum_{i,j=0}^{2^k-1} J_{ij} S_i S_j, \tag{2}
$$

where J_{ij} are Gaussian random variables with zero mean and variance σ_{ij}^2. The form of σ_{ij}^2 is given by the following expression: If only the last m digits in the binary representation of the points i and j are different, $\sigma_{ij}^2 = 2^{-2\sigma m}$. This form of the Hamiltonian corresponds to dividing the system in hierarchical embedded blocks of size 2^m, such that the interaction between two spins depends on the distance of the blocks to which they belong. It is important to observe that the quantity σ_{ij}^2 is not translational invariant, but it is invariant under a huge symmetry group, and this will be crucial in the study of the model. The two definitions (1) and (2) are equivalent.

We reproduce the IR behavior of the HEA and calculate its critical exponents by two different methods. Both methods assume the existence of a growing correlation scale length ξ, diverging for $T \to T_c$ as

$$
\xi \propto (T - T_c)^{-\nu},
$$

in such a way that for $T \to T_c$ the theory is invariant under reparametrizations of the length scale.

The first method is analogous to the coarse-graining Wilson's method for the Ising model: The scale-free limit is obtained by imposing invariance with respect to the composition operation of Eq. (1), taking two systems of 2^k spins and yielding a system of 2^{k+1} spins. As for the Dyson ferromagnetic model, thanks to the hierarchical structure of the Hamiltonian, one can obtain closed formulas for physical quantities with respect to such a composition operation, analyze the critical and noncritical fixed points, and extract ν.

The second method is more conventional: The IR divergences appearing for $k \to \infty$ and $T \to T_c$ are removed by constructing a renormalized IR-safe theory. The fundamental physical information one extracts from such a renormalized theory is the same as that of the original theory defined by Eq. (1). In particular, the correlation length and its power-law behavior close to the critical point must be the same, and so the critical exponent ν.

The rest of this paper is divided into three main sections: In Sec. II we go through the main steps of the computation with Wilson's method, show that the tensorial operations can be easily implemented diagrammatically, and thus performed by a computer program to compute high orders of the ϵ-expansion. Moreover, we give the two-loop result for ν. In Sec. III the same result is reproduced with the field-theoretical method, and the analogies between the two methods are discussed. In particular, we discuss why Wilson's method would be definitely better than the field-theoretical method for a high-order automatization of the ϵ-expansion. In Secs. II and III, we explicitly do all the steps of the calculation at one loop, giving to the reader all the information needed to reproduce the

two-loop result for ν. Finally, in Sec. IV the two-loop result is discussed in the perspective of the setup of a high-order ϵ-expansion.

II. WILSON'S METHOD

As mentioned before, the hierarchical symmetry structure of the model makes the implementation of a recursive RG equation simple enough to be solved within an approximation scheme. As a matter of fact, let us define the probability distribution of the overlap [1,2],

$$Q_{ab}, \quad a,b = 1,\ldots,n$$
$$Q_{ab} = Q_{ba}, \quad Q_{aa} = 0 \; \forall a,b = 1,\ldots,n \tag{3}$$

as

$$Z_k[Q] \equiv \mathbb{E}_J \left[\sum_{\{S_i^a\}_{i,a}} \exp\left(-\beta \sum_{a=1}^n H_k^J\big[S_0^a,\ldots,S_{2^k-1}^a\big]\right) \right.$$
$$\left. \times \prod_{a<b=1}^n \delta\left(Q_{ab} - \frac{1}{2^k}\sum_{i=0}^{2^k-1} S_i^a S_i^b\right) \right], \tag{4}$$

where $\beta \equiv 1/T$ is the inverse temperature and $\mathbb{E}_J$ the expectation value with respect to all the couplings $\{J_{12,ij}\}_{ij}$.

It is easy to show that the recursion relation (1) for the Hamiltonian results in a recursion relation for $Z_k[Q]$. Denoting by Tr the trace over the replica indexes, by $\int[dQ]$ the functional integral over $\{Q_{ab}\}_{a<b}$, and setting

$$C \equiv 2^{2(1-\sigma)}, \tag{5}$$

this recursion relation can be derived [23] as follows:

$$Z_k[Q] = \mathbb{E}_J \left\{ \sum_{\{S_i^a\}_{i,a}} \exp\left[-\beta \sum_{a=1}^n \left(H_{k-1}^{J_1}\big[S_0^a,\ldots,S_{2^{k-1}-1}^a\big] + H_{k-1}^{J_2}\big[S_{2^{k-1}}^a,\ldots,S_{2^k-1}^a\big] \right. \right.$$

$$\left. -\frac{1}{2^{k\sigma}} \sum_{i<j}^{0,2^k-1} J_{12,ij} S_i^a S_j^a \right) \right] \prod_{a<b=1}^n \delta\left(Q_{ab} - \frac{1}{2^k}\sum_{i=0}^{2^k-1} S_i^a S_i^b\right) \right\}$$

$$\times \int[dQ_1 dQ_2] \prod_{a<b=1}^n \left[\delta\left(Q_{1,ab} - \frac{1}{2^{k-1}}\sum_{i=0}^{2^{k-1}-1} S_i^a S_i^b\right) \delta\left(Q_{2,ab} - \frac{1}{2^{k-1}}\sum_{i=2^{k-1}}^{2^k-1} S_i^a S_i^b\right) \right]$$

$$= \int[dQ_1 dQ_2] \sum_{\{S_i^a\}_{i,a}} \mathbb{E}_{J_1} \left[\exp\left(-\beta \sum_{a=1}^n H_{k-1}^{J_1}[\vec{S}_1^a]\right) \prod_{a<b=1}^n \delta\left(Q_{1,ab} - \frac{1}{2^{k-1}}\sum_{i=0}^{2^{k-1}-1} S_i^a S_i^b\right) \right]$$

$$\times \mathbb{E}_{J_2} \left[\exp\left(-\beta \sum_{a=1}^n H_{k-1}^{J_2}[\vec{S}_2^a]\right) \prod_{a<b=1}^n \delta\left(Q_{2,ab} - \frac{1}{2^{k-1}}\sum_{i=2^{k-1}}^{2^k-1} S_i^a S_i^b\right) \right]$$

$$\times \mathbb{E}_{J_{12}} \left[\exp\left(\frac{\beta}{2^{k\sigma}} \sum_{a=1}^n \sum_{i<j}^{0,2^k-1} J_{12,ij} S_i^a S_j^a\right) \right] \prod_{a<b=1}^n \delta\left(Q_{ab} - \frac{Q_{1,ab}+Q_{2,ab}}{2}\right)$$

$$= \int[dQ_1 dQ_2] \sum_{\{S_i^a\}_{i,a}} \mathbb{E}_{J_1} \left[\exp\left(-\beta \sum_{a=1}^n H_{k-1}^{J_1}[\vec{S}_1^a]\right) \prod_{a<b=1}^n \delta\left(Q_{1,ab} - \frac{1}{2^{k-1}}\sum_{i=0}^{2^{k-1}-1} S_i^a S_i^b\right) \right]$$

$$\times \mathbb{E}_{J_2} \left[\exp\left(-\beta \sum_{a=1}^n H_{k-1}^{J_2}[\vec{S}_2^a]\right) \prod_{a<b=1}^n \delta\left(Q_{2,ab} - \frac{1}{2^{k-1}}\sum_{i=2^{k-1}}^{2^k-1} S_i^a S_i^b\right) \right]$$

$$
\times \exp\left[\frac{\beta^2}{4 2^{2k\sigma}} \sum_{i,j}^{0,2^k-1} \left(\sum_{a=1}^n S_i^a S_j^a\right)^2\right] \prod_{a<b=1}^n \delta\left(Q_{ab} - \frac{Q_{1,ab} + Q_{2,ab}}{2}\right)
$$

$$
= \int [dQ_1 dQ_2] \sum_{\{S_i^a\}_{i,a}} \mathbb{E}_{J_1}\left[\exp\left(-\beta \sum_{a=1}^n H_{k-1}^{J_1}[\vec{S}_1^a]\right) \prod_{a<b=1}^n \delta\left(Q_{1,ab} - \frac{1}{2^{k-1}} \sum_{i=0}^{2^{k-1}-1} S_i^a S_i^b\right)\right]
$$

$$
\times \mathbb{E}_{J_2}\left[\exp\left(-\beta \sum_{a=1}^n H_{k-1}^{J_2}[\vec{S}_2^a]\right) \prod_{a<b=1}^n \delta\left(Q_{2,ab} - \frac{1}{2^{k-1}} \sum_{i=2^{k-1}}^{2^k-1} S_i^a S_i^b\right)\right]
$$

$$
\times \exp\left[\frac{\beta^2}{4 2^{2k(\sigma-1)}} \sum_{a,b=1}^n \left(\frac{1}{2^k} \sum_i^{0,2^k-1} S_i^a S_i^b\right)^2\right] \prod_{a<b=1}^n \delta\left(Q_{ab} - \frac{Q_{1,ab} + Q_{2,ab}}{2}\right)
$$

$$
= \exp\left(\frac{\beta^2 C^k}{4} \mathrm{Tr}[Q^2]\right) \int [dQ_1 dQ_2] Z_{k-1}[Q_1] Z_{k-1}[Q_2] \prod_{a<b=1}^n \delta\left(Q_{ab} - \frac{Q_{1,ab} + Q_{2,ab}}{2}\right). \tag{6}
$$

The main steps of Eq. (6) can be summarized as follows. We observe first that in the composition operation of Eq. (1), a system 1 of 2^{k-1} spins $\vec{S}_1 \equiv \{S_0, \ldots, S_{2^{k-1}-1}\}$ with couplings $J_{1,ij}$ and a system 2 with 2^{k-1} spins $\vec{S}_2 \equiv \{S_{2^{k-1}}, \ldots, S_{2^k-1}\}$ and couplings $J_{2,ij}$ are put into interaction with couplings $J_{12,ij}$, and a system with 2^{k+1} spins is obtained. In the first line of Eq. (6) we used Eq. (1) and inserted the integrals over the Q_1, Q_2 that are both equal to 1. In the third line we performed the integral over J_{12}, which is found in the fourth line to depend only on the overlap Q_{ab}. In the fifth line we use the definition (4) of $Z_{k-1}[Q]$, and obtain the equation relating $Z_{k-1}[Q]$ to $Z_k[Q]$. Here and in the rest of this paper, all the Q-independent constants multiplying $Z_k[Q]$ are omitted for simplicity. Equation (6) is analogous to the recursion equation in Dyson's model [15–18], relating the probability distribution $g_k(m)$ of the magnetization at the k-th hierarchical level to $g_{k-1}(m)$. According to the general prescriptions of the replica approach, all the physics of the model is encoded in the $n \to 0$ limit of $Z_k[Q]$.

We define the rescaled overlap distributions as

$$
\mathcal{Z}_k[Q] \equiv Z_k[C^{-k/2}Q],
$$

and observe that the recursion relation (6) for $Z_k[Q]$ implies a recursion relation for $\mathcal{Z}_k[Q]$:

$$
\mathcal{Z}_k[Q] = \exp\left(\frac{\beta^2}{4} \mathrm{Tr}[Q^2]\right) \int [dP]
$$
$$
\times \mathcal{Z}_{k-1}\left[\frac{Q+P}{C^{1/2}}\right] \mathcal{Z}_{k-1}\left[\frac{Q-P}{C^{1/2}}\right]. \tag{7}
$$

To illustrate the technique used to solve (7) for $\mathcal{Z}_k[Q]$, we present our method in a simple toy example, where the matricial field Q_{ab} is replaced by a one-component field ϕ, the functional $\mathcal{Z}_k[Q]$ by a function $\Omega_k(\phi)$, and Eq. (7) by

$$
\Omega_k(\phi) = \exp\left(\frac{\beta^2}{4} \phi^2\right) \int d\chi\, \Omega_{k-1}\left[\frac{\phi+\chi}{C^{1/2}}\right] \Omega_{k-1}\left[\frac{\phi-\chi}{C^{1/2}}\right]. \tag{8}
$$

As for Dyson's model, Eq. (8) can be solved by making an ansatz for $\Omega_k(\phi)$. The simplest ansatz for $\Omega_k(\phi)$ is the Gaussian one:

$$
\Omega_k(\phi) = \exp[-(d_k\phi^2 + e_k\phi)]. \tag{9}
$$

This form corresponds to a mean-field solution. By inserting Eq. (9) into Eq. (8), one finds two recursion equations relating d_k, e_k to d_{k-1}, e_{k-1}:

$$
d_k = \frac{2d_{k-1}}{C} - \frac{\beta^2}{4},
$$
$$
e_k = \frac{2e_{k-1}}{C^{1/2}}.
$$

Non-Gaussian solutions can be explicitly constructed perturbatively. Indeed, by setting

$$
\Omega_k(\phi) = \exp\left[-\left(d_k\phi^2 + e_k\phi + \frac{u_k}{3}\phi^3\right)\right], \tag{10}
$$

and supposing that u_k is small, one can plug Eq. (10) into Eq. (8) and get

$$
\Omega_k(\phi) = \exp\left(-\left\{\left[\frac{2d_{k-1}}{C} - \frac{\beta^2}{4} - \frac{1}{4}\left(\frac{u_{k-1}}{C^{1/2}d_{k-1}}\right)^2\right]\phi^2 \right.\right.
$$
$$
+ \left(\frac{2e_{k-1}}{C^{1/2}} + \frac{u_{k-1}}{2C^{1/2}d_{k-1}}\right)\phi
$$
$$
\left.\left. + \frac{1}{3}\left[\frac{2u_{k-1}}{C^{3/2}} + \frac{1}{2}\left(\frac{u_{k-1}}{C^{1/2}d_{k-1}}\right)^3\right]\phi^3 + O\left(u_{k-1}^4\right)\right\}\right), \tag{11}
$$

where ϕ-independent constants multiplying $\Omega_k(\phi)$ are omitted for simplicity here and hereinafter. Comparing Eq. (11) with Eq. (10), one finds three recurrence equations relating d_k, e_k, u_k

to $d_{k-1}, e_{k-1}, u_{k-1}$:

$$d_k = \frac{2d_{k-1}}{C} - \frac{\beta^2}{4} - \frac{1}{4}\left(\frac{u_{k-1}}{C^{1/2}d_{k-1}}\right)^2 + O(u_{k-1}^4),$$

$$e_k = \frac{2e_{k-1}}{C^{1/2}} + \frac{u_{k-1}}{2C^{1/2}d_{k-1}} + O(u_{k-1}^4), \qquad (12)$$

$$u_k = \frac{2u_{k-1}}{C^{3/2}} + \frac{1}{2}\left(\frac{u_{k-1}}{C^{1/2}d_{k-1}}\right)^3 + O(u_{k-1}^4).$$

One can easily analyze the fixed points of the RG-flow equations (12), and the resulting critical properties. We will not enter into these details for the toy model, because all these calculations will be illustrated extensively for the HEA model.

Back to the original problem, Eq. (7) can be solved by making an ansatz for $\mathcal{Z}_k[Q]$, following the same lines as in the toy model case. The simplest form one can suppose for $\mathcal{Z}_k[Q]$ is the Gaussian one:

$$\mathcal{Z}_k[Q] = \exp(-r_k \mathrm{Tr}[Q^2]). \qquad (13)$$

This form corresponds to a mean-field solution. By inserting Eq. (13) into Eq. (7), one finds the evolution equation relating r_{k-1} to r_k:

$$r_k = \frac{2r_{k-1}}{C} - \frac{\beta^2}{4}. \qquad (14)$$

Corrections to the mean-field solution can be investigated by adding non-Gaussian terms in Eq. (13), which are proportional to higher powers of Q, and consistent with the symmetry properties of the model. It is easy to see [1] that the only cubic term in Q consistent with such symmetry conditions is $\mathrm{Tr}[Q^3]$, so that the non-mean field ansatz of $\mathcal{Z}_k[Q]$ reads

$$\mathcal{Z}_k[Q] = \exp\left[-\left(r_k \mathrm{Tr}[Q^2] + \frac{w_k}{3}\mathrm{Tr}[Q^3]\right)\right]. \qquad (15)$$

This correction can be handled by supposing that w_k is small for every k, and performing a systematic expansion in powers of it. By inserting Eq. (15) into Eq. (7), one finds

$$\mathcal{Z}_k[Q] = \exp\left\{-\left[\left(\frac{2r_{k-1}}{C} - \frac{\beta^2}{4}\right)\mathrm{Tr}[Q^2] + \frac{2w_{k-1}}{3C^{3/2}}\mathrm{Tr}[Q^3]\right]\right\}$$

$$\times \int [dP] \exp\left[-S_{k-1}^{(3)}[P,Q]\right], \qquad (16)$$

$$S_{k-1}^{(3)}[P,Q] \equiv \frac{2r_{k-1}}{C}\mathrm{Tr}[P^2] + \frac{2w_{k-1}}{C^{3/2}}\mathrm{Tr}[QP^2].$$

The Gaussian integral in Eq. (16) can be computed exactly. Indeed, defining $\forall a > b$ the super-index $A \equiv (a,b)$, one has

$$\frac{\partial^2 S_{k-1}^{(3)}[P,Q]}{\partial P_A \partial P_B} \equiv \frac{8r_{k-1}}{C}\delta_{AB} + \frac{4w_{k-1}}{C^{3/2}}M_{AB}[Q], \qquad (17)$$

where

$$M_{ab,cd}[Q] \equiv N_{ab,cd}[Q] + N_{ab,dc}[Q], \qquad (18)$$

$$N_{ab,cd}[Q] \equiv \delta_{bc}Q_{da} + \delta_{ac}Q_{db}. \qquad (19)$$

One thus finds

$$\mathcal{Z}_k[Q] = \exp\left\{-\left[\left(\frac{2r_{k-1}}{C} - \frac{\beta^2}{4}\right)\mathrm{Tr}[Q^2] + \frac{2w_{k-1}}{3C^{3/2}}\mathrm{Tr}[Q^3]\right]\right\}$$

$$\times \left[\det\left(\frac{8r_{k-1}}{C}\delta_{AB} + \frac{4w_{k-1}}{C^{3/2}}M_{AB}[Q]\right)\right]^{-\frac{1}{2}}. \qquad (20)$$

The determinant in the right-hand side of Eq. (20) can now be expanded in w_{k-1}. Denoting by **Tr** the trace over the A-type indexes, it is easy to show that $\mathbf{Tr}[M[Q]] = 0$, and one has to explicitly evaluate the traces $\mathbf{Tr}[M[Q]^2], \mathbf{Tr}[M[Q]^3]$ to expand the determinant to $O(w_{k-1}^3)$. Here we show how the trace $\mathbf{Tr}[M[Q]^2]$ can be evaluated, in order to show to the reader how the tensorial operations over the replica indexes can be generally carried out. By using Eqs. (18) and (19), one has

$$\mathbf{Tr}[M[Q]^2] = \sum_{AB} M[Q]_{AB} M[Q]_{BA}$$

$$= \sum_{a>b,c>d} (N_{ab,cd}[Q] + N_{ab,dc}[Q])$$

$$\times (N_{cd,ab}[Q] + N_{cd,ba}[Q])$$

$$= \sum_{a\neq b,c\neq d} N_{ab,cd}[Q] N_{cd,ab}[Q]$$

$$= \sum_{a\neq b,c\neq d} (\delta_{bc}Q_{da} + \delta_{ac}Q_{db})(\delta_{da}Q_{bc} + \delta_{ca}Q_{bd})$$

$$= \sum_{a\neq b,c\neq d} \delta_{ca}Q_{bd}^2$$

$$= \sum_{abcd} (1 - \delta_{ab})(1 - \delta_{cd})\delta_{ca}Q_{bd}^2$$

$$= (n-2)\sum_{ab} Q_{ab}^2$$

$$= (n-2)\mathrm{Tr}[Q^2]. \qquad (21)$$

The steps in Eq. (21) can be summarized as follows: In the second line we write the sums over the super indexes $A, B, \ldots$ in terms of the replica indexes $a, b, \ldots$, and in the third line we use the symmetry of $N_{ab,cd}[Q]$ with respect to $a \leftrightarrow b$ and rewrite the sum over $a > b, c > d$ in terms of a sum with $a \neq b, c \neq d$. In the fifth line we find out that just one of the terms stemming from the product $(\delta_{bc}Q_{da} + \delta_{ac}Q_{db})(\delta_{da}Q_{bc} + \delta_{ca}Q_{bd})$ does not vanish, because of the constraints $a \neq b, c \neq d, Q_{aa} = 0$, and because of the Kronecker δs in the sum. Once we are left with the nonvanishing term, in the sixth line we write explicitly the sum over $a \neq b, c \neq d$ in terms of an unconstrained sum over a, b, c, d by adding the constraints $(1 - \delta_{ab})(1 - \delta_{cd})$. In the seventh line we perform explicitly the sum over the replica indexes, and write everything in terms of the replica-invariant $I_1^{(2)}[Q] \equiv \mathrm{Tr}[Q^2]$ (see Table I).

The trace in Eq. (21) can also be computed with a purely graphical method, which can be easily implemented in a computer program to perform this computation at high orders

TABLE I. Invariants generated at the order $p = 5$. In each line of the table we show the invariants $I_1^{(j)}[Q], \ldots, I_{n_j}^{(j)}[Q]$ from left to right.

j			$I_l^{(j)}[Q]$	
2			$\mathrm{Tr}[Q^2]$	
3			$\mathrm{Tr}[Q^3]$	
4	$\mathrm{Tr}[Q^4]$	$\mathrm{Tr}[Q^2]^2$	$\sum_{a \neq c} Q_{ab}^2 Q_{bc}^2$	$\sum_{ab} Q_{ab}^4$
5	$\mathrm{Tr}[Q^5]$	$\mathrm{Tr}[Q^2]\mathrm{Tr}[Q^3]$	$\sum_{abcd} Q_{ab}^2 Q_{bc} Q_{bd} Q_{cd}$	$\sum_{abc} Q_{ab}^3 Q_{ac} Q_{bc}$

in w_k. Let us set

$$
\begin{aligned}
\mathbf{Tr}_2[f] &\equiv \sum_{a_1 \neq b_1, \cdots, a_k \neq b_k} f_{a_1 b_1, \ldots, a_k b_k} \\
&= \sum_{a_1 b_1, \cdots, a_k b_k} (1 - \delta_{a_1 b_1}) \cdots (1 - \delta_{a_k b_k}) f_{a_1 b_1, \ldots, a_k b_k} \quad (22)
\end{aligned}
$$

for any function of f the replica indexes, and make the graphical identifications shown in Fig. 1. The last line in Eq. (21) can now be reproduced by a purely graphical computation, as shown in Fig. 2. There we show that all the tensorial operations have precise a graphical interpretation, and so that they can be performed without using the cumbersome steps of Eq. (21). This graphical notation is suitable for an implementation in a computer program, which could push our calculation to high orders in w_k. For example, as shown in Fig. 2 in a simple example, while computing $\mathbf{Tr}[M[Q]^k]$ for $k \gg 1$, a proliferation of terms occurs, and some of these terms can be shown to be equal to each other, because they are represented by isomorph graphs, so that the calculation can be extremely simplified.

By following the steps shown in Eq. (21) (or their graphical implementation), all the other tensorial operations can be carried out. In particular, one finds

$$
\mathbf{Tr}[M[Q]^3] = (n - 2)\mathrm{Tr}[Q^3]. \quad (23)
$$

By plugging Eqs. (21) and (23) into Eq. (20), one finds

$$
\begin{aligned}
\mathcal{Z}_k[Q] = \exp\Bigg(&-\Bigg\{ \left[\frac{2r_{k-1}}{C} - \frac{\beta^2}{4} - \frac{n-2}{4}\left(\frac{w_{k-1}}{2r_{k-1}C^{1/2}}\right)^2 \right] \\
&\times \mathrm{Tr}[Q^2] + \frac{1}{3}\left[\frac{2w_{k-1}}{C^{3/2}} + \frac{n-2}{2}\left(\frac{w_{k-1}}{2r_{k-1}C^{1/2}}\right)^3 \right] \\
&\times \mathrm{Tr}[Q^3] + O\left(w_{k-1}^4\right) \Bigg\} \Bigg). \quad (24)
\end{aligned}
$$

$$
\begin{aligned}
\delta_{ab} &\equiv \quad a \; \longrightarrow\!\!\bullet\!\!\longrightarrow \; b, \\
Q_{ab} &\equiv \quad a \; \longrightarrow\!\!\blacklozenge\!\!\longrightarrow \; b.
\end{aligned}
$$

FIG. 1. Graphical identifications representing symbolically the mathematical objects used in tensorial operations. The basic objects are the δ_{ab} function, imposing that the replica indexes a and b are equal (top), and the matrix Q_{ab} (bottom). Once these elements are represented graphically, all the tensorial operations can be worked out by manipulating graphical objects composed by these elementary objects.

Comparing Eq. (24) with Eq. (15), one finds a recursion relation for the coefficients r_k, w_k:

$$
\begin{aligned}
r_k &= \frac{2r_{k-1}}{C} - \frac{\beta^2}{4} - \frac{n-2}{4}\left(\frac{w_{k-1}}{2C^{1/2}r_{k-1}}\right)^2 + O\left(w_{k-1}^4\right), \\
w_k &= \frac{2w_{k-1}}{C^{3/2}} + \frac{n-2}{2}\left(\frac{w_{k-1}}{2C^{1/2}r_{k-1}}\right)^3 + O\left(w_{k-1}^5\right). \quad (25)
\end{aligned}
$$

Setting

$$
\epsilon \equiv \sigma - 2/3,
$$

Equation (25) shows that if $\epsilon < 0$, $w_k \to 0$ for $k \to \infty$, i.e., the corrections to the mean field vanish in the IR limit. In this case, the critical fixed point (r_*, w_*) of Eq. (25) has $w_* = 0$. On the contrary, for $\epsilon > 0$ a nontrivial critical fixed point $w_* \neq 0$ arises. According to general RG arguments, this nontrivial fixed point is proportional to some power of ϵ [12]. In particular, one finds that $w_*^2 = O(\epsilon)$.

The critical exponent ν can be computed [13] by considering the 2×2 matrix $\mathcal{M}$ linearizing the transformation given by Eq. (25) around the critical fixed point (r_*, w_*),

$$
\begin{pmatrix} r_k - r_* \\ w_k - w_* \end{pmatrix} = \mathcal{M} \cdot \begin{pmatrix} r_{k-1} - r_* \\ w_{k-1} - w_* \end{pmatrix},
$$

and is given by

$$
\nu = \frac{\log 2}{\log \Lambda}, \quad (26)
$$

where Λ is the largest eigenvalue of $\mathcal{M}$.

Such a procedure can be systematically pushed to higher orders in w_k, and thus in ϵ, by taking into account further corrections to the mean-field solution. Indeed, if we go back to Eq. (20) and consider also the $O(w_{k-1}^4)$ terms on the right-hand side, we find

$$
\begin{aligned}
&\left[\det\left(\frac{8r_{k-1}}{C}\delta_{AB} + \frac{4w_{k-1}}{C^{3/2}} M_{AB}[Q] \right) \right]^{-\frac{1}{2}} \\
&= \exp\Bigg\{ -\frac{1}{2}\mathbf{Tr}\Bigg[-\frac{1}{2}\left(\frac{w_{k-1}}{2C^{1/2}r_{k-1}}\right)^2 M[Q]^2 \\
&\quad + \frac{1}{3}\left(\frac{w_{k-1}}{2C^{1/2}r_{k-1}}\right)^3 M[Q]^3 - \frac{1}{4}\left(\frac{w_{k-1}}{2C^{1/2}r_{k-1}}\right)^4 \\
&\quad \times M[Q]^4 + O\left(w_{k-1}^5\right) \Bigg] \Bigg\}. \quad (27)
\end{aligned}
$$

By computing explicitly the $O(w_{k-1}^4)$ term on the right-hand side of Eq. (27), one finds

$$\mathbf{Tr}[M[Q]^4] = nI_1^{(4)}[Q] + 3I_2^{(4)}[Q] - 16I_3^{(4)}[Q] - 8I_4^{(4)}[Q],$$
$$I_1^{(4)}[Q] \equiv \text{Tr}[Q^4],$$
$$I_2^{(4)}[Q] \equiv (\text{Tr}[Q^2])^2,$$
$$I_3^{(4)}[Q] \equiv \sum_{b \neq c} Q_{ab}^2 Q_{ac}^2, \tag{28}$$
$$I_4^{(4)}[Q] \equiv \sum_{ab} Q_{ab}^4.$$

Plugging Eq. (28) in Eq. (27) and Eq. (27) in Eq. (20), we see that at $O(w_{k-1}^4)$, Eq. (7) generates the fourth-order monomials $\{I_l^{(4)}[Q]\}_{l=1,\ldots,4}$, which are not included into the original ansatz (15). It follows that at $O(w_k^4)$, $\mathcal{Z}_k[Q]$ must be of the form

$$\mathcal{Z}_k[Q] = \exp\left[-\left(r_k \text{Tr}[Q^2] + \frac{w_k}{3}\text{Tr}[Q^3] \right. \right.$$
$$\left. \left. + \frac{1}{4}\sum_{l=1}^{4} \lambda_{l,k} I_l^{(4)}[Q] \right) \right], \tag{29}$$

with $\lambda_{l,k} = O(w_k^4)\,\forall l = 1,\ldots,4$.

By inserting Eq. (29) into Eq. (7) and expanding up to $O(w_{k-1}^4)$, we obtain six recursion equations relating $r_k, w_k, \lambda_{1,k}, \ldots, \lambda_{4,k}$ to $r_{k-1}, w_{k-1}, \lambda_{1,k-1}, \ldots, \lambda_{4,k-1}$.

Such a systematic expansion can be iterated to any order $O(w_k^p)$, obtaining

$$\mathcal{Z}_k[Q] = \exp\left\{ -\left[c_{1,k}^{(2)} I_1^{(2)}[Q] + \sum_{j=3}^{p} \frac{1}{j} \sum_{l=1}^{n_j} c_{l,k}^{(j)} I_l^{(j)}[Q] \right] \right\}, \tag{30}$$

where $c_{1,k}^{(2)} \equiv r_k$, $c_{1,k}^{(3)} \equiv w_k$, $c_{l,k}^{(4)} \equiv \lambda_{l,k}\,\forall l = 1,\ldots,4$, $n_3 = 1$, $n_4 = 4$, and $I_1^{(3)}[Q] \equiv \text{Tr}[Q^3]$. In this way, a recursion equation relating $\{c_{l,k-1}^{(j)}\}_{j,l}$ to $\{c_{l,k}^{(j)}\}_{j,l}$ is obtained.

The number n_j of monomials generated at the step j of this procedure proliferates for increasing j. In Table I we show the invariants $I_l^{(j)}[Q]$ obtained by performing this systematic expansion up to the order $p = 5$. It is interesting to observe that the invariants $\text{Tr}[Q^2]^2, \text{Tr}[Q^2]\text{Tr}[Q^3]$ that are generated, are of $O(n^2)$ if the matrix Q_{ab} is replica symmetric. Notwithstanding this, in general they will give a nonvanishing contribution to the recursion relations $\{c_{l,k-1}^{(j)}\}_{j,l} \to \{c_{l,k}^{(j)}\}_{j,l}$, and so to ν. The recurrence equations at $O(w_k^5)$ are the following:

$$c_{1,k}^{(2)} = \frac{2c_{1,k-1}^{(2)}}{C} - \frac{\beta^2}{4} - \frac{n-2}{4}\left(\frac{c_{1,k-1}^{(3)}}{2C^{1/2}c_{1,k-1}^{(2)}} \right)^2 + (2n-1)\frac{c_{1,k-1}^{(4)}}{8Cc_{1,k-1}^{(2)}} + \frac{c_{2,k-1}^{(4)}}{2Cc_{1,k-1}^{(2)}}\left[1 + \frac{n(n-1)}{4} \right]$$
$$+ (n-2)\frac{c_{3,k-1}^{(4)}}{8Cc_{1,k-1}^{(2)}} + \frac{3c_{4,k-1}^{(4)}}{8Cc_{1,k-1}^{(2)}} + O\big[(c_{1,k-1}^{(3)})^6\big], \tag{31}$$

$$c_{1,k}^{(3)} = \frac{2c_{1,k-1}^{(3)}}{C^{3/2}} + \frac{n-2}{2}\left(\frac{c_{1,k-1}^{(3)}}{2C^{1/2}c_{1,k-1}^{(2)}} \right)^3 + \frac{3nc_{1,k-1}^{(5)}}{4C^{3/2}c_{1,k-1}^{(2)}} + (n+3)\frac{3c_{2,k-1}^{(5)}}{20C^{3/2}c_{1,k-1}^{(2)}} + \frac{9c_{3,k-1}^{(5)}}{20C^{3/2}c_{1,k-1}^{(2)}}$$
$$+ \frac{3c_{4,k-1}^{(5)}}{20C^{3/2}c_{1,k-1}^{(2)}}[12 + n(n-1)] - \frac{3c_{1,k-1}^{(3)}}{4C^{1/2}c_{1,k-1}^{(2)}}\left[\frac{(n-1)c_{1,k-1}^{(4)}}{2Cc_{1,k-1}^{(2)}} + \frac{2c_{2,k-1}^{(4)}}{Cc_{1,k-1}^{(2)}} + \frac{c_{3,k-1}^{(4)}}{2Cc_{1,k-1}^{(2)}} \right] + O\big[(c_{1,k-1}^{(3)})^7\big], \tag{32}$$

$$c_{1,k}^{(4)} = \frac{2c_{1,k-1}^{(4)}}{C^2} - \frac{n}{2}\left(\frac{c_{1,k-1}^{(3)}}{2C^{1/2}c_{1,k-1}^{(2)}} \right)^4 + O\big[(c_{1,k-1}^{(3)})^6\big], \tag{33}$$

$$c_{4,k}^{(4)} = \frac{2c_{4,k-1}^{(4)}}{C^2} + 4\left(\frac{c_{1,k-1}^{(3)}}{2C^{1/2}c_{1,k-1}^{(2)}} \right)^4 + O\big[(c_{1,k-1}^{(3)})^6\big], \tag{36}$$

$$c_{2,k}^{(4)} = \frac{2c_{2,k-1}^{(4)}}{C^2} - \frac{3}{2}\left(\frac{c_{1,k-1}^{(3)}}{2C^{1/2}c_{1,k-1}^{(2)}} \right)^4 + O\big[(c_{1,k-1}^{(3)})^6\big], \tag{34}$$

$$c_{1,k}^{(5)} = \frac{2c_{1,k-1}^{(5)}}{C^{5/2}} + \frac{n+6}{2}\left(\frac{c_{1,k-1}^{(3)}}{2C^{1/2}c_{1,k-1}^{(2)}} \right)^5 + O\big[(c_{1,k-1}^{(3)})^7\big], \tag{37}$$

$$c_{3,k}^{(4)} = \frac{2c_{3,k-1}^{(4)}}{C^2} + 8\left(\frac{c_{1,k-1}^{(3)}}{2C^{1/2}c_{1,k-1}^{(2)}} \right)^4 + O\big[(c_{1,k-1}^{(3)})^6\big], \tag{35}$$

$$c_{2,k}^{(5)} = \frac{2c_{2,k-1}^{(5)}}{C^{5/2}} - 40\left(\frac{c_{1,k-1}^{(3)}}{2C^{1/2}c_{1,k-1}^{(2)}} \right)^5 + O\big[(c_{1,k-1}^{(3)})^7\big], \tag{38}$$

FIG. 2. Graphical computation of $\mathbf{Tr}[M[Q]^2]$ in Eq. (21). In the second line, the two addends of the matrix $N[Q]_{ab,cd}$ in Eq. (19) are represented graphically in terms of the graphical objects defined in Fig. 1. In the third line, the legs of such addends are contracted with each other, and four terms are generated. The second and the third term can be easily recognized to be topologically identical, and so equal. According to the condition $Q_{aa} = 0$ in Eq. (3), the first term in the third line vanishes. Indeed, in this term the lines coming out of the square vertex Q_{ab} are connected by a circuit, meaning that the matrix element Q_{ab} is computed with $a = b$, and thus vanishes. The second and third terms in the third line also vanish because, according to Eq. (22), the dummy indexes in $\mathbf{Tr}_2$ must satisfy $a_1 \neq b_1, a_2 \neq b_2$, while the graphical structure of the second and third terms enforces the constraint $a_2 = b_2, a_1 = b_1$ respectively. Moreover, the two top lines in the third term are actually equivalent to just one line, because of the relation $\delta_{ab}^2 = \delta_{ab}$. Hence, we are left with a single term in the fourth line. In the fifth line, we perform graphically the operation $\mathbf{Tr}_2$. Such an operation can be easily implemented graphically by looking at the second line of Eq. (22). Let us expand the product of δs in the second line of Eq. (22), and recall from Fig. 1 that δ_{ab} represents a line with a circular dot connecting a with b. Hence, given a graphical object O with external legs (indexes) $(a_1, b_1), \ldots, (a_k, b_k)$, $\mathbf{Tr}_2[O]$ is nothing but the sum of all the possible 2^k contractions (performed with a line with a circular dot) of these external legs, where each contracted term is multiplied by $(-1)^{\# \text{ of contractions of the term}}$. In this case $k = 2$, so we generate 2^2 terms in the fifth line. In the sixth line, we take into account the fact that the second and third terms in the fifth line are topologically isomorph, and that the fourth term in the fifth line vanishes because of the condition $Q_{aa} = 0$. In the seventh line the unconstrained sum over the replica indexes is finally performed. This can be done graphically in the following way: When we have an external line connected to a round vertex, summing over the replica index represented by that line means that one has to simply remove the line (this is the graphical implementation of the relation $\sum_b \delta_{ab} g_b = g_a$). We do this in the first term: We sum over the top-left index, and remove the line on the top. Then we sum over the top-right index by simply multiplying by n. The sum over the bottom-left and bottom-right indexes simply yields $\mathrm{Tr}[Q^2]$. We do the same for the second term: We sum over the top-right index and remove the top line, then sum over the top-left index and remove the top-left line. Then, the sum over the bottom-left and bottom-right indexes yields $\mathrm{Tr}[Q^2]$. Hence, we get the same result as in Eq. (21).

$$c_{3,k}^{(5)} = \frac{2c_{3,k-1}^{(5)}}{C^{5/2}} + 30 \left(\frac{c_{1,k-1}^{(3)}}{2C^{1/2}c_{1,k-1}^{(2)}} \right)^5 + O\left[\left(c_{1,k-1}^{(3)} \right)^7 \right], \quad (39)$$

$$c_{4,k}^{(5)} = \frac{2c_{4,k-1}^{(5)}}{C^{5/2}} + 5 \left(\frac{c_{1,k-1}^{(3)}}{2C^{1/2}c_{1,k-1}^{(2)}} \right)^5 + O\left[\left(c_{1,k-1}^{(3)} \right)^7 \right]. \quad (40)$$

By looking at Eqs. (33)–(40) and using the definition (5), it is easy to see that the coefficients $c_{l,k}^{(4)}, c_{l,k}^{(5)}$ scale to zero as $k \to \infty$ if $\epsilon < 1/12$. It is easy to find out that this is actually true for all the coefficients $c_{l,k}^{(j)}$ with $j > 3$. Such a critical value $\epsilon = 1/12$ will be reproduced also in the field-theoretical approach in Sec. III.

The evolution Eqs. (31)–(40) depend smoothly on the replica number n, so that the analytical continuation $n \to 0$, can be done directly. By linearizing the transformation (31)–(40) around the critical fixed point $\{c_{l*}^{(j)}\}_{j,l}$ and computing the matrix $\mathcal{M}$, one can extract Λ, and so ν for $n = 0$ to the order ϵ^2 by using Eq. (26). We find

$$\nu = 3 + 36\epsilon + [432 - 27(50 + 55 \times 2^{1/3} \\ + 53 \times 2^{2/3}) \log 2]\epsilon^2 + O(\epsilon^3). \quad (41)$$

At order ϵ, our result for ν is the same as that of the power-law interaction spin glass [11] [where $\epsilon \equiv 3(\sigma - 2/3)$]. Notwithstanding this, the coefficients of the expansion in these two models will be in general different at two or more loops. As a matter of fact, the binary-tree interaction structure of the HEA emerges in the nontrivial $\log 2, 2^{1/3}$ factors in the coefficient of ϵ^2 in Eq. (41), which cannot be there in the power-law case.

Before discussing the result in Eq. (41), we point out that Wilson's method explicitly implements the binary-tree structure of the model when approaching the IR limit. As a matter of fact, the hierarchical structure of the model is explicitly exploited to construct the steps of the RG transformation. Nevertheless, if the IR limit is unique and well defined, physical observables such as ν must not depend on the technique we use to compute them in such a limit. It is thus important to verify that Eq. (41) does not depend on the method we used to reproduce the IR behavior of the theory. This has been done by reproducing Eq. (41) with a quite different field-theoretical approach.

III. FIELD-THEORETICAL METHOD

Here the IR limit is performed by constructing a functional integral field theory and by removing its IR divergences within the minimal subtraction scheme.

While in Wilson's method the IR limit was performed by looking at the scale-invariant fixed points for $k \to \infty$ after solving the recursion relation (7), in this case we perform before the large-k limit, remove the resulting IR singularities through re-normalization, and then perform the scale-invariant (IR) limit by means of the Callan-Symanzik equation.

This computation is better performed by slightly changing the definition of the model. Indeed, the following redefinition of the interaction term in Eq. (1),

$$\sum_{i<j}^{0,2^{k+1}-1} J_{12,ij} S_i S_j \rightarrow \sum_{i=0}^{2^k-1} \sum_{j=2^k}^{2^{k+1}-1} J_{12,ij} S_i S_j \qquad (42)$$

is equivalent to the original definition (1) and makes the field-theory computations simpler. The equivalence of Eq. (42) with the original definition (1) can be shown [23] by observing that the scaling of the spin coupling in the model defined by Eq. (42) differs from that in Eq. (1) for a constant multiplicative factor, and thus that the two options are equivalent, and must yield the same critical exponents. Notwithstanding this, the critical temperature of the model defined by Eq. (1) and that of the model defined by Eq. (42) are different. This can be verified by considering how the recursion relation (6) is modified when one applies the redefinition (42).

The only difference is the third factor in the second line of Eq. (6), which is now given by

$$\mathbb{E}_{J_{12}}\left[\exp\left(\frac{\beta}{2^{k\sigma}}\sum_{a=1}^{n}\sum_{i=0}^{2^{k-1}-1}\sum_{j=2^{k-1}}^{2^k-1} J_{12,ij} S_i^a S_j^a\right)\right]$$
$$= \exp\left\{\frac{\beta^2 C^k}{4}\left[\mathrm{Tr}[Q^2] - \frac{1}{4}\left(\mathrm{Tr}[Q_1^2] + \mathrm{Tr}[Q_2^2]\right)\right]\right\}.$$

It follows that the recursion relation (6) becomes

$$Z_k[Q] = \exp\left(\frac{\beta^2 C^k}{4}\mathrm{Tr}[Q^2]\right)\int[dQ_1 dQ_2]$$
$$\times \exp\left(-\frac{\beta^2 C^k}{16}\mathrm{Tr}[Q_1^2]\right) Z_{k-1}[Q_1]$$
$$\times \exp\left(-\frac{\beta^2 C^k}{16}\mathrm{Tr}[Q_2^2]\right) Z_{k-1}[Q_2]$$
$$\times \prod_{a<b=1}^{n} \delta\left(Q_{ab} - \frac{Q_{1,ab} + Q_{2,ab}}{2}\right). \qquad (43)$$

Setting

$$\mathcal{X}_k[Q] \equiv \exp\left(-\frac{\beta^2 C}{16}\mathrm{Tr}[Q^2]\right) Z_k[C^{-k/2}Q],$$

one can rewrite Eq. (43) as

$$\mathcal{X}_k[Q] = \exp\left[\frac{\beta^2}{4}\left(1 - \frac{C}{4}\right)\mathrm{Tr}[Q^2]\right]\int[dP]$$
$$\times \mathcal{X}_{k-1}\left(\frac{Q+P}{C^{1/2}}\right)\mathcal{X}_{k-1}\left(\frac{Q-P}{C^{1/2}}\right). \qquad (44)$$

By comparing Eq. (44) with Eq. (7), it is finally clear that the redefinition (42) results in an effective redefinition of the inverse temperature β.

The redefinition (42) also has a clear physical meaning. Indeed, the original definition (1) is such that, when two subsystems of 2^k spins are coupled to form a system with 2^{k+1} spins, one introduces couplings $J_{12,ij}$ between the two subsystems *and* between the spins within each subsystem, while in Eq. (42) only couplings between the two subsystems are introduced.

By iterating the recursion relation (1), one has an explicit form for the Hamiltonian $H_k^J[\vec{S}]$ of a system of 2^k spins in the large-k limit. Then, the average of the replicated partition function is expressed as an integral over the local overlap field $Q_{iab} \equiv S_i^a S_i^b$:

$$\mathbb{E}_J[Z^n] = \mathbb{E}_J\left[\sum_{\{S_i^a\}_{i,a}}\exp\left(-\beta\sum_{a=1}^{n}H_k^J[S_0^a,\dots,S_{2^k-1}^a]\right)\right]$$
$$= \int[dQ]\, e^{-S[Q]}.$$

By using a dimensional analysis, it is easy to pick up the terms in $S[Q]$ that are relevant in the IR limit. It is easy to check that $S[Q]$ is given by the sum of a quadratic term in Q_{iab}, plus a cubic term, plus higher-degree terms. The dimensions of the field Q_{iab} can be computed by imposing the adimensionality of the quadratic term, and so the dimensions of the coefficient g of the cubic term and of those of the higher-degree terms. One finds that the dimensions of g in energy is $[g] = 3\epsilon$. Thus, as in Wilson's method, the cubic term scales to zero in the IR limit for $\epsilon < 0$, while a nontrivial fixed point appears for $\epsilon > 0$. As in Wilson's method, it is easy to see that for $\epsilon < 1/12$ all the higher-degree terms in $S[Q]$ scale to zero in the IR limit. Thus, the IR-dominant part of the action reads

$$S[Q] = \frac{1}{2}\sum_{i,j=0}^{2^k-1}\Delta_{ij}\mathrm{Tr}[Q_i Q_j] + \frac{g}{3!}\sum_{i=0}^{2^k-1}\mathrm{Tr}[Q_i^3]. \qquad (45)$$

In the derivation of Eq. (45), the bare propagator Δ_{ij} originally depends on i,j through the difference $\mathcal{I}(i) - \mathcal{I}(j)$, where the function $\mathcal{I}(i)$ is defined as follows: Given $i \in [0,2^k-1]$ and its expression in base 2,

$$i = \sum_{j=0}^{k-1} a_j 2^j, \quad \mathcal{I}(i) \equiv \sum_{j=0}^{k-1} a_{k-1-j} 2^j. \qquad (46)$$

Hence, the quadratic term of Eq. (45) is not invariant under spatial translations. This would make any explicit computation of the loop integrals, and so of the critical exponents, extremely difficult to perform. This problem can be overcome by a relabeling of the sites of the lattice [33],

$$\mathcal{I}(i) \rightarrow i, \forall i = 0,\dots,2^k-1.$$

After relabeling one obtains that Δ_{ij} depends on i,j just through the difference $i - j$, thus $S[Q]$ is translationally invariant, and the ordinary Fourier transform techniques [33,34] can be employed. In particular, the Fourier representation of the propagator is

$$\Delta_{ij} = \frac{1}{2^k}\sum_{p=0}^{2^k-1}\exp\left[\frac{-2\pi\iota p(i-j)}{2^k}\right]\left(|p|_2^{2\sigma-1} + m\right), \qquad (47)$$

where $|p|_2$ is the diadic norm of p [32], and the mass $m \propto T - T_c$ has dimensions $[m] = 2\sigma - 1$.

An interesting feature of the action (45) is the fact the propagator Δ in Eq. (47) depends on the momentum p through its diadic norm $|p|_2$. If we look at the original derivation of the recursion RG equation for the Ising model in finite dimension (in particular, to the Polyakov derivation [13]), we find that the

basic approximation was to introduce an ultrametric structure in momentum space: The momentum space is divided in shells, and the sum of two momenta of a given shell cannot give a momentum of a higher momentum scale cell. This has a nice similarity with the metric properties of the diadic norm, where if p_1, p_2 are two integers, their diadic norms satisfy [32] $|p_1 + p_2|_2 \leqslant \max(|p_1|_2, |p_2|_2)$.

The field theory defined by Eq. (45) reproduces the $\mathrm{Tr}[Q^3]$ interaction term of the well-know effective actions describing the spin-glass transition in short-range [35] and long-range [11,36] spin glasses. Notwithstanding this similarity, the novelty of the HEA is that a high-order ϵ-expansion can be quite easily automatized within Wilson's method, by means of a symbolic manipulation program solving the simple RG equation (7). This is not true for such short- and long-range [11,35,36] models, where the only approach to compute the exponents is the field-theoretical one. Indeed, to the best of our knowledge, nobody ever managed to automatize a high-order computation of the critical exponents within the field-theoretical minimal subtraction scheme, even for the Ising model, because such an automation is not an easy task [37].

The field theory defined by Eq. (45) can be now analyzed within the loop-expansion framework. The renormalized mass and coupling constant are defined as

$$m = m_r + \delta m, \tag{48}$$

$$g = m_r^{\frac{3\epsilon}{2\sigma-1}} g_r Z_g. \tag{49}$$

We define the one-particle-irreducible [12] (1PI) renormalized correlation functions $\Gamma_r^{(m,l)}$ in terms of the bare 1PI correlation functions $\Gamma^{(m,l)}$ as

$$\Gamma_r^{(m,l)}\left(a_1 b_1 i_1 \cdots a_m b_m i_m; j_1 \cdots j_l; g_r, m_r^{\frac{1}{2\sigma-1}}\right)$$
$$\equiv Z_2^l \Gamma^{(m,l)}\left(a_1 b_1 i_1 \cdots a_m b_m i_m; j_1 \cdots j_l; g, m^{\frac{1}{2\sigma-1}}\right).$$

Since this model has long-range interactions, the field Q_{ab} is not renormalized, and [12] $Z_Q = 1$. Hence, all we need to compute ν are [12] the renormalization constants Z_g, Z_2 and δm. These can be obtained by computing the IR-divergent parts of $\Gamma_r^{(3,0)}, \Gamma_r^{(2,1)}$ with the minimal subtraction scheme [12]. In other words, one takes the IR limit $m_r \to 0$, and systematically removes the resulting ϵ-singular parts of the correlations functions by absorbing them into the renormalization constants Z_g, Z_2.

The Feynman diagrams contributing to $\Gamma_r^{(2,1)}, \Gamma_r^{(3,0)}$ are shown in Figs. 3 and 4, respectively, and their singular parts are in the form of $1/\epsilon, 1/\epsilon^2$ poles.

Here we show by a simple example how the ϵ-divergent part of such diagrams can be computed. Let us consider the one-loop expansion of $\Gamma_r^{(3,0)}$. This is obtained by picking up the $\mathrm{Tr}[Q^3]$ term in the renormalized 1PI generating functional [12]:

$$\Gamma_r[Q] = \frac{1}{2} \sum_{i,j=0}^{2^k-1} \Delta_{ij} \mathrm{Tr}[Q_i Q_j] + \frac{m_r^{3\epsilon} g_r}{3!} \sum_{i=0}^{2^k-1} \mathrm{Tr}[Q_i^3]$$
$$\times \left(Z_g + \frac{n-2}{8} m_r^{\frac{6\epsilon}{2\sigma-1}} \mathscr{I}_7 g_r^2 \right) + O(g_r^5). \tag{50}$$
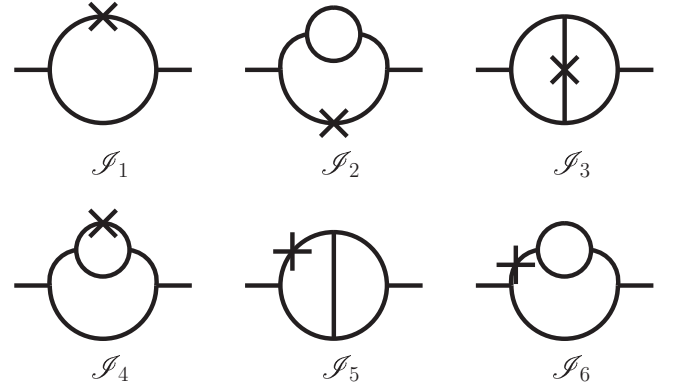

FIG. 3. One- and two-loop Feynman diagrams contributing to $\Gamma_r^{(2,1)}$. The crosses represent $\mathrm{Tr}[Q^2]$ insertions. From left to right, such diagrams computed at zero external momenta are equal to $\mathscr{I}_1, \mathscr{I}_2, \mathscr{I}_3, \mathscr{I}_4, \mathscr{I}_5, \mathscr{I}_6$, respectively.

The loop integral,

$$\mathscr{I}_7 \equiv \frac{1}{2^k} \sum_{p=0}^{2^k-1} \frac{1}{\left(m_r + \delta m + |p|_2^{2\sigma-1}\right)^3}, \tag{51}$$

is represented by the first diagram in Fig. 4.

Equation (51) has a well-defined limit for $k \to \infty$. Indeed, thanks to the translational invariance of the theory, the argument of the sum on the right-hand side of Eq. (51) depends on p just through its diadic norm. It follows that the sum $\mathscr{I}_7$ can be transformed into a sum over all possible values of $|p|_2$. Indeed, using the standard result [32] that the number of integers $p \in [0, 2^k - 1]$ such that $|p|_2 = 2^{-j}$, i.e., the volume of the diadic shell, is given by 2^{-j+k-1}, Eq. (51) becomes

$$\mathscr{I}_7 = \sum_{j=0}^{k-1} 2^{-j-1} \frac{1}{[m_r + \delta m + 2^{-j(2\sigma-1)}]^3}$$
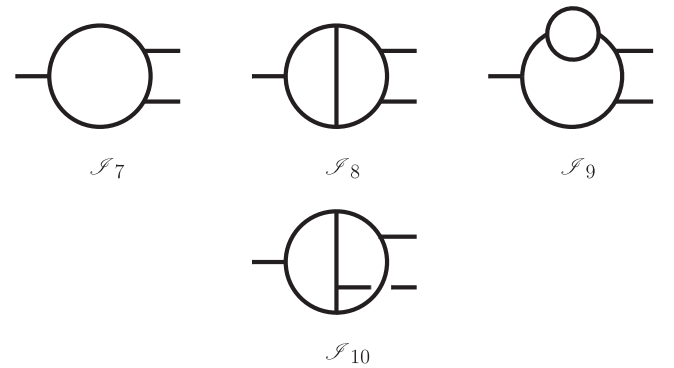$$\to \sum_{j=0}^{\infty} 2^{-j-1} \frac{1}{[m_r + \delta m + 2^{-j(2\sigma-1)}]^3}, \tag{52}$$

FIG. 4. One- and two-loop Feynman diagrams contributing to $\Gamma_r^{(3,0)}$. From left to right, such diagrams computed at zero external momenta are equal to $\mathscr{I}_7, \mathscr{I}_8, \mathscr{I}_9, \mathscr{I}_{10}$, respectively. The last diagram is nonplanar.

where in the second line of Eq. (52) the $k \to \infty$ limit has been taken, because the sum in the first line is convergent. By using the fact that $\delta m = O(g_r^2)$, we can rewrite Eq. (52) as

$$\mathscr{I}_7 = \sum_{j=0}^{\infty} 2^{-j-1} \frac{1}{[m_r + 2^{-j(2\sigma-1)}]^3} + O(g_r^2). \quad (53)$$

It is easy to see that $\mathscr{I}_7$ is IR divergent for $m_r \to 0$. Indeed, in the limit $m_r \to 0$ the sum over j in Eq. (53) is dominated by the terms in the IR region $2^{-j} = |p|_2 \to 0$. The js corresponding to this region go to infinity as $m_r \to 0$, yielding a divergent sum in $\mathscr{I}_7$.

In the IR region, the sum on the right-hand side of Eq. (53) can be approximated by an integral, because the integrand function is almost constant in the interval $[j, j+1]$ for large j. Setting $q \equiv 2^{-j}$, for $m_r \to 0$ we have $-q \log 2 \, dj = dq$, and

$$\begin{aligned}
\mathscr{I}_7 &= \frac{1}{2\log 2} \int_0^1 \frac{dq}{[m_r + q^{2\sigma-1}]^3} + O(g_r^2) \\
&= \frac{m_r^{-\frac{6\epsilon}{2\sigma-1}}}{2\log 2} \int_0^{m_r^{-\frac{1}{2\sigma-1}}} \frac{dx}{(1 + x^{2\sigma-1})^3} + O(g_r^2) \\
&\to \frac{m_r^{-\frac{6\epsilon}{2\sigma-1}}}{2\log 2} \int_0^{\infty} \frac{dx}{(1 + x^{2\sigma-1})^3} + O(g_r^2). \quad (54)
\end{aligned}$$

The integral on the right-hand side of the last line in Eq. (54) is convergent for $\epsilon > 0$, and diverges as $\epsilon \to 0$. Its ϵ-divergent part can be easily evaluated,

$$\begin{aligned}
\mathscr{I}_7 &= \frac{m_r^{-\frac{6\epsilon}{2\sigma-1}}}{4\log 2} \Gamma\left(3 + \frac{1}{1-2\sigma}\right) \\
&\quad \times \Gamma\left(1 + \frac{1}{1-2\sigma}\right) + O(g_r^2) \\
&= m_r^{-\frac{6\epsilon}{2\sigma-1}} \left[\frac{1}{12\epsilon \log 2} + O_\epsilon(1)\right] + O(g_r^2), \quad (55)
\end{aligned}$$

where Γ is the Euler-gamma function and $O_\epsilon(1)$ denotes terms that stay finite as $\epsilon \to 0$. As we will show in the following, these finite terms give a contribution to the renormalization constants at two loops. By plugging Eq. (55) into Eq. (50), one can compute the g_r^2 coefficient of Z_g by imposing that the ϵ-singular part of $\mathscr{I}_7$ is canceled by Z_g. For $n = 0$ we have

$$Z_g = 1 + \frac{1}{48\epsilon \log 2} g_r^2 + O(g_r^4). \quad (56)$$

By repeating the same computation for the generating functional $\Gamma_r[\mathcal{Q}, K]$ of correlation functions with $\text{Tr}[Q^2]$ insertions and imposing that the $\sum_{i=0}^{2^k-1} K_i \mathcal{Q}_i^2$ term is finite, i.e., that $\Gamma_r^{(2,1)}$ is finite, we obtain

$$Z_2 = 1 + \frac{1}{24\epsilon \log 2} g_r^2 + O(g_r^4).$$

Such a procedure has been pushed at two loops by an explicit calculation. Even if the evaluation of the ϵ-divergent part of the two-loop diagrams is more involved, the techniques and underlying ideas are exactly the same as those used to compute the one-loop diagram $\mathscr{I}_7$. In Figs. 3 and 4 we show the Feynman diagrams contributing to the finiteness conditions of $\Gamma_r^{(2,1)}$ and of $\Gamma_r^{(3,0)}$, respectively. We denote by $\mathscr{I}_7, \ldots, \mathscr{I}_6$ the diagrams in Fig. 3 evaluated at zero external momenta, and by $\mathscr{I}_7, \ldots, \mathscr{I}_{10}$ those in Fig. 4 evaluated at zero momenta. It is easy to show that the equalities

$$\begin{aligned}
\mathscr{I}_7 &= \mathscr{I}_7, \\
\mathscr{I}_2 &= \mathscr{I}_6 = \mathscr{I}_9, \\
\mathscr{I}_3 &= \mathscr{I}_{10}, \\
\mathscr{I}_4 &= \mathscr{I}_5 = \mathscr{I}_8
\end{aligned}$$

hold, and so that all we need to compute the renormalization constants are $\mathscr{I}_7, \mathscr{I}_2, \mathscr{I}_3, \mathscr{I}_4$. $\mathscr{I}_7$ is given by Eq. (51), while the other loop integrals are

$$\mathscr{I}_2 = \frac{1}{2^{2k}} \sum_{p=0}^{2^k-1} \sum_{q=0}^{2^k-1} \frac{1}{\left(m_r + \delta m + |p|_2^{2\sigma-1}\right)^4 \left(m_r + \delta m + |q|_2^{2\sigma-1}\right)\left(m_r + \delta m + |p - q|_2^{2\sigma-1}\right)},$$

$$\mathscr{I}_3 = \frac{1}{2^{2k}} \sum_{p=0}^{2^k-1} \sum_{q=0}^{2^k-1} \frac{1}{\left(m_r + \delta m + |p|_2^{2\sigma-1}\right)^2 \left(m_r + \delta m + |q|_2^{2\sigma-1}\right)^2\left(m_r + \delta m + |p - q|_2^{2\sigma-1}\right)^2},$$

$$\mathscr{I}_4 = \frac{1}{2^{2k}} \sum_{p=0}^{2^k-1} \sum_{q=0}^{2^k-1} \frac{1}{\left(m_r + \delta m + |p|_2^{2\sigma-1}\right)^3 \left(m_r + \delta m + |q|_2^{2\sigma-1}\right)^2\left(m_r + \delta m + |p - q|_2^{2\sigma-1}\right)}.$$

In the limit $m_r \to 0$, $\mathscr{I}_2, \mathscr{I}_3, \mathscr{I}_4$ are given by

$$\mathscr{I}_2 = m_r^{\frac{-12\epsilon}{2\sigma-1}} \left[\left(\frac{2}{2^{2/3}-1} - \frac{1}{2^{1/3}-1} - 1\right) \frac{1}{48\epsilon \log 2}\right] + O_\epsilon(1) + O(g_r^2),$$

$$\mathscr{I}_3 = m_r^{\frac{-12\epsilon}{2\sigma-1}} \left(\frac{1}{2^{1/3}-1} \frac{1}{16\epsilon \log 2}\right) + O_\epsilon(1) + O(g_r^2),$$

$$\mathscr{I}_4 = m_r^{\frac{-12\epsilon}{2\sigma-1}} \left\{ \frac{1}{2} \left[\frac{1}{(12\epsilon \log 2)^2} - \left(\frac{3}{8(\log 2)^2} + \frac{1}{48 \log 2} \right) \frac{1}{\epsilon} \right] + \left(\frac{1}{2^{1/3}-1} + \frac{1}{2^{2/3}-1} \right) \frac{1}{48\epsilon \log 2} \right\}$$
$$+ O_\epsilon(1) + O(g_r^2).$$

The finiteness of $\Gamma_r^{(3,0)}$ is imposed by making finite the $\sum_{i=0}^{2^k-1} \mathrm{Tr}[\mathcal{Q}_i^3]$ term in the 1PI generating functional $\Gamma_r[\mathcal{Q}]$. The finiteness of $\Gamma_r^{(2,1)}$ is imposed by making finite the $\sum_{i=0}^{2^k-1} K_i \mathcal{Q}_i^2$ term in the 1PI generating functional $\Gamma_r[\mathcal{Q},K]$. The two-loop expansion of $\Gamma_r[\mathcal{Q}]$ and of $\Gamma_r[\mathcal{Q},K]$ read

$$\Gamma_r[\mathcal{Q}] = g_r \sum_{i=0}^{2^k-1} \mathrm{Tr}[\mathcal{Q}_i^3] \left\{ \frac{m_r^{\frac{3\epsilon}{2\sigma-1}} Z_g}{3!} + \frac{g_r^2(n-2)}{6} \left(\frac{m_r^{\frac{3\epsilon}{2\sigma-1}} Z_g}{2} \right)^3 \mathscr{I}_7 \right.$$
$$\left. + \frac{g_r^4 m_r^{\frac{15\epsilon}{2\sigma-1}} Z_g^5}{3! 2^7} [6(n-2)^2 \mathscr{I}_9 + 6(n-2)^2 \mathscr{I}_8 + 2(n(n-1) - 4 - (n-2)^2) \mathscr{I}_{10}] + O(g_r^6) \right\}$$
$$+ \cdots, \tag{57}$$

$$\Gamma_r[\mathcal{Q},K] = \sum_{i=0}^{2^k-1} K_i \mathrm{Tr}[\mathcal{Q}_i^2] \left\{ \frac{Z_2}{4} + \frac{g_r^2 Z_2 Z_g^2 m_r^{\frac{6\epsilon}{2\sigma-1}} (n-2)}{16} \mathscr{I}_1 + \frac{g_r^4 m_r^{\frac{12\epsilon}{2\sigma-1}} (n-2)^2}{2^8} [2(3\mathscr{I}_2 + 2\mathscr{I}_4) \right.$$
$$\left. + 4\mathscr{I}_5 + \mathscr{I}_3] + O(g_r^6) \right\} + \cdots, \tag{58}$$

where the $\cdots$ in Eq. (57) stands for terms that are not cubic in $\mathcal{Q}_i$, while the $\cdots$ in Eq. (58) stands for terms that are not quadratic in $\mathcal{Q}_i$ and linear in K_i. The renormalization constants Z_g, Z_2 are calculated by imposing that the renormalized correlation functions $\Gamma_r^{(3,0)}$, $\Gamma_r^{(2,1)}$ are finite, i.e., that the term in curly brackets in Eq. (57) and that in Eq. (58) have no singularities [12] in ϵ. At this purpose, we observe that the finite part of the integral $\mathscr{I}_7$ contributes to the renormalization constants at two loops. For example, let us consider the second addend in curly brackets on the right-hand side of Eq. (57). By using Eq. (55) and the one-loop result (56) for Z_g, it is easy to see that this term produces an ϵ-divergent term, given by

$$\frac{g_r^2(n-2)}{48} m_r^{\frac{9\epsilon}{2\sigma-1}} \frac{3}{48\epsilon \log 2} g_r^2 O_\epsilon(1), \tag{59}$$

where $O_\epsilon(1)$ is the finite part of $\mathscr{I}_7$ in Eq. (55). The term in Eq. (59) is of $O(g_r^4)$ and singular in ϵ. Hence, it contributes to the $O(g_r^4)$ term in Z_g.

After setting $n = 0$ and imposing the finiteness conditions, we find

$$Z_g = 1 + \frac{g_r^2}{48\epsilon \log 2}$$
$$+ g_r^4 \left[\frac{1}{1536\epsilon^2(\log 2)^2} + \frac{5 + 2 \times 2^{2/3}}{512\epsilon \log 2} \right] + O(g_r^6), \tag{60}$$

$$Z_2 = 1 + \frac{g_r^2}{24\epsilon \log 2}$$
$$+ g_r^4 \left[\frac{1}{576\epsilon^2(\log 2)^2} - 5 \frac{(1 + 11 \times 2^{1/3} + 7 \times 2^{2/3})}{2304\epsilon \log 2} \right]$$
$$+ O(g_r^6). \tag{61}$$

It is also easy to verify that $\delta m = O(g_r^4)$.

Once the IR-safe renormalized theory has been constructed, the effective coupling constant $g(\lambda)$ at the energy scale λ is computed from the Callan-Symanzik equation in terms of the β function by setting $\mu \equiv m_r^{\frac{1}{2\sigma-1}}$,

$$\beta(g_r) = \mu \left. \frac{\partial g_r}{\partial \mu} \right|_{g,m}, \quad \beta(g(\lambda)) = \lambda \frac{dg(\lambda)}{d\lambda}. \tag{62}$$

$\beta(g_r)$ can be explicitly computed in terms of the renormalization constant Z_g by applying $\mu \frac{\partial}{\partial \mu}|_{g,m}$ on both sides of Eq. (49):

$$0 = \mu \left. \frac{\partial}{\partial \mu} \right|_{g,m} (\mu^{3\epsilon} g_r Z_g). \tag{63}$$

The right-hand side of Eq. (63) can then be worked out explicitly by using the two-loop result (60) and substituting systematically $\beta(g_r)$ to $\mu \frac{\partial g_r}{\partial \mu}|_{g,m}$. In this way, an explicit equation for $\beta(g_r)$ is obtained. One finds

$$\beta(g_r) = -3\epsilon g_r + \frac{g_r^3}{8 \log 2} + 3 \frac{5 + 2 \times 2^{2/3}}{128 \log 2} g_r^5 + O(g_r^7). \tag{64}$$

Setting $g_r^* \equiv g(\lambda = 0)$, we see from Eq. (64) that the fixed point $g_r^* = 0$ is stable only for $\epsilon < 0$, while for $\epsilon > 0$ a non-Gaussian fixed point g_r^* of order $\sqrt{\epsilon}$ arises, as predicted by dimensional considerations and by Wilson's method. Now the IR limit $\lambda \to 0$ can be safely taken, and the scaling relations yield ν, in terms of g_r^* and Z_2,

$$\eta_2[g_r] \equiv \mu \left. \frac{\partial \log Z_2}{\partial \mu} \right|_{g,m}, \quad \nu = \frac{1}{\eta_2[g_r^*] + 2\sigma - 1}. \tag{65}$$

By plugging the two-loop result for g_r^* and Z_2 into Eq. (65), we reproduce the result (41) derived within Wilson's method.

We observe that the analytical effort to derive the coefficients of the ϵ-expansion in this field-theoretical approach is much bigger than that of Wilson's method. Indeed, in the minimal subtraction scheme additional calculations are

needed to extract the coefficients of the ϵ poles of the Feynman diagrams in Figs. 3 and 4. It follows that for an automatized implementation of the high-order ϵ-expansion, Wilson's method turns out to be much better performing that the field-theoretical method. Notwithstanding this, the tensorial operations needed to compute the Q-dependence of the diagrams in this field-theoretical approach turn out to be exactly the same as those needed in Sec. II, and no additional effort has been required to compute them.

IV. CONCLUSIONS

In a previous work [26], we set up two perturbative approaches to compute the IR behavior of a strongly frustrated non-mean-field spin-glass system, the HEA model. The two methods are based on the replica approach, and in particular on the assumption that the physics of the system is encoded in the limit where the number of replicas n tends to zero. Within the ϵ-expansion framework, the two approaches yield the same prediction at two loops for the critical exponent ν related to the divergence of the correlation length.

In this work the two-loop computation is shown in all its most relevant details, so that the reader can reproduce it. Moreover, we show the underlying renormalization group ideas implemented in the two computation methods. One of these is the existence of a characteristic length ξ diverging at the IR critical fixed point, where the theory is invariant with respect to reparametrization of the length scale.

In addition, we show with an explicit example that such a computation of the critical exponents could be quite easily automatized, i.e., implemented in a computer program, in order to compute high orders of the ϵ-expansion, and so eventually make this theory physically predictive. Indeed, we give a graphical interpretation of the cumbersome tensorial operations needed to compute ν and previously used in Ref. [26]. Such a graphical method makes the calculations much more straightforward and suitable for an implementation in a computer program to compute high orders of the ϵ series. We observe that once this high-order series in ϵ will be known, some resummation technique will be needed to make the theory predictive, because the series probably has a nonconvergent behavior. If the high-order series could be made convergent by means of some appropriate resummation technique, this calculation would yield an analytical control on the critical exponents, resulting in a precise prediction for a non-mean-field spin glass mimicking a real system.

[1] M. Mézard, G. Parisi, and M. A. Virasoro, *Spin Glass Theory and Beyond* (World Scientific, Singapore, 1987).

[2] T. Castellani and A. Cavagna, J. Stat. Mech. (2005) P05012.

[3] G. Parisi, J. Phys. A **13**, 1101 (1980).

[4] B. Derrida, Phys. Rev. Lett. **45**, 79 (1980).

[5] W. L. McMillan, J. Phys. C **17**, 3179 (1984).

[6] A. J. Bray and M. A. Moore, Phys. Rev. Lett. **58**, 57 (1987).

[7] D. S. Fisher and D. A. Huse, Phys. Rev. B **38**, 373 (1988).

[8] T. R. Kirkpatrick, D. Thirumalai, and P. G. Wolynes, Phys. Rev. A **40**, 1045 (1989).

[9] C. De Dominicis and I. Giardina, *Random Fields and Spin Glasses: A Field Theory Approach* (Springer, Berlin, 2006).

[10] J. H. Chen and T. C. Lubensky, Phys. Rev. B **16**, 2106 (1977).

[11] G. Kotliar, P. W. Anderson, and D. L. Stein, Phys. Rev. B **27**, 602 (1983).

[12] J. Zinn-Justin, Int. Ser. Monogr. Phys. **113**, 1 (2002).

[13] K. G. Wilson and J. B. Kogut, Phys. Rept. **12**, 75 (1974).

[14] I. Giardina (private communication).

[15] F. J. Dyson, Commun. Math. Phys. **12**, 91 (1969).

[16] P. Collet and J. Eckmann, Lect. Notes Phys. **74** (1978).

[17] P. Collet and J. Eckmann, Commun. Math. Phys. **55**, 67 (1977).

[18] M. Cassandro and G. Jona-Lasinio, Adv. Phys. **27**, 6 (1978).

[19] A. Theumann, Phys. Rev. B **21**, 2984 (1980).

[20] A. Theumann, Phys. Rev. B **22**, 5441 (1980).

[21] A. N. Berker and S. Ostlund, J. Phys. C **12**, 4961 (1979).

[22] E. Gardner, J. Phys. (Paris) **45**, 1755 (1984).

[23] S. Franz, T. Jörg, and G. Parisi, J. Stat. Mech. (2009) P02002.

[24] M. Castellana, A. Decelle, S. Franz, M. Mézard, and G. Parisi, Phys. Rev. Lett. **104**, 127206 (2010).

[25] Y. V. Fyodorov, A. Ossipov, and A. Rodriguez, J. Stat. Mech. (2009) L12001.

[26] M. Castellana and G. Parisi, Phys. Rev. E **82**, 040105(R) (2010).

[27] H. G. Katzgraber and A. P. Young, Phys. Rev. B **67**, 134410 (2003).

[28] H. G. Katzgraber and A. P. Young, Phys. Rev. B **72**, 184416 (2005).

[29] H. G. Katzgraber, A. K. Hartmann, and A. P. Young, in *Condensed Matter Physics XXI*, edited by D. P. Landau, S. P. Lewis, and H. B. Schuttler (Springer, Heidelberg, 2008).

[30] L. Leuzzi, J. Phys. A **32**, 1417 (1999).

[31] L. Leuzzi, G. Parisi, F. Ricci-Tersenghi, and J. J. Ruiz-Lorenzo, Phys. Rev. Lett. **101**, 107203 (2008).

[32] G. Parisi and N. Sourlas, Eur. Phys. J. B **14**, 3 (2000).

[33] Y. Meurice, J. Math. Phys. **36**, 1812 (1995).

[34] M. Taibleson, *Fourier Analysis on Local Fields* (Princeton University Press, Princeton, NJ, 1976).

[35] A. B. Harris, T. C. Lubensky, and J. H. Chen, Phys. Rev. Lett. **36**, 415 (1976).

[36] M. C. Chang and J. Sak, Phys. Rev. B **29**, 2652 (1984).

[37] R. Guida and P. Ribeca, J. Stat. Mech. (2006) P02007.

Real-space Renormalization Group analysis of a non-mean-field spin-glass

M. CASTELLANA[(a)]

Dipartimento di Fisica, Università di Roma La Sapienza - 00185 Rome, Italy, EU and
LPTMS, CNRS and Université Paris-Sud, UMR8626 - Bâtiment 100, 91405 Orsay, France, EU

Abstract – A real-space Renormalization Group approach is presented for a non-mean-field spin-glass. This approach has been conceived in the effort to develop an alternative method to the Renormalization Group approaches based on the replica method. Indeed, non-perturbative effects in the latter are quite generally out of control, in such a way that such approaches are non-predictive. On the contrary, we show that the real-space method presented here yields a precise prediction of the critical behavior and exponents of the model.

Introduction. – Spin-glasses, structural glasses, and the physical description of their critical properties have interested statistical physicists for several decades. The mean-field theory of these models [1,2] provides a physically and mathematically rich picture of their physics and of their critical behavior. Notwithstanding the great success of such mean-field theories, real spin-glasses are non-mean-field systems, because they have short-range interactions. It follows that these systems cannot be described by mean-field models. Indeed, the generalization of the above mean-field theories to the non-mean-field case is an extremely difficult task that has still not been achieved, so that the development of a predictive and consistent theory of glassy phenomena for real systems is still one of the most hotly debated and challenging problems in this domain [3].

This task is difficult to achieve because the perturbative field-theoretical techniques [4,5] yielding the Ising model critical exponents with striking agreement with experimental data do not apply to locally interacting glassy systems. Indeed, a considerable difficulty in the set-up of a loop-expansion for a spin-glass with local interactions is that the mean-field saddle-point has a very complicated structure [1,6], and non-perturbative effects are not under control, in such a way that the properties of the large-scale behavior of these systems are still far from being clarified.

The physical properties of the paramagnetic-ferromagnetic transition emerge clearly in ferromagnetic systems in the original work of Wilson [4], where one can write a simple Renormalization Group (RG) transformation describing a flow under length-scale re-parametrizations. These RG equations are exact in non-mean-field models with power-law ferromagnetic interactions built on hierarchical lattices like Dyson Hierarchical Model (DHM) [7]. Indeed, in these models one can write an exact RG transformation for the probability distribution of the magnetization of the system, in such a way that all the relevant physical information on criticality and all the fundamental RG concepts are encoded into this equation, whose solution can be explicitly built up with the ϵ-expansion technique [8,9]. Accordingly, to investigate the RG properties of non-mean-field spin-glasses it is natural to consider spin-glass models built on hierarchical lattices. This study has been done heretofore only for some particular models. On the one hand, models with local interactions on hierarchical lattices built on diamond plaquettes [10] have been widely studied in their spin-glass version, and have been shown to lead to weakly frustrated systems even in their mean-field limit [11], and so are not a good representative of a realistic strongly frustrated spin-glass. On the other hand, a RG analysis of a different kind of random models on Dyson hierarchical lattice, and of their physical and non-physical infrared (IR) fixed points, has been done heretofore [12]. Unfortunately, also in these models spins belonging to the same hierarchical block interact with each other with the same [12] random coupling J, in such a way that frustration turns out to be relatively weak and they are not a good representative of a realistic strongly frustrated system.

[(a)]E-mail: `michele.castellana@u-psud.ft`

The study of such non-mean-field strongly frustrated spin-glasses is difficult also because it is hard to identify the correct order parameter and write the resulting RG equations for a function or functional of it without relying on the replica method, which is generally able to make predictions for the critical exponents only in the mean-field case [6].

In this letter we present a real-space RG method for a non-mean-field strongly frustrated spin-glass on a hierarchical lattice, the Hierarchical Edwards-Anderson model (HEA) [13], that does not rely on the replica method. Even if this method does not identify the order parameter of the system, it is interesting from the methodological point of view, because it yields a way to implement Kadanoff's [14] block-spin decimation rule in a strongly frustrated system, and to write the resulting RG equations. In this way, precise predictions on the critical exponents are obtained.

The HEA is defined as a system of 2^{k+1} spins $S_1, \ldots, S_{2^{k+1}}$, $S_i = \pm 1$, with an energy function defined recursively by coupling two systems, say system 1 and system 2, of 2^k spins

$$H_{k+1}[S_1, \ldots, S_{2^{k+1}}] = H_k^1[S_1, \ldots, S_{2^k}]$$
$$+ H_k^2[S_{2^k+1}, \ldots, S_{2^{k+1}}] - 2^{-\sigma(k+1)} \sum_{i=1}^{2^k} \sum_{j=2^k+1}^{2^{k+1}} J_{ij} S_i S_j,$$
$$(1)$$

where J_{ij} are random couplings distributed according to a Gaussian law with zero mean and unit variance, and $H_0[S] = 0$. σ is a parameter tuning the decay of the interaction strength between spins with distance. It turns out that for $\sigma < 1/2$ the thermodynamic limit is ill-defined, because the interaction energy grows with k faster than the volume 2^k, while for $\sigma > 1$ the interaction energy goes to zero for large k, and no finite-temperature phase transition occurs. Accordingly, in the following we will take $1/2 < \sigma < 1$. In this interval, the model is a non-mean-field one, and the mean-field limit is recovered for $\sigma \to 1/2$ [13].

The critical properties of the HEA have been studied heretofore within the replica formalism [15], showing that the system has a classical behavior in the region $1/2 < \sigma \leqslant 2/3$, where the mean-field approximation is correct, while non-mean-field effects are important for $2/3 < \sigma < 1$. This analysis makes a prediction for the critical exponents only in the classical region $1/2 < \sigma \leqslant 2/3$, because in the non-classical region $2/3 < \sigma < 1$ the first few orders of the $\sigma - 2/3 \equiv \epsilon$-expansion have a non-convergent behavior, and higher orders are not known.

Before exposing the real-space approach for the HEA, let us illustrate it in the case where the couplings J_{ij} in eq. (1) are ferromagnetic, i.e. for the well-known DHM [7], in order to test the consistency of our method.

The real-space approach for Dyson Hierarchical Model. – DHM is defined [7] as a system of 2^{k+1} spins

$S_1, \ldots, S_{2^{k+1}}$, $S_i = \pm 1$, with an energy function defined recursively by coupling two systems, say system 1 and system 2, of 2^k spins

$$H_{k+1}^F[S_1, \ldots, S_{2^{k+1}}] = H_k^F[S_1, \ldots, S_{2^k}]$$
$$+ H_k^F[S_{2^k+1}, \ldots, S_{2^{k+1}}] - J2^{2(1-\sigma_F)(k+1)}\left(\frac{1}{2^{k+1}}\sum_{i=1}^{2^{k+1}} S_i\right)^2,$$
$$(2)$$

where $H_0^F[S] = 0$, the suffix F stands for "ferromagnetic", and one can show that $1/2 < \sigma_F < 1$, with the same argument as that used to derive the constraints on σ for the HEA.

The real-space RG method is built up by iterating exactly k_0 times the recursion equation (2). In this way, a DHM with 2^{k_0} spins $S_1, \ldots, S_{2^{k_0}}$ and Hamiltonian $H_{k_0}^F[S_1, \ldots, S_{2^{k_0}}]$ is obtained. We now want to build up a 2^{k_0+1}-spin DHM starting from such a 2^{k_0}-spin DHM, which can be done as follows. We consider a 2^{k_0-1}-spin DHM, where J is replaced by another coupling J'. Such a 2^{k_0-1}-spin DHM is defined by iterating $k_0 - 1$ times eq. (2) with $J \to J'$, and its Hamiltonian is $H_{k_0-1}^{'F}[S_1', \cdots, S_{2^{k_0-1}}']$. Given J, the coupling J' is chosen in such a way that the 2^{k_0-1}-spin DHM represents as well as possible the 2^{k_0}-spin DHM, as qualitatively depicted in fig. 1. This approximation is practically implemented by considering a physical observable $O_{k_0}^F(\beta J)$ of the 2^{k_0}-spin DHM, and an observable $O_{k_0-1}^F(\beta J')$ of the 2^{k_0-1}-spin DHM, where β is the inverse temperature. The normalized magnetization on the left half of the 2^{k_0}-spin DHM is

$$m_L \equiv \left(\frac{1}{2^{k_0-1}}\sum_{i=1}^{2^{k_0-1}} S_i\right)\left\{\mathbb{E}_{\vec{S}}\left[\left(\frac{1}{2^{k_0-1}}\sum_{i=1}^{2^{k_0-1}} S_i\right)^2\right]\right\}^{-\frac{1}{2}},$$

and an analog expression holds for the right-half magnetization m_R, where $\mathbb{E}_{\vec{S}}$ stands for the thermal average at fixed β, performed with weight $\exp(-\beta H_{k_0}^F)$. The normalized magnetization on the left half of the 2^{k_0-1}-spin DHM is

$$m_L' \equiv \left(\frac{1}{2^{k_0-2}}\sum_{i=1}^{2^{k_0-2}} S_i'\right)\left\{\mathbb{E}_{\vec{S}'}\left[\left(\frac{1}{2^{k_0-2}}\sum_{i=1}^{2^{k_0-2}} S_i'\right)^2\right]\right\}^{-\frac{1}{2}},$$

and an analog expression holds for the right-half magnetization m_R', where $\mathbb{E}_{\vec{S}'}$ stands for the thermal average with weight $\exp(-\beta H_{k_0-1}^{'F})$. Mimicking Kadanoff's block-spin rule, for the 2^{k_0-1}-spin DHM to be a good approximation of the 2^{k_0}-spin DHM, we map the block of the spins in the left half of the 2^{k_0}-spin DHM into the block of the spins in the left half of the 2^{k_0-1}-spin DHM, and do the same for the right half. In order to do so, we choose the observables to be $O_{k_0}^F(\beta J) \equiv \mathbb{E}_{\vec{S}}[m_L m_R]$, $O_{k_0-1}^F(\beta J') \equiv \mathbb{E}_{\vec{S}'}[m_L' m_R']$, and impose the equation

$$O_{k_0}^F(\beta J) = O_{k_0-1}^F(\beta J'). \qquad (3)$$

For any fixed J, eq. (3) determines J' as a function of J, as the value of the coupling of the 2^{k_0-1}-spin DHM such that
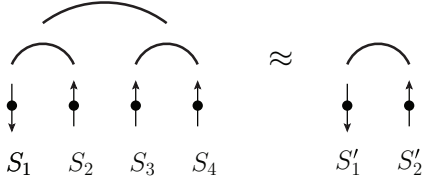
Fig. 1: Approximation of the real-space approach for $k_0 = 2$. In the implementation of the real-space approach for DHM, a 2^2-spin DHM is approximated by a 2-spin DHM. In the implementation of the real-space approach for the HEA, a 2^2-spin HEA is approximated by a 2-spin HEA.

Fig. 2: (Color online) $2^{1/\nu_F}$ as a function of σ_F for $1/2 \leqslant \sigma_F \leqslant 1$. The black dashed line represents the upper critical dimension $\sigma_F = 3/4$ discussed in [8]. The points are given by $2^{1/\nu_F}$ computed with the real-space method for $5 \leqslant k_0 \leqslant 12$, and the gray points are $2^{1/\nu_F}$ extrapolated to $k_0 \to \infty$ by fitting $\Lambda_{F\,RS}$ vs. k_0 with a function of the form $f(k_0) \equiv a - b \cdot \gamma^{k_0}$. The orange dashed curve and the green triangular points are $2^{1/\nu_F}$ obtained in [16]. Top inset: γ vs. σ_F. Bottom inset: $\Lambda_{F\,RS}$ vs. k_0 for $\sigma_F = 0.92$, its fitting function $f(k_0)$ and the extrapolated value a.

this yields the best possible approximation of the 2^{k_0}-spin DHM.

Let us take two copies of the 2^{k_0-1}-spin DHM. We make these two copies interact according to eq. (2), and form a 2^{k_0}-spin DHM. Since each of the DHMs that we make interact represents a 2^{k_0}-spin DHM, the 2^{k_0}-spin DHM result of this composition effectively represents a 2^{k_0+1}-spin DHM. Once again, this DHM is then approximated as a 2^{k_0-1}-spin DHM with coupling, say, J'', and so on. Setting $J_0 \equiv J, J_1 \equiv J', J_2 \equiv J'', \ldots$, eq. (3) establishes a relation between J_k and J_{k+1}, physically representing the RG flow of the coupling J_k under reparametrization of the unit length $2^k \to 2^{k+1}$.

The RG eq. (3) is not exact, because it relies on the fact that a 2^{k_0}-spin DHM is approximated by a 2^{k_0-1}-spin DHM. Nevertheless, such an approximation must become asymptotically exact in the large k_0-limit, where both 2^{k_0} and 2^{k_0-1} tend to infinity. Quite large values of k_0 can be reached by exploiting the hierarchical structure of the system [7], in such a way that the observables $O_{k_0}^F, O_{k_0-1}^F$ can be calculated with a computational cost proportional to 2^{k_0}. It is possible to show that for any k_0 the real-space method reproduces the constraints $1/2 < \sigma_F < 1$. Indeed, for $\sigma_F > 1$ eq. (3) gives $J' < J, \forall J, \beta$, so that the coupling J_k goes to 0 for large k, and no phase transition occurs. On the contrary, for $\sigma_F < 1/2$ one has $J' > J, \forall J, \beta$, and the model is thermodynamically unstable.

The critical exponent ν_F related to the divergence of the correlation length [5] is easily obtained by linearising the transformation $\beta J \to \beta J'$ in the neighborhood of the critical fixed point $\beta J = \beta J' \equiv K_c$ [4], $2^{1/\nu_F} = \frac{d\beta J'}{d\beta J}|_{\beta J = K_c}$. In fig. 2 we depict $2^{1/\nu_F}$ computed with this method, together with $2^{1/\nu_F}$ computed by Bleher [9,16] with an independent approach, as a function of $1/2 \leqslant \sigma_F \leqslant 1$. The latter calculation makes an exact prediction for $2^{1/\nu_F}$ in the region $1/2 < \sigma_F \leqslant 3/4$ where the mean-field approximation is exact, while it estimates $2^{1/\nu_F}$ in the non-mean-field region $3/4 < \sigma_F \leqslant 1$ by means of a series of successive approximations. In the bottom inset of fig. 2 we show how $\Lambda_{F\,RS}$ for finite k_0 has been extrapolated to the $k_0 \to \infty$-limit: for every σ_F the sequence $\Lambda_{F\,RS}$ vs. k_0 is fitted with a function of the form $a - b \cdot \gamma^{k_0}$, and a is the resulting extrapolated value. The parameter $\gamma < 1$ is an indicator of the speed of convergence with respect to
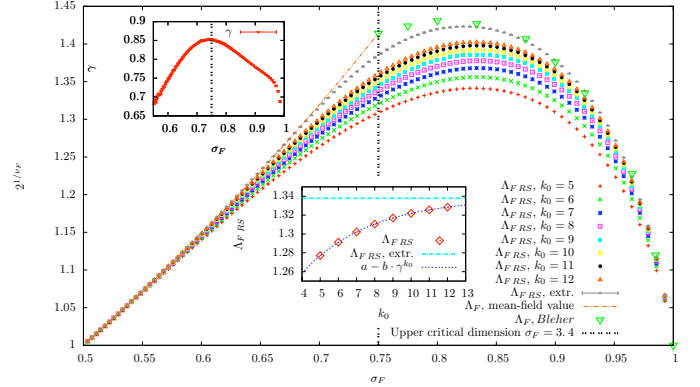
k_0: the larger γ the slower the convergence. In the main plot of fig. 2 the extrapolated value is depicted, and this is in good agreement with the value given in [9,16]. The region where the disagreement between the two methods is largest is $\sigma_F \approx 3/4$, where $2^{1/\nu_F}$ must be non-analytic [8]. This non-analiticity cannot show up for finite k_0. However, in the top inset of fig. 2 we show that the parameter γ has a maximum at $\sigma_F \approx 3/4$. This fact shows that the convergence slows down in the neighborhood of $\sigma_F = 3/4$, i.e. that the real-space method signals the appearance of a non-analiticity of ν_F at $\sigma_F = 3/4$, which results from the switchover from a mean-field to a non-mean-field regime.

It is now natural to generalise this real-space approach to the HEA model, to compare its predictions with those obtained with the replica method.

The real-space approach for the Hierarchical Edwards-Anderson model. – Let us now illustrate how to apply the real-space method to the HEA, by considering first the simplest case $k_0 = 2$. The reader should follow our derivation in close analogy with that exposed above for DHM. A HEA with 2^2 spins $S_1, \cdots, S_4$ and Hamiltonian $H_2[S_1, \ldots, S_4]$ is built up exactly by means of the recursion equation (1). We set $\mathcal{J}_{ij} \equiv 2^{-\sigma} J_{ij}$, where by definition the couplings $\{\mathcal{J}_{ij}\}_{ij}$ are independent identically distributed random variables, and the probability distribution of each of them will be denoted by $p(\mathcal{J})$. Thus, we consider a 2-spin HEA, whose Hamiltonian reads $H'_1[S'_1, S'_2] = -\mathcal{J}'_{12} S'_1 S'_2$. For each realization of the couplings $\{\mathcal{J}_{ij}\}_{ij}$, we choose $\mathcal{J}'_{12}$ as a function of $\{\mathcal{J}_{ij}\}_{ij}$ in such a way that the 2-spin HEA yields the best possible approximation of the 2^2-spin HEA, as qualitatively depicted in fig. 1.

In order to do so, let us consider a physical observable $O_2(\{\beta\mathcal{J}_{ij}\}_{ij})$ of the 2^2-spin HEA, depending on the 6 couplings $\{\mathcal{J}_{ij}\}_{ij}$ and β, and an observable $O_1(\beta\mathcal{J}'_{12})$ of the 2-spin HEA. Inspired by the fact that the order parameter in the mean-field case is the overlap [1], here we build up O_2 and O_1 as the thermal average of products of spin overlaps. To build up O_2 and O_1, consider two *real* replicas $\vec{S}^1, \vec{S}^2$ of the spins of the 2^2-spin model, and two real replicas $\vec{S'}^1, \vec{S'}^2$ of the spins of the 2-spin model. The normalized overlap between $\vec{S}^1$ and $\vec{S}^2$ on the left leaf of the 2^2-spin HEA is

$$Q_L \equiv \frac{S_1^1 S_1^2 + S_2^1 S_2^2}{2} \left\{ \mathbb{E}_{\vec{S}^1, \vec{S}^2} \left[\left(\frac{S_1^1 S_1^2 + S_2^1 S_2^2}{2} \right)^2 \right] \right\}^{-\frac{1}{2}},$$

and an analog expression holds for the right-leaf overlap Q_R, where $\mathbb{E}_{\vec{S}}$ stands for the thermal average at fixed disorder $\{\mathcal{J}_{ij}\}_{ij}$ and β. The normalized overlap between $\vec{S'}^1$ and $\vec{S'}^2$ on the left leaf of the 2-spin HEA is $Q'_L = S_1'^1 S_1'^2$, and an analog expression holds for the right-leaf overlap Q'_R. Following Kadanoff's decimation rule, we map the 2^2-spin HEA into the 2-spin HEA by imposing that the spins S_1, S_2 correspond to the spin S'_1, and that the spins S_3, S_4 correspond to the spin S'_2. This mapping results in a correspondence between Q_L and Q'_L, and between Q_R and Q'_R. By choosing the observables as $O_2(\{\beta\mathcal{J}_{ij}\}) \equiv \mathbb{E}_{\vec{S}^1, \vec{S}^2}[Q_L Q_R]$, $O_1(\beta\mathcal{J}'_{12}) \equiv \mathbb{E}_{\vec{S'}^1, \vec{S'}^2}[Q'_L Q'_R]$, Kadanoff's decimation rule can be practically implemented by imposing the equality

$$O_2(\{\beta\mathcal{J}_{ij}\}) = O_1(\beta\mathcal{J}'_{12}), \tag{4}$$

where $\mathbb{E}_{\vec{S'}}$ stands for the thermal average at fixed disorder $\mathcal{J}'_{12}$ and β. For any realization of the couplings $\{\mathcal{J}_{ij}\}_{ij}$, eq. (4) determines $\mathcal{J}'_{12}$ as a function of $\{\mathcal{J}_{ij}\}_{ij}$ in such a way that the 2-spin HEA yields the best possible approximation of the 2^2-spin HEA. Accordingly, the distribution $p(\mathcal{J})$ induces a distribution of $\mathcal{J}'_{12}$, that we will denote by $p'(\mathcal{J}'_{12})$. The mapping between $p(\mathcal{J})$ and $p'(\mathcal{J}')$ can be shown to be given by

$$p'(\mathcal{J}') = \int \left[\prod_{i<j} p(\mathcal{J}_{ij}) \mathrm{d}\mathcal{J}_{ij} \right] \frac{1}{2}$$

$$\times \left[\delta\left(\mathcal{J}' - \frac{1}{\beta}\mathrm{arctanh}\left(\sqrt{O_2(\{\beta\mathcal{J}_{ij}\})} \right) \right) \right.$$

$$\left. + \delta\left(\mathcal{J}' + \frac{1}{\beta}\mathrm{arctanh}\left(\sqrt{O_2(\{\beta\mathcal{J}_{ij}\})} \right) \right) \right]. \tag{5}$$

According to the iterative construction of eq. (1), a new HEA is then constructed by taking two realizations of the 2-spin HEA. Each realization is given by throwing the coupling $\mathcal{J}'$ according to its probability distribution $p'(\mathcal{J}')$. We make these two copies interact to form a 2^2-spin HEA. Since each of the HEAs that we put into interaction represents a 2^2-spin HEA, the 2^2-spin HEA result of this composition effectively represents a 2^3-spin

HEA. At the next step of the iteration, this 2^2-spin HEA is again approximated as a 2-spin HEA with coupling, say, $\mathcal{J}''_{12}$, and the probability distribution $p''(\mathcal{J}''_{12})$ of $\mathcal{J}''_{12}$ is computed from $p'(\mathcal{J}')$, and so on. This step is repeated k-times, and a system representing a 2^{2+k}-spin HEA is obtained.

Setting $p_0(\mathcal{J}) \equiv p(\mathcal{J})$, $p_1(\mathcal{J}) \equiv p'(\mathcal{J})$, $p_2(\mathcal{J}) \equiv p''(\mathcal{J}), \ldots$, eq. (5) establishes a relation between $p_k(\mathcal{J})$ and $p_{k+1}(\mathcal{J})$, physically representing the RG flow of the probability distribution of the coupling $p_k(\mathcal{J})$ under reparametrization of the unit length $2^k \to 2^{k+1}$.

Equation (5) has been solved by means of the population dynamics algorithm. In population dynamics, one represents the function $p(\mathcal{J})$ as a population of $P \gg 1$ numbers $\{\mathcal{J}_i\}_{i=1,\ldots,P}$, where each $\mathcal{J}_i$ has been drawn with probability $p(\mathcal{J}_i)$. The mapping $p(\mathcal{J}) \to p'(\mathcal{J}')$ given by eq. (5) results into a mapping between $\{\mathcal{J}_i\}_i$ and the population $\{\mathcal{J}'_i\}_i$ representing $p'(\mathcal{J}')$.

The structure of the fixed points of eq. (5) has been thus investigated numerically, showing that there exists a finite value of $\beta = \beta_c$ such that for $\beta < \beta_c$ $p_k(\mathcal{J})$ shrinks to a $\delta(\mathcal{J})$ as k is increased, while for $\beta > \beta_c$ $p_k(\mathcal{J})$ broadens, *i.e.* its variance is an ever-increasing function of k. The physical interpretation of these two temperature regimes is that for $\beta < \beta_c$ $p_k(\mathcal{J})$ flows to the attractive high-temperature fixed point with $\mathcal{J} = 0$ where spins are decorrelated, while for $\beta > \beta_c$ it flows to the attractive low-temperature fixed point with $\mathcal{J} = \infty$ where spins are strongly correlated. This fact implies that as the temperature is lowered below $T_c = 1/\beta_c$ a phase transition occurs, resulting in the appearance of a collective and strongly interacting behavior of spins in the low-temperature phase. The existence of such a finite-temperature phase transition for a diluted version of HEA model has already been established heretofore in MC simulations by means of finite-size scaling techniques [13].

The population dynamics approach reproduces the fact that for $\sigma < 1/2$ the thermodynamic limit is ill-defined, as we discussed above. Indeed, the numerics show that for $\sigma \to 1/2$ $\beta_c \to 0$, in such a way that the variance of $p_k(\mathcal{J})$, and so that of H_2, is an ever-increasing function of k, and the thermodynamic limit $k \to \infty$ is ill-defined. Unfortunately, the second constraint $\sigma < 1$ is not reproduced. This is presumably due to the fact that eq. (5) implements only the lowest-order approximation of the real-space method, $k_0 = 2$, and that the method is exact only for large k_0. This hypothesis is supported by the estimate of the critical exponents that we will discuss in the following, suggesting that the closer σ to one, the larger the values of k_0 needed to have a good estimate of the exact result. Accordingly, for $\sigma \to 1$ a significantly better description would be obtained if larger values of k_0 were accessible, and the $\sigma < 1$-limit would be recovered.

The numerical implementation of eq. (5) also reveals the existence of a repulsive critical fixed point with a finite width, that we will denote by $p_*(\mathcal{J})$, and that is reached by iterating eq. (5) with $\beta = \beta_c$. The critical exponent

ν governing the power-law divergence of the correlation length at $\beta = \beta_c$ is determined [4] from the spectrum of the matrix linearising the transformation (5) in the neighborhood of $p_*(\mathcal{J})$.

Before discussing the numerical results for $p_*(\mathcal{J})$ and ν, let us discuss better implementations with $k_0 > 2$ of this method. The only new element with respect to the $k_0 = 2$-case is the following. For $k_0 > 2$, a 2^{k_0}-spin HEA is approximated as a 2^{k_0-1}-spin HEA. The latter has $2^{k_0-1}(2^{k_0-1} - 1)/2 \equiv M' > 1$ couplings $\{\mathcal{J}'_{ij}\}_{ij}$. It turns out that even if the couplings $\{\mathcal{J}_{ij}\}_{ij}$ of the 2^{k_0}-spin HEA are independent, $\{\mathcal{J}'_{ij}\}_{ij}$ are not, and are distributed according to a joint distribution that we denote by $p'_C(\{\mathcal{J}'_{ij}\}_{ij})$. In other words, correlations are introduced when iterating the RG transformation. In the present treatment these correlations have been neglected by assuming that each of the $\{\mathcal{J}'_{ij}\}_{ij}$ behaves as an independent random variable distributed according to a distribution obtained as the average of M' distributions, each obtained by marginalising $p'_C(\{\mathcal{J}'_{ij}\}_{ij})$ with respect to $M' - 1$ couplings $\mathcal{J}'_{ij}$.

The real-space approach has been thus implemented for $k_0 = 2, 3, 4$. Larger values of k_0 were not accessible, because the computational cost scales as $2^{2^{k_0}}$. All the qualitative features emerging for $k_0 = 2$ and discussed above are preserved for $k_0 = 3, 4$. In fig. 3 we depict $p_*(\mathcal{J})$ as a function of $\mathcal{J}$ for several values of σ in the $k_0 = 3, 4$ approximations. Two interesting features emerge from fig. 3. Firstly, the discrepancy between $p_*(\mathcal{J})$ in the $k_0 = 3$-approximation and $p_*(\mathcal{J})$ in the $k_0 = 4$-approximation is relatively small, signaling that $k_0 = 4$ is hopefully large enough for the real-space approach to give a reasonably good estimate of the critical fixed point, at least for the values of σ considered in fig. 3. Secondly, a plausible scenario resulting from the inset of fig. 3 is that, for large k_0, $p_*(0) = 0$ for $\sigma < 2/3$, while $p_*(0) > 0$ for $\sigma > 2/3$. Interestingly, the analysis of the HEA based on the replica approach [13,15] predicts a sharp change of behavior from a mean-field regime for $1/2 < \sigma \leqslant 2/3$ to a non-mean-field regime for $2/3 < \sigma < 1$. In the real-space approach $\mathcal{J}_{ij}$ is nothing but the effective coupling between spins S_i and S_j of a 2^{k_0}-spin HEA. At the critical point, S_i is obtained as the coarse-graining of a group of 2^l, $l \gg 1$ spins, which have been progressively decimated and reduced to a single, effective degree of freedom S_i, and the same property holds for S_j. For $\sigma < 2/3$ the model is effectively mean-field, and should thus behave as a fully connected one. Accordingly, the 2^l spins represented by S_i must interact with all the other spins, and so with the 2^l spins represented by S_j. Thus, the effective coupling between S_i and S_j cannot vanish, i.e. $p_*(0) = 0$. In the non-mean-field case $\sigma > 2/3$ the system is not fully connected, because the effective interaction range is finite. Accordingly, there is a finite probability that the 2^l spins represented by S_i do not interact with the 2^l spins represented by S_j. Thus, the effective coupling between S_i and S_j can vanish, i.e. $p_*(0) > 0$. According to this argument, this change of
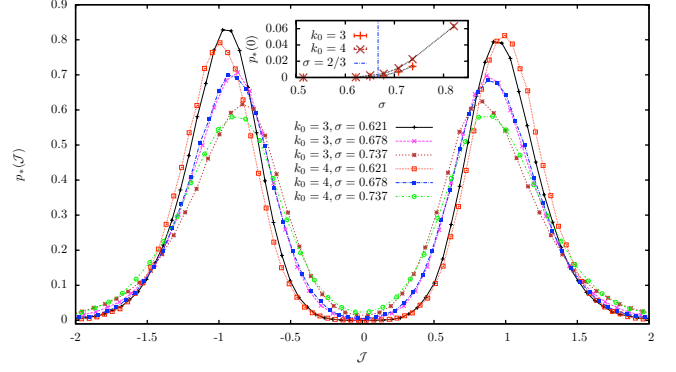

Fig. 3: (Color online) Fixed point $p_*(\mathcal{J})$ as a function of $\mathcal{J}$ for $k_0 = 3$ and $\sigma = 0.621, 0.678, 0.737$ (in black, violet and brown, respectively), and for $k_0 = 4$ and $\sigma = 0.621, 0.678, 0.737$ (in red, blue and green, respectively). For these values of σ, the discrepancy between $p_*(\mathcal{J})$ in the $k_0 = 3$-approximation and $p_*(\mathcal{J})$ in the $k_0 = 4$-approximation is relatively small, signaling that $k_0 = 4$ is presumably large enough for the method to give a reasonably good estimate of the critical fixed point. Inset: $p_*(0)$ vs. σ for $k_0 = 3, 4$. A plausible picture resulting from the data is that, for large k_0, $p_*(0) = 0$ for $\sigma < 2/3$ and $p_*(0) > 0$ for $\sigma > 2/3$. This picture has a clear physical interpretation given in the text, and suggests a change of behavior at $\sigma = 2/3$, reminiscent of the switchover from a mean-field regime for $\sigma < 2/3$ to a non-mean-field regime for $\sigma > 2/3$ predicted by the replica approach.

behavior of $p_*(0)$ at $\sigma = 2/3$ can be seen as the switchover from a mean-field behavior to a non-mean-field one, and is predicted independently and confirmed by the replica analysis of the HEA.

Let us now consider the predictions on the critical exponent ν. In fig. 4 we depict $2^{1/\nu}$ obtained with the $k_0 = 2$, 3, 4-approximation and $2^{1/\nu}$ obtained with the replica approach [15] as a function of σ, both in the mean-field region $\sigma \leqslant 2/3$ and in the non-mean-field region $\sigma > 2/3$, where the first two orders of the ϵ-expansion are depicted. The agreement between $2^{1/\nu}$ computed with the real-space approach for $k_0 = 2$ and $2^{1/\nu}$ computed with the replica approach is not satisfying. Nevertheless, for $k_0 = 3, 4$ the agreement in the mean-field region $1/2 < \sigma \leqslant 2/3$ is very good, and serves as an important test of the real-space method. A quantitative comparison between $2^{1/\nu}$ of the real-space approach and that of the replica approach in the non-mean-field region cannot be done, because in the latter the ϵ-expansion is out of control, i.e. the first two orders of the expansion have a non-convergent behavior, and higher orders are not known. Accordingly, the ϵ-expansion curve depicted in fig. 4 must not be considered as an estimate of $2^{1/\nu}$. A prediction for ν in the non-classical region $\sigma > 2/3$ for a diluted version [13] of the HEA is given by Monte Carlo (MC) simulations [17]. According to [17], for $\sigma > 2/3$ $2^{1/\nu}$ is a decreasing function of σ in the neighborhood of $\sigma = 2/3$, which is in disagreement with the results of the real-space approach, fig. 4. This discrepancy will be discussed in the following.
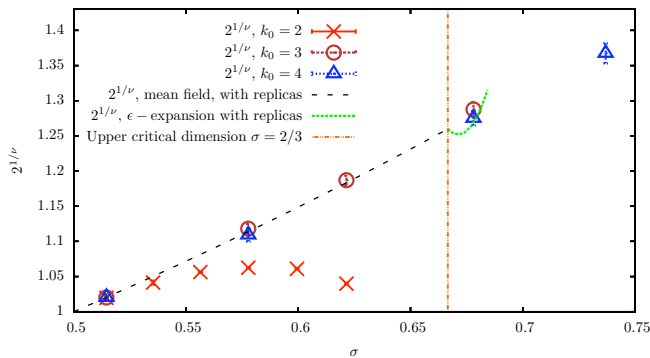
Fig. 4: (Color online) $2^{1/\nu}$ as a function of σ. The red, brown and blue points are $2^{1/\nu}$ computed with the real-space approach for $k_0 = 2, 3, 4$, respectively. The black dashed curve and the green dashed curve are $2^{1/\nu}$ obtained with the replica approach [15], and the orange dashed line is the relative upper critical dimension $\sigma = 2/3$ [13]: the black dashed curve is the mean-field value of $2^{1/\nu}$ for $\sigma \leqslant 2/3$, while the green dashed curve is the two-loops result obtained with the ϵ-expansion.

Discussion and conclusions. – In this letter we developed a real-space RG approach for a non-mean-field spin-glass, the Hierarchical Edwards-Anderson model (HEA). This approach is innovative with respect to the RG approaches to disordered, strongly frustrated systems developed heretofore that generally rely on the replica method [6]. Indeed, the present approach does not make use of the replica method, which is generally predictive only in the mean-field case, and cannot handle perturbatively fluctuations around the mean-field saddle-point, because these turn out to be out of control [6]. Through a systematic approximation scheme, the present approach implements Kadanoff's block-spin decimation rule [14] on spins. The implementation of such a decimation rule to a disordered, strongly frustrated system has not been developed heretofore because of the intrinsic difficulties introduced by frustration, and allows for an effective reduction of the degrees of freedom of the system. Kadanoff's block-spin rule is practically implemented by approximating a 2^{k_0}-spin HEA as a 2^{k_0-1}-spin HEA. Such an approximation is practically performed by imposing that some observables of the 2^{k_0}-spin HEA are equal to some corresponding observables of the 2^{k_0-1}-spin HEA. For large k_0, the method is asymptotically exact, and so are its predictions on the critical features of the system. The method has been tested in the simplest case of Dyson Hierarchical Model [7], which is the ferromagnetic version of the HEA, and the resulting predictions for the critical exponents are in good agreement with the results obtained heretofore [16].

The method has been then applied to the HEA, and identifies the existence of a phase transition in the system, yielding a prediction on the critical exponent ν related to the power-law divergence of the correlation length at the critical point. Above the upper critical dimension

($\sigma < 2/3$), the results for ν are in very good quantitative agreement with those given by the replica method [15] even for small $k_0 = 3, 4$. Below the upper critical dimension ($\sigma > 2/3$), the ϵ-expansion for the critical exponents performed within the replica method is not predictive, because the first few orders have a non-convergent behavior, and higher orders are not known. Hence, a quantitative comparison between the real-space approach and the replica approach is not possible. On the contrary, Monte Carlo (MC) simulations [17] for a diluted version of the HEA yield a prediction for the critical exponents in this region. These are in disagreement with those of the real-space approach. This discrepancy could be due both to the smallness of k_0 in the real-space approach, or to the non-universality of the exponent ν when switching from the HEA defined here to its diluted version, or to the fact that correlations between the spin couplings have been neglected in the real-space approach. Accordingly, the quantitative estimate of ν below the upper critical dimension is a still untamed issue, which could be suitable for future investigations and developments of the present real-space method.

$* * *$

REFERENCES

[1] Parisi G., *Phys. Rev. Lett.*, **43** (1979) 1754.
[2] Derrida B., *Phys. Rev. Lett.*, **45** (1980) 79.
[3] Fisher D. S. and Huse D. A., *Phys. Rev. Lett.*, **56** (1986) 1601.
[4] Wilson K. and Kogut J., *Phys. Rep.*, **12** (1974) 75.
[5] Zinn-Justin J., *Int. Ser. Monogr. Phys.*, **113** (2002) 1.
[6] Dominicis C. D. and Giardina I., *Random Fields and Spin-glasses: A Field-theory Approach* (Springer) 2006.
[7] Dyson F., *Commun. Math. Phys.*, **12** (1969) 91.
[8] Collet P. and Eckmann J., *Lect. Notes Phys.*, **74** (1978).
[9] Collet P., Eckmann J. P. and Hirsbrunner B., *Phys. Lett. B*, **71** (1977) 385.
[10] Berker A. N. and Ostlund S., *J. Phys. C: Solid State Phys.*, **12** (1979) 4961.
[11] Gardner E., *J. Phys.*, **45** (1984) 1755.
[12] Theumann A., *Phys. Rev. B*, **21** (1980) 2984.
[13] Franz S., Jörg T. and Parisi G., *J. Stat. Mech.: Theory Exp.* (2009) P02002.
[14] Kadanoff L. P., *Physics*, **2** (1966) 263.
[15] Castellana M. and Parisi G., *Phys. Rev. E*, **82** (2010) 040105; **83** (2011) 041134.
[16] Bleher P. M., Preprint, Institute of Applied Mathematics of the Academy of Sciences USSR (1975).
[17] Franz S. and Decelle A., in preparation.

Role of Tracy-Widom distribution in finite-size fluctuations of the critical temperature of the Sherrington-Kirkpatrick spin glass

Michele Castellana[1,2,*] and Elia Zarinelli[1,†]

[1]*LPTMS, CNRS and Université Paris-Sud, UMR8626, Bât. 100, F-91405 Orsay, France*
[2]*Dipartimento di Fisica, Università di Roma 'La Sapienza', I-00185 Rome, Italy*

We investigate the finite-size fluctuations due to quenched disorder of the critical temperature of the Sherrington-Kirkpatrick spin glass. In order to accomplish this task, we perform a finite-size analysis of the spectrum of the susceptibility matrix obtained via the Plefka expansion. By exploiting results from random matrix theory, we obtain that the fluctuations of the critical temperature are described by the Tracy-Widom distribution with a nontrivial scaling exponent 2/3.

I. INTRODUCTION

The characterization of phase transitions in terms of a nonanalytic behavior of thermodynamic functions in the infinite-size limit has served as a milestone[1–5] in the physical understanding of critical phenomena. In laboratory and numerical experiments, the system size is always finite so that the divergences that would result from such a nonanalytic behavior are suppressed, and are replaced by smooth maxima occurring in the observation of physical quantities as a function of the temperature. In disordered systems, the pseudocritical temperature, defined as the temperature at which this maximum occurs, is a fluctuating quantity depending on the realization of the disorder. A question naturally arises: Can the fluctuations of the pseudocritical temperature be understood and determined with tools of probability theory? Several efforts have been made to study the fluctuations of the pseudocritical temperature for disordered finite-dimensional systems[6–9] and their physical implications. For instance, recently Sarlat *et al.*[10] showed that the theory of finite-size scaling, which is valid for pure systems, fails in fully-connected disordered models because of strong sample-to-sample fluctuations of the critical temperature.

The extreme value statistics of independent random variables is a well-established problem with a long history dating from the original work of Gumbel,[11] while less results are known in the case where the random variables are correlated. The eigenvalues of a Gaussian random matrix are an example of strongly-correlated random variables.[12] Only recently, Tracy and Widom calculated[13–16] exactly the probability distribution of the typical fluctuations of the largest eigenvalue of a Gaussian random matrix around its infinite-size value. This distribution, known as Tracy-Widom distribution, appears in many different models of statistical physics, such as directed polymers[17,18] or polynuclear growth models,[19] showing profound links between such different systems. Conversely, to our knowledge no evident connections between the Tracy-Widom distribution and the physics of spin glasses have been found heretofore.[20]

The purpose of this work is to try to fill this gap. We consider a mean-field spin glass model, the Sherrington-Kirkpatrick (SK) model,[21] and propose a definition of finite-size critical temperature inspired by a previous analysis.[8] We investigate the finite-size fluctuations of this pseudocritical temperature in the framework of extreme value statistics and show that the Tracy-Widom distribution naturally arises in the description of such fluctuations.

II. THE MODEL

The SK model[21] is defined by the Hamiltonian

$$H[\{S_i\},\{x_{ij}\}] = -\frac{J}{N^{1/2}} \sum_{i>j=1}^{N} x_{ij} S_i S_j + \sum_{i=1}^{N} h_i S_i, \quad (1)$$

where $S_i = \pm 1$, the couplings $\{x_{ij}\}_{i>j=1,...,N} \equiv \{x\}$, $x_{ji} \equiv x_{ij} \forall i > j$ are distributed according to normal distribution with zero mean and unit variance

$$P(x) = \frac{1}{\sqrt{2\pi}} e^{-\frac{x^2}{2}}, \quad (2)$$

and J is a parameter tuning the strength of the interaction energy between spins.

The low-temperature features of the SK model have been widely investigated in the past and are encoded in Parisi's solution,[22–27] showing that the SK has a finite-temperature spin glass transition at $T_c = J$ in the thermodynamic limit $N \to \infty$. The critical value T_c can be physically thought of as the value of the temperature where ergodicity breaking occurs and the spin glass susceptibility diverges.[25–27]

While Parisi's solution has been derived within the replica method framework, an alternative approach to study the SK model had been previously proposed by Thouless, Anderson, and Palmer (TAP).[28] Within this approach, the system is described in terms of a free energy at fixed local magnetization, and the physical features derived in terms of the resulting free-energy landscape. Later on, Plefka[29] showed that the TAP free energy can be obtained as the result of a systematic expansion in powers of the parameter

$$\alpha \equiv \frac{\beta J}{N^{1/2}},$$

where β is the inverse temperature of the model. This α expansion, known as Plefka expansion, has thus served as a method for deriving the TAP free energy for several classes of models, and has been extensively used in different contexts in physics, from classical disordered systems,[30–32] to general quantum systems.[33–36] It is a general fact that, if the model is

defined on a complete graph, the Plefka expansion truncates to a finite order in α, because higher-order terms should vanish in the thermodynamic limit. In particular, for the SK model, the orders of the expansion larger than three are believed[37] to vanish in the limit $N \to \infty$ in such a way that the expansion truncates, and one is left with the first three orders of the α series, which reads

$$
\begin{aligned}
-\beta f(\{m_i\}, \beta) = & -\sum_i \left[\frac{1+m_i}{2} \ln\left(\frac{1+m_i}{2}\right) + \frac{1-m_i}{2} \right. \\
& \left. \times \ln\left(\frac{1-m_i}{2}\right) \right] + \alpha \sum_{i>j} x_{ij} m_i m_j \\
& + \frac{\alpha^2}{2} \sum_{i>j} x_{ij}^2 (1-m_i^2)(1-m_j^2),
\end{aligned} \tag{3}
$$

where $m_i \equiv \langle S_i \rangle$ is the local magnetization, i.e., the thermal average $\langle \rangle$ of the spin S_i performed with the Boltzmann weight given by Eq. (1) at fixed disorder $\{x\}$.

In the thermodynamic limit $N \to \infty$, for temperatures $T > T_c$, the only minimum of $\beta f(\{m\}, \beta)$ is the paramagnetic one $m_i = 0 \, \forall i$. Below the critical temperature, the TAP free energy has exponentially many different minima: the system is in a glassy phase. In this framework, the phase transition at T_c can be characterized by the inverse susceptibility matrix, which is also the Hessian of βf

$$
\beta \chi_{ij}^{-1} \equiv \beta \frac{\partial h_i}{\partial m_j} = \frac{\partial^2 (\beta f)}{\partial m_i \partial m_j}. \tag{4}
$$

The inverse susceptibility matrix in the paramagnetic minimum at leading order in N is

$$
\beta \chi_{ij}^{-1} = (1 + \beta^2 J^2) \delta_{ij} - \alpha x_{ij}. \tag{5}
$$

Random-matrix theory states that the average density of eigenvalues of x,

$$
\rho_N(\lambda) \equiv \mathbb{E}_x \left[\frac{1}{N} \sum_{i=1}^N \delta(\lambda - \lambda_i(\{x\})) \right], \tag{6}
$$

has a semicircular shape[38] on a finite support $[-2\sqrt{N}, 2\sqrt{N}]$, where $\mathbb{E}_x$ denotes expectation value with respect to the random bonds $\{x\}$, and $\lambda_i(\{x\})$ is the ith eigenvalue of x. Equation (6) is nothing but the density of eigenvalues of the Gaussian orthogonal ensemble (GOE) of Gaussian random matrices.[12,39]

Due to self-averaging properties, the minimal eigenvalue of $\beta \chi^{-1}$ in the paramagnetic minimum is $\lambda = (1 - \beta J)^2$. This shows that, for $T > T_c$, λ is strictly positive and vanishes at T_c, implying the divergence[25] of the spin glass susceptibility $1/\beta^2 \mathrm{Tr}[\chi^2]$. Since λ is also the minimal eigenvalue of the Hessian matrix of βf in the paramagnetic minimum, we deduce that this is stable for $T > T_c$ and becomes marginally stable at T_c.

This analysis sheds some light on the nature of the spin glass transition of the SK model in terms of the minimal eigenvalue λ of the inverse susceptibility matrix (Hessian matrix) in the thermodynamic limit. In this paper we generalize such analysis to finite sizes, where no diverging susceptibility nor uniquely-defined critical temperature exists, and the minimal eigenvalue λ acquires fluctuations due to quenched disorder.

We show that a finite-size pseudocritical temperature can be suitably defined and investigate its finite-size fluctuations with respect to disorder. As a result of this work, these fluctuations are found to be described by the Tracy-Widom distribution.

The rest of the paper is structured as follows. In Sec. III, we generalize Eq. (5) to finite sizes, in the simplifying assumption that the Plefka expansion can be truncated up to order α^2, which is known as the TAP approach. We then study the finite-size fluctuations of the minimal eigenvalue λ of the susceptibility matrix, and show that they are governed by the TW distribution. In Sec. IV, we extend this simplified approach by taking into account the full Plefka expansion, by performing an infinite re-summation of the series. Hence, in Sec. V, we give a suitable definition of a finite-size pseudocritical temperature, and show that its fluctuations are governed by the TW distribution. In Sec. VI, this result is discussed in the perspective of generalizing it to more realistic spin glass models.

III. FINITE-SIZE ANALYSIS OF THE SUSCEPTIBILITY IN THE TAP APPROXIMATION

In this section, we study the finite-size fluctuations due to disorder of the minimal eigenvalue of the inverse susceptibility matrix $\beta \chi^{-1}$ at the paramagnetic minimum $m_i = 0 \, \forall i$, by considering the free energy f in the TAP approximation, Eq. (3). We want to stress the fact that large deviations of thermodynamics quantities of the SK model have been already studied heretofore. For example, Parisi *et al.* have studied[40,41] the probability distribution of large deviations of the free energy within the replica approach. The same authors studied the probability of positive large deviations of the free energy per spin in general mean-field spin-glass models,[42] and showed that such fluctuations can be interpreted in terms of the fluctuations of the largest eigenvalue of Gaussian matrices, in analogy with the lines followed in the present work.

Back to the TAP equations (3), the inverse susceptibility matrix in the paramagnetic minimum for finite N reads

$$
\begin{aligned}
\beta \chi_{ij}^{-1} &= -\alpha x_{ij} + \delta_{ij} \left(1 + \alpha^2 \sum_{k \neq i} x_{ki}^2 \right) \\
&= -\alpha x_{ij} + \delta_{ij}(1 + \beta^2 J^2) + \delta_{ij} \frac{(\beta J)^2}{\sqrt{N}} z_2^i,
\end{aligned} \tag{7}
$$

where

$$
z_2^i \equiv \sqrt{N} \left(\frac{1}{N} \sum_{k \neq i} x_{ki}^2 - 1 \right). \tag{8}
$$

According to Eq. (8), z_2^i is given by the sum of $N - 1$ independent identically-distributed random variables x_{ij}^2. By the central limit theorem, at leading order in N the variable z_2^i is distributed according to a Gaussian distribution with zero mean and variance 2

$$
p_N(z_2^i = z) \overset{N \to \infty}{\to} \frac{1}{\sqrt{4\pi}} e^{-z^2/4}, \tag{9}
$$

where $p_N(z_2^i = z)$ denotes the probability that z_2^i is equal to z at finite size N.

We set

$$\beta \chi_{ij}^{-1} \equiv \delta_{ij}(1 + \beta^2 J^2) + \alpha M_{ij}. \tag{10}$$

According to Eq. (8), the diagonal elements of M_{ij} are random variables correlated to out-of-diagonal elements. The statistical properties of the spectrum of a random matrix whose entries are correlated to each other has been studied heretofore only in some cases. For instance, Stäring *et al.*[43] studied the average eigenvalue density for matrices with a constraint implying that the row sum of matrix elements should vanish, and other correlated cases have been investigated both from a physical[44] and mathematical[45] point of view.

In recent years, a huge amount of results has been obtained on the distribution of the minimal eigenvalue of a $N \times N$ random matrix drawn from Gaussian ensembles, such as GOE. In particular, Tracy and Widom[13–16] deduced that for large N, small fluctuations of the minimal eigenvalue λ_{GOE} of a GOE matrix around its leading-order value $-2\sqrt{N}$ are given by

$$\lambda_{\mathrm{GOE}} = -2\sqrt{N} + \frac{1}{N^{1/6}} \phi_{\mathrm{GOE}}, \tag{11}$$

where ϕ_{GOE} is a random variable distributed according to the Tracy-Widom (TW) distribution for the GOE ensemble $p_{\mathrm{GOE}}(\phi)$. It follows that for $\beta J = 1$ if z_2^i was independent on $\{x\}$, the matrix M_{ij} would belong to the GOE ensemble, and the minimal eigenvalue λ of $\beta \chi^{-1}$ would define a variable ϕ according to

$$\lambda = \frac{1}{N^{2/3}} \phi, \tag{12}$$

and ϕ would be distributed according to the TW distribution $p_{\mathrm{GOE}}(\phi)$.

As shown in Appendix A, this is indeed the case for z_2^i, which can be treated, at leading order in N, as a random variable independent on x_{ij}. The general idea is that z_2^i is given by the sum of $N - 1$ terms all of the same order of magnitude, and only one amongst these $N - 1$ terms depends on x_{ij}. It follows that at leading order in N, z_2^i can be considered as independent on x_{ij}. Since in Eq. (7) z_2^i is multiplied by a sub-leading factor $1/\sqrt{N}$, in Eq. (7) we can consider z_2^i at leading order in N, and treat it as independent on x_{ij}.

To test this independence property, we set $\beta J = 1$, generate numerically $S \gg 1$ samples of the $N \times N$ matrix $\beta \chi^{-1}$, and compute the average density of eigenvalues of $\beta \chi^{-1}$, defined as in Eq. (6), together with the distribution of the minimal eigenvalue λ for several sizes N. The eigenvalue distribution $\rho_N(\lambda)$ as a function of λ is depicted in Fig. 1, and tends to the Wigner semicircle as N is increased, showing that the minimal eigenvalue λ tends to 0 as $N \to \infty$.

The finite-size fluctuations of λ around 0 are then investigated in Fig. 2. Defining ϕ in terms of λ by Eq. (12), in Fig. 2 we depict the distribution $p_N(\phi)$ of the variable ϕ for several sizes N, and show that for increasing N, $p_N(\phi)$ approaches the TW distribution $p_{\mathrm{GOE}}(\phi)$. Let us introduce the central moments

$$\mu_1^N \equiv \mathbb{E}_N[\phi],$$
$$\mu_i^N \equiv \mathbb{E}_N[(\phi - \mathbb{E}_N[\phi])^i] \; \forall i > 1$$
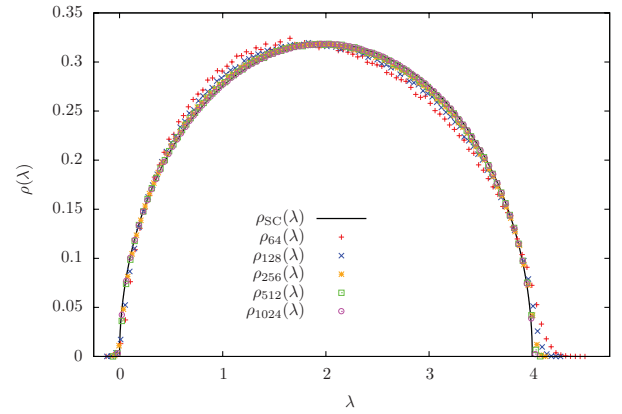

FIG. 1. (Color online) Density of eigenvalues $\rho_N(\lambda)$ of the matrix $\beta \chi^{-1}$ for $N = 64, 128, 256, 512, 1024$ (in red, blue, yellow, green, violet respectively), $\beta J = 1$ and $S = 16 \times 10^3$, and Wigner semicircular law $\rho_{\mathrm{SC}}(\lambda) = 1/(2\pi)\sqrt{4 - (2 - \lambda)^2}$ (black) as a function of λ. $\rho_N(\lambda)$ approaches $\rho_{\mathrm{SC}}(\lambda)$ as N is increased.

of $p_N(\phi)$, and the central moments

$$\mu_1^{\mathrm{GOE}} \equiv \mathbb{E}_{\mathrm{GOE}}[\phi],$$
$$\mu_i^{\mathrm{GOE}} \equiv \mathbb{E}_{\mathrm{GOE}}[(\phi - \mathbb{E}_{\mathrm{GOE}}[\phi])^i] \; \forall i > 1$$

of the TW distribution, where

$$\mathbb{E}_N[\cdot] \equiv \int d\phi \, p_N(\phi) \cdot ,$$

$$\mathbb{E}_{\mathrm{GOE}}[\cdot] \equiv \int d\phi \, p_{\mathrm{GOE}}(\phi) \cdot .$$

In the inset of Fig. 2 we depict μ_i^N for several sizes N and μ_i^{GOE} as a function of i, showing that μ_i^N converges to μ_i^{GOE} as N is increased.

In Fig. 3, this convergence is clarified by depicting $\Delta \mu_i^N \equiv (\mu_i^N - \mu_i^{\mathrm{GOE}})/\mu_i^{\mathrm{GOE}}$ for several values of $i > 1$ as a function of N. $\Delta \mu_i^N$ is found to converge to 0 for large N. In the inset of Fig. 3, we depict $\Delta \mu_1^N$ as a function of N, showing that the convergence of the first central moment with N is much slower than that of the other central moments. It is interesting to observe that a slowly-converging first moment has been recently found also in experimental[46] and numerical[47] data of models of growing interfaces where the TW distribution appears.

The analytical argument proving the independence property of z_2^i has been thus confirmed by this numerical calculation. Hence, the main result of this section is that the finite-size fluctuations of the minimal eigenvalue of the susceptibility matrix $\beta \chi^{-1}$ in the TAP approximation for $\beta J = 1$ are of the order of $N^{-2/3}$ and are distributed according to the TW law. These fluctuations have already been found to be of the order of $N^{-2/3}$ in a previous work,[48] and more recently reconsidered,[49] following an independent derivation based on scaling arguments, even though the distribution has not been worked out. Our approach sheds some light on the nature of the scaling $N^{-2/3}$, which is nontrivial, since it comes from the $N^{-1/6}$ scaling of the TW distribution, which is found to govern the fluctuations of λ. Moreover, the fact that we find the same scaling as that found in such previous works can be considered as a consistency test of our calculation.
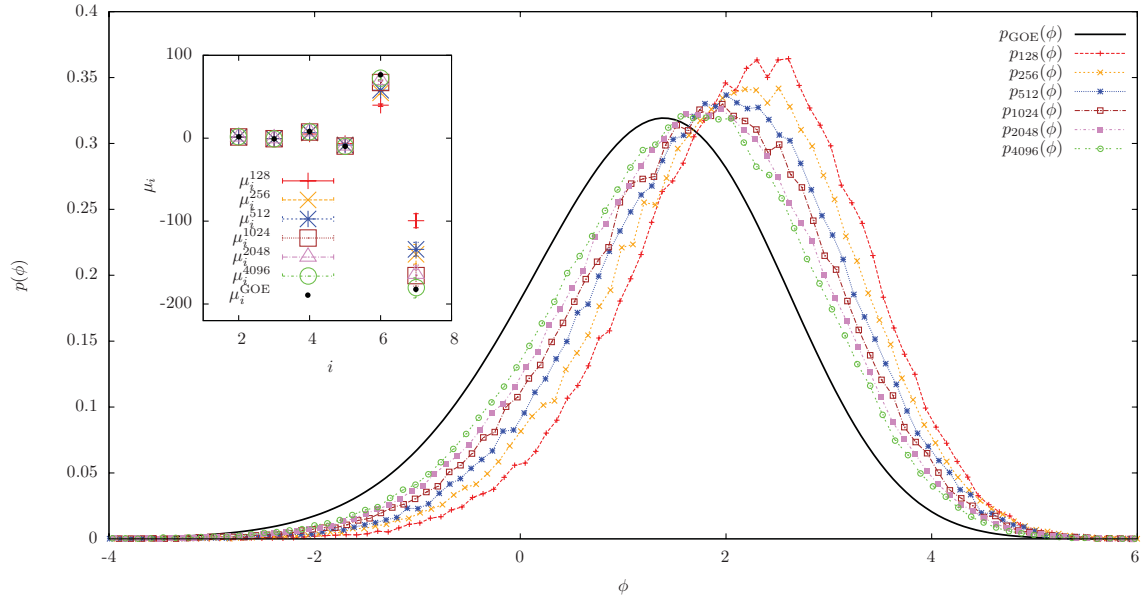
FIG. 2. (Color online) Distribution $p_N(\phi)$ for $N = 128, 256, 512, 1024, 2048, 4096$ (in red, yellow, blue, brown, violet, green respectively) and $10^5 \leqslant S \leqslant 4 \times 10^5$ samples, and the Tracy-Widom distribution $p_{\mathrm{GOE}}(\phi)$ for the GOE ensemble (black), as a function of ϕ. For increasing N, $p_N(\phi)$ approaches $p_{\mathrm{GOE}}(\phi)$, confirming the asymptotic independence of the diagonal elements (11) by each of the off-diagonal elements x_{ij} for large N. Inset: μ_i^N for sizes $N = 128, 256, 512, 1024, 2048, 4096$ (in red, yellow, blue, brown, violet, green respectively), $10^5 \leqslant S \leqslant 4 \times 10^5$, and μ_i^{GOE} (black) as a function of $i > 1$.

We now recall that both the derivation of this section and the previously-developed analysis of Bray and Moore[48] rely on the TAP approximation, i.e., neglect the terms of the Plefka expansion (13) of order larger than 2 in α. As we will show in the following section, these terms give a non-negligible contribution to the finite-size corrections of the TAP equations, and so to the finite-size fluctuations of the critical temperature,

and thus must be definitely taken into account in a complete treatment.

IV. FINITE-SIZE ANALYSIS OF THE SUSCEPTIBILITY WITHIN THE FULL PLEFKA EXPANSION

In this section, we compute the inverse susceptibility matrix $\beta \chi^{-1}$ by taking into account all the terms of the Plefka expansion, in the effort to go beyond the TAP approximation of Sec. III. Notwithstanding its apparent difficulty, here we show that this task can be pursued by a direct inspection of the terms of the expansion. Indeed, let us formally write the free-energy f as a series[29] in α,

$$f(\{m\}, \beta) = \sum_{n=0}^{\infty} \alpha^n f_n(\{m\}, \beta). \quad (13)$$

For $n < 3$, the f_n's are given by Eq. (3). For $n > 3$, f_n is given by the sum of several different addends,[37] which proliferate for increasing n.

It is easy to show that at leading order in N, there is just one term contributing to f_n, and that such a term can be written explicitly as
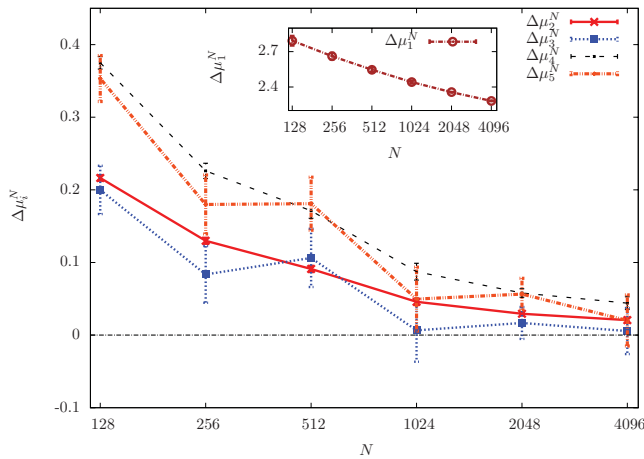

FIG. 3. (Color online) Relative difference $\Delta \mu_i^N$ between the central moments μ_i^N of the distribution $p_N(\phi)$ for $10^5 \leqslant S \leqslant 4 \times 10^5$, and the central moments μ_i^{GOE} of the Tracy-Widom distribution as a function of $N = 128, 256, 512, 1024, 2048, 4096$, for $i = 2, 3, 4, 5$ (in red, blue, black, orange respectively). For increasing N, μ_i^N approaches μ_i^{GOE}, confirming the asymptotic independence of z_2^i by each of the off-diagonal elements x_{ij} for large N. Inset: relative difference of the first central moment $\Delta \mu_1^N$ as a function of N (brown). $\Delta \mu_1^N$ approaches 0 very slowly as N is increased.

$$f_n(\{m\}, \beta) \overset{N \to \infty}{\approx} \sum_{i_1 > \cdots > i_{n-1}} x_{i_1 i_2} x_{i_2 i_3} \cdots x_{i_{n-1} i_1} \\ \times \left(1 - m_{i_1}^2\right) \times \cdots \times \left(1 - m_{i_{n-1}}^2\right). \quad (14)$$

It follows that by plugging Eq. (14) into Eq. (13) and computing $\beta\chi^{-1}$ for $m_i = 0$, one obtains a simple expression for the inverse susceptibility at the paramagnetic solution

$$\beta\chi_{ij}^{-1} = -\alpha x_{ij} + \delta_{ij}\left(1 + \alpha^2 \sum_{k \neq i} x_{ki}^2 + 2 \sum_{n=3}^{\infty} \alpha^n \right.$$
$$\times \left. \sum_{i_1 > \cdots > i_{n-1}} x_{ii_1} x_{i_1 i_2} \cdots x_{i_{n-1} i}\right)$$
$$= -\alpha x_{ij} + \delta_{ij}(1 + \beta^2 J^2) + \delta_{ij}\frac{1}{\sqrt{N}}$$
$$\times \left[(\beta J)^2 z_2^i + 2 \sum_{n=3}^{\infty} \frac{(\beta J)^n}{\sqrt{(n-1)!}} z_n^i\right]. \quad (15)$$

where

$$z_n^i \equiv \frac{\sqrt{(n-1)!}}{N^{\frac{n-1}{2}}} \sum_{i_1 > \cdots > i_{n-1}} x_{ii_1} x_{i_1 i_2} \cdots x_{i_{n-1} i}, \forall n > 2. \quad (16)$$

According to Eq. (16), one has that at leading order in N,

$$\mathbb{E}_x\left[z_n^i\right] = 0 \,\forall n > 2,$$
$$\mathbb{E}_x\left[\left(z_n^i\right)^2\right] = 1 \,\forall n > 2, \quad (17)$$

where in the second line of Eq. (17) the multiple sum defining z_n^i has been evaluated at leading order in N.

We observe that the random variables z_n^i and x_{jk} in Eq. (15) are not independent, since each z_n^i depends on the bond variables $\{x\}$. Following an argument similar to that given in Sec. III for z_2^i, we observe that, by Eq. (16) and at leading order in N, z_n^i is given by a sum of $O(N^{n-1})$ terms which are all of the same order of magnitude. Each term is given by the product of $n-1$ bond variables $x_{ii_1} x_{i_1 i_2} \cdots x_{i_{n-1} i}$ forming a loop passing by site i. For any fixed i, j, k, and n, only $O(N^{n-2})$ terms amongst the $O(N^{n-1})$ terms of z_n^i are entangled with the random bond variable x_{jk}. It follows that at leading order in N, z_n^i can be considered as independent by x_{jk}. Since the sum in the second line of Eq. (15) has a $1/\sqrt{N}$ factor multiplying each of the z_n^i's, we can consider the z_n^i at leading order in N. Hence, in Eq. (15) we can consider each of the z_n^i's as independent on x_{jk}.

In Appendix B we show that at leading order in N, the distribution of z_n^i is a Gaussian with zero mean and unit variance for every i and $n > 2$, while in Appendix C we show that at leading order in N the variables $\{z_n^i\}_{n,i}$ are mutually independent. Both these predictions are confirmed by numerical tests, illustrated in Appendix B and C respectively.

Hence, at leading order in N the term in square brackets in Eq. (15) is nothing but the sum of independent Gaussian variables, and is thus equal to a random variable $\sigma \times \zeta_i$, where ζ_i is Gaussian with zero mean and unit variance, and

$$\sigma^2 = 2(\beta J)^4 + 4 \sum_{n=3}^{\infty} \frac{(\beta J)^{2n}}{(n-1)!}$$
$$= 2(\beta J)^2\{2(e^{(\beta J)^2} - 1) - (\beta J)^2\}.$$

It follows that Eq. (15) becomes

$$\beta\chi_{ij}^{-1} = -\alpha x_{ij} + \delta_{ij}\left(1 + \beta^2 J^2 + \frac{\sigma}{\sqrt{N}}\zeta_i\right)$$
$$= -\alpha x_{ij}' + \delta_{ij}(1 + \beta^2 J^2), \quad (18)$$

where

$$x_{ij}' \equiv x_{ij} - \delta_{ij}\frac{\sigma}{\beta J}\zeta_i. \quad (19)$$

Because of the additional diagonal term in Eq. (19), the matrix x_{ij}' does not belong to the GOE ensemble. Notwithstanding this fact, it has been shown by Soshnikov[50] that the presence of the diagonal elements in Eq. (19) does not alter the universal distribution of the maximal eigenvalue of x_{ij}', which is still distributed according to the TW law. Hence, denoting by λ the minimal eigenvalue of $\beta\chi^{-1}$, we have

$$\lambda = (1 - \beta J)^2 + \frac{\beta J}{N^{2/3}}\phi_{\text{GOE}}, \quad (20)$$

where ϕ_{GOE} is a random variable depending on the sample x_{ij}, and distributed according to the TW law.

In this section, we have calculated the inverse susceptibility matrix $\beta\chi^{-1}$, by considering the full Plefka expansion. In this framework, additional diagonal terms are generated that were not present in the TAP approximation. These additional terms can be handled via a resummation to all orders in the Plefka expansion. As a result, we obtain that the fluctuations of the minimal eigenvalue λ of the susceptibility $\beta\chi^{-1}$ are still governed by the TW law, as in the TAP case treated in Sec. III.

V. FINITE SIZE FLUCTUATIONS OF THE CRITICAL TEMPERATURE

We can now define a finite-size critical temperature, and investigate its finite-size fluctuations due to disorder. In the previous sections, we have shown that for a large but finite size N, the minimal eigenvalue of the inverse susceptibility matrix, i.e., the Hessian matrix of $\beta f(\{m\}, \beta)$ evaluated in the paramagnetic minimum $m_i = 0$, is a function of the temperature and of a quantity ϕ_{GOE}, which depends on the realization of the disorder $\{x\}$. Since the TW law, i.e., the distribution of ϕ_{GOE}, has support for both positive and negative values of ϕ_{GOE}, the subleading term in Eq. (20) can be positive or negative. Accordingly, for samples $\{x\}$ such that $\phi_{\text{GOE}} < 0$, there exists a value of $\beta J \approx 1$ such that $\lambda(\beta J) = 0$, in such a way that the spin-glass susceptibility in the paramagnetic minimum diverges. This fact is physically meaningless, since there cannot be divergences in physical quantities at finite size. This apparent contradiction can be easily understood by observing that if $\lambda(\beta J) = 0$, the true physical susceptibility is no more the paramagnetic one, but must be evaluated in the low-lying nonparamagnetic minima of the free energy, whose appearance is driven by the emergent instability of the paramagnetic minimum. According to this discussion, in the following we will consider only samples $\{x\}$ such that $\phi_{\text{GOE}} > 0$.

For these samples, the spectrum of the Hessian matrix at the paramagnetic minimum has positive support for every temperature: The paramagnetic solution is always stable, and the paramagnetic susceptibility matrix χ is physical and finite. We define a pseudoinverse critical temperature $\beta_c J$ as the value of βJ such that λ has a minimum at $\beta_c J$:

$$
\left. \frac{d\lambda}{d\beta J} \right|_{\beta J = \beta_c J} \equiv 0
$$
$$
= -2(1 - \beta_c J) + \frac{1}{N^{2/3}} \phi_{\text{GOE}}, \quad (21)
$$

where in the second line of Eq. (21), Eq. (20) has been used. This definition of pseudocritical temperature has a clear physical interpretation: The stability of the paramagnetic minimum, which is encoded into the spectrum of the Hessian matrix $\beta \chi^{-1}$, has a minimum at $\beta = \beta_c$. According to Eq. (21), the finite-size critical temperature β_c is given by

$$
\beta_c J = 1 - \frac{1/2}{N^{2/3}} \phi_{\text{GOE}}, \quad (22)
$$

where ϕ_{GOE} depends on the sample $\{x\}$, and is distributed according to the TW law.

Eq. (22) shows that the pseudocritical temperature of the SK model is a random variable depending on the realization of the quenched disorder. Finite-size fluctuations of the pseudocritical temperature are of the order of $N^{-2/3}$, and are distributed according to the TW law. This has to be considered the main result of this paper.

VI. DISCUSSION AND CONCLUSIONS

In this paper, the finite-size fluctuations of the critical temperature of the Sherrington-Kirkpatrick spin glass model have been investigated. The analysis is carried on within the framework of the Plefka expansion for the free energy at fixed local magnetization. A direct investigation of the expansion shows that an infinite resummation of the series is required to describe the finite-size fluctuations of the critical temperature. By observing that the terms in the expansion can be treated as independent random variables, one can suitably define a finite-size critical temperature. Such a critical temperature has a unique value in the infinite-size limit, while it exhibits fluctuations due to quenched disorder at finite sizes. These fluctuations with respect to the infinite-size value have been analyzed, and have been found to be of the order of $N^{-2/3}$, where N is the system size, and to be distributed according to the Tracy-Widom distribution.

The exponent 2/3 describing the fluctuations of the pseudocritical temperature stems from the fact that the finite-size fluctuations of the minimal eigenvalue λ of the inverse susceptibility matrix are of the order of $N^{-2/3}$. Such a scaling for λ at the critical temperature had already been obtained in a previous work,[48] where it was derived by a completely independent method, by taking into account only the first three terms of the Plefka expansion. The present work shows that a more careful treatment, including an infinite resummation of the expansion, is needed to handle finite-size effects. The exponent 2/3 derived by Bray and Moore[48] is here rederived by establishing a connection with recently-developed results in random matrix theory, showing that the scaling $N^{-2/3}$ comes from the scaling of the Tracy-Widom distribution, which was still unknown when the paper by Bray and Moore[48] was written.

As a possible development of the present work, it would be interesting to study the fluctuations of the critical temperature for a SK model where the couplings are distributed according to a power law. Indeed, in a recent work[52] the distribution of the largest eigenvalue λ of a random matrix M whose entries M_{ij} are power-law distributed as $p(M_{ij}) \sim M_{ij}^{-1-\mu}$ has been studied. The authors show that if $\mu > 4$, the fluctuations of λ are of the order of $N^{-2/3}$ and are given by the TW distribution, while if $\mu < 4$ the fluctuations are of the order of $N^{-2/\mu-1/2}$ and are governed by Fréchet's statistics. This result could be directly applied to a SK model with power-law distributed couplings. In particular, it would be interesting to see if there exists a threshold in the exponent μ separating two different regimes of the fluctuations of T_c.

Another interesting perspective would be to generalize the present approach to realistic spin glass models with finite-range interactions. For instance, a huge amount of results has been quite recently obtained for the three-dimensional Ising spin glass,[53–60] and for the short-range p-spin glass model in three dimensions,[61] yielding evidence for a finite-temperature phase transition. It would be interesting to try to generalize the present work to that systems, and compare the resulting fluctuations of the critical temperature with sample-to-sample fluctuations observed in these numerical works. Accordingly, the finite-size fluctuations deriving from the generalization of this work to the three-dimensional Ising spin glass could be hopefully compared with those observed in experimental spin glasses,[62] such as $Fe_{0.5}Mn_{0.5}TiO_3$.

Finally, a recent numerical analysis[63] inspired by the present work has investigated the sample-to-sample fluctuations of a given pseudocritical temperature for the SK model, which is different from that defined in this work. Even though the relatively small number of samples did not allow for a precise determination of the probability distribution of that pseudocritical point, the analysis yields a scaling exponent equal to 1/3, which is different from that of the pseudocritical temperature defined here. As a consequence, the general scaling features of the pseudocritical temperature seem to depend on the actual definition of the pseudocritical point itself, even though different definitions of the pseudocritical temperature must all converge to the infinite-size pseudocritical temperature as the system size tends to infinity. As a future perspective, it would be interesting to investigate which amongst the features of the pseudocritical point are definition-independent, if any.

APPENDIX A: PROOF OF THE ASYMPTOTIC INDEPENDENCE OF x_{ij} AND z_2^i

Here we show that at leading order in N, the variables x_{ij} and z_2^i are independent, i.e., that at leading order in N

$$p_N(x_{ij} = x, z_2^i = z) = p_N(x_{ij} = x) \times p_N(z_2^i = z). \quad (A1)$$

Let us explicitly write the left-hand size of Eq. (A1) as

$$
\begin{aligned}
p_N&(x_{ij} = x, z_2^i = z) \\
&= \mathbb{E}_{\{x_{ik}\}_{k \neq i}} [\delta(x_{ij} - x)\delta(z_2^i - z)], \\
&= \mathbb{E}_{x_{ij}} \Bigg[\delta(x_{ij} - x)\mathbb{E}_{\{x_{ik}\}_{k \neq i, k \neq j}} \\
&\quad \times \left\{ \delta\left[\sqrt{N}\left(\frac{1}{N}\sum_{k \neq i, k \neq j} x_{ki}^2 - 1 \right) - \bar{z}_2^{ij} \right] \right\} \Bigg], \quad (A2)
\end{aligned}
$$

where $\mathbb{E}_{x_{lm}, x_{no}, \ldots}$ denotes the expectation value with respect to the probability distributions of the variables $x_{lm}, x_{no}, \ldots, \delta$ denotes the Dirac delta function, and

$$\bar{z}_2^{ij} \equiv z - \frac{x_{ij}^2}{\sqrt{N}}. \quad (A3)$$

Proceeding systematically at leading order in N, the second expectation value in the second line of Eq. (A2) is nothing but the probability that the variable $\sqrt{N}(\frac{1}{N}\sum_{k \neq i, k \neq j} x_{ki}^2 - 1)$ is equal to $\bar{z}_2^{ij}$. We observe that according to the central limit theorem, at leading order in N this probability is given by

$$
\begin{aligned}
\mathbb{E}_{\{x_{ik}\}_{k \neq i, k \neq j}} &\left[\delta\left(\sqrt{N}\left(\frac{1}{N}\sum_{k \neq i, k \neq j} x_{ki}^2 - 1 \right) - \bar{z}_2^{ij} \right) \right] \\
&= \frac{1}{\sqrt{4\pi}} e^{-\frac{(\bar{z}_2^{ij})^2}{4}}. \quad (A4)
\end{aligned}
$$

By plugging Eq. (A4) into Eq. (A2) and using Eq. (A3), one has

$$
\begin{aligned}
p_N(x_{ij} = x, z_2^i = z) &= \frac{1}{\sqrt{4\pi}} \int dx_{ij} P(x_{ij})\delta(x_{ij} - x) \\
&\quad \times e^{-\frac{(z - x_{ij}^2/\sqrt{N})^2}{4}} \\
&= P(x)\frac{1}{\sqrt{4\pi}} e^{-\frac{(z - x^2/\sqrt{N})^2}{4}} \quad (A5) \\
&= p_N(x_{ij} = x) \times p_N(z_2^i = z),
\end{aligned}
$$

where in the first line we explicitly wrote the expectation value with respect to x_{ij} in terms of the probability distribution (2), while in the third line proceeded at leading order in N, and used Eq. (9).

APPENDIX B: COMPUTATION OF THE PROBABILITY DISTRIBUTION OF z_n^i

Here we compute the probability distribution of z_n^i at leading order in N. Let us define a super index $L \equiv \{i_1, \ldots, i_{n-1}\}$, where L stands for loop, since L represents a loop passing by the site i. Let us also set $X_L \equiv x_{ii_1}x_{i_1 i_2}\cdots x_{i_{n-1}i}$. By Eq. (16)

one has

$$z_n^i = \frac{\sqrt{(n-1)!}}{N^{\frac{n-1}{2}}} \sum_L X_L, \forall n > 2. \quad (B1)$$

We observe that the probability distribution of X_L is the same for every L. Hence, according to Eq. (B1), z_n^i is given by the sum of equally distributed random variables. Now pick two of these variables, X_L and $X_{L'}$. For some choices of L, L', X_L and $X_{L'}$ are not independent, since they can depend on the same bond variables x_{ij}. If one picks one variable X_L, the number of variables appearing in the sum (B1) which are dependent on X_L are those having at least one common edge with the edges of X_L. The number of these variables, at leading order in N, is $O(N^{n-2})$, since they are obtained by fixing one of the $n-1$ indexes $i_1, \ldots, i_{n-1}$. The latter statement is equivalent to saying that if one picks at random two variables X_L and $X_{L'}$, the probability that they are correlated is

$$O(N^{n-2}/N^{n-1}) = O(N^{-1}). \quad (B2)$$

Hence, at leading order in N, we can treat the ensemble of the variables $\{X_L\}_L$ as independent. According to the central limit theorem, at leading order in N, the variable

$$\frac{\sqrt{(n-1)!}}{N^{\frac{n-1}{2}}} z_n^i = \frac{1}{\frac{N^{n-1}}{(n-1)!}} \sum_L X_L$$

is distributed according to a Gaussian distribution with mean $\mathbb{E}_x[X_L] = 0$ and variance

$$\mathbb{E}_x\left[\left(\frac{\sqrt{(n-1)!}}{N^{\frac{n-1}{2}}} z_n^i \right)^2 \right] = \frac{\mathbb{E}_x[X_L^2]}{\frac{N^{n-1}}{(n-1)!}} = \frac{1}{\frac{N^{n-1}}{(n-1)!}}, \quad (B3)$$

where in Eq. (B3) Eq. (2) has been used. It follows that at leading order in N, z_n^i is distributed according to a Gaussian distribution with zero mean and unit variance

$$p_N(z_n^i = z) \overset{N \to \infty}{\longrightarrow} \frac{1}{\sqrt{2\pi}} e^{-\frac{z^2}{2}}, \quad (B4)$$

where $p_N(z_n^i = z)$ is defined as the probability that z_n^i is equal to z at size N.

Eq. (B4) has been tested numerically for the first few values of n: $p_N(z_n^i = z)$ has been computed by generating $S \gg 1$ samples of $\{x\}$, and so of z_n^i. For $n = 3$ and 4, the resulting probability distribution $p_N(z_n^i = z)$ converges to a Gaussian distribution with zero mean and unit variance as N is increased, confirming the result (B4). This convergence is shown in Fig. 4, where $p_N(z_4^1 = z)$ is depicted for different values of N together with the right-hand side of Eq. (B4), as a function of z.

APPENDIX C: INDEPENDENCE OF THE z_n^i's AT LEADING ORDER IN N

Let us consider two distinct variables z_n^i and z_m^j, and proceed at leading order in N. Following the notation of Appendix B, we write Eq. (16) as

$$z_n^i = \frac{\sqrt{(n-1)!}}{N^{\frac{n-1}{2}}} \sum_L X_L, \quad (C1)$$

$$z_m^j = \frac{\sqrt{(m-1)!}}{N^{\frac{m-1}{2}}} \sum_{L'} X_{L'}, \quad (C2)$$
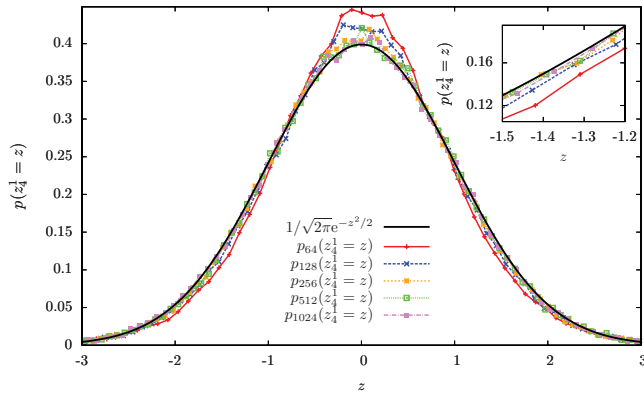
FIG. 4. (Color online) Probability distribution $p_N(z_4^1 = z)$ for $S = 10^5$ and different values of $N = 64, 128, 256, 512, 1024$ (in red, blue, yellow, green, violet respectively) together with a Gaussian distribution $1/\sqrt{2\pi}e^{-z^2/2}$ with zero mean and unit variance (black), as a function of z. As N is increased, $p_N(z_4^1 = z)$ converges to $1/\sqrt{2\pi}e^{-z^2/2}$, as predicted by the analytical calculation, Eq. (B4). Inset: zoom of the above plot explicitly showing the convergence of $p_N(z_4^1 = z)$ to $1/\sqrt{2\pi}e^{-z^2/2}$ as N is increased.

where L, L' represent a loop of length n, m passing by the site i, j respectively. Some of the variables X_L depend on some of the variables $X_{L'}$, because they can depend on the same bond variables x_{ij}. Let us pick at random one variable X_L appearing in z_n^i, and count the number of variables $X_{L'}$ in z_m^j that are dependent on X_L. At leading order in N, these are given by the number of $X_{L'}$ having at least one common bond with X_L, and are $O(N^{m-2})$. Hence, if one picks at random two variables $X_L, X_{L'}$ in Eqs. (C1), (C2) respectively, the probability that $X_L, X_{L'}$ are dependent is
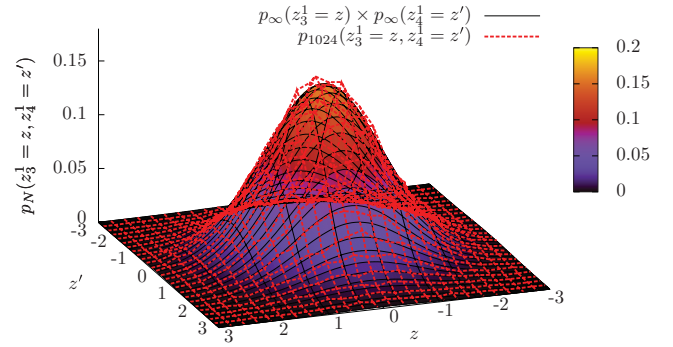
$$O(N^{m-2}/N^{m-1}) = O(N^{-1}).$$

FIG. 5. (Color online) $p_{1024}(z_3^1 = z, z_4^1 = z')$ for $S = 10^5$ samples (red), and the $N \rightarrow \infty$ limit of the right-hand side of Eq. (C3) (black), as a function of z, z'. For large N, $p_N(z_3^1 = z, z_4^1 = z')$ equals $p_N(z_3^1 = z) \times p_N(z_4^1 = z')$, as predicted by Eq. (C3). Hence, at leading order in N, the variables z_3^1 and z_4^1 are independent.

It follows that z_n^i and z_m^j are independent at leading order in N, i.e., for $N \rightarrow \infty$

$$p_N(z_n^i = z, z_m^j = z') = p_N(z_n^i = z) \times p_N(z_m^j = z'), \quad \text{(C3)}$$

where $p_N(z_n^i = z, z_m^j = z')$ denotes the joint probability that z_n^i equals z and z_m^j equals z', at fixed size N.

Eq. (C3) has been tested numerically for $n = 3, m = 4$: $p_N(z_3^1 = z, z_4^1 = z')$ has been computed by generating $S \gg 1$ samples of $\{x\}$, and so of z_3^1, z_4^1. As a result, the left-hand side of Eq. (C3) converges to the right-hand side as N is increased, confirming the predictions of the above analytical argument. This is shown in Fig. 5, where $p_{1024}(z_3^1 = z, z_4^1 = z')$ is depicted together with the $N \rightarrow \infty$ limit of the right-hand side of Eq. (C3) [see Eq. (B4)], as a function of z, z'.

---

*michele.castellana@lptms.u-psud.fr

†elia.zarinelli@lptms.u-psud.fr

[1] T. D. Lee and C. N. Yang, Phys. Rev. **87**, 410 (1952).

[2] C. Yang, Phys. Rev. **87**, 404 (1952).

[3] K. Huang, *Statistical mechanics* (Wiley, New York, 1987).

[4] M. Biskup, C. Borgs, J. T. Chayes, L. J. Kleinwaks, and R. Kotecký, Phys. Rev. Lett. **84**, 4794 (2000).

[5] D. Ruelle, Phys. Rev. Lett. **26**, 303 (1971).

[6] C. Monthus and T. Garel, J. Stat. Mech.: Theory Exp. **2005**, P12011.

[7] C. Monthus and T. Garel, Eur. Phys. J. B **48**, 393 (2005).

[8] F. Iglói, Y. C. Lin, H. Rieger, and C. Monthus, Phys. Rev. B **76**, 064421 (2007).

[9] C. Monthus and T. Garel, Phys. Rev. E **74**, 011101 (2006).

[10] T. Sarlat, A. Billoire, G. Biroli, and J. P. Bouchaud, J. Stat. Mech.: Theory Exp. **2009**, P08014.

[11] E. J. Gumbel, *Statistics of extremes* (Columbia University Press, New York, 1958).

[12] M. L. Mehta, *Random matrices* (Academic Press, Amsterdam, 2004).

[13] C. A. Tracy and H. Widom, *Distribution Functions for Largest Eigenvalues and Their Applications*, in *Proceedings of the*

International Congress of Mathematicians, Vol. I, edited by LI Tatsien (Higher Education Press, Beijing, 2002), pp. 587–596.

[14] C. A. Tracy and H. Widom, Commun. Math. Phys. **177**, 727 (1996).

[15] C. A. Tracy and H. Widom, Commun. Math. Phys. **159**, 151 (1994).

[16] C. A. Tracy and H. Widom, Phys. Lett. B **305**, 115 (1993).

[17] K. Johansson, Commun. Math. Phys. **209**, 437 (2000).

[18] J. Baik and E. M. Rains, J. Stat. Phys. **100**, 523 (2000).

[19] M. Prähofer and H. Spohn, Phys. Rev. Lett. **84**, 4882 (2000).

[20] G. Biroli, J. P. Bouchaud, and M. Potters, J. Stat. Mech.: Theory Exp. **2007**, P07019.

[21] D. Sherrington and S. Kirkpatrick, Phys. Rev. Lett. **35**, 1792 (1975).

[22] G. Parisi, J. Phys. A: Math. Gen. **13**, 1101 (1980).

[23] G. Parisi, Phys. Rev. Lett. **50**, 1946 (1983).

[24] M. Talagrand, Comptes Rendus Mathematique **337**, 111 (2003).

[25] M. Mézard, G. Parisi, and M. A. Virasoro, *Spin Glass Theory and Beyond* (World Scientific, Singapore, 1987).

[26] M. Mézard and A. Montanari, *Information, Physics and Computation* (Oxford University Press, Oxford, 2009).

[27] H. Nishimori, *Statistical Physics of Spin Glasses and Information Processing: An Introduction* (Oxford University Press, Oxford, UK, 2001).

[28] D. J. Thouless, P. W. Anderson, and R. G. Palmer, Philos. Mag. **35**, 593 (1977).

[29] T. Plefka, J. Phys. A: Math. Gen. **15**, 1971 (1982).

[30] A. Georges, M. Mézard, and J. S. Yedidia, Phys. Rev. Lett. **64**, 2937 (1990).

[31] J. S. Yedidia and A. Georges, J. Phys. A: Math. Gen. **23**, 2165 (1990).

[32] T. Yokota, Phys. Rev. B **51**, 962 (1995).

[33] T. Plefka, Phys. Rev. E **73**, 016129 (2006).

[34] H. Ishii and T. Yamamoto, J. Phys. C **18**, 6225 (1985).

[35] L. De Cesare, K. L. Walasek, and K. Walasek, Phys. Rev. B **45**, 8127 (1992).

[36] G. Biroli and L. F. Cugliandolo, Phys. Rev. B **64**, 014206 (2001).

[37] J. S. Yedidia, in *Advanced Mean Field Methods: Theory and Practice* (MIT Press, Cambridge, MA, 2001), pp. 21–36.

[38] E. P. Wigner, The Annals of Mathematics **62**, 548 (1955).

[39] Y. V. Fyodorov, in *Recent Perspectives in Random Matrix Theory and Number Theory*, Vol. 322 (Cambridge Univ. Press, 2005), p. 31.

[40] G. Parisi and T. Rizzo, Phys. Rev. Lett. **101**, 117205 (2008).

[41] G. Parisi and T. Rizzo, Phys. Rev. B **79**, 134205 (2009).

[42] G. Parisi and T. Rizzo, Phys. Rev. B **81**, 094201 (2010).

[43] J. Stäring, B. Mehlig, Y. V. Fyodorov, and J. M. Luck, Phys. Rev. E **67**, 047101 (2003).

[44] P. Shukla, Phys. Rev. E **71**, 026226 (2005).

[45] Z. Bai and W. Zhou, Statistica Sinica **18**, 425 (2008).

[46] K. A. Takeuchi and M. Sano, Phys. Rev. Lett. **104**, 230601 (2010).

[47] J. Rambeau and G. Schehr (unpublished).

[48] A. J. Bray and M. A. Moore, J. Phys. C **12**, L441 (1979).

[49] T. Aspelmeier, A. Billoire, E. Marinari, and M. A. Moore, J. Phys. A: Math. Theor. **41**, 324008 (2008).

[50] A. Soshnikov, Commun. Math. Phys. **207**, 697 (1999).

[51] P. J. Forrester, S. N. Majumdar, and G. Schehr, Nucl. Phys. B **844**, 500 (2011).

[52] G. Biroli, J. P. Bouchaud, and M. Potters, Europhys. Lett. **78**, 10001 (2007).

[53] R. A. Banos, A. Cruz, L. A. Fernandez, J. M. Gil-Narvion, A. Gordillo-Guerrero, M. Guidetti, A. Maiorano, F. Mantovani, E. Marinari, V. Martin-Mayor *et al.*, J. Stat. Mech.: Theory Exp. **2010**, P06026.

[54] M. Hasenbusch, A. Pelissetto, and E. Vicari, Phys. Rev. B **78**, 214205 (2008).

[55] R. Alvarez Baños *et al.*, Phys. Rev. Lett. **105**, 177202 (2010).

[56] F. Belletti, A. Cruz *et al.*, J. Stat. Phys. **135**, 1121 (2009).

[57] P. Contucci, C. Giardinà, C. Giberti, G. Parisi, and C. Vernia, Phys. Rev. Lett. **99**, 057206 (2007).

[58] P. Contucci, C. Giardinà, C. Giberti, G. Parisi, and C. Vernia, Phys. Rev. Lett. **103**, 017201 (2009).

[59] F. Krzakala and O. C. Martin, Phys. Rev. Lett. **85**, 3013 (2000).

[60] E. Marinari, G. Parisi, and J. J. Ruiz-Lorenzo, Phys. Rev. B **58**, 14852 (1998).

[61] M. Campellone, B. Coluzzi, and G. Parisi, Phys. Rev. B **58**, 12081 (1998).

[62] K. Gunnarsson, P. Svedlindh, P. Nordblad, L. Lundgren, H. Aruga, and A. Ito, Phys. Rev. B **43**, 8199 (1991).

[63] A. Billoire, L. A. Fernandez, A. Maiorano, E. Marinari, V. Martin-Mayor, and D. Yllanes, e-print arXiv:1108.1336.

P H Y S I C A L   R E V I E W   L E T T E R S

Extreme Value Statistics Distributions in Spin Glasses

Michele Castellana,[1,2,*] Aurélien Decelle,[1] and Elia Zarinelli[1]

[1]*LPTMS, CNRS and Université Paris-Sud, UMR8626, Bât. 100, 91405 Orsay, France*
[2]*Dipartimento di Fisica, Università di Roma "La Sapienza", 00185 Rome, Italy*

We study the probability distribution of the pseudocritical temperature in a mean-field and in a short-range spin-glass model: the Sherrington-Kirkpatrick and the Edwards-Anderson (EA) model. In both cases, we put in evidence the underlying connection between the fluctuations of the pseudocritical point and the extreme value statistics of random variables. For the Sherrington-Kirkpatrick model, both with Gaussian and binary couplings, the distribution of the pseudocritical temperature is found to be the Tracy-Widom distribution. For the EA model, the distribution is found to be the Gumbel distribution. Being the EA model representative of uniaxial magnetic materials with quenched disorder like $Fe_{0.5}Mn_{0.5}TiO_3$ or $Eu_{0.5}Ba_{0.5}MnO_3$, its pseudocritical point distribution should be *a priori* experimentally accessible.

Disordered uniaxial magnetic materials having a glassy behavior like $Fe_{0.5}Mn_{0.5}TiO_3$ [1] and $Eu_{0.5}Ba_{0.5}MnO_3$ [2] have interested physicists for decades. Since the first pioneering work of Edwards and Anderson (EA) [3], these systems have been studied by means of spin-glass models with quenched disorder, which were later considered in their mean-field version by Sherrington and Kirkpatrick (SK) [4]. In the thermodynamic limit, Parisi's solution for the SK model [5] predicts a phase transition at a finite critical temperature separating a high-temperature paramagnetic phase from a low-temperature glassy phase. Differently, for the EA model there is no analytical solution and the existence of a finite-temperature phase transition relies entirely on numerical simulations [6].

Even though criticality in a physical system can emerge only in the thermodynamic limit [7,8], in laboratory and numerical experiments the system size is always finite: singularities of physical observables are smeared out and replaced by smooth maxima. In order to characterize the critical point of finite-size systems, a suitably defined pseudocritical temperature must be introduced, e.g., the temperature at which such maxima occur. In finite-size systems with quenched disorder, such a pseudocritical temperature is a random variable depending on the realization of the disorder. The characterization of the distribution of the pseudocritical point and of its scaling properties is still an open problem which has drawn the attention of physicists since the very first works of Harris [9–13]. Further studies of such distributions in spin glasses have been performed in a recent work [14], where some of the authors showed a connection between the fluctuations of the pseudocritical temperature of the SK model and the theory of extreme value statistics (EVS) of correlated random variables.

The EVS of independent identically distributed (IID) random variables is a well-established problem: a fundamental result [15] states that the limiting Probability Distribution Function (PDF) of the maximum of IID random variables belongs to three families of distributions: the Gumbel, Fréchet, or Weibull distribution. Much less is known about the EVS of correlated random variables. A noteworthy case of an EVS distribution of correlated random variables that has been recently discovered is the Tracy-Widom (TW) distribution [16], describing the fluctuations of the largest eigenvalue of a Gaussian random matrix. The TW distribution has been found to describe the fluctuations of observables of a broad number of physical and mathematical models, like the longest common sequence in a random permutation [17], directed polymers in disordered media [18], and polynuclear growth models [19], which can be described by the Kardar-Parisi-Zhang equation [20,21]. Recently the TW distribution has been found to describe the conductance fluctuations in two- and three- dimensional Anderson insulators [22,23] and has been measured in growing interfaces of liquid-crystal turbulence [24,25] experiments.

In this Letter we study the distribution of the pseudocritical temperature in the SK and in the EA model by means of numerical simulations. Our numerical findings show that the fluctuations of the pseudocirtical temperature of the SK model both with Gaussian and binary couplings are described by the TW distribution. This result suggests that the features of the fluctuations of the pseudocritical temperature are universal, i. e., stable with respect to the distribution of the disorder. To our knowledge, this is the first time that the ubiquitous TW distribution is shown to play a role in spin glasses. Moreover, our numerical analysis shows that the fluctuations of the pseudocritical point of the EA model are described by the Gumbel distribution. These two results shed light on the role played by EVS in spin glasses.

To pose the problem, let us consider a system of N spins $S_i = \pm 1$ located at the vertices of a graph, interacting via the Hamiltonian $H[\vec{S}] = -\sum_{(i,j)} J_{ij} S_i S_j$, where the sum runs over the interacting spin pairs (i, j). For the SK model

with Gaussian couplings (GSK) and for the SK model with binary couplings (BSK) the interacting spin pairs are all the distinct pairs. The couplings J_{ij} are IID Gaussian random variables with zero mean and variance $1/N$ for the GSK model [4], and are equal to $\pm 1/\sqrt{N}$ with equal probability for the BSK model [26]. For the EA model the interacting spin pairs are the nearest-neighbor pairs on a three-dimensional cubic lattice with periodic boundary conditions, and J_{ij} are IID random variables equal to ± 1 with equal probability [3]. For the BSK and EA model, the binary structure of the couplings allowed for the use of an efficient asynchronous multispin-coding simulation technique [6], yielding an extensive number of disorder samples and system sizes.

Let us now define the physical observables used to carry on the numerical analysis of the problem. Given two real spin replicas $\vec{S}^1$, $\vec{S}^2$, their mutual overlap $q \equiv \frac{1}{N} \sum_{i=1}^{N} S_i^1 S_i^2$ is a physical quantity characterizing the spin-glass transition in the thermodynamic limit [5,6]: $\overline{\langle q^2 \rangle_{\mathcal{J}}(\beta)} = 0$ if $\beta < \beta_c$, $\overline{\langle q^2 \rangle_{\mathcal{J}}(\beta)} > 0$ if $\beta > \beta_c$, where $\langle \cdots \rangle_{\mathcal{J}}$ denotes the thermal average performed with the Boltzmann weight defined by the Hamiltonian $H[\vec{S}]$, $\beta \equiv 1/T$ is the inverse temperature, and $\overline{\cdots}$ stands for the average over quenched disorder $\mathcal{J} \equiv \{J_{ij}\}_{ij}$. The finite-size inverse pseudocritical temperature $\beta_{c\,\mathcal{J}}$ of a sample with a realization $\mathcal{J}$ of the disorder can be defined as the value of β at which $\langle q^2 \rangle_{\mathcal{J}}(\beta)$ *significantly differs from zero*, i. e., becomes critical. This qualitative definition is made quantitative by setting

$$\langle q^2 \rangle_{\mathcal{J}}(\beta_{c\,\mathcal{J}}) = \overline{\langle q^2 \rangle_{\mathcal{J}}(\beta_c^N)}. \tag{1}$$

Both for the GSK and BSK model, β_c^N is chosen to be the average critical temperature at size N, which is defined as the temperature at which the Binder ratio $B \equiv 1/2(3 - \overline{\langle q^4 \rangle_{\mathcal{J}}}/\overline{\langle q^2 \rangle_{\mathcal{J}}}^2)$ of a system of size N equals the Binder ratio of a system of size $2N$. For the EA model we simply take β_c^N to be equal to the infinite-size critical temperature $\beta_c = 0.855$ [27], because in this case the Binder ratios cross at a temperature which is very close to the infinite-size critical temperature β_c. The definition (1) and β_c^N are qualitatively depicted in Fig. 1. The distribution of $\beta_{c\,\mathcal{J}}$ can be characterized by its mean $\overline{\beta_{c\,\mathcal{J}}}$, its variance $\sigma_{\beta N}^2 \equiv \overline{\beta_{c\,\mathcal{J}}^2} - \overline{\beta_{c\,\mathcal{J}}}^2$, and by the PDF $p_N(x_{\mathcal{J}})$ of the natural scaling variable $x_{\mathcal{J}} \equiv (\beta_{c\,\mathcal{J}} - \overline{\beta_{c\,\mathcal{J}}})/\sigma_{\beta N}$. We can expect that, to leading order in N, $\sigma_{\beta N} \sim N^{-\phi}$, and that for large N, $p_N(x_{\mathcal{J}})$ converges to a nontrivial limiting PDF $p_\infty(x_{\mathcal{J}})$.

Sherrington-Kirkpatrick model.—Let us start discussing the distribution of $\beta_{c\,\mathcal{J}}$ for the GSK and BSK model. Monte Carlo (MC) simulations have been performed with parallel tempering for system sizes $N = 32, 64, 128, 256$ (GSK) and $N = 16, 32, 64, 128, 256, 512, 1024, 2048, 4096$ (BSK), allowing for a numerical computation of $\langle q^2 \rangle_{\mathcal{J}}$ and so of $\beta_{c\,\mathcal{J}}$ for several samples $\mathcal{J}$. The data shows that as the system size N is increased, $\overline{\beta_{c\,\mathcal{J}}}$
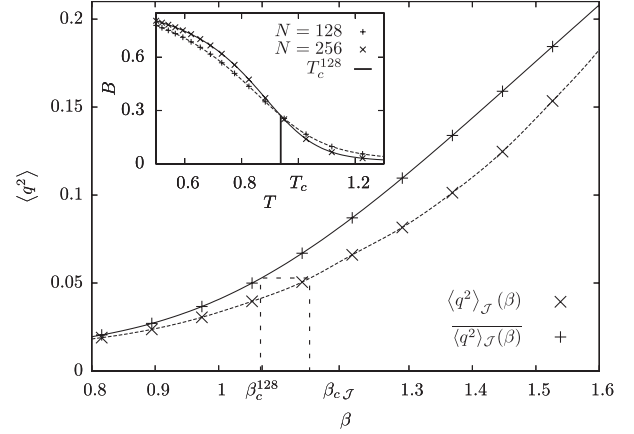

FIG. 1. Square value of the overlap $\langle q^2 \rangle_{\mathcal{J}}$ for a sample $\mathcal{J}$ (dashed curve) for the binary Sherrington-Kirkpatrick model with $N = 128$, its average $\overline{\langle q^2 \rangle_{\mathcal{J}}}$ over the samples $\mathcal{J}$ (solid curve) as a function of the inverse-temperature β, and critical temperatures β_c^N and $\beta_{c\,\mathcal{J}}$. The dashed vertical lines depict the definition (1) of $\beta_{c\,\mathcal{J}}$. Inset: Binder parameter B as a function of the temperature T for $N = 128, 256$, and average pseudocritical temperature T_c^{128}, with $T_c^N \equiv 1/\beta_c^N$.

approaches β_c. Setting $T_{c\,\mathcal{J}} \equiv 1/\beta_{c\,\mathcal{J}}$, $\sigma_{TN}^2 \equiv \overline{T_{c\,\mathcal{J}}^2} - \overline{T_{c\,\mathcal{J}}}^2 \sim N^{-\phi}$, the power law fit of σ_{TN} shown in Fig. 2 gives the value of the scaling exponent $\phi = 0.31 \pm 0.07$ (GSK) and $\phi = 0.34 \pm 0.05$ (BSK). These values of ϕ are both consistent with the value $\phi = 1/3$ one would expect from scaling arguments by considering the variable $y \equiv N^{1/3}(T - T_c)$ [28].

The PDF p_N of the rescaled variable $x_{\mathcal{J}}$ is depicted in Fig. 2. The curves $p_N(x_{\mathcal{J}})$ collapse quite satisfyingly indicating that we are close to the asymptotic regime $N \to \infty$. Even though one could naively expect the fluctuations of the pseudocritical point to be Gaussian, Fig. 2 shows that this is not the case.

To understand this fact, let us recall the analysis proposed in a recent work [14] by some of the authors. In order to study the sample-to-sample fluctuations of the pseudocritical temperature one uses the Thouless-Anderson-Palmer approach for the SK model. In the TAP approach a free energy function of the local magnetization is built up for any sample $\mathcal{J}$ of the disorder, and its Hessian matrix H_{ij} calculated at the paramagnetic minimum is a random matrix in the Gaussian orthogonal ensemble. In the thermodynamic limit, the spectrum of H_{ij} is described by the Wigner semicircle, centered in $1 + \beta^2$ and with radius 2β. The critical temperature $\beta_c = 1$ of the SK model is identified as the value of β such that the minimal eigenvalue of H_{ij} vanishes. In [14] the fluctuations of the pseudocritical temperature are investigated in terms of the fluctuations of the minimal eigenvalue of H_{ij}. One introduces a definition of pseudocritical temperature $\hat{\beta}_{c\,\mathcal{J}}$, which is different from that considered in the present work. The finite-size fluctuations of $\hat{\beta}_{c\,\mathcal{J}}$ are found to be described by the relation
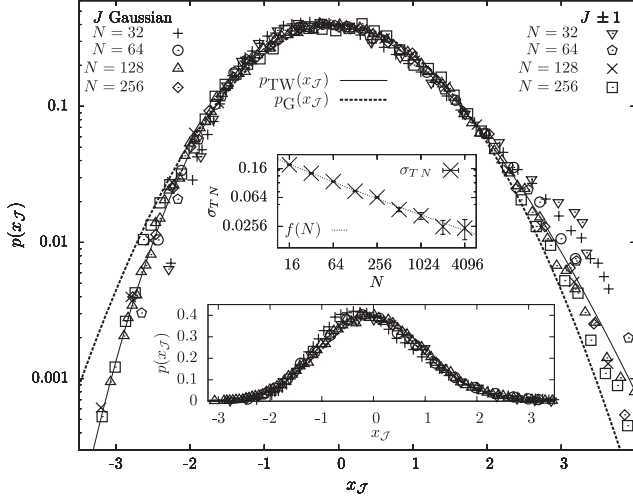
FIG. 2. Distribution of the pseudocritical point both for the Sherrington-Kirkpatrick (SK) model with Gaussian couplings (GSK) and for the SK model with binary couplings (BSK). PDF $p_N(x_{\mathcal{J}})$ of the rescaled critical temperature $x_{\mathcal{J}}$ for system sizes $N = 32, 64, 128, 256$ with $1.6 \times 10^4 \le S \le 4.7 \times 10^4$ (GSK) and $2.9 \times 10^4 \le S \le 9.8 \times 10^4$ (BSK) disorder samples, Tracy-Widom distribution $p_{\text{TW}}(x_{\mathcal{J}})$ (solid curve) and Gaussian distribution $p_G(x_{\mathcal{J}})$ (dashed curve), both with zero mean and unit variance. The plot has no adjustable parameters, and is in logarithmic scale to highlight the behavior of the distributions on the tails. Top inset: width σ_{TN} for the BSK as a function of N and fitting function $f(N) = aN^{-\phi} + bN^{-2\phi}$, yielding $\phi = 0.34 \pm 0.05$. Bottom inset: same plot as in the main plot in linear scale.

$\hat{\beta}_{c\,\mathcal{J}} = \beta_c - \chi_{\mathcal{J}}/(2N^{2/3})$, where $\chi_{\mathcal{J}}$ is distributed according to the TW distribution in the high-temperature region $\hat{\beta}_{c\,\mathcal{J}} < 1$. According to Fig. 2, MC simulations confirm this analysis: the limiting distribution of $p_N(x_{\mathcal{J}})$ is described with good accuracy by the TW distribution in the high-temperature regime $\beta_{c\,\mathcal{J}} < 1$ ($x_{\mathcal{J}} < 0$). The TW distribution is robust with respect to the choice of the disorder distribution and to the definition of pseudocritical temperature. On the other hand, since the exponent ϕ obtained from MC simulations is not compatible with the exponent $2/3$ of $\hat{\beta}_{c\,\mathcal{J}}$, we conclude that the scaling exponent is definition dependent [14,29].

Edwards-Anderson model.—The same analysis has been performed for the three-dimensional EA model. Physical observables have been computed with parallel tempering for system sizes $N = L^3$ with $L = 4, 8, 12, 16$. Similarly to the SK model, the width $\sigma_{\beta N}$ of the distribution of the pseudocritical point $\beta_{c\,\mathcal{J}}$ shrinks to zero as the system size N is increased: a power law fit $\sigma_{\beta N} = aN^{-\phi}$ gives the value of the scaling exponent $\phi = 0.23 \pm 0.03$ (inset of Fig. 3). The PDFs $p_N(x_{\mathcal{J}})$ of the rescaled critical temperature seem to have a finite limit as N is increased, as depicted in Fig. 3, and this limit coincides with the Gumbel distribution. Both ϕ and the PDF have the following interesting
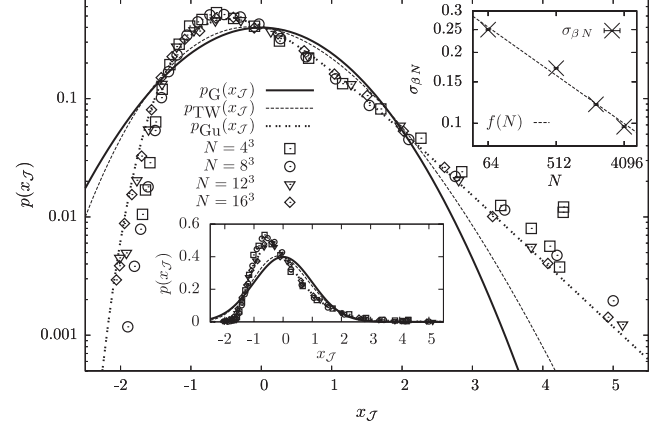

FIG. 3. Distribution of the pseudocritical point for the Edwards-Anderson model. PDF $p_N(x_{\mathcal{J}})$ of the rescaled critical temperature $x_{\mathcal{J}}$ for systems sizes $N = 4^3, 8^3, 12^3, 16^3$ with $2.4 \times 10^4 \le S \le 3.2 \times 10^4$ disorder samples, Gaussian distribution $p_G(x_{\mathcal{J}})$ (solid curve), Tracy-Widom distribution $p_{\text{TW}}(x_{\mathcal{J}})$ (dashed curve), and Gumbel distribution $p_{\text{Gu}}(x_{\mathcal{J}})$ (dotted curve), all with zero mean and unit variance. The plot has no adjustable parameters, and is in logarithmic scale to highlight the behavior of the distributions on the tails. Top inset: width $\sigma_{\beta N}$ as a function of N, and fitting function $f(N) = aN^{-\phi}$, with scaling exponent $\phi = 0.23 \pm 0.03$. Bottom inset: same plot as in the main plot in linear scale.

features. As far as the exponent ϕ is concerned, we recall [10] that for systems known to be governed by a random fixed point like the EA model, it was predicted that the scaling exponent satisfies $1/\phi = d\nu$, where d is the dimensionality of the system. The value of the critical exponent $\nu = 1.8 \pm 0.2$ for the EA model is known from numerical simulations [6], yielding a value of $\phi = 0.19 \pm 0.02$ which is compatible with that measured from the fluctuations of the critical temperature. As far as the limiting distribution $p_\infty(x_{\mathcal{J}})$ is concerned, we recall that [30] a disordered system like the EA behaves as an ensemble of independent subsystems $\mathcal{S}_1, \ldots, \mathcal{S}_M$, where each subsystem $\mathcal{S}_i$ has a random local critical temperature β_c^i, the local critical temperatures $\{\beta_c^i\}_i$ being IID random variables depending on the *local* realization of the disorder. We can argue that, for a single realization of the disorder $\mathcal{J}$, the pseudocritical temperature $\beta_{c\,\mathcal{J}}$ results from the fact that β has to be taken large enough to bring all of the subsystems $\{\mathcal{S}_i\}_i$ to criticality. Thus, $\beta_{c\,\mathcal{J}}$ is the maximum over the ensemble of the local critical temperatures $\beta_{c\,\mathcal{J}} = \max_i \beta_c^i$. If this picture is correct, $\beta_{c\,\mathcal{J}}$ is distributed according to one of the EVS limiting distributions of independent variables [15]: the Gumbel, Fréchet, or Weibull distribution. Assuming that the distribution of β_c^i decays exponentially for large β_c^i, the distribution of $\beta_{c\,\mathcal{J}}$ is the Gumbel one. We want to stress that this argument would not hold for the SK model, where there is no geometric structure.

Conclusions.—In this Letter, we have performed a numerical analysis of the distribution of the pseudocrtical

temperature in two mean-field spin glasses, the Sherrington-Kirkpatrick model with Gaussian couplings and with binary couplings, and in a short-range spin glass, the Edwards-Anderson model. The analysis for the Sherrington-Kirkpatrick models shows that the distribution of the pseudocritical temperature in the high-temperature phase is described with good accuracy by the Tracy-Widom distribution, as suggested by an analytical prediction previously published by some of the authors [14]. To our knowledge, this is the first time that the Tracy-Widom distribution is shown to play a role in spin glasses. The fact that both the Sherrington-Kirkpatrick model with Gaussian couplings and the Sherrington-Kirkpatrick model with binary couplings yield the Tracy-Widom distribution suggests that the Tracy-Widom distribution is universal with respect to the bonds' distribution.

The analysis pursued for the three-dimensional Edwards-Anderson model shows that the liming distribution of the pseudocritical temperature is the Gumbel distribution. An argument to understand this result has been proposed. These two numerical analyses put in evidence a connection between the critical regime of spin-glass models and the extreme value statistics theory which has never been proposed heretofore.

The present Letter opens several perspectives. As far as the Sherrington-Kirkpatrick model is concerned, we recall that the Tracy-Widom distribution describes typical fluctuations of the maximal eigenvalue of a Gaussian orthogonal ensemble random matrix, while the large deviations regime of these fluctuations has been studied only recently [31]. It would be interesting to study numerically the large deviations regime of the fluctuations of the critical temperature, where the distribution of the pseudocritical point could be described by the large deviations function derived in [31]. It would be also interesting to consider the case where the couplings J_{ij} are Gaussian with a positive bias J_0 [32]. Depending on the value of J_0, the Sherrington-Kirkpatrick model has a phase transition from a paramagnetic to a spin-glass phase or from a ferromagnetic to a mixed phase [32]: it would be interesting to investigate, both analytically and numerically, the fluctuations of these pseudocritical points. Moreover, in order to bridge the gap between a mean-field and a short-range interactions regime, it could be interesting to investigate the fluctuations of the pseudocritical temeperature in spin-glass models with tunable long-range interactions, like those introduced in [33]. As far as the Edwards-Anderson model is concerned, it would be interesting to test experimentally the scenario found here in $Fe_{0.5}Mn_{0.5}TiO_3$ [1] or $Eu_{0.5}Ba_{0.5}MnO_3$ [2] spin-glass materials. Indeed, ac-susceptibility measurements in these systems show [1] that the spin-glass critical temperature can be identified as the temperature where the susceptibility has a cusp. Accordingly, the pseudocritical point could be identified and measured, and one could test whether the resulting

rescaled pseudocritical point distribution converges to the Gumbel distribution as the system size is increased.

*michele.castellana@lptms.u-psud.fr

[1] K. Gunnarsson *et al.*, Phys. Rev. B **43**, 8199 (1991).
[2] S. Nair and A. K. Nigam, Phys. Rev. B **75**, 214415 (2007).
[3] S. F. Edwards and P. W. Anderson, J. Phys. F **5**, 965 (1975).
[4] D. Sherrington and S. Kirkpatrick, Phys. Rev. Lett. **35**, 1792 (1975).
[5] M. Mézard, G. Parisi, and M. A. Virasoro, *Spin glass theory and beyond* (World Scientific, Singapore, 1987).
[6] M. Palassini and S. Caracciolo, Phys. Rev. Lett. **82**, 5128 (1999).
[7] T. D. Lee and C. N. Yang, Phys. Rev. **87**, 410 (1952).
[8] C. Yang, Phys. Rev. **87**, 404 (1952).
[9] A. Harris, J. Phys. C **7**, 1671 (1974).
[10] A. Aharony and A. B. Harris, Phys. Rev. Lett. **77**, 3700 (1996).
[11] S. Wiseman and E. Domany, Phys. Rev. Lett. **81**, 22 (1998).
[12] K. Bernardet, F. Pázmándi, and G. G. Batrouni, Phys. Rev. Lett. **84**, 4477 (2000).
[13] F. Iglói *et al.*, Phys. Rev. B **76**, 064421 (2007).
[14] M. Castellana and E. Zarinelli, Phys. Rev. B **84**, 144417 (2011).
[15] J. Galambos, *The asymptotic Theory of Extreme Order Statistics* (R. E. Krieger Publishing Co., Malabar, Florida, 1987).
[16] C. A. Tracy and H. Widom, in *Proc. International Congress of Mathematicians (Beijing, 2002)* (Higher Education Press, Beijing, 2002), Vol. 1.
[17] J. Baik, P. Deift, and K. Johansson, J. Am. Math. Soc. **12**, 1119 (1999).
[18] K. Johansson, Commun. Math. Phys. **209**, 437 (2000).
[19] M. Prähofer and H. Spohn, Phys. Rev. Lett. **84**, 4882 (2000).
[20] M. Kardar, G. Parisi, and Y. C. Zhang, Phys. Rev. Lett. **56**, 889 (1986).
[21] P. Calabrese and P. Le Doussal, Phys. Rev. Lett. **106**, 250603 (2011).
[22] A. M. Somoza, M. Ortuño, and J. Prior, Phys. Rev. Lett. **99**, 116602 (2007).
[23] C. Monthus and T. Garel, Phys. Rev. B **79**, 205120 (2009).
[24] K. A. Takeuchi and M. Sano, Phys. Rev. Lett. **104**, 230601 (2010).
[25] K. A. Takeuchi *et al.*, Sci. Rep. **1** (2011) 34.
[26] B. Coluzzi *et al.*, J. Phys. A **33**, 3851 (2000).
[27] T. Nakamura *et al.*, J. Phys. A **36**, 10895 (2003).

[28] G. Parisi *et al.*, J. Phys. A **26**, 247 (1993).

[29] A. Billoire *et al.*, J. Stat. Mech. (2011) P10019.

[30] T. Vojta, J. Phys. A **39**, R143 (2006).

[31] D. S. Dean and S. N. Majumdar, Phys. Rev. Lett. **97**, 160201 (2006).

[32] H. Nishimori, *Statistical Physics of Spin Glasses and Information Processing: An Introduction* (Oxford University Press, Oxford, UK, 2001).

[33] G. Kotliar, P. W. Anderson, and D. L. Stein, Phys. Rev. B **27**, 602 (1983).

Bibliography

[1] Phase transitions. In *Proceedings of the Cargese Summer Institute* (edited by M. Lévy, J. C. Le Guillou and J. Zinn-Justin), vol. B72. Plenum (1982).

[2] ABOU-CHACRA, R., THOULESS, D. J., AND ANDERSON, P. W. A selfconsistent theory of localization. *Journal of Physics C: Solid State Physics*, **6** (1973), 1734.

[3] ALVAREZ BAÑOS, R., ET AL. Static versus dynamic heterogeneities in the $d = 3$ Edwards-Anderson Ising spin glass. *Physical Review Letters*, **105** (2010), 177202.

[4] ANDERSON, P. W. Through the glass lightly. *Science*, **267** (1995), 1615.

[5] BAILLIE, C. F., GUPTA, R., HAWICK, K. A., AND PAWLEY, G. S. Monte Carlo renormalization-group study of the three-dimensional Ising model. *Physical Review B*, **45** (1992), 10438.

[6] BAKER JR, G. Ising model with a scaling interaction. *Physical Review B*, **5** (1972), 2622.

[7] BALLESTEROS, H. G., ET AL. Critical behavior of the three-dimensional Ising spin glass. *Physical Review B*, **62** (2000), 14237.

[8] BAÑOS, R. A., ET AL. Nature of the spin-glass phase at experimental length scales. *Journal of Statistical Mechanics: Theory and Experiment*, (2010), P06026.

[9] BARAHONA, F. On the computational complexity of Ising spin glass models. *Journal of Physics A: Mathematical and General*, **15** (1982), 3241.

[10] BELLETTI, F., ET AL. An in-depth view of the microscopic dynamics of Ising spin glasses at fixed temperature. *Journal of Statistical Physics*, **135** (2009), 1121.

[11] BERKER, A. AND OSTLUND, S. Renormalization group calculations of finite systems: order parameter and specific heat for epitaxial ordering. *Journal of Physics C: Solid State Physics*, **12** (1979), 4961.

[12] BERNARDI, L. AND CAMPBELL, I. A. Violation of universality for Ising spin-glass transitions. *Physical Review B*, **52** (1995), 12501.

[13] BERNARDI, L. W., PRAKASH, S., AND CAMPBELL, I. A. Ordering temperatures and critical exponents in Ising spin glasses. *Physical Review Letters*, **77** (1996), 2798.

[14] BERT, F., DUPUIS, V., VINCENT, E., HAMMANN, J., AND BOUCHAUD, J. P. Spin anisotropy and slow dynamics in spin glasses. *Physical Review Letters*, **92** (2004), 167203.

[15] BHATT, R. N. AND YOUNG, A. P. Numerical studies of Ising spin glasses in two, three, and four dimensions. *Physical Review B*, **37** (1988), 5606.

[16] BIROLI, G. AND BOUCHAUD, J. P. The random first-order transition theory of glasses: a critical assessment (2009). `arXiv:0912.2542`.

[17] BIROLI, G., BOUCHAUD, J. P., CAVAGNA, A., GRIGERA, T. S., AND VERROCCHIO, P. Thermodynamic signature of growing amorphous order in glass-forming liquids. *Nature Physics*, **4** (2008), 771.

[18] BIROLI, G. AND MÉZARD, M. Lattice glass models. *Physical Review Letters*, **88** (2001), 025501.

[19] BIROLI, G., MONASSON, R., AND WEIGT, M. A variational description of the ground state structure in random satisfiability problems. *The European Physical Journal B-Condensed Matter and Complex Systems*, **14** (2000), 551.

[20] BLEHER, P. AND SINAI, J. Investigation of the critical point in models of the type of Dyson's hierarchical models. *Communications in Mathematical Physics*, **33** (1973), 23.

[21] BLEHER, P. M. *Tr. Mosc. Mat. Ob.*, **33**.

[22] BLEHER, P. M. Investigation of the vicinity of the critical point in models of the type of Dyson's hierarchical models. *Institute of Applied Mathematics of the Academy of Sciences of the USSR, Moscow*, (1973).

[23] BLEHER, P. M. Critical indices for models with long range forces (numerical calculations). *Preprint of the Institute of Applied Mathematics of the Academy of Sciences of the USSR*, (1975).

[24] BLEHER, P. M. AND SINAI, Y. G. Critical indices for Dyson's asymptotically-hierarchical models. *Communications in Mathematical Physics*, **45** (1975), 247.

[25] BOUCHAUD, J. P. AND BIROLI, G. On the Adam-Gibbs-Kirkpatrick-Thirumalai-Wolynes scenario for the viscosity increase in glasses. *The Journal of Chemical Physics*, **121** (2004), 7347.

[26] BOUCHAUD, J. P., CUGLIANDOLO, L., KURCHAN, J., AND MÉZARD, M. In *Lecture notes in Slow Relaxation and Nonequilibrium Dynamics in Condensed Matter, Les Houches 2002 Summer School, Session 77*. Berlin (2002).

[27] BRAY, A. J. AND MOORE, M. A. Heidelberg Colloquium on Glassy Dynamics and Optimization. Springer-Verlag, Heidelberg, (1986).

[28] CALLAN, C. Broken scale invariance in scalar field theory. *Physical Review D*, **2** (1970), 1541.

[29] CALLAN, C. Methods in field theory. In *Les Houches 1975* (edited by R. Balian and J. Zinn-Justin). North-Holland, Amsterdam (1976).

[30] CAMPOSTRINI, M., PELISSETTO, A., ROSSI, P., AND VICARI, E. Improved high-temperature expansion and critical equation of state of three-dimensional Ising-like systems. *Physical Review E*, **60** (1999), 3526.

[31] CASSANDRO, M. AND JONA-LASINIO, G. Critical point behaviour and probability theory. *Advances in Physics*, **27** (1978), 913.

[32] CASTELLANA, M., DECELLE, A., FRANZ, S., MÉZARD, M., AND PARISI, G. Hierarchical random energy model of a spin-glass: critical behavior of the correlation length. To be published.

[33] CASTELLANA, M., DECELLE, A., FRANZ, S., MÉZARD, M., AND PARISI, G. Hierarchical random energy model of a spin glass. *Physical Review Letters*, **104** (2010), 127206.

[34] CASTELLANA, M. AND PARISI, G. Renormalization group computation of the critical exponents of hierarchical spin glasses. *Physical Review E*, **82** (2010), 040105.

[35] CASTELLANA, M. AND PARISI, G. Renormalization group computation of the critical exponents of hierarchical spin glasses: Large-scale behavior and divergence of the correlation length. *Physical Review E*, **83** (2011), 041134.

[36] CASTELLANA, M. Real-space renormalization group analysis of a non-mean-field spin-glass. *Europhysics Letters*, **95** (2011), 47014.

[37] CASTELLANI, T. AND CAVAGNA, A. Spin-glass theory for pedestrians. *Journal of Statistical Mechanics: Theory and Experiment*, (2005), P05012.

[38] CHANG, M. AND SAK, J. Spin-glass with long-range random exchange interaction. *Physical Review B*, **29** (1984), 2652.

[39] CHEN, J. AND LUBENSKY, T. Mean field and ε-expansion study of spin glasses. *Physical Review B*, **16** (1977), 2106.

[40] CHETYRKIN, K., KATAEV, A., AND TKACHOV, F. Errata. *Physics Letters B*, **101** (1981), 457.

[41] CHETYRKIN, K., KATAEV, A., AND TKACHOV, F. Five-loop calculations in the $g\phi^4$ model and the critical index η. *Physics Letters B*, **99** (1981), 147.

[42] CHETYRKIN, K. G., GORISHNY, S. G., LARIN, S. A., AND TKACHOV, F. V. Five-loop renormalization group calculations in the $g\phi^4$ theory. *Physics Letters B*, **132** (1983), 351.

[43] CHETYRKIN, K. G. AND TKACHOV, F. V. Integration by parts: The algorithm to calculate β-functions in 4 loops. *Nuclear Physics B*, **192** (1981), 159.

[44] COLLET, P. AND ECKMANN, J. A renormalization group analysis of the hierarchical model in statistical mechanics. *Lecture Notes in Physics*, **74** (1978).

[45] COLLET, P. AND ECKMANN, J. P. The ϵ-expansion for the hierarchical model. *Communications in Mathematical Physics*, **55** (1977), 67.

[46] COLLET, P., ECKMANN, J. P., AND HIRSBRUNNER, B. A numerical test of Borel summability in the ϵ-expansion of the hierarchical model. *Physics Letters B*, **71** (1977), 385.

[47] CONTUCCI, P., GIARDINÀ, C., GIBERTI, C., PARISI, G., AND VERNIA, C. Ultrametricity in the Edwards-Anderson model. *Physical Review Letters*, **99** (2007), 057206.

[48] CONTUCCI, P., GIARDINÀ, C., GIBERTI, C., PARISI, G., AND VERNIA, C. Contucci et al. reply:. *Physical Review Letters*, **100** (2008), 159702.

[49] CONTUCCI, P., GIARDINÀ, C., GIBERTI, C., PARISI, G., AND VERNIA, C. Structure of correlations in three dimensional spin glasses. *Physical Review Letters*, **103** (2009), 017201.

[50] CRISANTI, A. AND SOMMERS, H. J. The spherical p-spin interaction spin glass model: the statics. *Zeitschrift für Physik B Condensed Matter*, **87** (1992), 341.

[51] DABOUL, D., CHANG, I., AND AHARONY, A. Test of universality in the Ising spin glass using high temperature graph expansion. *The European Physical Journal B-Condensed Matter and Complex Systems*, **41** (2004), 231.

[52] DE DOMINICIS, C. AND KONDOR, I. On spin glass fluctuations. *Journal de Physique Lettres*, **45** (1984), 205.

[53] DERRIDA, B. Random-energy model: Limit of a family of disordered models. *Physical Review Letters*, **45** (1980), 79.

[54] DERRIDA, B. Random-energy model: An exactly solvable model of disordered systems. *Physical Review B*, **24** (1981), 2613.

[55] DOMINICIS, C. D. AND GIARDINA, I. *Random fields and spin-glasses: a field-theory approach*. Springer (2006).

[56] DUPUIS, V., VINCENT, E., ALBA, M., AND HAMMANN, J. Aging, rejuvenation and memory effects in re-entrant ferromagnets. *The European Physical Journal B-Condensed Matter and Complex Systems*, **29** (2002), 19.

[57] DYSON, F. Existence of a phase transition in a one-dimensional Ising ferromagnet. *Communications in Mathematical Physics*, **12** (1969), 91.

[58] EARL, D. J. AND DEEM, M. W. Parallel tempering: Theory, applications, and new perspectives. *Physical Chemistry Chemical Physics*, **7** (2005), 3910.

[59] EDWARDS, S. AND ANDERSON, P. Theory of spin glasses. *Journal of Physics F: Metal Physics*, **5** (1975), 965.

[60] FISHER, D. AND HUSE, D. Absence of many states in realistic spin glasses. *Journal of Physics A: Mathematical and General*, **20** (1987), L1005.

[61] FISHER, D. AND HUSE, D. Pure states in spin glasses. *Journal of Physics A: Mathematical and General*, **20** (1987), L997.

[62] FISHER, D. AND HUSE, D. Equilibrium behavior of the spin-glass ordered phase. *Physical Review B*, **38** (1988), 386.

[63] FISHER, D. AND HUSE, D. Nonequilibrium dynamics of spin glasses. *Physical Review B*, **38** (1988), 373.

[64] FISHER, D. S. AND HUSE, D. A. Ordered phase of short-range Ising spin-glasses. *Physical Review Letters*, **56** (1986), 1601.

[65] FRANZ, S., JÖRG, T., AND PARISI, G. Overlap interfaces in hierarchical spin-glass models. *Journal of Statistical Mechanics: Theory and Experiment*, (2009), P02002.

[66] FRANZ, S. AND PARISI, G. On non-linear susceptibility in supercooled liquids. *Journal of Physics: Condensed Matter*, **12** (2000), 6335.

[67] GARDNER, E. A spin glass model on a hierarchical lattice. *Journal de Physique*, **45** (1984), 1755.

[68] GORISHNY, S. G., LARIN, S. A., AND TKACHOV, F. V. ϵ-expansion for critical exponents: The $O(\epsilon^5)$ approximation. *Physics Letters A*, **101** (1984), 120 .

[69] GUERRA, F. Broken replica symmetry bounds in the mean field spin glass model. *Communications in Mathematical Physics*, **233** (2003), 1.

[70] GUIDA, R. AND RIBECA, P. Towards a fully automated computation of RG functions for the three-dimensional $O(N)$ vector model: parametrizing amplitudes. *Journal of Statistical Mechanics: Theory and Experiment*, (2006), P02007.

[71] GUNNARSSON, K., SVEDLINDH, P., NORDBLAD, P., LUNDGREN, L., ARUGA, H., AND ITO, A. Static scaling in a short-range Ising spin glass. *Physical Review B*, **43** (1991), 8199.

[72] HARRIS, A. B., LUBENSKY, T. C., AND CHEN, J.-H. Critical properties of spin-glasses. *Physical Review Letters*, **36** (1976), 415.

[73] HASENBUSCH, M., PELISSETTO, A., AND VICARI, E. Critical behavior of three-dimensional Ising spin glass models. *Physical Review B*, **78** (2008), 214205.

[74] HUANG, K. *Statistical mechanics.* Wiley (1987).

[75] HUSE, D. Private communication (2011).

[76] ITO, A., ARUGA, H., TORIKAI, E., KIKUCHI, M., SYONO, Y., AND TAKEI, H. Time-dependent phenomena in a short-range Ising spin-glass, $Fe_{0.5}Mn_{0.5}TiO_3$. *Physical Review Letters*, **57** (1986), 483.

[77] ITZYKSON, C. AND DROUFFE, J. M. *Statistical Field Theory (Cambridge Monographs on Mathematical Physics)*. Cambridge University Press (1991).

[78] JOH, Y. G., ORBACH, R., AND HAMMANN, J. Spin glass dynamics under a change in magnetic field. *Physical Review Letters*, **77** (1996), 4648.

[79] JONA-LASINIO, G. The renormalization group: A probabilistic view. *Il Nuovo Cimento B (1971-1996)*, **26** (1975), 99.

[80] JONA-LASINIO, G. Renormalization group and probability theory. *Physics Reports*, **352** (2001), 439.

[81] JONASON, K., VINCENT, E., HAMMANN, J., BOUCHAUD, J. P., AND NORD-BLAD, P. Memory and chaos effects in spin glasses. *Physical Review Letters*, **81** (1998), 3243.

[82] JÖRG, T., KATZGRABER, H., AND KRZAKALA, F. Behavior of Ising spin glasses in a magnetic field. *Physical Review Letters*, **100** (2008), 197202.

[83] JÖRG, T. AND KRZAKALA, F. Comment on "Ultrametricity in the Edwards-Anderson model". *Physical Review Letters*, **100** (2008), 159701.

[84] KADANOFF, L. P. Scaling laws for Ising models near T_c. *Physics (Long Island. City, N.Y.)*, **2** (1966), 263.

[85] KATORI, H. A. AND ITO, A. Experimental study of the de Almeida-Thouless line by using typical Ising spin-glass $Fe_xMn_{1-x}TiO_3$ with $x = 0.41, 0.50, 0.55$ and 0.57. *Journal of the Physical Society of Japan*, **63** (1994), 3122.

[86] KATZGRABER, H. AND HARTMANN, A. Ultrametricity and clustering of states in spin glasses: A one-dimensional view. *Physical Review Letters*, **102** (2009), 37207.

[87] KATZGRABER, H., PALASSINI, M., AND YOUNG, A. Monte Carlo simulations of spin glasses at low temperatures. *Physical Review B*, **63** (2001), 184422.

[88] KATZGRABER, H. AND YOUNG, A. Monte Carlo studies of the one-dimensional Ising spin glass with power-law interactions. *Physical Review B*, **67** (2003), 134410.

[89] KATZGRABER, H. AND YOUNG, A. Probing the Almeida-Thouless line away from the mean-field model. *Physical Review B*, **72** (2005), 184416.

[90] KATZGRABER, H. G., HARTMANN, A. K., AND YOUNG, A. P. *Computer Simulation Studies in Condensed Matter Physics*, vol. XXI. Springer Verlag, Heidelberg (2008).

[91] KATZGRABER, H. G., KÖRNER, M., AND YOUNG, A. P. Universality in three-dimensional Ising spin glasses: A Monte Carlo study. *Physical Review B*, **73** (2006), 224432.

[92] KATZGRABER, H. G., LARSON, D., AND YOUNG, A. P. Study of the de Almeida-Thouless line using power-law diluted one-dimensional Ising spin glasses. *Physical Review Letters*, **102** (2009), 177205.

[93] KAUZMANN, W. The nature of the glassy state and the behavior of liquids at low temperatures. *Chemical Reviews*, **43** (1948), 219.

[94] KAZAKOV, D. The method of uniqueness, a new powerful technique for multiloop calculations. *Physics Letters B*, **133** (1983), 406.

[95] KIRKPATRICK, S. AND SHERRINGTON, D. Infinite-ranged models of spin-glasses. *Physical Review B*, **17** (1978), 4384.

[96] KIRKPATRICK, T. R., THIRUMALAI, D., AND WOLYNES, P. Scaling concepts for the dynamics of viscous liquids near an ideal glassy state. *Physical Review A*, **40** (1989), 1045.

[97] KLEINERT, H., NEU, J., SCHULTE-FROHLINDE, N., CHETYRKIN, K. G., AND LARIN, S. A. Five-loop renormalization group functions of $O(n)$-symmetric ϕ^4-theory and ϵ-expansions of critical exponents up to ϵ^5. *Physics Letters B*, **272** (1991), 39.

[98] KLEINERT, H., NEU, J., SCHULTE-FROHLINDE, V., CHETYRKIN, K. G., AND LARIN, S. A. Erratum (Five-loop renormalization group functions of $O(n)$-symmetric ϕ^4-theory and ϵ-expansions of critical exponents up to ϵ^5: (*Physics Letters B **272** (1991), 39*)). *Physics Letters B*, **319** (1993), 545.

[99] KOTLIAR, G., ANDERSON, P., AND STEIN, D. One-dimensional spin-glass model with long-range random interactions. *Physical Review B*, **27** (1983), 602.

[100] KRZAKALA, F. AND MARTIN, O. C. Spin and link overlaps in three-dimensional spin glasses. *Physical Review Letters*, **85** (2000), 3013.

[101] LANDAU, L. AND LIFSHITZ, E. M. *Statistical Physics: Course of Theoretical Physics, Vol. 5*. Pergamon (1980).

[102] LANGER, J. The mysterious glass transition. *Physics Today*, **60** (2007), 8.

[103] LAUGHLIN, W. T. AND UHLMANN, D. R. Viscous flow in simple organic liquids. *The Journal of Physical Chemistry*, **76** (1972), 2317.

[104] LEUZZI, L. Critical behaviour and ultrametricity of Ising spin-glass with long-range interactions. *Journal of Physics A: Mathematical and General*, **32** (1999), 1417.

[105] LEUZZI, L., PARISI, G., RICCI-TERSENGHI, F., AND RUIZ-LORENZO, J. Ising spin-glass transition in a magnetic field outside the limit of validity of mean-field theory. *Physical Review Letters*, **103** (2009), 267201.

[106] LEUZZI, L., PARISI, G., RICCI-TERSENGHI, F., AND RUIZ-LORENZO, J. J. Dilute one-dimensional spin glasses with power law decaying interactions. *Physical Review Letters*, **101** (2008), 107203.

[107] LOEFFEL, J. J. Transformation of an asymptotic series in a convergent one. In *Workshop on Padé approximants*. Marseille (1975).

[108] MARI, P. O. AND CAMPBELL, I. A. Ising spin glasses: Corrections to finite size scaling, freezing temperatures, and critical exponents. *Physical Review E*, **59** (1999), 2653.

[109] MARINARI, E., PARISI, G., AND RITORT, F. On the $3d$ Ising spin glass. *Journal of Physics A: Mathematical and General*, **27** (1994), 2687.

[110] MARINARI, E., PARISI, G., AND RUIZ-LORENZO, J. J. Phase structure of the three-dimensional Edwards-Anderson spin glass. *Physical Review B*, **58** (1998), 14852.

[111] MCMILLAN, W. L. Scaling theory of Ising spin glasses. *Journal of Physics C: Solid State Physics (1968-1988)*, **17** (1984), 3179.

[112] MENON, N., O'BRIEN, K. P., DIXON, P. K., WU, L., NAGEL, S. R., WILLIAMS, B. D., AND CARINI, J. P. Wide-frequency dielectric susceptibility measurements in glycerol. *Journal of Non-Crystalline Solids*, **141** (1992), 61.

[113] MEURICE, Y. The high-temperature expansion of the hierarchical Ising model: From Poincaré symmetry to an algebraic algorithm. *Journal of Mathematical Physics*, **36** (1995), 1812.

[114] MEURICE, Y., NIERMANN, S., AND ORDAZ, G. The oscillatory behavior of the high-temperature expansion of Dyson's hierarchical model: A renormalization group analysis. *Journal of Statistical Physics*, **87** (1997), 363.

[115] MÉZARD, M. AND MONTANARI, A. *Information, Physics and Computation*. Oxford University Press (2009).

[116] MÉZARD, M. AND PARISI, G. The Bethe lattice spin glass revisited. *The European Physical Journal B-Condensed Matter and Complex Systems*, **20** (2001), 217.

[117] MÉZARD, M., PARISI, G., SOURLAS, N., TOULOUSE, G., AND VIRASORO, M. Replica symmetry breaking and the nature of the spin glass phase. *Journal de Physique*, **45** (1984), 843.

[118] MÉZARD, M., PARISI, G., AND VIRASORO, M. A. SK model: The replica solution without replicas. *Europhysics Letters*, **1** (1986), 77.

[119] MÉZARD, M., PARISI, G., AND VIRASORO, M. A. *Spin glass theory and beyond*. World Scientific (1987).

[120] MÉZARD, M., PARISI, G., AND ZECCHINA, R. Analytic and algorithmic solution of random satisfiability problems. *Science*, **297** (2002), 812.

[121] MÉZARD, M. AND VIRASORO, M. The microstructure of ultrametricity. *Journal de Physique*, **46** (1985), 1293.

[122] Mézard, M. and Zecchina, R. Random *K*-satisfiability problem: From an analytic solution to an efficient algorithm. *Physical Review E*, **66** (2002), 056126.

[123] Monasson, R. and Zecchina, R. Statistical mechanics of the random *K*-satisfiability model. *Physical Review E*, **56** (1997), 1357.

[124] Moore, M. A. Ordered phase of the one-dimensional Ising spin glass with long-range interactions. *Physical Review B*, **82** (2010), 014417.

[125] Moore, M. A., Bokil, H., and Drossel, B. Evidence for the droplet picture of spin glasses. *Physical Review Letters*, **81** (1998), 4252.

[126] Moore, M. A. and Bray, A. J. Disappearance of the de Almeida-Thouless line in six dimensions. *Physical Review B*, **83** (2011), 224408.

[127] Naimzhanov, A. Hierarchical models of spin glasses. *Theoretical and Mathematical Physics*, **51** (1982), 416.

[128] Naimzhanov, A. Hierarchical model of spin glass. *Theoretical and Mathematical Physics*, **57** (1983), 1163.

[129] Nair, S. and Nigam, A. K. Critical exponents and the correlation length in the manganite spin glass $Eu_{0.5}Ba_{0.5}MnO_3$. *Physical Review B*, **75** (2007), 214415.

[130] Nishimori, H. *Statistical physics of spin glasses and information processing: An introduction.* Oxford University Press, Oxford, UK (2001).

[131] Ogielski, A. T. Dynamics of three-dimensional Ising spin glasses in thermal equilibrium. *Physical Review B*, **32** (1985), 7384.

[132] Palassini, M. and Caracciolo, S. Universal finite-size scaling functions in the 3-*d* Ising spin glass. *Physical Review Letters*, **82** (1999), 5128.

[133] Parisi, G. Infinite number of order parameters for spin-glasses. *Physical Review Letters*, **43** (1979), 1754.

[134] Parisi, G. Toward a mean field theory for spin glasses. *Physics Letters A*, **73** (1979), 203 .

[135] Parisi, G. A sequence of approximated solutions to the SK model for spin glasses. *Journal of Physics A: Mathematical and General*, **13** (1980), L115.

[136] Parisi, G. The order parameter for spin glasses: A function on the interval $0 - 1$. *Journal of Physics A: Mathematical and General*, **13** (1980), 1101.

[137] Parisi, G. Order parameter for spin-glasses. *Physical Review Letters*, **50** (1983), 1946.

[138] Parisi, G. *Statistical Field Theory (Advanced Book Classics).* Westview Press (1998).

[139] PARISI, G. AND SOURLAS, N. *p*-adic numbers and replica symmetry breaking. *The European Physical Journal B-Condensed Matter and Complex Systems*, **14** (2000), 535.

[140] PAWLEY, G. S., SWENDSEN, R. H., WALLACE, D. J., AND WILSON, K. G. Monte Carlo renormalization-group calculations of critical behavior in the simple-cubic Ising model. *Physical Review B*, **29** (1984), 4030.

[141] PLEFKA, T. Convergence condition of the TAP equation for the infinite-ranged Ising spin glass model. *Journal of Physics A: Mathematical and General*, **15** (1982), 1971.

[142] POLYAKOV, A. M. Interaction of Goldstone particles in two dimensions. Applications to ferromagnets and massive Yang-Mills fields. *Physics Letters B*, **59** (1975), 79 .

[143] RICHERT, R. AND ANGELL, C. Dynamics of glass-forming liquids. V. On the link between molecular dynamics and configurational entropy. *The Journal of Chemical Physics*, **108** (1998), 9016.

[144] SHERRINGTON, D. AND KIRKPATRICK, S. Solvable model of a spin-glass. *Physical Review Letters*, **35** (1975), 1792.

[145] SWENDSEN, R. H. AND WANG, J.-S. Replica Monte Carlo simulation of spin-glasses. *Physical Review Letters*, **57** (1986), 2607.

[146] SYKES, M., GAUNT, D., ROBERTS, P., AND WYLES, J. High temperature series for the susceptibility of the Ising model. II. Three dimensional lattices. *Journal of Physics A: General Physics*, **5** (1972), 640.

[147] SYMANZIK, K. Small distance behaviour in field theory and power counting. *Communications in Mathematical Physics*, **18** (1970), 227.

[148] TAIBLESON, M. *Fourier analysis on local fields.* Princeton University Press, Princeton, NJ (1976).

[149] TALAGRAND, M. The Parisi formula. *Annals of Mathematics-Second Series*, **163** (2006), 221.

[150] TARJUS, G. AND KIVELSON, D. The viscous slowing down of supercooled liquids and the glass transition: phenomenology, concepts, and models. *Jamming and rheology: constrained dynamics on microscopic and macroscopic scales*, (2001), 20. arXiv:cond-mat/0003368v1.

[151] THEUMANN, A. Critical properties of the random hierarchical model. *Physical Review B*, **21** (1980), 2984.

[152] THEUMANN, A. Ferromagnetic and spin-glass behavior in the random hierarchical model. *Physical Review B*, **22** (1980), 5441.

[153] THOULESS, D. J., ANDERSON, P. W., AND PALMER, R. G. Solution of 'Solvable model of a spin-glass'. *Philosophical Magazine*, **35** (1977), 593.

[154] VAN DUIJVENDIJK, K., SCHEHR, G., AND VAN WIJLAND, F. Slow relaxation, dynamic transitions, and extreme value statistics in disordered systems. *Physical Review E*, **78** (2008), 011120.

[155] VAN HEMMEN, J. L. AND PALMER, R. G. The replica method and solvable spin glass model. *Journal of Physics A: Mathematical and General*, **12** (1979), 563.

[156] VINCENT, E., DUPUIS, V., ALBA, M., HAMMANN, J., AND BOUCHAUD, J. P. Aging phenomena in spin-glass and ferromagnetic phases: Domain growth and wall dynamics. *Europhysics Letters*, **50** (2000), 674.

[157] VLADIMIROV, A. A., KAZAKOV, D. I., AND TARASOV, O. V. Calculation of the critical indices by the methods of quantum field theory. *Zhurnal Eksperimental'noi i Teoreticheskoi Fiziki*, **77** (1979), 1035.

[158] WEINBERG, S. *The quantum theory of fields, Volume I: Foundations.* Cambridge University Press (2005).

[159] WEINBERG, S. *The quantum theory of fields, Volume II: Modern applications.* Cambridge University Press (2005).

[160] WELSH, D. J. A. *Complexity: Knots, colourings and counting. Volume 186 of London Mathematical Society Lecture Notes Series.* Cambridge University Press (1993).

[161] WILSON, K. The renormalization group and critical phenomena, Nobel lecture, 8 December 1982. *Nobel Lectures, Physics*, **1990** (1982).

[162] WILSON, K. The renormalization group and critical phenomena. *Reviews of Modern Physics*, **55** (1983), 583.

[163] WILSON, K. AND KOGUT, J. The renormalization group and the ϵ expansion. *Physics Reports*, **12** (1974), 75.

[164] WILSON, K. G. Renormalization group and critical phenomena. I. Renormalization group and the Kadanoff scaling picture. *Physical Review B*, **4** (1971), 3174.

[165] WILSON, K. G. Renormalization group and critical phenomena. II. Phase-space cell analysis of critical behavior. *Physical Review B*, **4** (1971), 3184.

[166] WILSON, K. G. Feynman-graph expansion for critical exponents. *Physical Review Letters*, **28** (1972), 548.

[167] WILSON, K. G. Quantum field-theory models in less than 4 dimensions. *Physical Review D*, **7** (1973), 2911.

[168] WILSON, K. G. Critical phenomena in 3.99 dimensions. *Physica*, **73** (1974), 119.

[169] WILSON, K. G. AND FISHER, M. E. Critical exponents in 3.99 dimensions. *Physical Review Letters*, **28** (1972), 240.

[170] WOLFRAM, S. *The Mathematica book, third edition.* Cambridge University Press (1996).

[171] YOUNG, A. AND KATZGRABER, H. Absence of an Almeida-Thouless line in three-dimensional spin glasses. *Physical Review Letters*, **93** (2004), 207203.

[172] ZINN-JUSTIN, J. Analysis of Ising model critical exponents from high-temperature series expansion. *Journal de Physique*, **40** (1979), 969.

[173] ZINN-JUSTIN, J. Quantum field theory and critical phenomena. *International Series of Monographs on Physics*, **113** (2002), 1.

[174] ZINN-JUSTIN, J. *Phase transitions and renormalization group.* Oxford University Press (2007).